Sílvio Vaz Jr. *Editor*

Analytical Techniques and Methods for Biomass

Springer

Analytical Techniques and Methods for Biomass

Sílvio Vaz Jr.
Editor

Analytical Techniques and Methods for Biomass

Springer

Editor
Sílvio Vaz Jr.
Brazilian Agricultural Research Corporation
National Research Center for Agroenergy (Embrapa Agroenergy)
Embrapa Agroenergia, Parque Estação Biológica
Brasília, DF, Brazil

ISBN 978-3-319-41413-3 ISBN 978-3-319-41414-0 (eBook)
DOI 10.1007/978-3-319-41414-0

Library of Congress Control Number: 2016954461

Printed on acid-free paper

This Springer imprint is published by Springer Nature
The registered company is Springer International Publishing AG
The registered company address is: Gewerbestrasse 11, 6330 Cham, Switzerland

Preface

The use of biomass as a renewable raw material to substitute oil is a topic of strong academic, industrial and marketing appeal due to the establishment of a green economy (or bioeconomy) less harmful to the environment. Thus, more than ever, it has sought to expand the biomass uses beyond those already in use, such as agriculture and energy. In order to develop new products and processes, and ensure the quality of existing ones, it is fundamental to carry out chemical analysis of raw materials as both the products and their co-products and residues.

The objectives of the book are (1) to demonstrate the importance of analytical chemistry in understanding the chemical composition of biomass and its products and (2) to introduce modern techniques and their methods of analysis, which can positively influence in a direct way the improvements of products and processes and reduce the environmental impacts of biomass chains, focusing on plant. These precedents are based on great efforts seeking to advance scientific knowledge of chemical analysis, which has been occurring over decades of work by the chemical community.

The authors conducted a thorough survey of the relevant analytical techniques to the biomass, based on their academic and professional experience and the trends in current analytical science, as well as consideration of other relevant aspects such as the proposal for a more sustainable chemistry. The theoretical principles of analytical techniques are presented in order to direct their applications, since the book is aimed at researchers, scientists, biomass professionals and graduate students who already have knowledge in analytical chemistry and organic chemistry. Thus, it is intended to transmit a sound knowledge about the most useful analytical techniques and methods applied to the main types of biomass and their products, in order to allow them to develop their analytical methods and interpret the results.

Good lecture!

Brasília, Brazil — Sílvio Vaz Jr.

Contents

Contributors

Patrícia Verardi Abdelnur EMBRAPA Agroenergy, Brazilian Agricultural Research Corporation, National Center for Agroenergy Research, Brasília, DF, Brazil

Institute of Chemistry, Mass Spectrometry and Chromatography Laboratory, Federal University of Goiás, Goiânia, GO, Brazil

Carlos Alciaturi Chemometrics and Optimization Unit, Zulian Institute of Technological Research, La Cañada de Urdaneta, Venezuela

Juliana A. Aricetti Brazilian Bioethanol Science and Technology Laboratory at Brazilian Center for Research in Energy and Materials, Campinas, SP, Brazil

Eduardo Ribeiro de Azevêdo Instituto de Física de São Carlos, Universidade de São Paulo, São Carlos, SP, Brazil

Oigres Daniel Bernardinelli Instituto de Física de São Carlos, Universidade de São Paulo, São Carlos, SP, Brazil

Camila Caldana Brazilian Bioethanol Science and Technology Laboratory at Brazilian Center for Research in Energy and Materials, Campinas, SP, Brazil

Max Planck Partner Group at Brazilian Bioethanol Science and Technology Laboratory/CNPEM, Campinas, SP, Brazil

Julián Carrillo-Reyes Unidad Académica Juriquilla, Instituto de Ingeniería, Universidad Nacional Autónoma de México, Querétaro, Mexico

Luiz Alberto Colnago Embrapa Instrumentação, São Carlos, SP, Brazil

Mauro Vicentini Correia EMBRAPA, Embrapa Agroenergy, Brasília, DF, Brazil

Vincenza Cozzolino Centro Interdipartimentale di Ricerca sulla Risonanza Magnetica Nucleare per l'Ambiente, l'Agro-Alimentare ed i Nuovi Materiali (CERMANU), Portici, Italy

Marios Drosos Centro Interdipartimentale di Ricerca sulla Risonanza Magnetica Nucleare per l'Ambiente, l'Agro-Alimentare ed i Nuovi Materiali (CERMANU), Portici, Italy

Alexis Faneite Chemical Engineering Laboratory, Chemical Engineering School, Engineering Faculty, University of Zulia, Maracaibo, Venezuela

Alexis Ferrer Analytical Instrumentation Laboratory, Science Faculty, University of Zulia, Maracaibo, Venezuela

Luz Marina Flórez-Pardo Department of Energy and Mechanics, Autónoma of Occidente University, Cali, Colombia

Basma El Khaldi-Hansen Research Institute Bioactive Polymer Systems and BTU Cottbus, Berlin-Teltow, Germany

Birgit Kamm Research Institute Bioactive Polymer Systems and BTU Cottbus, Berlin-Teltow, Germany

Jorge Enrique López-Galán School of Chemical Engineering, University of Valle, Cali, Colombia

Pierluigi Mazzei Centro Interdipartimentale di Ricerca sulla Risonanza Magnetica Nucleare per l'Ambiente, l'Agro-Alimentare ed i Nuovi Materiali (CERMANU), Portici, Italy

Artemisa Medina-López Laboratorio de Fitomejoramiento Molecular, Instituto Politécnico Nacional, Centro Interdisciplinario de Investigación para el Desarrollo Integral Regional Unidad Sinaloa (CIIDIR-IPN Unidad Sinaloa), Guasave, Sinaloa, Mexico

Antonio Nebbioso Centro Interdipartimentale di Ricerca sulla Risonanza Magnetica Nucleare per l'Ambiente, l'Agro-Alimentare ed i Nuovi Materiali (CERMANU), Portici, Italy

Etelnivo Enrique Novotny Embrapa Solos, Rio de Janeiro, RJ, Brazil

Assunta Nuzzo Centro Interdipartimentale di Ricerca sulla Risonanza Magnetica Nucleare per l'Ambiente, l'Agro-Alimentare ed i Nuovi Materiali (CERMANU), Portici, Italy

Vanda Maria de Oliveira EMBRAPA, Embrapa Agroenergy, Brasília, DF, Brazil

UCB, Catholic University of Brasília, Brasília, DF, Brazil

Alessandro Piccolo Centro Interdipartimentale di Ricerca sulla Risonanza Magnetica Nucleare per l'Ambiente, l'Agro-Alimentare ed i Nuovi Materiali (CERMANU), Portici, Italy

Francisco R. Quiroz-Figueroa Laboratorio de Fitomejoramiento Molecular, Instituto Politécnico Nacional, Centro Interdisciplinario de Investigación para el Desarrollo Integral Regional Unidad Sinaloa (CIIDIR-IPN Unidad Sinaloa), Guasave, Sinaloa, Mexico

Maria Esther Ricci-Silva EMBRAPA Agroenergy, Brazilian Agricultural Research Corporation, National Center for Agroenergy Research, Brasília, DF, Brazil

Josybel Ríos Agrifoods Unit, Zulian Institute of Technological Research, La Cañada de Urdaneta, Venezuela

Clenilson Martins Rodrigues EMBRAPA, Embrapa Agroenergy, Brasília, DF, Brazil

Wanderson Romão Department of Chemistry, Petroleomic and Forensic Laboratory, Federal University of Espírito Santo, Vitoria, ES, Brazil

Davide Savy Centro Interdipartimentale di Ricerca sulla Risonanza Magnetica Nucleare per l'Ambiente, l'Agro-Alimentare ed i Nuovi Materiali (CERMANU), Portici, Italy

Margit Schulze Department of Natural Sciences, Bonn-Rhein-Sieg University of Applied Sciences, Rheinbach, Germany

Viviane Cândida da Silva EMBRAPA, Embrapa Agroenergy, Brasília, DF, Brazil

Wesley Pereira da Silva UFGD, Faculty of Science and Technology, Federal University of Grande Dourados, Dourados, MS, Brazil

Augusto Lopes Souto EMBRAPA, Embrapa Agroenergy, Brasília, DF, Brazil

Riccardo Spaccini Centro Interdipartimentale di Ricerca sulla Risonanza Magnetica Nucleare per l'Ambiente, l'Agro-Alimentare ed i Nuovi Materiali (CERMANU), Portici, Italy

Magno Aparecido Gonçalves Trindade UFGD, Faculty of Science and Technology, Federal University of Grande Dourados, Dourados, MS, Brazil

Idania Valdez-Vazquez Unidad Académica Juriquilla, Instituto de Ingeniería, Universidad Nacional Autónoma de México, Querétaro, Mexico

Géssica Adriana Vasconcelos Chemistry Institute, Mass Spectrometry and Chromatography Laboratory, Federal University of Goiás, Goiânia, GO, Brazil

Boniek Gontijo Vaz Institute of Chemistry, Mass Spectrometry and Chromatography Laboratory, Federal University of Goiás, Goiânia, GO, Brazil

Sílvio Vaz Jr. Brazilian Agricultural Research Corporation, National Research Center for Agroenergy (Embrapa Agroenergy), Embrapa Agroenergia, Parque Estação Biológica, Brasília, DF, Brazil

Chapter 1
The Use of Analytical Chemistry to Understand Biomass

Sílvio Vaz Jr.

Abstract Modern chemistry plays a strong economic role in industrial activities based on biomass, with an increasing trend in the importance of its application from the deployment of biorefineries and the principles of green chemistry, which make use of the potential of biomass with decreasing negative environmental impact. In this context, analytical chemistry can contribute significantly to the biomass supply chains, be they of plant or animal origin, but with the first offering the greatest challenges and the greatest opportunity for technical and scientific advances, given its diversified chemical constitution. This chapter presents a general outlook on the application of analytical chemistry to understand biomass composition and to promote its usages.

Keywords Biomass constitution • Chemical analysis • Instrumental analysis

1.1 Introduction

The use of biomass by humans goes back to the principles of humanity, where it was used as a heat source, food, fiber, and various items, such as weapons. With the development of societies, biomass was in great demand and uncontrolled use of this natural resource led to massive deforestation of native forests in almost every continent of the globe, to a greater or lesser extent. On the other hand, agriculture also developed, leading to an increase in the production and productivity of crops, especially for human and animal consumption.

From the mid-20th century, there was a "boom" of consumer society based on petroleum derivatives, which is a nonrenewable source and highly polluting raw material; this might be noticed by the large amount of produced plastic products.

S. Vaz Jr. (✉)
Brazilian Agricultural Research Corporation, National Research Center for Agroenergy (Embrapa Agroenergy), Embrapa Agroenergia, Parque Estação Biológica, s/n, Av. W3 Norte (final), 70770-901 Brasília, DF, Brazil
e-mail: silvio.vaz@embrapa.br

S. Vaz Jr. (ed.), *Analytical Techniques and Methods for Biomass*,
DOI 10.1007/978-3-319-41414-0_1

However, the same society began to notice that oil is a finite source, with serious problems observed in several producing countries, such as political and social instability, wars, and environmental disasters.

Modern chemistry plays a strong economic role in industrial activities based on biomass, with an increasing trend in the importance of its application from the deployment of biorefineries and the principles of green chemistry, which make use of the potential of biomass with decreasing negative environmental impact. In this context, analytical chemistry can contribute significantly to the biomass supply chains, be they of plant or animal origin, but the first offers the greatest challenges and the greatest opportunity for technical and scientific advances, given its diversified chemical constitution. It is worth mentioning that chemical analysis is used to examine the composition, for the characterization of physical

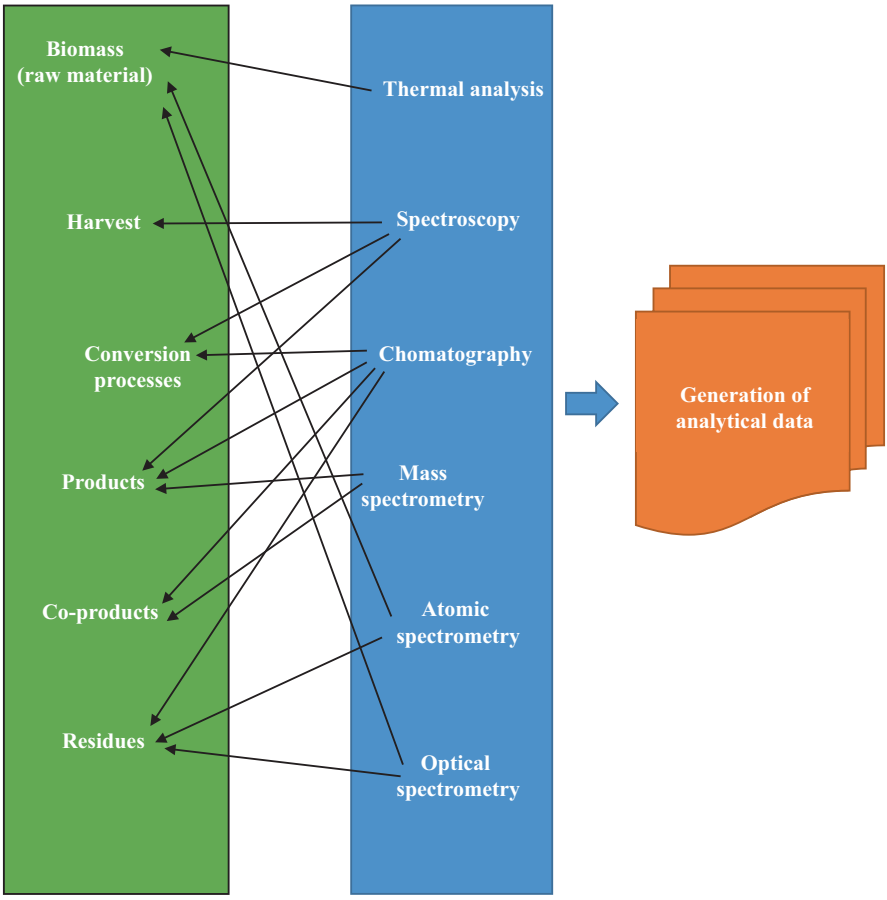

Fig. 1.1 A flowchart of the relationship between components of a biomass chain and chemical analyses to generate analytical data. This relationship is a proposal of use and other combinations can be established according to physicochemical properties, economic aspects, and equipment availability

and chemical properties, and for determining the concentration of chemical species of interest. Figure 1.1 shows, in a simplified way, components of an economic chain from biomass and the application of analytical techniques.

This chapter presents a general outlook on the application of analytical chemistry in order to understand biomass composition and to promote its usages.

1.2 Plant Biomass Diversity and Composition

According to data from the Food and Agriculture Organization of the United Nations (UN FAO), global biomass production for agri-industrial usages has reached 1,558.5 Gtons, with a huge contribution to the bioeconomy; it comprises cereals, oil crops, roots and tubers, vegetables, fruit, and fiber (UN FAO 2013). The high heterogeneity and consequent large chemical complexity of plant biomass become the raw material for various end products, such as energy, food, chemicals, pharmaceuticals, and materials. We can highlight four types of plant biomass of great economic interest, and to which we turn our attention: oil, saccharides (or sugars), starch, and lignocellulosic. Soybean (*Glycine max*) and palm oil (*Elaeis guineensis*) are examples of oil plant species; sugarcane (*Saccharum* spp.) and sorghum (*Sorghum bicolor* (L.) Moench) are biomass saccharides; maize (*Zea mays*) is a starchy biomass; and bagasse, straw, and wood biomass are lignocellulosic biomass. Each has its structural features and its chemical characteristics, which are directly related to analytical technology and the best technical approach to be applied during chemical analysis (Vaz 2014, 2015). Figures 1.2 1.3, 1.4, 1.5, 1.6, and 1.7 show the chemical structure of components of these biomass types, and Tables 1.1, 1.2, 1.3, and 1.4 show their m/m percentages.

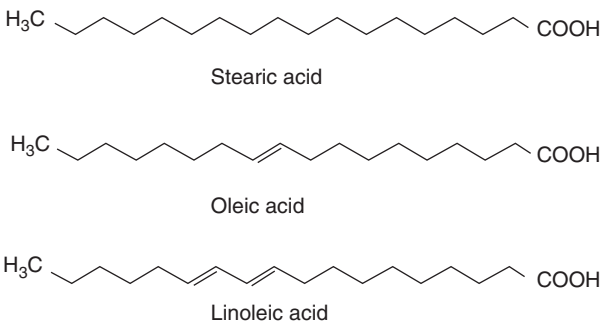

Fig. 1.2 Some chemical structures of fatty acids from oleaginous plants, such as soybean

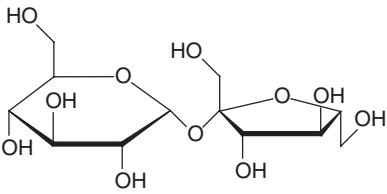

Fig. 1.3 Chemical structure of sucrose, a disaccharide present in sugarcane (author). The D-glucose moiety is on the *left* and the D-fructose moiety is on the *right*, linked by *α*–*β*–D-disaccharide bonds

Fig. 1.4 Chemical structure of starch polymer; the glucose unities (monomers) are linked by *α*–1–4–D-disaccharide bonds

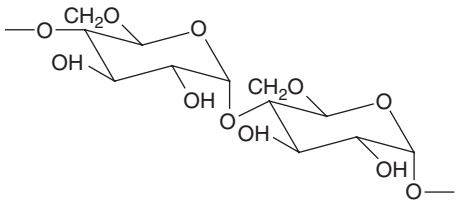

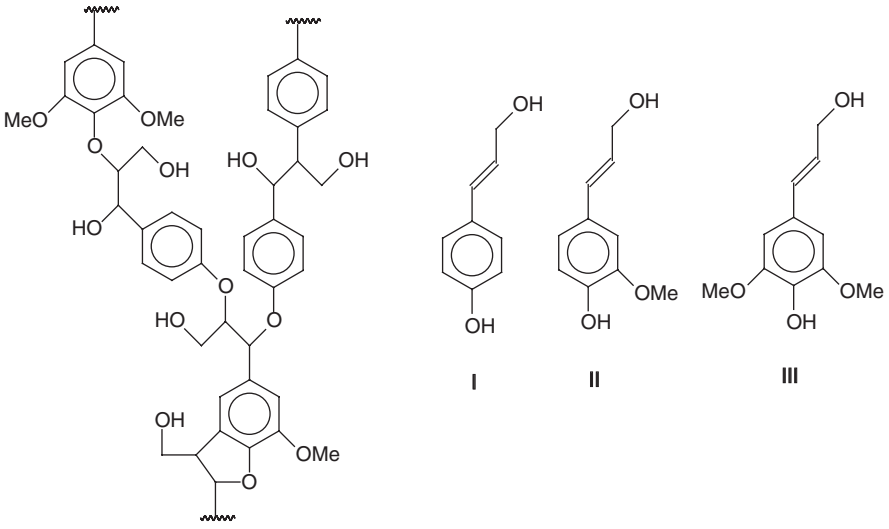

Fig. 1.5 Lignin structure (*left*) and its precursors (*right*): (*I*) *p*-coumaryl alcohol, (*II*) coniferyl alcohol, and (*III*) sinapyl alcohol

Fig. 1.6 Chemical structure of cellulose; the glucose units are linked by a 1,4–*β*–D bond

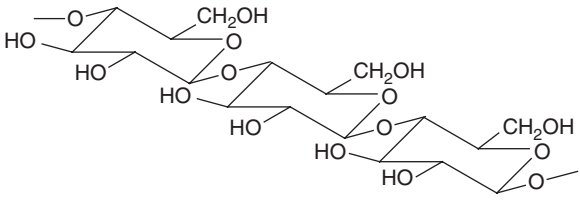

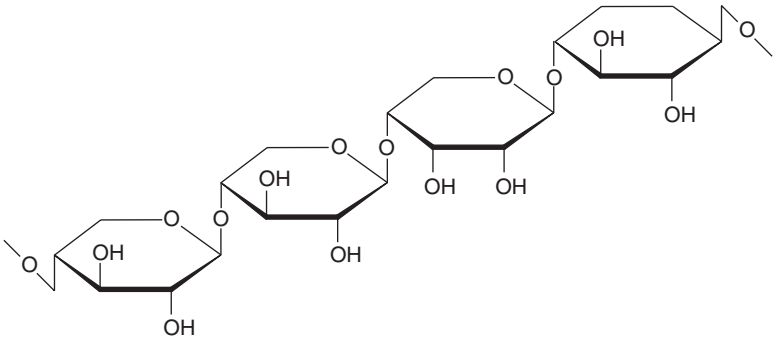

Fig. 1.7 Chemical structure of hemicellulose; the oligomeric units composed of D-glucose and pentoses (mainly D-xylose) are linked by means of a 1,4–β–D bond

Table 1.1 Chemical composition of oils extracted from oleaginous biomass (Gunstone 2004)

Plant	% m/m Palmitic acid	% m/m Stearic acid	% m/m Oleic acid	% m/m Linoleic acid	% m/m Triacylglycerols
Palm oil	44	4	39	10	3
Soybean	11	4	23	8	1

Table 1.2 Chemical composition of broth extracted from sugarcane (Faria et al. 2011) and sweet sorghum (Mamma et al. 1995)

Plant	% m/m Sucrose	% m/m Glucose	% m/m Organic acid
Sugarcane	85.3	–	24
Sweet sorghum	14.8	1.5	–

Table 1.3 Chemical composition of corn grain flour (Sandhu et al. 2007), cassava (Charles et al. 2005), and potato (Liu et al. 2007)

Plant	% m/m Starch	% m/m Protein	% m/m Fiber	% m/m Others
Corn (flour from grain)	90.1	6.5	0.52	1.99 (lipd)
Cassava (pulp)	83.8	1.5	2.5	0.2 (lipd)
Potato (pulp)	71.5	8.6	5.4	–

Table 1.4 Chemical composition of cellulosic biomasses (Vassilev et al. 2012)

Biomass	% m/m Cellulose	% m/m Hemicellulose	% m/m Lignin
Barley straw	48.6	29.7	21.7
Corn cobs	48.1	37.2	14.7
Grasses	34.2	44.7	21.1
Sugarcane bagasse	42.7	33.1	24.2
Rice husks	43.8	31.6	24.6
Wheat straw	44.5	33.2	22.3
Eucalyptus	52.7	15.4	31.9

1.3 Chemical Analysis and Its Application in Biomass Study

Chemical analysis, in a general way, can be considered as the use of concepts of analytical chemistry and its technical and analytical methods in the research and actual troubleshooting of varying complexity in different scientific and technological fields. Chemical analysis can generate both qualitative and quantitative information. Techniques and analytical methods provide support for the implementation of regulatory legislation and the market environment, such as the carbon credit market in order to ensure the quality of raw materials and yields of manufacturing processes, while also allowing the development of new products and materials that add value to the biomass. Chemical analyses play an important role in the exploitation of biomass and are supporting technologies for all processing stages of production chains, such as sugarcane, soybean, corn, forestry, pulp and paper, and agribusiness waste, among others.

In the study of biomass and its transformation, or conversion processes, the application of chemical analysis can take place as follows:

- Determining the chemical constitution of various biomass (raw materials), products, by-products, co-products, and wastes
- Monitoring of chemical, biochemical, and thermochemical conversion processes
- Observation of physical and chemical properties and characteristics of biomass and their molecular constituents

Nowadays, there are several possible methodological approaches, as well as a large number of analytical techniques, available and chemical analysis can be applied to all operations in a biomass chain, hence its importance for monitoring and quality control of raw materials, products, processes, and waste.

The analytical techniques used in the quantification of *analytes*—the species of interest for the analysis—are divided into two classes: classical techniques, based on mass, volume, charge, and mol measurement, which provide absolute values; and instrumental techniques, based on relative values, expressed as mg L^{-1}, mg kg^{-1}, μg m^{-3}, and so on.

Until the early 20th century, chemists employed the separation of analytes by techniques such as extraction, precipitation, and distillation. For qualitative analysis, these separated analytes were treated with appropriate reagents to produce compounds that could be identified by properties such as solubility, color, and melting and boiling points. Quantitative analysis was done using simple techniques with good accuracy, which are used to this day, volumetry (volume measurement) and gravimetry (mass measurement); these are typical examples of classical techniques.

Since then, different aspects of the observed classical techniques began to be investigated and several experiments have been carried out aiming to measure analytes from some particular physicochemical property, usually associated with phenomena such as the absorption and emission of radiation, which are the beginning of instrumental techniques, such as atomic spectrometry and molecular spectroscopy.

These findings stimulated the development of a wide variety of instruments that are used in this technical class. The techniques are generally faster than the classical ones and are used in the determination of low concentrations of analyte, such as trace concentrations of ng L^{-1} values or below it.

The following equations express the foundations of these two sets of techniques:

$$A_{S(c)} = kn_{A(c)} \tag{1.1}$$

$$A_{S(c)} = kC_{A(f)} \tag{1.2}$$

Equation 1.1 applies to classical techniques, where $A_{S(c)}$ is the measured signal—or the response—of the analyte, k is the proportionality constant to be standardized, and $n_{A(c)}$ is the number of moles, charge, or mass obtained from the measuring. On the other hand, Equation 1.2 applies to instrumental techniques, where the measured signal $A_{S(i)}$ is also the response of the analyte, k is the proportionality constant to be standardized again, and $C_{A(i)}$ is the relative concentration of the analyte measurement. However, some spectroscopic and microscopic techniques covered in this book do not necessarily obey these two concepts, but mainly report the structural characteristics of the sample.

Table 1.5 lists certain physical properties operated by analytical techniques and promoting the measured response.

The instrumental techniques measure a physical phenomenon resulting from a molecular or atomic property that is qualitatively or quantitatively related to the

Table 1.5 Physical properties used in analytical techniques most commonly used in the chemical analysis of biomass (modified from Skoog et al. 1996)

Properties	Instrumental technique
Absorption of radiation	Spectrophotometry and photometry (ultraviolet and visible) Atomic spectrometry Infrared spectroscopy (near, medium, and far) Nuclear magnetic resonance (solid and liquid states)
Electric current	Voltammetries (cyclic, square wave, anodic, cathodic, polarography)
Diffraction of radiation	X-ray diffraction
Emission of radiation	Emission spectroscopy (X-ray, ultraviolet, and visible) Optical emission spectrometry Fluorescence (X-ray, ultraviolet, and visible)
Mass	Gravimetry
Electrical potential	Potentiometry
Thermal properties	Gravimetric and volumetric Calorimetry Thermal analysis
Ratio mass/charge	Mass spectrometry
Refraction of radiation	Refractometry and interferometry
Electric resistance	Conductimetry

Table 1.6 Some examples of analytical techniques and their uses in the chemical analysis of biomass (modified from Vaz 2014)

Technique	Principle of measurement	Example of use	Advantages	Disadvantages
Differential scanning calorimetry	Enthalpy changes	Determination of combustion properties of biomass (exothermic or endothermic)	Small quantity of sample; high sensitivity; determines physicochemical changes in materials impossible to determine by other techniques	–
Capillary electrophoresis	Migration of ions or charged particles	High-efficiency separation for polar compounds from biomass degradation	High separation efficiency	Limitation for nonpolar compounds
Mass spectrometry	Molecular fragmentation	Structural identification and quantification of several organic compounds based on the m/z ratio	Identification and resolution of complex molecular structures	Necessity of separation techniques, such as chromatography, for a better resolution
X-ray fluorescence spectroscopy	Emission of characteristic X-rays	Multielemental quantification in solid and liquid samples from biomass residues	Easy to handle; nondestructive	Chemical composition and morphology of the sample can affect the result
Infrared spectroscopy (near and medium)	Vibrational energy absorption	Structural identification of organic compounds and lignocellulosic components	Easy to handle, mainly for near-infrared	Low resolution for compounds with same functional groups (sum of bands); however, the application of chemometrics can help to overcome this limitation
X-ray diffractometry	Intensity of X-rays diffracted	Determination of crystallinity and chemical composition of cellulose	Important physical information for natural fiber and polymer usages	Long acquisition time (hours or days) for process control

(continued)

Table 1.6 (continued)

Technique	Principle of measurement	Example of use	Advantages	Disadvantages
Scanning electron microscopy	Surface scanning with a primary electron beam	Surface and structural analysis of materials (e.g., catalysts)	Important physical information for natural fiber and polymer usages	Long acquisition time (hours or days) for process control
Nuclear magnetic resonance (e.g., ^{13}C in solid state)	Transition of nuclear spin inside atomic nuclei; interactions between nuclei–nuclei and nuclei–surrounding electrons	Structural identification of organic compounds from biomass processing (e.g., lignocellulosic and oleaginous)	Resolution of complex molecular structures	Long acquisition time (hours or days) for process control, except under a high concentration of the analyte (e.g., fatty acids)
Voltammetry (e.g., cyclic and square wave)	Changes in current as a function of potential	Chemical speciation and quantification of metals and nonmetals (e.g., catalysts for glycerin use), or verification of glucose or starchy oxidation processes	Rapid response	Search for the better electrolyte or voltammetric technique can expend time

analyte; that is, the physical phenomenon will produce a signal that is directly correlated to the presence or concentration of analyte in the sample. Table 1.6 shows some examples related to the use of instrumental techniques for the analysis of biomass and its products, and Table 1.7 shows analytical techniques widely used in the analyses of the chemical composition of raw materials.

In general, the application of an analytical method for biomass products must follow the steps presented in Fig. 1.8. Any failure or absence of the sequence compromises the reliability of the obtained results.

1.4 Sustainability and Economic Aspects of Analytical Chemistry

Based on the understanding that we should reduce or eliminate negative environmental impacts of processes and products, combined with a social and economic improvement—that is, ensure the *sustainability* of an entire production chain—we

Table 1.7 Examples of analytical techniques widely used in the analysis of the chemical composition of raw materials from biomass (modified from Vaz 2014)

Raw material	Parameter	Analytical technique	Advantages	Disadvantages
Sugarcane for ethanol production	Content of sugars	HPLC refractive index detector	Methods established	Long acquisition time for chromatographic run (approximately 30 min)
Vegetable oils for biodiesel production	Content of fatty acids and esters	GC flame ionization detector	Methods established	Necessity of organic solvent to extract the analyte
Bioenergy crops	Energetic characteristics	Near-infrared spectroscopy	Rapid response and easy to handle	Low band resolution, which can be improved by chemometrics application
Residues for gasification	Energy content	Differential scanning calorimetry	Rapid response and easy to handle	–

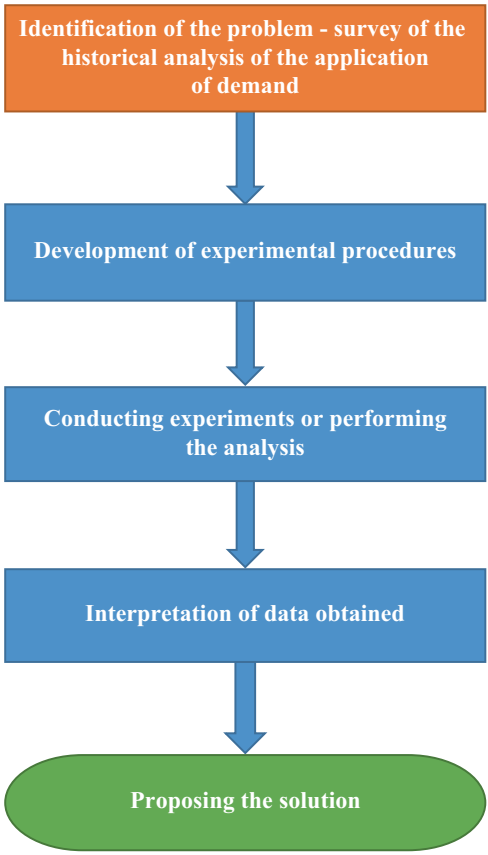

Fig. 1.8 A flowchart describing the steps for the application of an analytical method for biomass

began to consider biomass as a potential source of raw material for energy, chemicals, food, pharmaceuticals, and materials, among others. On the other hand, analytical chemistry has the commitment also to become sustainable in its application, for instance, by means of the use of green chemistry principles and strategies (de la Guardia and Garrigues 2011).

To establish a sustainable method with positive impacts to the environment, society, and economy, we can apply some of the 12 principles of green chemistry (Anastas and Warner 1998):

- Prevent the generation of waste instead of treating it.
- All reagents should be consumed for the formation of product; there should be an atom economy.
- The use of solvents, separation agents, and the like should be unnecessary if possible and innocuous when done.
- Reduce or avoid the formation of derivatives, because this involves the use of additional reagents, which can generate more waste.
- Develop analytical methodologies that can be used for real-time monitoring and control prior to the formation of toxic compounds, in order to contribute to the prevention of pollution.

Furthermore, the analysis of biomass should be, per se, based on the principles of green chemistry, inasmuch as the first use of context is reflected in the sustainability of raw materials.

Finally, the choice of an analytical technique or an analytical method should take into account the following technical and economic aspects:

- The analyte of interest and its physicochemical characteristics (solubility, p*K*a, speciation, etc.): a technical factor that can reduce or increase costs and the final price.
- The analytical matrix to which the analyte is sorbed (water, air, soil, sludge, biological fluid, plant, industrial waste, etc.) and physical state (solid, liquid, or gaseous): a technical factor that can reduce or increase costs and the final price.
- The need to obtain results in the short, medium, or long period of time: a market factor that can reduce or increase the final price.
- Existence of an analytical method developed and/or validated that meets the limits of detection or quantification required by law for the analyte: less effort, faster, and cost reduction.
- Impact generated by the analytical result (e.g., release of a batch of product or monitoring of effluent): as a market factor, reduces or increases the final price.
- The technique robustness, low standard deviation of the results, regardless of condition: parameters of quality control to be taken into account.
- Destructive or nondestructive technique: reduces costs.
- Satisfactory analytical response: of course, without the correct response, will not be viable.
- Cost per analysis: limiting, but not fundamental.

More detailed information about the choice of the technique and/or method can be obtained in the *Handbook of Instrumental Techniques for Analytical Chemistry* (Settle 1997).

It is always important to consider the toxicological and occupational aspects when applying analytical procedures, because chemicals usually offer a potential risk to those who handle them. Therefore, the laboratory team must be aware of implementing safety procedures and, above all, take care to follow them.

1.5 Conclusions

The chemical analysis of biomass is an important branch of analytical chemistry because it can provide information about the constitution of raw materials, products, by-products and co-products, residues, and so on. Analytical techniques can be applied to a whole biomass chain to solve many technical and scientific problems related, but not limited, to the best uses for a biomass, improvement of conversion processes, increase in the quality of products, and control of residues.

Plant biomass is a very complex analytical matrix and it needs cutting-edge techniques to understand its composition and properties, which can be replicated for its products obtained from conversion processes. Furthermore, to explore all the possibilities offered by techniques and methods is desirable for the procedure of sustainable and economic evaluation.

References

Anastas PT, Warner JC (1998) Green chemistry: theory and practice. Oxford University Press, New York, NY

Charles AL, Sriroth K, Huang T-C (2005) Proximate composition, mineral contents, hydrogen cyanide and phytic acid of 5 cassava genotypes. Food Chem 92:615–620

de la Guardia M, Garrigues S (2011) Challenges in green analytical chemistry. RSC Publishing, Cambridge

Faria S, de Oliveira Petkowicz CL, de Morais SAL, Terrones MGH, de Resende MM, de França FP, Cardoso VL (2011) Characterization of xanthan gum produced from sugar cane broth. Carbohydr Polym 86:469–476

Food and Agriculture Organization of the United Nations (UN FAO) (2013) FAO statistical yearbook 2013. FAO, Rome

Gunstone FD (2004) The chemistry of oils and fats: sources, composition, properties and uses. Blackwell, Oxford

Liu Q, Tarn R, Lynch D, Skjodt NM (2007) Physicochemical properties of dry matter and starch from potatoes grown in Canada. Food Chem 105:897–907

Mamma D, Christakopoulos P, Koullas D, Kekos D, Macris BJ, Koukios E (1995) An alternative approach to the bioconversion of sweet sorghum carbohydrates to ethanol. Biomass Bioenergy 8:99–103

Sandhu KS, Singh N, Malhi NS (2007) Some properties of corn grains and their flours I: physicochemical, functional and chapati-making properties of flours. Food Chem 101:938–946

Settle FA (1997) Handbook of instrumental techniques for analytical chemistry. Prentice Hall, Upper Saddle River
Skoog DA, West DM, Holler FJ (1996) Fundamentals of analytical chemistry. Saunders College, New York, NY
Vassilev SV, Baxter D, Andersen LK, Vassileva CG, Morgan TJ (2012) An overview of the organic and inorganic phase composition of biomass. Fuel 94:1–33
Vaz S Jr (2014) Analytical techniques for the chemical analysis of plant biomass and biomass products. Anal Methods 6:8094–8105
Vaz S Jr (2015) An analytical chemist's view of lignocellulosic biomass. BioResources 10:3815–3817

Chapter 2
Qualitative and Quantitative Analysis of Lignins from Different Sources and Isolation Methods for an Application as a Biobased Chemical Resource and Polymeric Material

Basma El Khaldi-Hansen, Margit Schulze, and Birgit Kamm

Abstract Lignins in general have been extensively studied, though the relation between source, isolation method and application is rarely described. In the present work, lignin from different sources (wheat straw and beech wood) and isolation methods (steam explosion, Organosolv) has been characterized regarding their application as a chemical resource and polymeric material. A range of analytical methods were applied including elemental analysis, FT-IR, ^{31}P NMR, SEC, Py-GC-MS and HPLC to gain information about establish the purity, structure, molecular weight, thermal behavior and to determine carbohydrate residues according to the NREL protocol. TGA and DSC were used to study the thermal behavior of the isolated lignins and showed relatively low glass transition temperatures around 120 °C and decomposition temperatures between 340 and 380 °C. NREL analysis presented a carbohydrate-free lignin fraction derived from beech wood via Organosolv process which has not been achieved to date. The finding of this work supports Organolsolv as an efficient method to isolate pure lignin fractions from beech wood with practical value in industry, in particular for application in polyurethanes and phenolic resins.

Keywords Lignin • Organosolv process • Beech wood • Analytics • Chemical resource • Biobased polymeric material

---

Dedicated to Michael Kamm, Founder of biorefinery.de GmbH.

B. El Khaldi-Hansen • B. Kamm (✉)
Research Institute Bioactive Polymer Systems and BTU Cottbus,
Kantstraße 55, 14513 Berlin-Teltow, Germany
e-mail: kamm@biopos.de

M. Schulze
Department of Natural Sciences, Bonn-Rhein-Sieg University of Applied Sciences,
von-Liebig-Str. 20, 53359 Rheinbach, Germany

S. Vaz Jr. (ed.), *Analytical Techniques and Methods for Biomass*,
DOI 10.1007/978-3-319-41414-0_2

2.1 Introduction and Research Question

The application and use of renewable raw materials for the production of base and fine chemicals is becoming increasingly significant. Although the petroleum prices plunged in 2014, the more significant need is to reduce the vast CO_2 emissions which are responsible for global warming (Hoglund 2015). The use and/or processing of fossil-based raw materials must be reduced. This can only happen by substituting fossil fuels with alternative energy sources such as rapeseed oil, bioethanol or wind energy. Another means of reducing CO_2 emissions is the production of energy and of base and fine chemicals from renewable raw materials such as biomass that contains lignocellulose (Kamm et al. 2006) Obtaining chemicals used industrially from renewable raw materials would lessen dependency on crude oil. Interest in researching lignocellulose-containing biomass has greatly increased in the last decade, since it definitely has potential as a source of raw materials for base chemicals. In Western Europe, approx. 40.5 million metric tons of ethylene and propylene are required every year. Today, the global production of base and fine chemicals including polymers is at more than 500 million metric tons (VdCI 2004). This illustrates the major requirement in quantity terms for renewable raw materials.

Worldwide, nature offers us approx. 170 billion metric tons of plant biomass annually, but currently only approx. 3 % ($1.8–2 \times 10^{11}$ t) of this is used worldwide in production annually in the "non-food" sector as, among other things, fuels (methanol, heating oil, biodiesel), bio-based chemicals (phenols, furfurals, fatty acids) and biopolymers (in paints, varnishes, cleaning agents, additives) (RBACAS 2004; Froböse 2004).

The principle of sustainability was introduced in 1992 in the Rio Declaration and Agenda 21 at the United Nations Conference on Environment and Development (R.o.t.U.N.C.o.E.a. 1992). For the implementation of sustainable development, the American chemical industry, for example, decided upon the Vision 2020 programme which described recommendations for attaining specific sustainability goals. One recommendation alludes to the use of renewable raw materials as a source of chemicals, specifically cellulose and carbohydrates (TUCI 1992).

The EU, too, is aiming to obtain 30 % of chemicals sustainably from renewable raw materials by 2025 (ETPSC 2005). One possible approach for achieving this is the construction of lignocellulose biorefineries (Kamm et al. 2007). Figure 1.1 shows the schematic structure and the product tree of a lignocellulose biorefinery. Lignocellulose-containing biomass contains cellulose (40–50 %), lignin (16–33 %), hemicelluloses (15–30 %) and extractive constituents (1–10 %). Cellulose is an unbranched glucose polymer which, by virtue of the linked structure of the linear β-1,4-glycosidic bonds, forms microfibrils which bundle to form crystalline macrofibrils (Krässig 1993). These fibrils link up with one another through hemicelluloses, which produces the "backbone" of plant cell walls (Jayme and Hunger 1957).

Hemicellulose is an amorphous, branched heteropolymer. This association of cellulose and hemicellulose is surrounded by lignin, a three-dimensional network of phenylpropane units (Fengel and Wegener 1989). Lignin constitutes approx. 20 % of terrestrial biomass and is therefore quantitatively the second largest organic material (Blazei 1979). Currently it is still primarily used as a fuel, but structurally has major

potential for replacing fossil-based sources of carbon (Tomani and Axegard 2011). The US Department of Energy estimates that approx. 1.3 billion metric tons of biomass are available in the USA alone for use in biorefineries (Perlack and Wright 2005). The utilization of these quantities in turn generates approx. 225 million metric tons of lignin, which is then available for further use. Assuming that 20 % of this biorefinery lignin (approx. 45 million metric tons) was used for processing into BTX chemicals and hydrocarbons, this would mean a substitution of approx. 10 % of fossil-based with bio-based base chemicals (Holladay et al. 2007). Translating crude oil refinery systems to biorefineries requires the complete separation of the biomass into its precursors, carbohydrates, lignin, proteins and fats.

Figure 2.1 shows, in diagram form, a lignocellulose feedstock (LCF) biorefinery and the resulting products. Promising, among other things, is the extraction of furfural, which is used as a starting material for the production of nylon-6 and nylon-6,6 and also the manufacture of (bio)ethanol by means of hydrolysis reactions (Kamm and Kamm 2007). Current utilization of the lignin polymer is aimed at its use as a fuel or adhesive or filler. This utilization is not satisfactory, since the structure of lignin has monoaromatic compounds which, viewed on their own, constitute an important foundation for the production of base chemicals (e.g. phenols) (Ringpfeil 2002). It is known that the lignin structure varies depending on the plant source, but above all is altered by the particular digestion process. Currently, 60 million metric tons of lignin accumulate per year as a

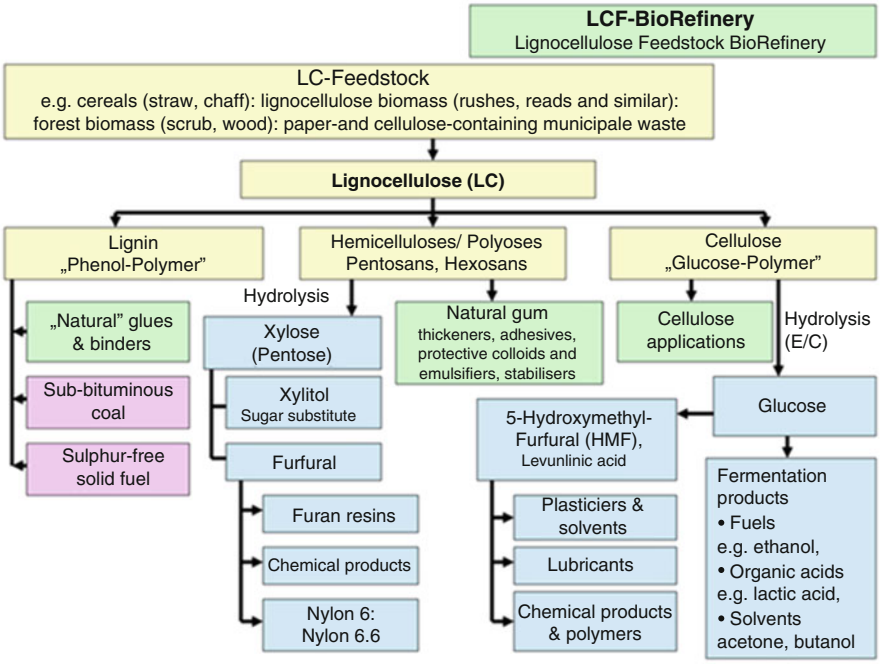

Fig. 2.1 Diagram of a LCF biorefinery (Kamm et al. 2006)

by-product in the waste lyes from the cellulose industries (Lora 2010). Enhancing the value of this accumulating lignin is desirable. Although research has been taking place into lignins for over 100 years, detailed characterization of the heterogeneous lignin structure still constitutes a major challenge.

2.2 The Understanding of the Lignin Structure

Today, lignin accumulates in significant quantities as a by-product and has major structural potential for generating platform chemicals. A prerequisite for material utilization is detailed and comprehensive knowledge of the structure and properties of the corresponding lignins. The following results show investigated lignins from beech wood, isolated by different conditions during Organosolv process. Analytical processes are used which provide a very comprehensive picture of the isolated fractions. The results should enable an estimation as to which method combining the source quality is suitable for the material utilization of lignin. The characterization of the lignin fractions comprises purity analyses in accordance with the NREL protocol, chromatographic (pyrolysis-GC/MS, GPC), thermal (TGA, DSC), spectroscopic (UV–Vis, FT-IR, ^{31}P-NMR) and additional methods, including the testing of solubility behaviour, water content and elementary analyses.

The results constitute a basis for making lignin marketable. The main focus here is on its use as a source of raw materials for the generation of base chemicals, comparable to the products which at the moment are still produced by the petroleum industry. The focus of the decomposition products lies primarily on the generation of phenolic products. The results shall also be considered in relation to use as a polymeric material. Knowledge of the thermal behaviour in particular is necessary for this.

The objective of the chapter is to produce instructions concerning steps and/or analytical methods to be carried out, firstly in the case of use as a raw material, secondly as a polymeric material as you can see in Fig. 2.2. A generally applicable protocol is to be derived for this.

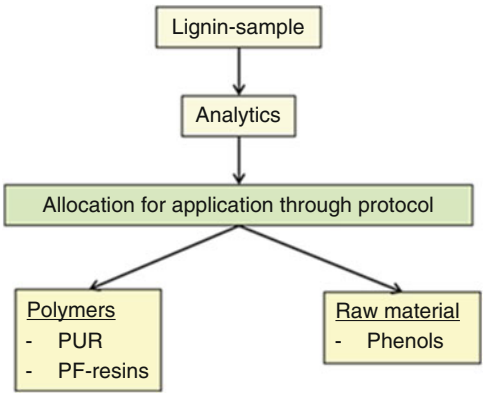

Fig. 2.2 Work scheme

2.3 Current Level of Research

2.3.1 Lignin

Lignin is by definition a polymeric natural product which is generated through enzymatically initiated dehydration polymerization of three primary precursors: *p*-coumaryl, coniferyl and sinapyl alcohol (Lai and Sarkanen 1971; Bunzel and Steinhart 2003; Bunzel et al. 2005). These monomer units, also called main monolignols, are divided into **g**uaiacyl, **s**yringyl and *p*-**h**ydroxylbenzaldehyde types. The monomeric building blocks of lignin are derived from the *p*-hydroxycinnamyl alcohols (Nimz et al. 1981). Figure 2.3 shows the chemical relationship of the *p*-hydroxycinnamyl alcohols generated from biosynthesis to the monolignols. Lignins from conifers (gymnosperms) differ from lignins from deciduous trees and shrubs (dicotyledons) and grasses in respect of the ratio of these three phenylpropane units and are differentiated accordingly into: guaiacyl lignins (G lignins), guaiacyl-syringyl lignins (GS lignins) and guaiacyl-syringyl-*p*-hydroxybenzaldehyde lignins (GSH lignins). Lignins from conifers have a G/S/H ratio of 90/2/8; here, coniferyl alcohol is the predominant monomeric subunit. These lignins belong to the G lignins. Lignins from deciduous trees and shrubs are classed among the GS lignins. Unlike with the gymnosperms, more sinapyl alcohols units are introduced during polymerization. The monomer composition in the lignins of the monocotyledons likewise differs from the other categories; they have an increased proportion of *p*-**h**ydroxylbenzaldehyde (H units) (30 % and over) (Adler 1977).

These monomeric subunits are phenylpropanoids, i.e. phenols with a propenol group in the *para* position. In nature, the macromolecular structure of the lignin is generated from the oxidation of the *p*-hydroxycinnamyl alcohols to phenoxy radicals (Freudenberg 1965). Through the dehydrogenation of the alcohols, the phenoxy radicals are produced; these are present in five mesomeric formulae illustrated in Fig. 2.4 using the example of coniferyl alcohol.

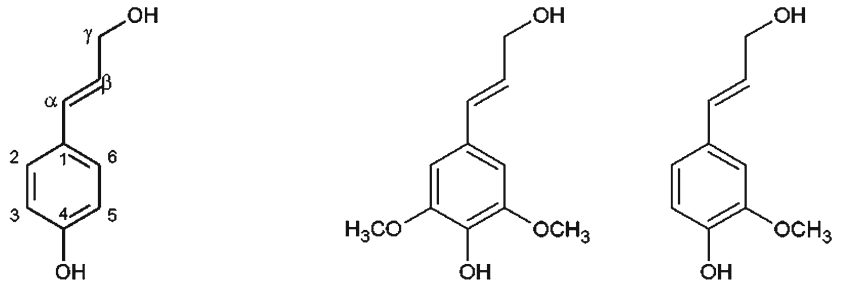

Fig. 2.3 Monomeric units of the lignin structure

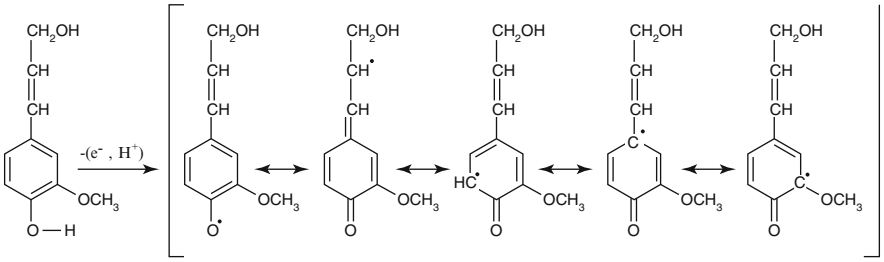

Fig. 2.4 Mesomeric formulae of the phenoxy radical

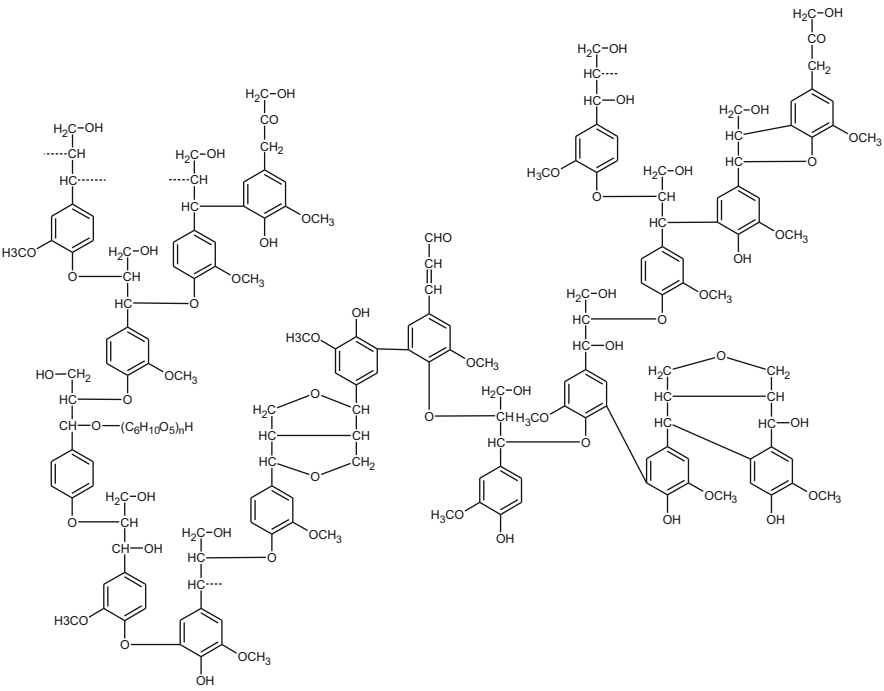

Fig. 2.5 Lignin structure referring to Freudenberg and Neish (1968)

Figure 2.5 shows the structure of lignin which was postulated by Freudenberg (Freudenberg and Neish 1968). The most frequently occurring bonds are aryl ether linkages (α-O-4 and β-O-4); they occur, with a frequency of approx. 50–65 %, as the most important linkages in the lignin structures (Glasser 1980). Lignins from deciduous wood have, as a result of the high proportion of aryl ether bonds, only a few free phenolic hydroxyl groups. The S units also form β-O-4 bonds more frequently than G units. In spruce lignin hardly any S units

occur; consequently the proportion of β-O-4 bonds is significantly lower. Alongside these ether bonds, one also encounters C-C linkages in the lignin structure such as the β-1 bond which occurs in beech lignin at 15 % and leads to 1,2-diaryl compounds. Glasser and Adler were able to show that spruce lignins contain 10 % β-5, 5-5 and α-β bonds (Nimz 1974; Glasser 1981).

2.3.2 Recovery of Lignin

The chemical pulping processes provide every year about 70 million tons of lignin (Römpp 1995). The various industrial processes serve as the selective isolation of cellulose from the cell wall matrices. Lignin is produced as a by-product. The macromolecular structure of lignin is fragmented with cleavage of α-O-4 and β-O-4-bonds.

Digestions in aqueous media require insertion of hydrophilic sulphuric or sulphonic acid groups at the decomposed lignin products to enhance their solubility. These hydrophilization steps do not apply to processes employing organic solvents. The most important method is the sulphate digestion (kraft cooking) with about 76 % share (Sjöström 1981), followed by the sulphite process with about 8 % (Ullman's Enzyklopädie 1979).

The search for alternative methods is becoming more important as the processes mentioned are very harmful to the environment. There are a number of alternative special pulping processes; they are primarily aimed at the production of high-quality pulps (about 16 % share).

2.3.2.1 Organosolv Process

The Organosolv process is as a pulping process with a use of organic solvents to improve lignin solubility (Alcell process: ethanol/water mixtures (Nimz 1986)).

The solvent (or solvent mixture) must be able to dissolve the lignin completely and should have a low boiling point, so that a slight recovery is possible.

Due to the improved solubility a hydrophilization of the lignin in contrast to sulphite processes are not necessary. El Hage (2009) were able to show that in this process preferably β-O-4 bonds are cleaved. Advantages of this method are the sulphur-free treatment and hemicellulose-free products. A disadvantage is that during the cooking process a lot of phenolic and aliphatic hydroxyl groups are etherified, which impedes a subsequent application as a component for polycondensation processes. Another drawback is that not all types of wood can be pulped, including woods with high syringyl content due to the blocking of ortho positions. Preference should be given grasses with high *p*-hydroxybenzaldehyde units.

2.3.2.2 Steam Explosion

This procedure is one of the pretreatments of wood species for the enzymatic hydrolysis (Lindorfer et al. 2010). To be treated, shredded material is pulped with saturated steam under pressure and subsequent relaxation. By steaming the lignocellulose structure is digested, the hemicellulose hydrolyzed and lignin depolymerized. The process temperature is about 200 °C. Pretreatment proceeds without catalyst, only an addition of acid is enough to release the monomeric sugars of the hemicellulose. After washing with distilled water and subsequent precipitation by addition of sodium hydroxide solution, the lignin may be recovered in pure form. Li et al. (2009) showed that under the steam explosion mainly β-O-4 bonds are cleaved. In addition, a high percentage of phenolic OH groups could be detected.

2.3.3 Use of Lignins

Lignin is a versatile product that can be used for lots of different applications. The possibilities and challenges relating specifically to biorefinery lignins have been described in a detailed study by Holladay et al. (2007). This shows the diversity of lignin for potential applications, which are subdivided into three groups:

1. Energy, fuel, synthesis gas.
2. Macromolecules.
3. Aromatic compounds.

In group 1, the lignin is used as a source of carbon for energy production and/or for reprocessing as a synthesis gas. The second group makes use of the natural macromolecular structure of the lignin. The lignin can be used in major application areas such as binders, carbon fibres or polyurethane foams. The third group requires technologies for the degradation of the macromolecular structure to obtain monomeric units while retaining the aromatic structure. This is a prerequisite for the production of the polymer building blocks benzene, toluene and xylene (BTX), phenols and vanillin.

Table 2.1 shows areas of research concerning the use of lignins. It is noticeable that until now, prior characterization of the lignin fractions has not always been carried out; industrially accumulating fractions are used among other things for the manufacture of epoxy and phenol formaldehyde resins. One focuses on the differences in the finished polymer product and observes the mechanical properties such as strength and notched impact strength. Khan et al. (2004) investigated bagasse lignins for use as adhesives following characterization carried out during FT-IR and/or UV spectroscopy and thermal analyses. It should be noted that the results of the end products in the case of the studies by Wang et al. (1992) show that polymers with improved mechanical properties can be obtained if phenol is substituted with lignin. A prerequisite for use in resins is good solubility and the associated optimum distribution in an unhardened resin system. Cazacu et al.

Table 2.1 Use of lignins

Source/pulping process	Use	Lignin analytics	Tested parameters final product	Comment	Literature
Lignin (bagasse)	Wood adhesive	IR UV DSC TGA CHN	Adhesive strength IS 851-1978, shearing behavior ASTM D 2339-94A, IR, Tg	Comparable stability regarding commercial resins when substitution of phenol through lignin (50 %), structure of lignin resins similar to the commercial resins	Khan et al. (2004)
Kraft (hardwood)	Epoxide resins	IR NMR TGA solubility	Strength (E-Modul), impact strength	Improved mechanical properties at good solubility in uncured resin system	Wang et al. (1992)
Lignosulphonate	Polyolefins (blend polymers)	CHN solubility	DSC, TGA, IR, breaking elongation	Improved mechanical properties	Cazacu et al. (2004)
Lignosulphonate	Phenol formaldehyde resins	No	Viscosity Curing time	Higher viscosities and curing times	Peng and Riedl (1994)
Lignosulphonates (from softwood), Kraft	Vanillin	UV IR NMR	–	–	Araújo et al. (2010)
Organosolv	Phenol formaldehyde resins	No	Strength, curing time, density	Improved curing time, unchanged density compared to commercial resins	Cetin and Özmen (2002)
Organosolv	Epoxide resins	No	Glass transition, dielectrical constant	Higher glass transition temp., unchanged dielectric constant	Kosbar et al. (2001)
Organosolv/Kraft	Carbon fibre	1H-NMR DSC TGA SEM	Strength	Unchanged strength	Kadla et al. (2002)

(2004) were also able to show similar results. Here, lignosulphonates were used as a blend material. Beforehand attention was, here too, devoted chiefly to the solubility. The end product exhibits improved mechanical properties (here, elongation at break was tested). In the USA there are already several patented phenolic resin systems on the basis of lignin. Here the attempt was made to substitute lignins for phenols. Peng and Riedl (1994) found that using up to 40 % w/w lignosulphonates, the hardening times increase *vis-à-vis* conventional phenol formaldehyde systems and the viscosities increase with a greater lignin proportion. The main field of use of lignin-based phenolic resins is the glueing of chipboard; polyurethane-lignin systems are also a possible option for this application. Another research field which is not mentioned in the list below is the field of lignin-polyurethane chemistry, research groups led by Feldman (Feldman 1994; Feldman and Lacasse 1989; Feldman and Lacasse 1994; Feldman et al. 1988; Glasser et al. 1982; Toffey and Glasser 1997; Kelley et al. 1988, 1989a, b; Saraf et al. 1985) and Hirose and Hatakeyama (Hirose et al. 1989; Yoshida et al. 1990) have carried out many investigations. By Hatakeyama, polyurethanes were synthesized from a kraft lignin and different polyethylene glycols using up to 40 % w/w lignin. The end products were soft-elastic to hard.

Polyurethane systems with up to 20 % w/w kraft lignin were investigated by Feldman. The rigidity values increased with higher lignin content. The materials had the best mechanical properties at a lignin content of 5 % w/w (Reimann et al. 1990).

Use is made mainly of lignosulphonates for application in industrial products. Owing to their viscosity behaviour, lignosulphonates have high cohesive force and adhesive power Windeisen and Wegener 2012). By occupying with hydrophilic sulphonic acid groups, the solubility of the native lignin changes considerably. Today, up to 200,000 metric tons of lignosulphonates are sold annually as a cement additive. They contribute to the deagglomeration of the cement particles and liquefy the mortar by reducing the viscosity. In the petroleum industry, too, lignosulphonates are used as flow improvers for water–oil emulsions (Booregard Lignotech 2015). The use of technical lignins permits significantly lower water quantities and facilitates the recovery of drilling water.

2.3.4 Lignin Analytics

Lignins from a variety of plant sources and digestion processes are often characterized in wood and lignin research. Admittedly, the analysis is frequently aimed at the direct application. One example of this is the research field of Methacanon et al. (2010); here, kraft lignins were investigated in relation to their direct use in phenol formaldehyde resins (PF resins). The techniques employed were IR spectroscopy, GPC, TGA and DSC. Mansouri et al. (2006), in addition to investigating kraft lignins, also investigated lignosulphonates and organosolv lignins. Here, too, the investigation aimed at the use of lignins in PF resins. Alongside the analysis of the proportions of sugar and ash, GPC was used for the

determination of the molecular weight, and ^{1}H-NMR to investigate the bond types in the lignin. The focus of characterization is on the detection of the hydroxyl groups. Here is a priority list of the features that lignins ought to have for use in PF resins: (1) Presence of phenolic hydroxyl groups, (2) Presence of aliphatic hydroxyl groups, (3) Structures that can form quinone methide intermediates, (4) Non-substituted 3- or 5-positions on phenolic C_9 units, (5) Low molar masses (M_w).

In recent years a number of different lignins have been analyzed from various pulping processes and were characterized. Focus of this work is the development of a reliable, reproducible procedure for lignin characterization and the adaptation of established methods on the lignins from the applied isolation methods. Among the most important parameters to be determined are the molecular weight (M_w and M_n) and its distribution (MWD), as well as the thermal behavior, in particular the glass transition temperature (T_g). These parameters affect the later processing in a significant way. The melting behavior is important for the technical processing and application. The melting range and the glass transition temperature are dependent on the type of pulping conditions and the content of impurities or the (remaining) water content of the sample.

The analytical methods can be divided into two categories: the analysis of the chemical structure of lignin and the characterization of its physico-chemical properties, see Fig. 2.6.

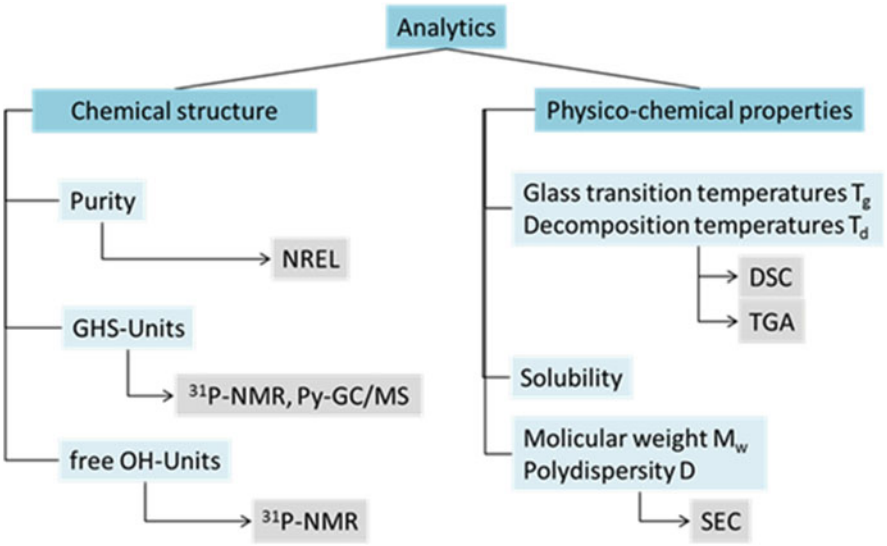

Fig. 2.6 Analytical methods of lignin fractions

2.3.5 *Prerequisites for Lignin Properties from Literature Values, for Use in Polyurethanes (Thermoplastic/ Thermosetting)*

For the purpose of the approach of this chapter described above, a specific use is to be derived for the lignin-containing samples investigated using detailed characterizing analyses. Use as a polymeric material is made more specific in the form of thermoplastic and thermosetting polyurethanes and phenolic resins. The extraction of phenols from the lignins considered is contemplated as a second important use. Current applications have been researched for this specific data. In the case of thermoplastic polyurethane, Alcell lignin was successfully processed into thermoplastic polyurethanes at a level of up to 65 % w/w by Saito et al. Here, lignin is considered the "hard segment", which significantly influences the mechanical strength. The polybutadiene is hence the "soft segment" component and responsible for the rubber-like property in the polymer overall. For this, the lignin must initially be pretreated with formaldehyde in order to keep the molecular weight and the glass transition temperature controllable. In this specific example, the setting of the molecular weight M_w at over 800,000 g mol^{-1} and a glass transition temperature of T_g: 150 °C were ideal for the resulting mechanical properties. The DSC analyses of the finished polymer showed a two-phase morphology as is typical of thermoplastic copolymers (Saito et al. 2013).

Glasser and Leitheiser (1984) were able to produce polyether adducts following a reaction of lignin with epoxides. This reaction is initiated by a base attacking the phenolic hydroxyl groups of the lignin, so that phenoxides are generated. Through the alkoxylation of the lignin, physical properties of the molecule change: the glass transition temperature is lowered. This results in a low viscosity in all temperature ranges. The alkoxylation reaction is a very important step for the manufacture of thermosetting polyurethanes with isocyanates. The modification of the lignin delivers primary alcohols which are chemically more reactive than phenolic hydroxyl groups. In addition, through the necessary lowering of the glass transition temperature the lignin becomes liquid at relatively low temperatures. A reaction condition for the polymerization to polyurethanes is the use of liquid reactants at temperatures around 60 °C. The lignin modified through the alkoxylation consequently constitutes the liquid polyol component of the reaction, which can be processed using injection moulding. If one now observes the structure of the lignin, it becomes clear that such alkoxylation reactions can only take place sterically unimpeded, hence the reaction is more successful if the basic structure of the isolated lignin has few syringyl units.

2.3.6 *Prerequisites for Lignin Properties from Literature Values, for Use in PF Resins*

If the lignin is considered for possible use as a phenol substitute in phenol formaldehyde resins, the lignin batch must contain certain physical and chemical properties. The main use of lignin-based PF resins is currently the glueing of chipboards. With this application, the phenol component is substituted completely or partially with lignin. In order to achieve comparable quality in the end product, the raw material used must be free from accompanying substances. Fliedner and van Herwijnen (2011) were able to substitute 30 % of the phenol quantity through the use of lignin as a component. The resulting resins were tested on the basis of their mechanical properties using standard methods (DIN EN 319, DIN EN 312, DIN EN 314, DIN EN 310). The results compare well with the conventionally manufactured PF resins. Here too, the reaction with formaldehyde requires a lignin structure where H/G units dominate. Syringyl units act as a steric hindrance. Tejado et al. (2007) were able to achieve good results for the manufacture of lignin-based PF resins, with lignin input values with molecular weights up to 8000 g mol^{-1} and glass transition temperatures of up to 150 °C and decomposition temperatures of between 300 and 400 °C. The physico-chemical requirements on lignins of this study are summarized in Table 2.2.

2.4 Analytical Data

Investigated lignins:

The investigated Organosolv lignin fractions are products from a biorefinery pilot plant in Leuna, Germany using beech wood as the feedstock material. The pulping process parameters for OBL_1 are a 50/50 ethanol/water mixture, a reaction temperature of 170 °C, a reaction time of 120 min and sulphuric acid as a catalyst with 0.94 % w/w. OBL_2 is a result of isolating beech wood with a 50/50 ethanol/water mixture at a temperature of 180 °C and a reaction time of 240 min. The fraction of LigSteam results from an acid steam explosion process using wheat straw as raw material. The applicated process parameters cannot be published.

Table 2.2 Requirements on lignins

Analytics	Lignin for PF resins	Lignin for polyurethanes (thermoplastic)
Solubility	Good solubility in polar-protic organic solvents	Good solubility in polar-protic organic solvents
Ligningehalt [%]	From 90	From 90
M_w [g mol^{-1}]	Between 600 and 8000	Up to 4000
T_d [°C]	>200	>200
T_g [°C]	–	100–150
G/H/S	Dominant G/H-units	Dominant G/H-units

2.4.1 Purity and Fractional Yield of Lignin: LigSteam vs OBL_1 and OBL_2

The results of moisture, ash, elemental sugars, Klason (AIL) and acid-soluble (ASL) lignin contents (w/w %) are summarized in Table 2.3. The results show highly pure lignin fractions for isolated beech wood lignin (91.4-94.0 %). The sugar content is under the quantification limit (<0.1 ppm). The fraction of the isolated wheat straw lignin via steam explosion show less purity with high contents of sugars (<21 %).

In comparison to other studies these results of Organosolv samples are unique. El Mansouri and Salvadó (2006) investigated lignosulphonates, Kraft, soda-anthraquinone, Organosolv and ethanol process lignins for the industrial production of adhesives. The results of these lignins also show high contents of total lignin yield but all considered lignins exhibit carbohydrates contents. Erdocia et al. (2014) studied different Organosolv conditions on olive wood. They used the Acetosolv, Formosolv and a mixture of both processes at a temperature of 130 °C and a reaction time of 90 min. The resulting lignin fractions had contents of Klason lignin between 69.05 and 79.01 % w/w. The sugar contents were between 1.88 and 5.87 w/w %.

2.4.2 Solubility

It is known that lignins have limited solubility in organic solvents due to the heterogeneous three-dimensional molecular structures. Therefore it is essential to find appropriate solvents, especially for detailed structural analysis using spectroscopic or chromatographic methods. Lignins are generally insoluble in water and

Table 2.3 Analysis of moisture, ash, lignin and carbohydrates

	OBL_1 [% w/w on dry matter]	OBL_2 [% w/w on dry matter]	LigSteam [% w/w on dry matter]
Moisture content	3.48	3.81	4.92
Ash content	0.22	0.47	16.95
Total lignin[a]	94.32	91.71	51.95
Klason lignin (AIL)	92.71	87.77	51.75
Acid-soluble lignin (ASL)	1.61	3.95	0.2
Carbohydrate	NF[b]	NF	21.14
Carbohydrate composition			
Glucose	NF	NF	17.68
Arabinose	NF	NF	3.46
Galactose	NF	NF	NF
Mannose	NF	NF	NF

[a]*AIL* acid insoluble lignin, *ASL* acid soluble lignin

[b]*NF* not found

most of the organic solvents, with the exception of Organosolv-processed lignins which show a higher solubility in organic solvents than industrial lignins. In this study, the solubility of OBL and LigSteam was examined in a variety of nonpolar to polar solvents and corresponding mixtures (Table 2.4) as classified by Reichardt (2010). The solvents are mainly divided in terms of their polarity and protic behaviour. Organosolv lignin and LigSteam lignin show insolubilities in water.

OBL_1 and OBL_2 fractions show good solubility in protic polar solvents such as methanol and ethanol and aprotic polar solvents like acetonitrile and acetone. The highest solubilites for these fractions were observed in dioxane, tetrahydrofuran and pyridine which belong to the classes of aprotic apolar, protic polar and aprotic dipolar solvents, respectively.

In general, there are few studies on solubility characteristics of lignins.

Cybulska et al. (2012) investigated the solubility of Organosolv lignins derived from cord grass, switch grass and corn stover in DMSO, dioxane, methanol, ethanol, ethyl acetate and methyl isobutyl ketone MIBK. The results show best solubility values in methanol as protic polar solvent and dioxane as aprotic apolar solvent and rather poor solubility in DMSO, ethyl acetate and MIBK as aprotic polar solvents in particular for cord grass lignin. Lignin from steam explosion processes show slightly solubility in all applied solvents. This is due to the less purity and the high contents of sugars. Modification methods are required (e.g. acetylation) to enhance the solubility in organic matters.

2.4.3 Physico-chemical Characteristics of Organosolv Derived Lignin

2.4.3.1 Fourier Transform Infrared (FT-IR) Spectroscopy

FTIR-spectra of Organosolv lignins and LigSteam lignin are given in Fig. 2.7; the corresponding assignments and references are summarized in Table 2.5. According to former studies, the network of hardwood lignin like beech wood is mainly composed by GS units. Wheat straw lignin is composed by GHS units.

Table 2.4 Solubility behaviour of OBL and LigSteam

Solvent[a]	Classification[b]	OBL_1 [% w/w]	OBL_2 [% w/w]	LigSteam [% w/w]
Water	HBSA	25	27	27
Methanol	HB	72	73	50
Ethanol	HB	60	60	50
Tetrahydrofuran	HB	96	97	46
Pyridine	AHD	97	98	45
Acetone	AD	71	73	30
Acetonitrile	AD	58	60	34
Dioxane	EPD	97	98	40

[a] $C_{M\%} = 2$; $T = 25$ °C in ultrasonic bath for 30 min

[b] Classification according to Reichardt [12] *HBSA* hydrogen bonding, strongly associated, *HB* hydrogen bonding, *AHD* aprotic, highly dipolar, *AD* aprotic, dipolar, *EPD* electron pair donor

The broad absorption band at 3430 cm^{-1} is assigned to aromatic and aliphatic OH groups, bands at 2940, 2840 and 1460 cm^{-1} are related to C-H vibration of CH_2 and CH_3 groups, absorptions at 1600, 1515 and 1425 cm^{-1} are related to aromatic ring vibrations of the phenyl propane skeleton. The absorption at 1700 cm^{-1} can be attributed to non-conjugated carbonyl groups. Phenolic OH groups are shown by absorption bands at 1330 and 1365 cm^{-1}, whereas the one at 1030 cm^{-1} is related to primary alcohols. Absorptions at 1330, 1220 and 834 cm^{-1} are assigned to the syringyl units, while small shoulders at 1270, 1120 and 1153 cm^{-1} can be attributed to the guaiacyl units. The Organosolv process results in cleavage of the β-O-4-linkages which are mainly present in beech wood lignin generating both phenolic hydroxyl (1365 cm^{-1}) and carbonyl groups (1700 cm^{-1}) (Nimz 1974).

2.4.3.2 ^{31}P NMR Spectroscopy

The lignin samples were first phosphitylated with 2-chloro-4,4,5,5-tetramethyl-1,2,3-dioxaphospholane and analyzed via quantitative ^{31}P NMR spectroscopy (with endo-*N*-hydroxy-5-norbornene-2,3-dicarboximide as internal standard) according to the method described by Granata and Argyropoulos (1995). The obtained spectrum (Fig. 2.8) provides information about the concentration of each hydroxyl group calculated in reference to the hydroxyl content (mmol g^{-1}) of the internal standard.

According to the results obtained from ^{31}P NMR spectra, Organosolv-isolated lignin samples exhibit considerable quantities of G and H units and rather low amounts of S units (see Table 2.6). It shows the presence of aliphatic hydroxyl groups (δ 146–149 ppm, 0.38 mmol g^{-1}), amounts of syringyl units (δ 143–144 ppm, 0.12 mmol g^{-1}), guaiacyl units (δ 142–143 ppm, 0.25 mmol g^{-1}), hydroxyphenyl units (δ 139–140 ppm, 0.27 mmol g^{-1}) and low amounts of carboxylic acid (δ

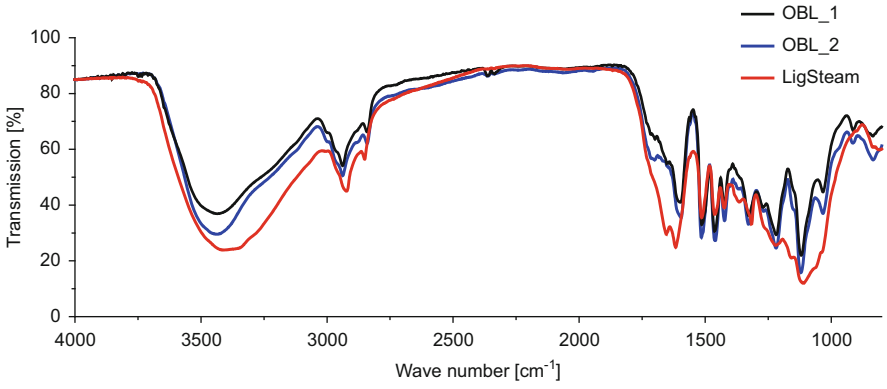

Fig. 2.7 FT-IR spectra Organosolv lignin and LigSteam

Table 2.5 FT-IR bands assignment

Band [cm^{-1}]	Assignment	Vibration[a]
3435	Phenolic OH + aliphatic OH	st O-H
2938	$CH_3 + CH_2$	st C-H
2841	CH_3	st C-H
1699	Non-conjugated C=O	st C=O
1595	Aromatic skeleton (S>G)	st C-C
1514	Aromatic skeleton (S<G)	st C-C
1459	$CH_3 + CH_2$	$\delta_{asymmetric}$C-H
1423	Aromatic skeleton	st C-C
1369	Phenolic OH	δ_{ip} O-H
1327	Aromatic skeleton (S)	st C-O
1268	Guaiacyl unit	st C-O
1218	Phenolic OH	st C-O (H)
1152	Aromatic ether	st C-O-C
1120	Guaiacyl unit	δ_{ip}Ar C-H
1032	First order aliphatic OH	st C-O (H)
970	CH=CH	δ_{op} C-C
914	Aromatic ring	δ_{op} C-H
834	Aromatic ring (S)	δ_{op} C-H

[a]*st* stretching vibration, δ_{ip} in-plane deformation vibration, δ_{op} out-of-plane deformation vibration

135 ppm, 0.02 mmol g^{-1}). The high amount of guaiacyl hydroxyl units in OBL is a consequence of cleavages of β-O-4 linkages. The resulting ratios of monomeric units (H/G/S) were 32/49/19 for OBL_1 and 43/40/17 for OBL_2. The beech wood lignin data obtained by Faix et al. (1987) show monomeric ratios of beech milled wood lignin of 4/56/40. El Hage (2009) investigated Organosolv lignin from Miscanthus and found hydroxyl amounts: aliphatic 1.19 mmol g^{-1}, syringyl 0.13 mmol g^{-1}, guaiacyl 1.33 mmol g^{-1} and hydroxyphenyl 0.61 mmol g^{-1}. Regarding the results of Faix et al. (1987) our beech wood lignins show higher amounts of hydroxyphenyl units arising from Organosolv isolation method cleaving mainly the β-O-4 bonds. The spectra of steam exploded wheat straw lignin LigSteam shows presence of GHS units with 42/13/45. References give a GHS ratio of 49/5/46 (Lapierre 1993). These results were also confirmed by pyrolysis gas chromatography (Fig. 2.9).

2.4.3.3 Thermogravimetric Analysis (TGA)

Thermal analysis of lignins determined their thermal behavior which was based by thermogravimetric analysis (TGA) and differential scanning calorimetry (DSC). The thermograms of Organosolv beech wood lignin and LigSteam (Fig. 2.9) show that the thermal degradation of lignin occurs in a broad temperature range (100–700 °C). This is due to the complex structure of lignin consisting of phenolic hydroxyl,

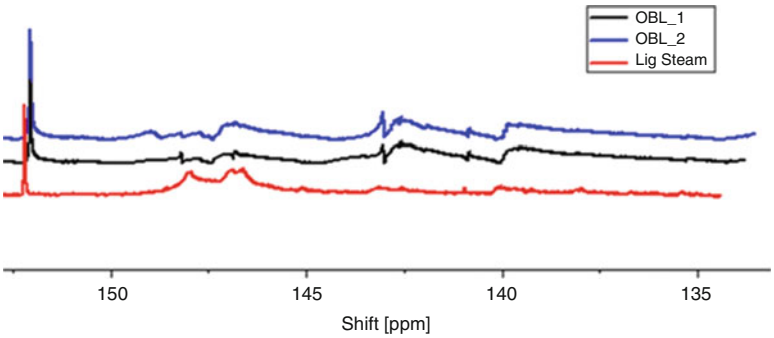

Fig. 2.8 ^{31}P NMR spectra of OBL_1,OBL_2 and LigSteam

Table 2.6 Signal assignment for ^{31}P NMR spectroscopy of OBL and LigSteam

Chemical shift range δ ^{31}P-NMR [ppm]	Assignment	OBL_1 [mmol g^{-1}]	OBL_2 [mmol g^{-1}]	LigSteam
146.5–150	Aliphatic OH	0.50	0.38	2.85
152	e-HNDI (IS)			
143	Syringyl OH	0.14	0.10	0.48
142–143	Guaiacyl OH	0.38	0.24	0.44
139–140	*p*-hydroxyphenyl OH	0.25	0.26	0.14
135	Carboxylic acid	0.02	0.01	0.02

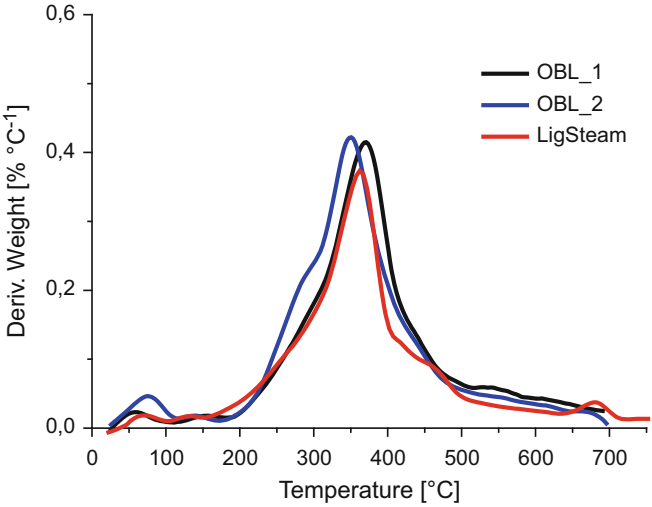

Fig. 2.9 DTG of Organosolv lignins and LigSteam

carbonyl and benzylic hydroxyl functionalities. Several stages of weight-loss can be observed in the TG curves. Initially, the decrease in loss of weight was attributable to moisture present in the lignin sample and to the release of volatile products such as carbon dioxide and carbon monoxide up to 200 °C (Domínguez et al. 2008). According to Wittkowski et al. (1992), the degradation of propanoid side chains of lignin occurs between 230 and 260 °C with formation of methyl, ethyl and vinyl guaiacol derivatives. Aryl ether bonds can be cleaved at temperatures below 310 °C due to their low thermal stability. According to the studies of Nimz, more than 65 % of the monomer units of beech wood lignin are connected by β-O-4 linkages (Nimz 1974). The major degradation occurs between 200 and 600 °C. The first derivative of the TG curves leads to the DTG curve which shows the corresponding rate of weight-loss. The curves are presented in Fig. 2.10 and show maximal values at 381 and 346 °C (DTG_{max}), respectively, with a weight-loss value of 0.4 % $°C^{-1}$. The sample of LigSteam presents a decomposition temperature of 367 °C and a weight-loss 0.37 %. In general, DTG_{max} values vary between 350 and 425 °C for softwood and hardwood lignins (Tejado et al. 2007). The decomposition temperature strongly depends on the molecular structure of lignin. Lignins with high contents of G units exhibit higher molecular weights caused by intermolecular C-C bonds, which have a high stability and are not cleaved during the pulping processes (El-Saied and Nada 1993). Domínguez et al. (2008) investigated the thermal stability of Organosolv lignins from *Eucalyptus* and found average DTG_{max} values of 340 °C. Nitsos et al. (2013) performed a systematic investigation of the hydrothermal pretreatment of beech wood. Amongst other characterizations they used TGA to compare the DTG curves of untreated biomass and samples pretreated by hydrothermal processes. The

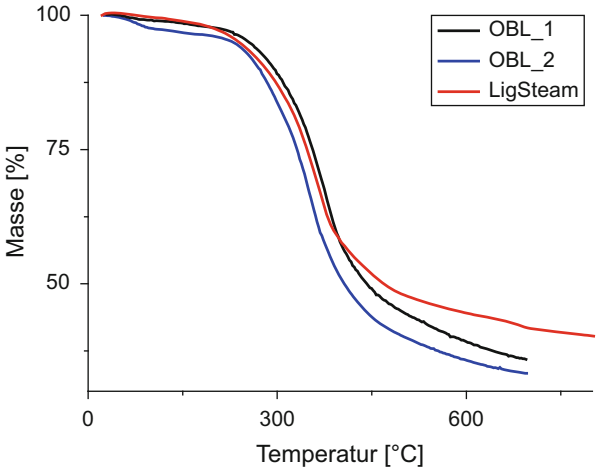

Fig. 2.10 Thermograms of OBL_1, OBL_2 and LigSteam

isolated beech wood lignin shows a DTG_{max} of 375 °C. Monteil-Rivera et al. (2013) performed thermal analysis on wheat straw lignins and flax lignins. They observed degradation temperatures of 375 °C.

2.4.3.4 Differential Scanning Calorimetry (DSC)

DSC is the most common method to determine thermal behavior and glass transition temperatures (T_g) of polymers, also used for various lignins (Glasser 2000). The glass transition is a reversible phenomenon; it is correlated to the viscoelastic behavior of amorphous polymers. At temperatures below the glass transition viscoelastical materials are stiff and glassy. This stiffness decreases in the transition region; a rubber-like elasticity is shown by the material resulting from chain entanglements (Kaelbe 1971; Aklonis et al. 1972). Glass transitions are correlated local rotational or translational flowings of chain-segments of the molecules at increasing temperature. Thermal expansion increases the free volume allowing these motions to take place. Visthal reported glass transitions for Organosolv lignin with T_g value of 97 °C; these studies were performed in order to study lignins as components in polymer blends (Vishtal and Kraslawski 2011). Softwood Kraft lignins show higher T_g values than Organosolv lignins derived from hardwoods (Glasser and Jain 1993). The studied Organosolv beech wood lignin samples also show relative low T_g values of 123 °C (see Figs. 2.11 and 2.12). There are no documented studies on DSC analysis from steam exploded wheat straw samples. LigSteam exhibits a glass transition temperature of 75 °C (see Fig. 2.13). The studies of Sameni et al. (2014) present glass transitions for steam exploded hardwood lignins at temperatures about 149 °C.

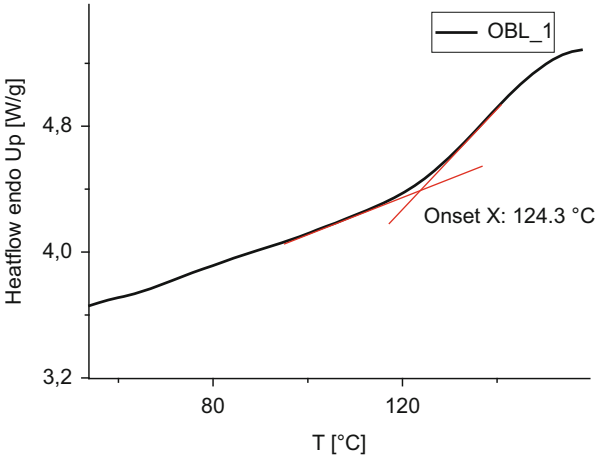

Fig. 2.11 DSC curve of OBL_1

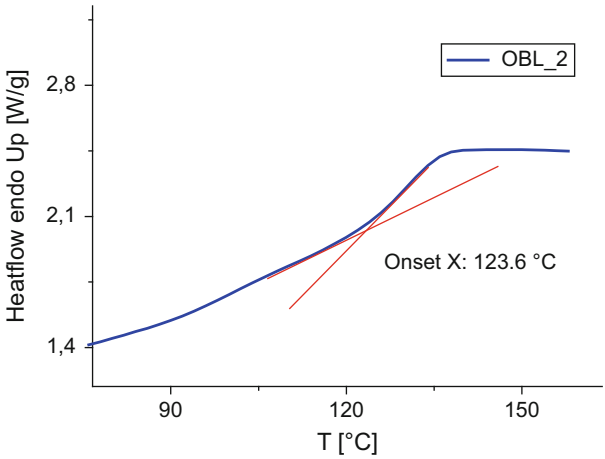

Fig. 2.12 DSC curve of OBL_2

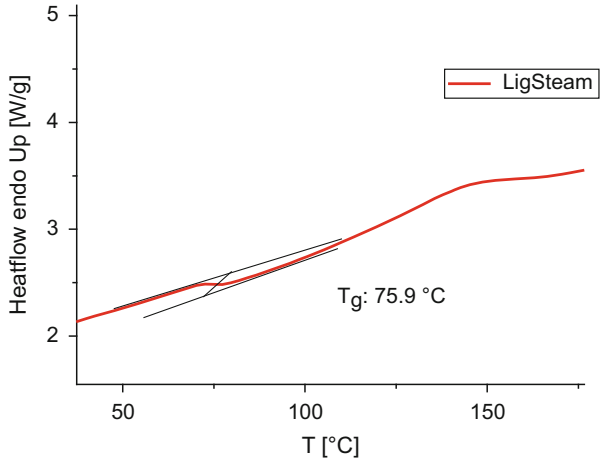

Fig. 2.13 DSC curve of LigSteam

2.4.3.5 Size Exclusion Chromatography (SEC)

The molecular weight and the molecular weight distribution of lignin has been analyzed through THF-eluted SEC. Due to polystyrene calibration standards the obtained data are discussed in comparison to literature studies performed under the same calibration conditions. Tejado et al. (2007) have investigated Kraft softwood lignins, Soda softwood lignins and Organosolv hardwood lignins. Technical Kraft lignins showed a weight average of 8700 g mol^{-1}, Organosolv lignins from hardwood (tamarind) exhibited a molecular weight of 3100 g mol^{-1}. Results of Kim et al. (2013) show molecular weights of 4168 g mol^{-1} for Organosolv-treated poplar wood using an alkaline catalyst.

curve of LigSteam.

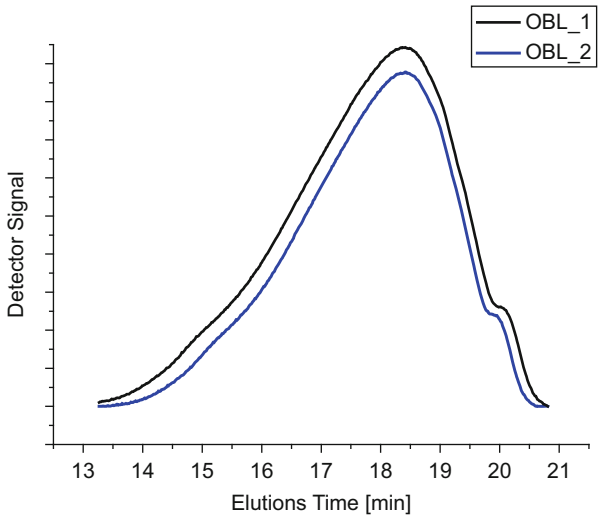

Fig. 2.14 SEC Elugram of OBL_1 and OBL_2

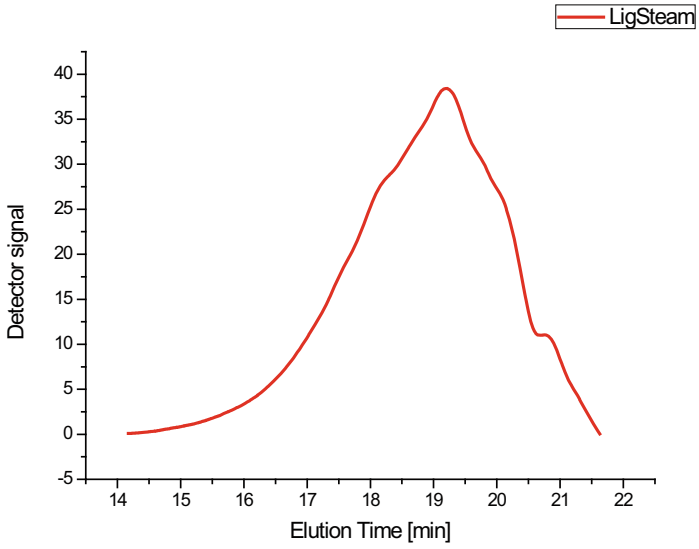

Fig. 2.15 SEC Elugram of LigSteam

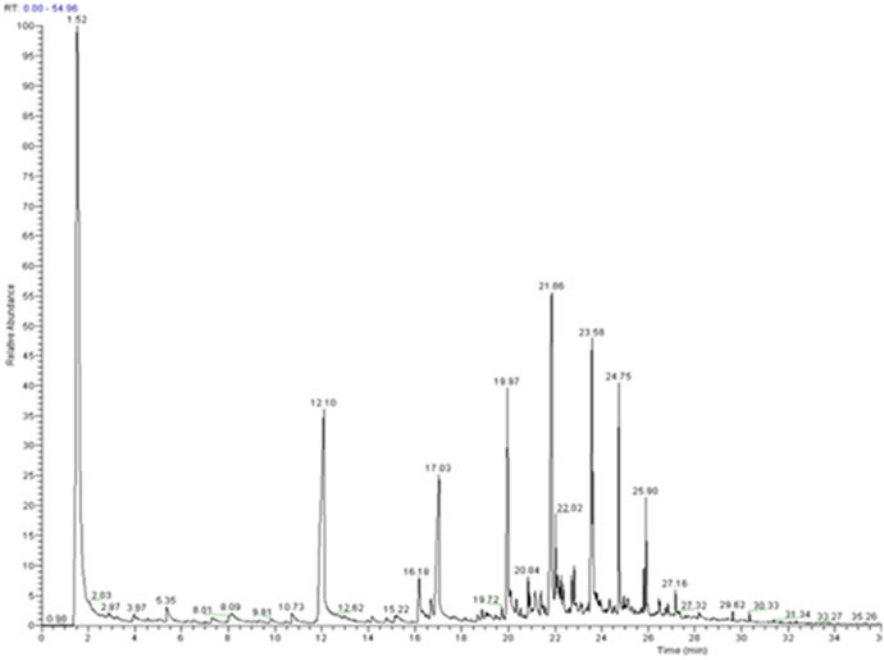

Fig. 2.16 Chromatogram of OBL_1

As confirmed by solubility tests a previous acetylation was necessary for the LigSteam sample. Figure 2.14 shows the chromatogram for the Organosolv-treated and steam-exploded lignin samples. LigSteam show higher molecular weights, this is an indication of less degradation during the process (see Fig. 2.15).

2.4.3.6 Pyrolysis GC/MS

Among the different degradation techniques, pyrolysis in combination with gas chromatography and mass spectrometry detection (Py-GC-MS) allows an online degradation and fragment analysis of the samples. Today, Py-GC-MS is an established technique to determine decomposition characteristics and monomeric contents. Pyrolysis decomposes a sample in the absence of oxygen into molecules of lower mass which can be detected by GC or MS. That results in a pool of fragments, a fingerprint, which is characteristic for each sample. There are basically two methods which are applied in pyrolysis research studies: the continuous mode and the pulse mode. In the continuous mode the sample is placed into a furnace and the temperature is kept fixed during the pyrolysis procedure. The pulse mode requires an introduction of the sample on a cold pyrolysis probe, which is then rapidly heated to the desired pyrolysis temperature (mainly applied: Curie-point pyrolysis). Curie-point pyrolysis of beech milled wood lignin has been investigated by Faix et al. (1987).

Table 2.7 Compounds identified by Py-GC-MS from lignin fragments of OBL_1

Compound	Molecular weight [g mol^{-1}]	Origin
CO_2	44	
2-Methyl 2-cyclopenten-1-one	96	C
2,3-dimethylphenol	96	C
4-ethyl-2-methylphenol	124	H
Phenol	94	H
2-methoxy-4-methylphenol (4-methylguaiacol)	138	G
4-ethyl-2-methoxyphenol	122	H
2,3-dimethoxybenzyl alcohol	138	G
2,3-dimethylhydroquinone	138	G
2-methylphenol	108	H
4-ethylphenol	108	H
4-ethylcatechol	138	H
2,3-dimethylhydroquinone	138	H
2-methoxy-4-propenyl-phenol (isoeugenol)	164	G
Phenol, 2-methoxy-4-propyl-(4-propylguaiacol)	138	H
Phenol, 2-methoxy-4-(1-propenyl)-	138	H
3-methoxy-5-methylphenol	164	G
Phenol, 4-(3-hydroxy-1-propenyl)-2-methoxy-	164	G
Phenol, 2,6-dimethoxy-4-(2-propenyl)-(4-allyl syringol)	194	S
Benzene, 1,2,4-trimethoxy-5-(1-propenyl)-, (Z)-	208	S
Phenol, 2,6-dimethoxy-4-(2-propenyl)-	194	S
Ethanone, 1-(2,6-dihydroxy-4-methoxyphenyl)-	182	G
1,2-dimethoxy-4-*n*-propylbenzene	180	S
2,6-dimethoxyphenol (syringol)	154	S
1,2-dimethoxy-4-*n*-propylbenzene	180	S

Their results specifically show fragments of syringyl (S), guaiacyl (G) and *p*-hydroxyphenyl units (H) which is in line with the estimated SGH ratio on the basis of chemical degradation by Nimz (1974). The pyrogram also reveals fragments derived from carbohydrates. Lignin and polysaccharides are connected through covalent bonds to lignin carbohydrate complexes (LCC) (Jung and Deetz 1993). Carbohydrates, which are not completely removed, can be detected by Py-GC-MS. So, pyrolysis coupled to GC-MS gives valuable information about the relative amounts of lignin and carbohydrates. The pyrogram of Organosolv lignin OBL_1 is shown in Fig. 2.16. The nature and molecular weight of the released compounds after pyrolysis at a temperature of 550 °C are listed in Tables 2.7 and 2.8. Besides the fragments of GHS units there are small quantities of fragments originating from carbohydrate residues. Here, we found these small quantities of carbohydrates due to the lower detection limit of 1 ppb. The detection limit of HPLC is 10 ppb, so carbohydrates were not found. NMR results show a higher content of H and G units for OBL_2. These results are confirmed by Py-GC-MS fragment analysis.

Table 2.8 Compounds identified by Py-GC-MS from lignin fragments of OBL_2

Component	Molecular weight [g mol^{-1}]	Origin
CO_2	44	
Benzene	78	C
Toluene	92	C
Ethylbenzene	106	C
p-xylene	106	C
5-methyl-2-furalaldehyde	110	C
Phenol	94	H
2-propenylbenzene	118	H
2-methylphenol (*o*-cresol)	108	H
3-methylphenol	108	H
Mequinol	124	G
2,4-dimethylphenol	122	H
3-ethyl-5-methyl-phenol	136	G
2-methoxy-4-methylphenol (4-methylguaiacol)	138	G
1,2-dihydroxybenzene (pyrocatechol)	110	H
3-methoxypyrocatechol	140	H
p-ethylguaicol	152	G
4-allylphenol	134	H
2-methoxy-4-vinylphenol (4-vinylguaicol)	150	G
2,6-dimethoxyphenol (syringol)	154	S
4-ethylcatechol	138	H
Vanillic acid	168	G
2-methoxy-4-propenyl-phenol (isoeugenol)	164	G
4-ethylsyringol	182	S
4-vinylsyringol	180	S
2,6-dimethoxy-4-allylphenol	194	S
Syringaldehyde	182	S

LigSteam shows degradation products which can be correlated to a molecular structure consisting GHS units which are typical for wheat straw. The fragments of pyrolized Lig Steam are listed in Table 2.9.

2.5 Summary

Beech wood lignin isolated via Organosolv treatment and wheat straw lignin isolated via Steam explosion have been characterized. Organosolv lignins of different process parameters mainly result in different molecular weights and decomposition temperatures. OBL_1 has been isolated using sulphuric acid as catalyst, whereas OBL_2 has been extracted without catalyst but at double

Table 2.9 Compounds identified by Py-GC-MS from lignin fragments of LigSteam

Component	Molecular weight [g mol^{-1}]	Origin
CO_2	44	
Benzene	78	C
Toluene	92	C
Ethylbenzene	106	C
p-xylene	106	C
5-methyl-2-furalaldehyde	110	C
Phenol	94	H
2-propenylbenzene	118	H
2-methylphenol (*o*-cresol)	108	H
3-methylphenol	108	H
Mequinol	124	G
2,4-dimethylphenol	122	H
3-ethyl-5-methyl-phenol	136	G
2-methoxy-4-methylphenol (4-methylguaiacol)	138	G
1,2-dihydroxybenzene (pyrocatechol)	110	H
3-methoxypyrocatechol	140	H
p-ethylguaicol	152	G
4-allylphenol	134	H
2-methoxy-4-vinylphenol (4-vinylguaicol)	150	G
2,6-dimethoxyphenol (syringol)	154	S
4-ethylcatechol	138	H
Vanillic acid	168	G
2-methoxy-4-propenyl-phenol (isoeugenol)	164	G
4-ethylsyringol	182	S
4-vinylsyringol	180	S
2,6-dimethoxy-4-allylphenol	194	S
Syringaldehyde	182	S

process duration time. The fractionated lignins are found to be highly pure without carbohydrate residues. This enables conclusions to the pulping and isolation processes and the corresponding bond cleavages between lignin and carbohydrates. NMR studies revealed a GHS ratio of 49/32/19 for OBL_1 and 40/43/17 for OBL_2. Furthermore, the lignin showed a high solubility in the applied solvents like THF, pyridine and 1,4 dioxane. Concerning the three dimensional macromolecular structure, the samples exhibit a rather low molecular weight and polydisperisty. Thermal analysis studies using TGA and DSC demonstrated typical thermal behavior for Organosolv-fractionated lignins. Organosolv-treated beech wood lignin samples exhibit decomposition temperatures (T_d) of 381 and 348 °C and glass transition temperatures (T_g) of 123 and 124 °C. Pyrolysis studies presented an individual pyrogram with fragments that originated from GHS units which are in agreement with NMR analyses. Lignin isolated via steam explosion

show impurities with high content of carbohydrates. As a result of solubility tests, a modification, in particular an acetylation, was required to enhance the solubility in organic solvents. LigSteam lignin exhibits a lower glass transition temperature (75 °C) compared to Organosolv lignins. The molecular weight of this fraction is higher than Organosolv lignin which means less depolymerization during the isolation process. The monomeric GHS composition of the fraction has been detected by ^{31}P NMR analysis and pyrolysis. The results can be compared with the literature values for wheat straw lignins.

In summary, the Organosolv process seems to be an efficient method to isolate pure lignin fractions. Resulting molecular weights are dependent on reaction time and catalysts used for lignin isolation. Thus, the presented data provides beneficial information for the utilization of beech wood lignin for chemical synthesis and material development. Referring to Table 3.2 OBL lignins meet the requirements for use as a component in phenol formaldehyde resin and polyurethane systems.

2.6 Analytical Methods

2.6.1 Purity, Ash and Sugar Contents

The chemical composition (%, w/w) was performed according to National Renewable Energy Laboratory's (NREL) standard analytical procedure (Sluiter et al. 2008). A Macherey-Nagel HPLC was used with a flow rate of 0.4 mL/min, a column (300 × 7.8 mm) of Macherey-Nagel at a temperature of 90 °C. This analysis was kindly performed by the biorefinery.de GmbH.

2.6.2 Solubility

Solutions were prepared in 5 mL volumetric flasks, using 0.1 g of lignin sample. The solutions were kept for 30 min in an ultrasonic bath and then filtered through a paper filter. The solid residue was dried and weighed. Comparison of the initial sample weight and the remaining solid residue after filtration is the percent solubility value.

2.6.3 FT-IR Spectroscopy

FT-IR spectra of the lignin samples were recorded on a Jasco FT/IR 410 spectrometer in the range of 4000–400 cm^{-1} using a KBr disc containing 1 % finely ground samples. The spectrum recorded over 30 scans with a resolution of 4 cm^{-1}.

2.6.4 ^{31}P NMR Spectroscopy

Quantitative ^{31}P NMR spectra were performed on a Bruker DRX-400 spectrometer using pyridine-d5/$CDCl_3$ (1.6:1 v/v) as the solvent, endo-*N*–hydroxy-5-norbornene-2,3-dicarboxiimide as the internal standard, chromium acetylacetonate as the relaxation reagent, and 2-chloro-4,4,5,5-tetramethyl-1,3,2-dioxapholane as the phosphitylation reagent.

2.6.5 SEC

The lignin sample was completely dissolved in THF (1 mg mL^{-1}) at room temperature with gentle stirring at room temperature. Size exclusion was performed at room temperature with THF as the mobile phase (flow rate 1.0 mL min^{-1}) and a UV detector (280 nm) using an Agilent 1100 instrument. Calibration was performed with polystyrene standards (PSS Standards).

2.6.6 TGA

TGA was performed with about 10 mg of lignin using a Netzsch TGA 209F1 with a heating rate of 20 °C min^{-1} under nitrogen atmosphere. The temperature ranged from ambient to 800 °C.

Acknowledgements Professor Bodo Saake (vTI Hamburg) is gratefully acknowledged for the kind delivery of lignin samples, FNR 22027405.

References

Adler E (1977) Wood Sci Technol 11:169–217
Aklonis JJ, MacKnight WJ, Shen M (1972) Introduction to polymer viscoelasticity. Wiley Interscience, New York
Araújo DP, Grande CA, Rodrigues AE (2010) Chem Eng Res Design 88:1024–1032
Blazei A (1979) Chemie des Holzes. VEB- Fachbuchverlag, Leipzig Booregaard Lignotech USA, Homepage, www.ltus.com, Accessed March 2015
Booregaard Lignotech USA, Homepage: www.ltus.com
Bunzel M, Steinhart H (2003) Chem unserer Zeit 37:188–196
Bunzel M, Seiler A, Steinhart H (2005) J Agric Food Chem 53:9553–9559
Cazacu G, Mihaies M, Pascu MC, Profire L, Kowarskik AL, Vasile C (2004) Macromol Mater Eng 9:880–888
Cetin NS, Özmen N (2002) Int J Adhes Adhes 422:481–486
Ullmanns Enzyklopadie der technischen Chemie (1979) 4th edn, Verlag Chemie, Weinheim
Cybulska I, Brudecki G, Rosentrater K, Julson J, Lei H (2012) Bioresour Technol 118:30

VdCI Verband der Chemischen Industrie (2004) Chemiewirtschaft in Zahlen, Frankfurt
Domínguez JC, Oliet M, Gilarranz MA, Rodríguez F (2008) Ind Crop Prod 27:150
El Hage R (2009) Polym Degrad Stab 94:1632–1638
El Mansouri N, Salvadó J (2006) Ind Crop Prod 24:8–16
El-Saied H, Nada AMA (1993) Polym Degrad Stab 40:417
Erdocia X, Prado R, Ángeles Corcuera M, Labidi J (2014) J Ind Eng Chem 20:1103–1108
European Technology Platform for Sustainable Chemistry, Industrial Biotechnology Section, Brüssel (2005) www.suschem.org. Accessed March 2015
Faix O, Genuit W, Boon JJ (1987) Anal Chem 59:508
Feldman D, Lacasse MA (1989) Materials research society symposiums proceedings 153:193–198
Feldman D, Lacasse MA (1994) J Appl Polym Sci 51:701–709
Feldman D, Lacasse MA, Manley J (1988) J Appl Polym Sci 35:247–257
Fengel D, Wegener G (1989) Wood. Walter de Gruyter Verlag, Berlin-New York, p 145
Fliedner E, van Herwijnen HWG (2011) Stoffliche Nutzung von Organosolv-Lignin zur Herstellung von Phenolharzen, 11. Schwarzheider Kunststoffkolloquium, 5. KuvBB Berlin Brandenburg, Berlin, p 44
Freudenberg K (1965) Holzforschung 18:3–9
Freudenberg K, Neish AC (1968) Constitution and biosynthesis of lignin. Springer Verlag, Berlin, p 132
Froböse R (2004) Nachr Chem 52:660
Glasser WG (1980) In: Casey J P (ed) Lignin – pulp and paper. Chemistry and chemical technology. Wiley Interscience, New York, NY, pp 39–111
Glasser WG (1981) Paperi ja Puu 63:71–83
Glasser WG (2000) Am Chem Soc 216
Glasser WG, Jain RK (1993) Holzforschung 47:225
Glasser WG, Leitheiser RH (1984) Polym Bull 12:1–5
Glasser WG, Saraf VP, Newman WH (1982) J Adhes 14:233–255
Granata A, Argyropoulos DS (1995) J Agric Food Chem 43:1538
Hirose S, Yano S, Hatakeyama T, Hatakeyama H (1989) Heat resistant polyurethanes from solvolysis lignin, lignin – properties and materials. ACS symposium, series 397, Washington, pp 382–389
Hoglund LE (2015) Gasoline prices: cyclical trends and market developments. http://www.bls.gov/opub/btn/volume-4. Accessed 1 June 2015
Holladay JE, White JF, Bozell JJ, Johnson D (2007) Top value-addes chemicals from biomass, results of screening for potential candidates from biorefinery lignin. Pacific Northwest National Laboratory (PNNL) and the National Renewable Energy Laboratory (NREL)
Jayme G, Hunger G (1957) Das Papier 11:140145
Jung HG, Deetz DA (1993) Forage cell wall structure and digestibility. American Society of Agronomy, Crop Science Society of America, Soil Science Society of America, Madison. WI, pp 315–346
Kadla KF, Kubo S, Venditti RA, Gilbert RD, Compere AL, Griffith W (2002) Carbon 40:2913–2920
Kaelbe DH (1971) Physical chemistry of adhesion. Wiley Interscience, New York, NY
Kamm B, Kamm M (2007) Chemie-Ingenieur-Technik 79:592–603
Kamm B, Gruber PR, Kamm M (2006) Biorefineries—industrial processes and products: status quo and future directions, 1st edn. Wiley-VCH, Weinheim, p 441
Kamm B, Gruber PR, Kamm M (2007) Biorefineries—industrial processes and products, Ullmann's encyclopedia of industrial chemistry, electronic release, 7th edn. Wiley-VCH, Weinheim, p 321
Kelley SS, Glasser W, Ward T (1988) J Appl Polym Sci 36:759–772
Kelley SS, Glasser W, Ward T (1989a) Effect of soft-segment content on the properties of lignin-based polyurethanes, lignin – properties and materials. ACS symposium, series 397, Washington, pp 402–413

Kelley SS, Ward T, Rials T, Glasser W (1989b) J Appl Polym Sci 37:2961–2971
Khan MA, Ashraf SM, Malhotra VP (2004) Int J Adhes Adhes 24:485–493
Kim JY, Oh S, Hwang H (2013) Polym Degrad Stab 98:1671–1678
Kosbar LL, Gelorme JD, Japp RM (2001) Ind Ecol 4:93–98
Krässig HA (1993) Cellulose structure, accessibility and reactivity, polymer monographs. Gordon and Breach Science Publishers, Philadelphia, PA
Lai YZ, Sarkanen KV (1971) Isolation and structural studies. In: Sarkanen KV, Ludwig CH (eds) Lignins, occurrence, formation, structure and reactions. Wiley Interscience, New York, pp 165–240
Lapierre C (1993) Application of new methods for the investigation of lignin structure. American Society of Agronomy, Madison, WI, pp 133–166
Li J, Gellerstedt G, Toven K (2009) Bioresour Technol 100:2556–2561
Lindorfer J, Steinmüller H, Auer W (2010) Chem Ingen Tech 82:1169–1176
Lora J (2010) Utilization opportunities for biorefinery lignins: an industrial perspective. International lignin biocemicals conference in Toronto, Canada
Methacanon P, Weerawatsophon U, Thainthongdee M, Lekpittaya P (2010) Kasetsart J (Nat Sci) 44:680–690
Monteil-Rivera F, Phuong M, Ye M, Halasz A, Hawari J (2013) Ind Crop Prod 41:356–364
Nimz H (1974) Angew Chem 9:336
Nimz H (1986) Holzforschung 40:125–132
Nimz H, Faix O, Nemr M (1981) Holzforschung 35:12–26
Nitsos CK, Konstantinos AM, Triantafyllidis KS (2013) ChemSusChem 6:110
Peng W, Riedl B (1994) Polymer 35:1280–1286
Perlack R, Wright L (2005) Biomass as feedstock for a bioenergy and bioproducts industry: the technical feasibility of a billion-ton annual supply
RBACAS (2004) Industrial biotechnology and sustainable chemistry. Royal Belgian Academy Council of Applied Science, Brüssel
Reichardt C (2010) Solvents and solvent effects in organic chemistry. Wiley VCH, Weinheim, p 336
Reimann A, Mörck R, Yoshida H, Hatakeyama H (1990) J Appl Polym Sci 41:39–50
Report on the United Nations Conference on Environment and Development R.o.t.U.N.C.o.E.a. (1992) Rio de Janeiro. https://sustainabledevelopment.un.org/content/documents/1709riodeclarationeng.pdf
Ringpfeil M (2002) Biobased industrial products and biorefinery systems—Industrielle Zukunft des 21. Jahrhunderts? Berlin
Römpp Chemie Lexikon (1995) 9th edn. Thieme Verlag, Stuttgart
Saito T, Perkins JH, Jackson DC (2013) RSC Adv 3:21832
Sameni J, Krigstin S, Rosa DS, Leao A, Sain M (2014) BioResources 9:725–737
Saraf V, Glasser W, Wilkes G (1985) J Appl Polym Sci 30:3809–3823
Sjöström E (1981) Wood chemistry: fundamentals and applications. Academic, New York, NY
Sluiter A, Hames B, Ruiz R, Scarlata C, Sluiter J, Templeton D, Crocker D (2008) Determination of structural carbohydrates and lignin in biomass, laboratory analytical procedure (LAP). Technical report NREL/TP-510-42618
Tejado A, Pena C, Labidi J, Echeverria JM, Mondragon I (2007) Bioresour Technol 98:1655–1663
Toffey A, Glasser W (1997) Holzforschung 51:71–78
Tomani P, Axegard P (2011) LignoBoost Kraft lignin – a new renewable fuel and a valuable fuels additive. International Bioenergy & Bioproducts Conference, Atlanta, AL
TUCI The US Chemical Industry (1992) http://www.industrytoday.com, Accessed 25 Feb 2015
Vishtal A, Kraslawski A (2011) BioResources 6:3547
Wang J, Banu D, Feldman D (1992) J Adhes Sci Technol 6:587–598
Windeisen E, Wegener G (2012) Lignin as building unit for polymers. Technische Universität München, München
Wittkowski R, Ruther J, Drinda H, Rafiei-Taghanaki F (1992) ACS symposium series 490:232
Yoshida H, Mörck R, Kringstad K (1990) J Appl Polym Sci 40:1819–1832

Chapter 3
Analyses of Biomass Fibers by XRD, FT-IR, and NIR

Alexis Ferrer, Carlos Alciaturi, Alexis Faneite, and Josybel Ríos

Abstract This chapter involves the description and application of three advanced analytical techniques that are currently used to assess the potential of biomass for the production of biofuels, feeds, and chemicals. X-ray diffraction, FT-IR, and NIR may be used to study the structure of fibers in native biomass as well as changes during conditioning, pretreatment, and processing in a modern biorefinery. X-ray diffraction is used mainly to study the crystallinity of the samples based on the cellulose fraction which is one of the two major barriers for hydrolysis. FT-IR is used to get insight about the presence and interactions of main components of the fiber such as cellulose, hemicelluloses, and lignin. NIR is mainly used for a fast chemical characterization of the biomass and it is gaining a place to study changes caused by the pretreatments.

Keywords Biomass fibers • Molecular properties • X-Ray • Spectroscopy

3.1 Introduction

Nowadays, there is a paramount need to look for alternative ways to produce fuels, feeds, and chemicals in the world. Biomass constitutes the major source of carbon and should play a major part in the bioeconomy. However, biomass is so diverse and

A. Ferrer (✉)
Analytical Instrumentation Laboratory, Science Faculty, University of Zulia, Maracaibo, Venezuela
e-mail: alexis.ferrer@gmail.com

C. Alciaturi
Chemometrics and Optimization Unit, Zulian Institute of Technological Research, La Cañada de Urdaneta, Venezuela
e-mail: alciaturi@gmail.com

A. Faneite
Chemical Engineering Laboratory, Chemical Engineering School, Engineering Faculty, University of Zulia, Maracaibo, Venezuela
e-mail: afaneite@fing.luz.edu.ve

J. Ríos
Agrifoods Unit, Zulian Institute of Technological Research, La Cañada de Urdaneta Venezuela
e-mail: josybelrios_28@hotmail.com

S. Vaz Jr. (ed.), *Analytical Techniques and Methods for Biomass*,
DOI 10.1007/978-3-319-41414-0_3

heterogeneous that robust analytical methods are greatly needed to estimate its composition, potential for byproducts, and changes during pretreatment and processing, purity of the fractions, and so on. There are different sources of biomass, including forest and agricultural main materials as well as residues. Harvesting aquatic plants is also a potential source of fiber and feed and food protein. The chemical composition of a biomass feedstock varies as a function of many factors that introduce a great deal of variance. In this respect, the advanced analytical techniques of X-ray diffraction, FT-IR, and NIR comprise easy and rapid ways to assess the composition and changes in biomass fibers, which are critical for the establishment of a biorefinery. Both chemical and physical changes can be assessed by these techniques. The chemical changes are associated with cleavage of linkages, formation and disappearance of chemical groups and changes on the fiber surface, whereas physical changes are mainly associated with changes in crystallinity. The use of these methods, although equipment-expensive, turns out to be less costly than standard wet chemical methods since the last ones are expensive in labor, equipment, and reactants and usually do not provide results in a time frame useful for industrial purposes. The main components of the fibers are cellulose, hemicelluloses, and lignin, among others. These compounds will be the target in this chapter. The first two are important energy feeds for ruminants and the major feedstocks for bioethanol production from lignocellulosic materials through enzymatic hydrolysis and fermentation of the sugars produced, mainly glucose and xylose. On the other hand, the sugars produced may be used for production of a great variety of chemicals, including furans, polymers, etc. (Gallezot 2012). Cellulose nanofibers are being considered as a very unique reinforcing material for industrial packaging (Siqueira et al. 2010) and composites and nanocomposites (Miao and Hamad 2013). In this chapter, X-ray diffraction (XRD), FT-IR, and NIR are discussed as relevant techniques that are currently used to analyze the fiber from a great diversity of biomass.

3.2 X-Ray Powder Diffraction

3.2.1 Theory

Powder and single-crystal X-ray diffraction (XRD) are the two main methods currently used to study the crystal structures of materials. In fact, single-crystal XRD is regarded to be the most powerful technique for elucidating crystal structures, but for biomass the use of powder XRD techniques becomes essential to studying its crystalline structure. In this respect, powder XRD is an analytical technique for characterizing crystalline materials, or with a certain degree of crystallinity, finely ground and homogenized, with respect to the crystalline system of the unit cell and its dimensions, the crystalline allomorphs present, and the crystallinity index of the sample. The technique is based on impinging a beam of X-rays on the sample, which rotates in the plane, with a θ angle relative to the X-ray beam, which is reflected when it encounters a crystal plane that causes a diffraction of the beam,

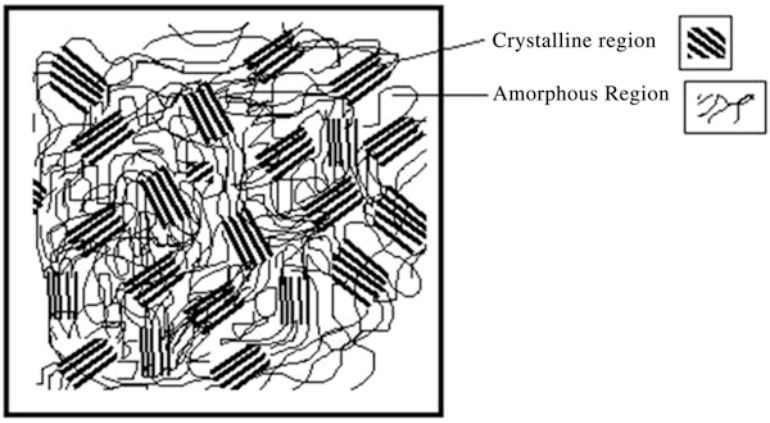

Fig. 3.1 Mixed amorphous and crystalline regions in a polymer (Reproduced from Hegde et al. 2004)

and the intensity of the reflected radiation is counted by a detector forming an angle 2θ with the sample. As opposed to single-crystal XRD, in powder diffraction, all the symmetry-equivalent reflections have the same d spacing with the result that individual intensities cannot be measured.

3.2.1.1 Crystallinity

For a polymer, the crystallinity may be considered a packing of the molecular chains that produces an array in space. It can also be seen as the number of regions where the chains of a polymer have a geometric order (crystalline regions) with respect to the number of regions where the polymer chains are disordered (amorphous regions), in a given sample (Fig. 3.1). This arrangement of the chains is due to the formation of intermolecular hydrogen bonds.

3.2.1.2 Cellulose Crystallinity

Cellulose is a linear poly (1-4)-α-D-glucan, normally biosynthesized in a metastable form known as Cellulose I which is comprised of crystalline micro fibrils like thin rods (Langan et al. 2001) shown in Fig. 3.2, where the intermolecular and intramolecular types of hydrogen bonds that characterize the crystal structure are shown.

Cellulose I can be subjected to an irreversible transition toward a stable crystalline form by two different processes: regeneration and mercerization, which generates a marked difference in the pattern of XRD. The modification is known as "hydrated cellulose", "mercerized cellulose", "regenerated cellulose", or more generally as "cellulose II". Regeneration involves the preparation of a cellulose solution

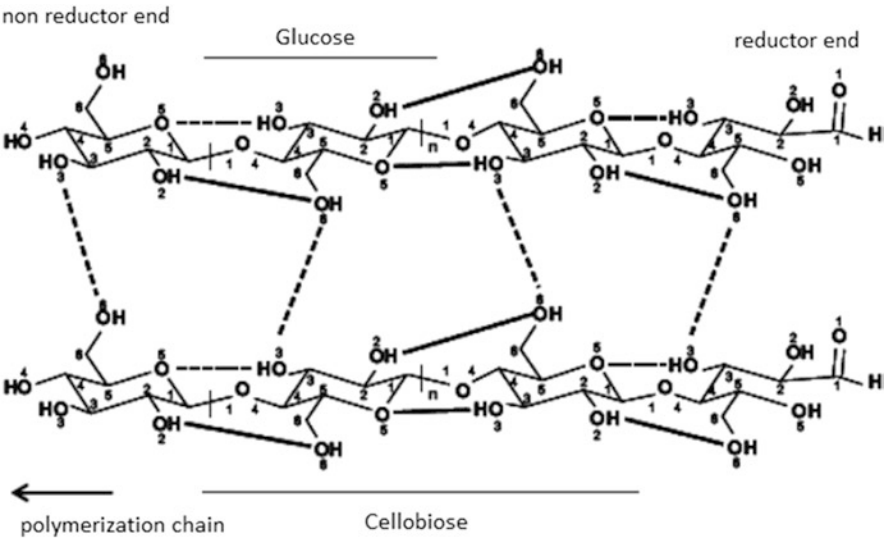

Fig. 3.2 Structure and bridges examples of the inter- and intra-chain hydrogen bonding patterns in cellulose I. *Dashed lines*: inter-chain hydrogen bonding. *Dotted lines*: intra-chain hydrogen bonding (Reproduced from Festucci-Buselli et al. 2007)

with a suitable solvent or preparation of an intermediate derivative followed by coagulation and recrystallization. This process is used for producing rayon fibers. Mercerizing involves intra-crystalline swelling of cellulose in concentrated aqueous NaOH followed by washing and recrystallization. This process is used to improve the properties of yarn and natural fabrics (Marchessault and Sarko 1968; Langan et al. 2001).

Differences between the reticular structures of cellulose I and II have been described by Krässig (1993). Cellulose II is the most thermodynamically stable form because hydrogen bonds are extended in *c*-axis direction (Marchessault and Sarko 1968). Besides being responsible for the chemical reactivity of the cellulose, the ability of the hydroxyl groups to form hydrogen bonds between them is the cause of the high tendency of the cellulose to get organized as parallel arrangements of crystallites and intertwined crystallites, which are the basic elements of the supramolecular structure of cellulose fibers (Krässig 1993).

There are two other types of regenerated cellulose, called cellulose III and IV, produced by swelling and regeneration, with monoclinic unit cells, but slightly different interplanar spacings (Marchessault and Sarko 1968). Cellulose III is obtained by treatment of cellulose I or II with liquid ammonia below −30 °C and then recrystallization of the sample by evaporation of the ammonia (Klemm et al. 1998). Cellulose IV is obtained at high temperatures on glycerol or formamide. Using regenerated fibers make it easier the obtainment of cellulose IV since they have a low order of crystallinity, therefore requiring lower energies for these changes to happen (Marchessault and Sarko 1968).

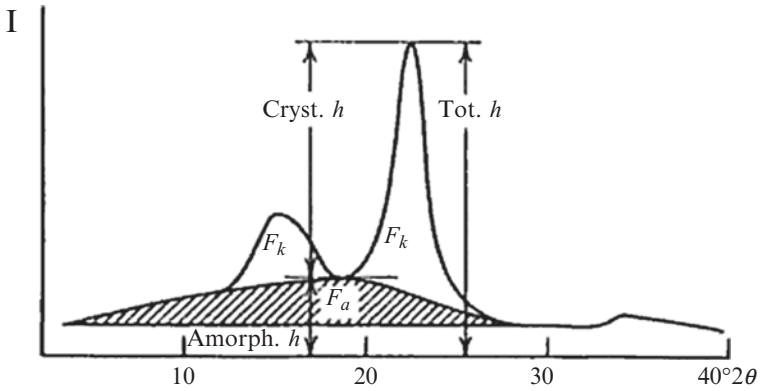

Fig. 3.3 Typical diffractogram of cellulose I (Reproduced from Jayme and Knolle 1964)

3.2.2 Cellulose Crystallinity Index

Although there are a large number of methods that have been used to determine the crystallinity and the availability of celluloses, there are few suitable for determining the crystallinity of wood, pulp, and other lignocellulosic materials. XRD, infrared spectroscopy, and nuclear magnetic resonance spectroscopy are usually sensitive to different aspects of order and disorder, but it is not surprising that they give rise to different values of ordered and unordered cellulose for the same sample, since they have different sensitivities. Other methods are not suitable due to interference of hemicellulose and lignin (Krässig 1993).

A typical diffractogram of cellulose I obtained with the XRD technique is shown in Fig. 3.3. Diffractograms corresponding to other crystalline cellulose allomorphs and polymorphs are shown elsewhere (Marchessault and Sarko 1968). The maximum observed are produced by specific reflections of the crystalline regions. To determine the percent crystallinity of the sample, different methods and approximations have been proposed in the literature (Roncero 2001).

A simple approach used by many authors is to take from the diffractogram the intensity of an appropriate maximum and a minimum to give a "crystallinity index" (CrI) (Segal et al. 1959) defined as:

$$\%\mathrm{CrI}_{\mathrm{Segal}} = \left[\frac{I_{002} - I_{\mathrm{am}}}{I_{002}}\right] \times 100 = \left[1 - \frac{I_{\mathrm{am}}}{I_{002}}\right] \times 100, \tag{3.1}$$

where I_{002} (Tot. h in Fig. 3.3) is the intensity of the crystalline peak at the maximum 2θ between 22° and 23° for cellulose I (between 18° and 22° for cellulose II) and I_{am} (Amorph. h in Fig. 3.3) is the intensity at the minimum 2θ between 18° and 19° for cellulose I (between 13° and 15° for cellulose II) (Roncero 2001).

The crystallinity index of Segal is highly susceptible to the normalization of the spectrum and its softening, so that the handling and treatment of the data should be made evenly for all samples for comparative purposes. Raw data must be softened,

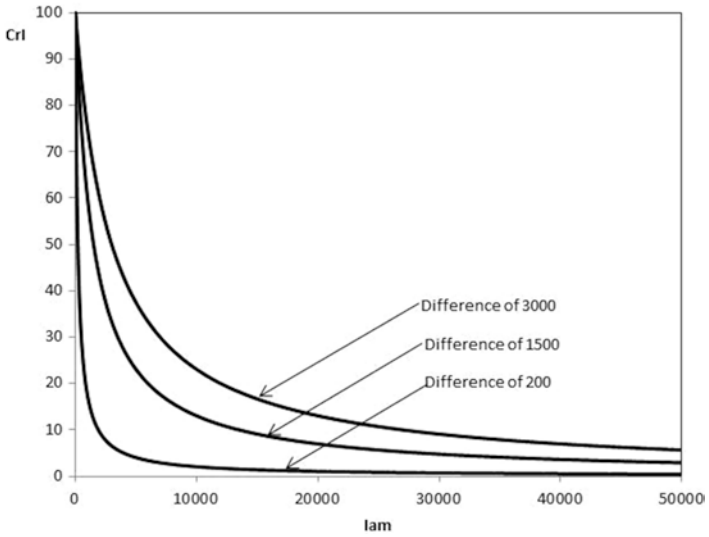

Fig. 3.4 Segal's crystallinity index of three samples, with different $I_{002} - I_{am}$ (difference of 3000, 1500, and 200, respectively) by varying the position of the spectrum in the *y* axis (Intensity)

and in the case of Excel® the "moving average" trendline with a period of 30 may be used. Then the baseline is taken to 0 and the amorphous and crystalline intensities are measured. Figure 3.4 shows the crystallinity index when the position of the spectrum on the *y*-axis (Intensity) for normalization purposes is varied. It is noted that the equation of Segal is highly susceptible to the normalization of the spectra and to the difference between crystalline and amorphous intensities, so one should carefully follow the suggestions given in this paragraph.

Landis (1971) proposed a graphical method to estimate the index of crystallinity of carbonaceous materials, which is very simple and is not influenced by normalization of the data. Equation (3.2) represents the crystallinity index of Landis:

$$\mathrm{CrI} = \frac{2 \times h}{w}, \tag{3.2}$$

where h is the height of peak 002 and w is the base of the peak, both values in consistent units.

Diffractograms of other crystalline allomorphs of cellulose have been reported by Nelson and O'Connor (1964) as shown in Fig. 3.5.

3.2.3 X-Ray Powder Diffraction Applications

Lignocellulosic materials relevant to the area of biorefining are mostly field residues that can be processed and chemically refined to obtain several products. Many processes, whose primary interest is the use of cellulose, have different levels of

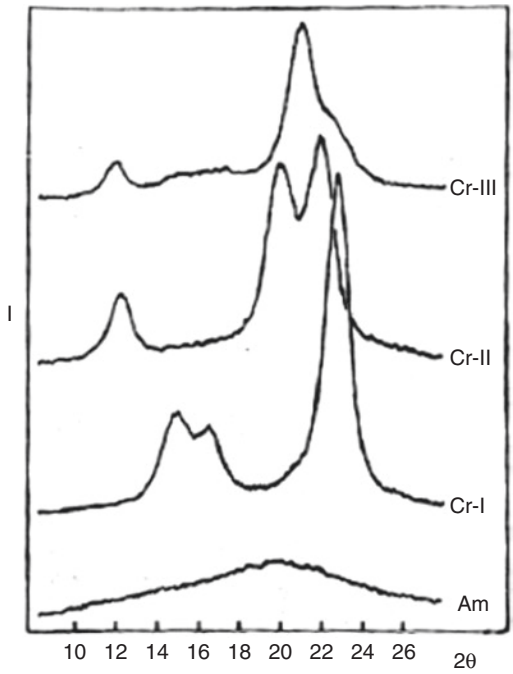

Fig. 3.5 X-ray diffractograms of hydrocelluloses prepared from cotton cellulose (Cr-III), fortisan rayon (Cr-II), and native cotton (Cr-I) and of vibratory ball-milled cotton (Am) (Reproduced from Nelson and O'Connor 1964)

complexity depending on the type of desired product. If the major interest is as a feed for polygastric animals (cattle, buffalo, sheep, and goats), ammonia processes greatly enhance the dry matter digestibility of the materials (Ferrer et al. 1997). For sugar production as a feedstock for downstream processing, cellulose must be separated from the original vegetable matrix and be hydrolyzed mainly by enzymes or acids. Sugars can be fermented to produce a variety of chemicals such as ethanol, butanol, 2-propanol, lactic acid, followed by a dehydration process.

In any case, two major obstacles to access the cellulose must be overcome. One is the barrier created by the other components of the cell wall such as pectin, hemicelluloses, and lignin, both physically and chemically. The second relates directly to the degree of crystallinity of the cellulose. In these regions, the attacks of agents that normally produce changes in cellulose, such as enzymes or acids are greatly ineffective. For this reason, physicochemical pretreatments are applied.

When designing a biorefinery one should take into account the crystallinity of the cellulose present in the raw material and the changes that occur in such crystallinity during the preconditioning steps, including drying. To maximize the amount of cellulose available, one should be careful about the selection of the pretreatment since a greater severity of a pretreatment could remove more barriers to cellulose, but could also make it more crystalline or more recalcitrant due to the formation of crystalline allomorphs or the formation of new bonds between the cell wall polymers (Ferrer et al. 2000). In some cases, the technological proposal is to pelletize the unreacted fraction and send it to the boiler as an energy source but this depends on the particular technical and economic feasibility in each situation in terms of available fuels and the cost of converting this cellulose crystalline fraction into a product.

Table 3.1 Crystallinity index (CrI) of some lignocellulosic materials

Material	$\%CrI_{Faneite}$ (proposal)	Van Soest Cellulose content (%, dry basis)	CrI_{Landis}	$\%CrI_{Segal}$ (Faneite (2010)
Microcrystalline cellulose (Merck Art. 2330)	91.84	97.00	12.62	91.84
Guinea grass (GG)	24.99	26.97	3.16	67.47
King grass (KG)	20.38	37.75	2.80	64.29
Sugarcane bagasse (SCB)	18.70	49.32	2.57	71.08
Sugarcane leaves (SCL)	12.95	29.93	1.78	65.18
Bermuda grass (BG)	12.95	28.30	1.78	62.17
Midrib of plantain leaves (MPL)	9.68	34.48	1.33	67.44
Maize leaves (ML)	5.46	18.79	0.75	60.00
Plantain leaves (PL)	2.84	15.47	0.39	50.00
Cassava foliage (CF)	2.84	15.83	0.39	50.00
Cassava leaves (CL)	2.40	8.21	0.33	29.27
Old duckweed (ODw)	2.40	12.73	0.33	50.00
Young duckweed (YDw)	1.82	10.28	0.25	47.06

It is not considered as necessary to have XRD routine analysis in a biorefinery unless operating conditions, technologies, processes or raw materials are changed, however, information about the crystallinity of the raw materials, changes during processing, and selection of pretreatment play a major role in the performance of the biorefinery.

3.2.3.1 Crystallinity Index of Materials

The crystallinity index of Segal yields values that could create confusion, as some materials have values fairly close to the microcrystalline cellulose values, such as the case of bagasse (Table 3.1). We can see in Fig. 3.6 that the bagasse, although it is one of the most crystalline samples, does not generate intensities in the 2θ angle of the plane 002, such that are equivalent to that expressed by the equation from Segal. The calculation of a crystallinity percentage is proposed by using the simple rule of three where the Landis index of each sample is expressed as a percentage by using the ratio of the percentage crystallinity index of Segal over the index of Landis both for microcrystalline cellulose (MCC). The values are presented in Table 3.1 expressed as % CrI (proposed). Equation (3.3) shows the proposed model.

$$\%CrI_{Faneite} = CrI_{Landis\,material} \times \frac{\%CrI_{Segal}MCC}{CrI_{Landis}MCC}. \tag{3.3}$$

Thus, the percent crystallinity index of bagasse becomes 18.70 %, which keeps a more accurate relationship with the comparison of spectra of Fig. 3.6. Equation (3.3)

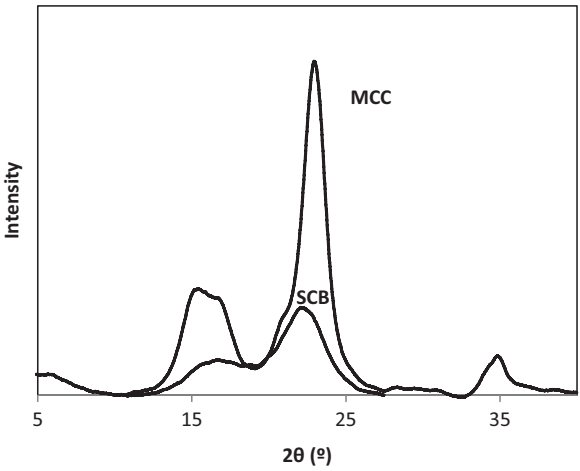

Fig. 3.6 Normalized XRD spectra of sugarcane bagasse (SCB) and microcrystalline cellulose (MCC)

represents the "Faneite model" for the percent crystallinity index of lignocellulosic materials. It is important that the conditions of the diffractometer and graphics scales are the same for the diffractograms of the microcrystalline cellulose and samples.

The crystallinity index of a raw material is strongly related to the morphology of the plant material and the part of the plant from which it was obtained. Certain grasses and supporting tissues such as Guinea and King grass and sugarcane bagasse have the highest crystallinities of the evaluated materials. Other grasses such as Bermuda, hard leaves such as those from sugarcane and corn and the midrib of the banana leaf, which is a supporting tissue, have intermediate to low crystallinities. On the other hand, cassava and banana leaves, and duckweed (an aquatic plant), have rather a low crystallinity. All this relates directly to the cellulose content of Van Soest (Goering and Van Soest 1970), with which, the percentage crystallinity index (Landis or Faneite) has a correlation coefficient of more than 0.82. This was expected, since the main function of the cellulose in the plant is for stiffness. Typical diffraction patterns of X-rays of various potential raw materials for biorefineries can be seen in Fig. 3.7. Results for foliage of cassava and cassava leaves were expected because the foliage contains a mixture of petioles and leaves, this being a more crystalline mixture. Regarding duckweed, the old one has a higher fiber content and thus greater rigidity. XRD of materials such as those presented in this section is very useful for predicting whether a material will likely be more recalcitrant to enzymatic attack than others, at least in terms of crystallinity. This is useful both for biofuels and feeds applications. Undoubtedly, lignin and hemicellulose also play an important part.

3.2.3.2 Crystallinity Changes During Drying

In scientific literature, changes in crystallinity have been attributed to pretreatments (Yue et al. 2015; Sannigrahi et al. 2010), but drying makes important changes that are frequently overlooked.

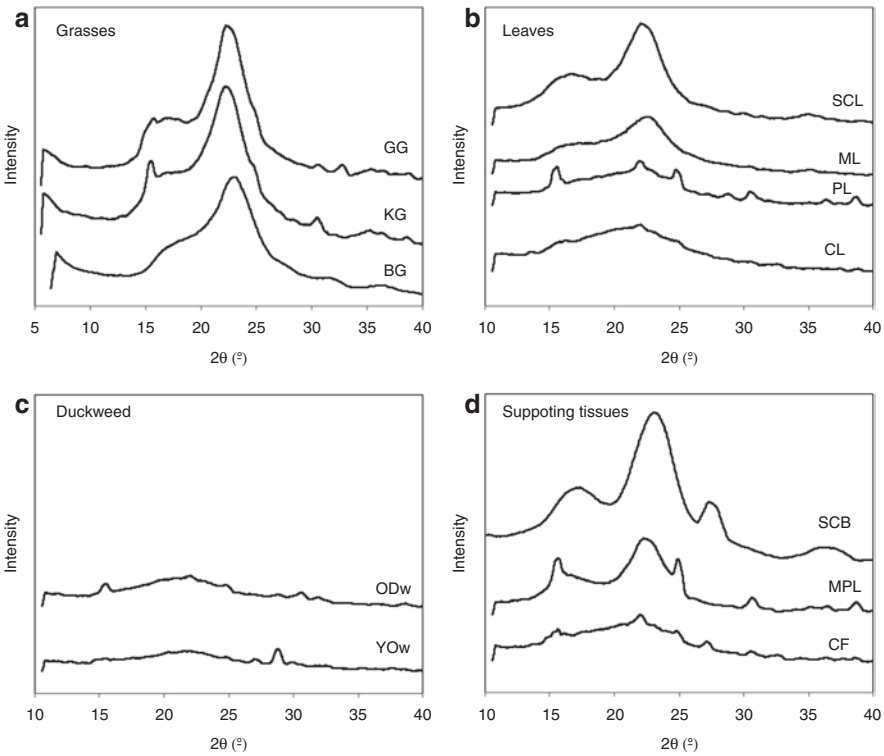

Fig. 3.7 XRD spectra of (**a**) grasses (*GG* guinea grass, *KG* king grass, *BG* Bermuda grass), (**b**) Leaves (*SCL* sugarcane leaves, *ML* maize leaves, *PL* plantain leaves, *CL* cassava leaves); (**c**) Duckweed (*ODw* old duckweed, *YDw* young duckweed); and (**d**) Supporting tissues (*SCB* sugarcane bagasse, *MPL* midrib of plantain leaves, *CF* cassava foliage)

Figure 3.8 shows XRD spectra for a material of low crystallinity such as duckweed (a), and one of higher crystallinity guinea grass (b), respectively, dried at 55, 75, 95, and 115 °C. The highest intensity (related to carbohydrate) occurs at an angle of 2θ, between 18° and 22°, characteristic of cellulose II. However, a harder fiber such that from guinea grass has the greatest intensity between 22 and 23, typical of cellulose I. Table 3.2 has the percentage crystallinity indices of Faneite for the different samples presented in Fig. 3.8. For duckweed, cellulose I and II crystallinities were calculated.

Drying produces morphological changes in the material (Therdthai and Zhou 2009) such that modifies the paracrystalline structure, and in the case of duckweed, which is a very special case due to its high water content (94 % on wet basis), causes the change from cellulose I to cellulose II. This may be due to plasticization of the cellulose chains in contact with water that is being desorbed during drying, which also destroys the cell wall, and substances present in the cytoplasm impregnate the cellulose chains, for example accumulated minerals which may appear in the spec-

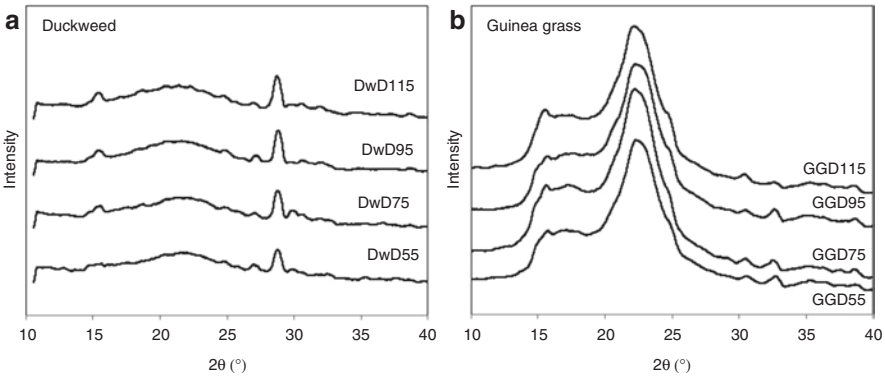

Fig. 3.8 Effect of drying temperature on crystalline characteristics of lignocellulosic materials (**a**) Duckweed (Dw) and (**b**) Guinea grass (GG), dried (D) at 55, 75, 95, and 115 °C (Reproduced from Faneite 2010)

Table 3.2 Faneite's crystallinity percentage index (%CrI) of duckweed and guinea grasse dried at different temperatures (Faneite 2010)

Samples	%CrI (Faneite)	%Cellulose I	%Cellulose II
Duckweed			
DwD55	5.68	33.24	66.76
DwD75	5.72	31.61	68.39
DwD95	6.35	13.34	86.66
DwD115	6.45	4.67	95.33
Guinea grass			
GGD55	24.99	–	–
GGD75	23.43	–	–
GGD95	23.18	–	–
GGD115	22.41	–	–

trum. Duckweed cellulose does not greatly exert a support function as in the case of guinea grass, reason why duckweed cellulose is more susceptible to plasticization, also adding the effect of the high water content. Crystallinity increases with drying, specifically as cellulose-II, which is thermodynamically the most stable crystalline conformation.

In the case of guinea grass, crystallinity decreases, and this was expected by the hornification effect, which mainly involves shrinkage, formation of internal hydrogen bonds, and the irreversible loss of water absorption capacity and swelling (Weise 1998). It is presumed that shrinkage is the phenomenon responsible for the decrease in crystallinity of this material because it forces the chains, whether packed or not, to change position and being a very rigid material tends to lose crystalline regions since the amorphous regions remain amorphous after these modifications.

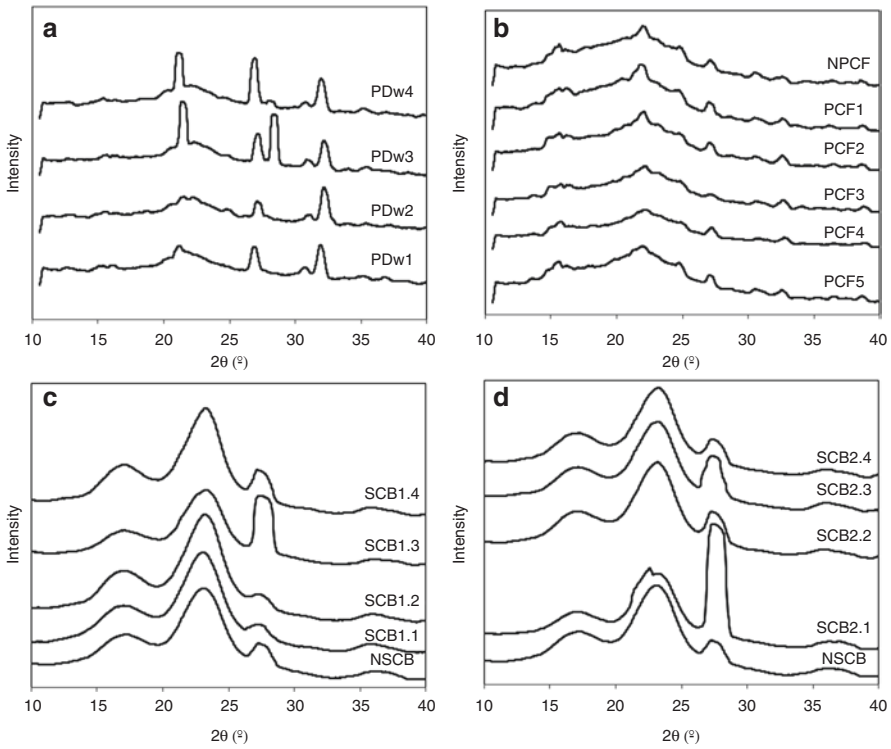

Fig. 3.9 XRD spectra of untreated and PDA treated (**a**) duckweed (PDw); (**b**) cassava foliage (NPCF and PCF); (**c**) and (**d**) sugarcane bagasse (Data from Ríos 2009; Montiel and Rodriguez 2008 and Urribarrí 2011)

3.2.3.3 Changes in Crystallinity Due to Physicochemical Pretreatments

The following discussion refers to materials subjected to an ammonia pretreatment at Ammonia Pressurization-Depressurization (PDA) conditions.

Figure 3.9 present the XRD spectra for (a) treated duckweed with PDA (Ríos 2009), previously rehydrated to 60 % (wet basis) at reaction conditions of 2 min, 75 °C, and 150 psi, varying the ammonia/biomass ratio (*r*, in dry basis), 0, 0.25, 0.50, and 0.75 (samples: PDw1, PDw2, PDw3, and PDw4, respectively); (b) cassava foliage untreated (NPCF) and PDA treated (Montiel and Rodriguez 2008), rehydrated to 60 % (wet basis) at reaction conditions for 2 min and 75 °C, varying r-reaction pressure as 0–120, 0.25–150, 0.50–155, 1.0–180 and 1.5–200 psi (samples: PCF1, PCF2, PCF3, PCF4, and PCF5, respectively); (c) and (d) bagasse untreated (NSCB) and PDA treated (Urribarrí 2011) at 100 °C for 5 min at 300 psi. Samples were rehydrated to 30 % (*r* 0.25, 0.5, 1.0 and 1.25, for SCB1.1, SCB1.2, SCB1.3, and SCB1.4, respectively) and 50 % (*r* 0.25, 0.5, 1.0 and 1.25, for SCB2.1, SCB2.2, SCB2.3, and SCB2.3, respectively).

In Fig. 3.9a–c, it is seen that the spectra of all the materials do not greatly differ in the intensity of the I_{002} signal, so that crystallinity changes caused by the pretreatment PDA were very light. Well-defined signals more intense that the signal for I_{002}, especially for bagasse and duckweed, were likely generated by mineral contaminants. The signal intensity at I_{002} for untreated duckweed (PDw1, Fig. 3.9a) moved into the range of cellulose II; a cellulose II content of 54.16 % was estimated. Plasticization of cellulose I to cellulose II likely occurred by the effect of swelling when the sample was exposed to an environment with ammonia vapors at pressures above atmospheric, and not by the effect of pre-drying samples at 55 °C which was the drying temperature for all the samples (Rios 2009).

No presence of cellulose II was observed in cassava leaves samples at different severity conditions of treatment PDA (Fig. 3.9b), although the peak of the plane 002 is at an angle of 2θ, where both allomorphs coincide (22°). No shift of this signal was seen with changes in pretreatment conditions. They look as very amorphous samples even though they are the mixture of leaves and supporting tissue (petioles). No evidence of formation of cellulose II was found in untreated and PDA treated bagasse at different conditions, which may be due to the fact that it is a fibrous material, with high cellulose content, being a supportive tissue of the plant, and for transport of nutrients, therefore, it must have some degree of rigidity.

In Fig. 3.10, the effect of the treatment PDA is shown at several ammonia/biomass ratios on (a) the percentage of Van Soest solubles in duckweed (Rios 2009), cassava leaves (Montiel and Rodriguez 2008), sugarcane bagasse (Urribarrí 2011); (b) the percentage crystallinity index of these same samples; and (c) the protein extraction yield for cassava foliage (Urribarrí et al. 2009) and the production of sugars from sugarcane bagasse (Urribarrí 2011). Solubles usually increase with the PDA treatment due to partial hemicellulose and lignin solubilization. When treatment conditions are severe, condensation reactions may occur which change the behavior (Ferrer et al. 2000).

Comparing Fig. 3.10a, b, it can be observed that the solubles content is inverse to Van Soest crystallinity of samples. As usual, crystallinity is directly related to the cellulose content. Percent crystallinity for duckweed is greater than for cassava foliage, which is contrary to what was observed in Table 3.1, and this is because the duckweed treated sample is much higher in fiber with 17.25 % (dry basis) of Van Soest cellulose, and lower in crude protein content with 13.23 % (dry basis) (Ríos 2009), therefore it is much older than the old lemna shown in Table 3.1. Old duckweed is usually subjected to a high level of environmental stress or a low nutrient medium, and usually has longer roots which are richer in cellulose compared to the fronds (leaves). Thus, the XRD becomes a valuable tool to quickly determine the quality of a raw material such as duckweed.

A relationship between the crystallinity of samples and the solubles content of Van Soest (Fig. 3.10a, b) produced by the PDA treatment of the same samples is observed, where the PDA condition that produced the sample with the highest amount of solubles is also that one with the greatest crystallinity. This is consistent with what was observed by Peters (2003) for PDA-treated dwarf elephant

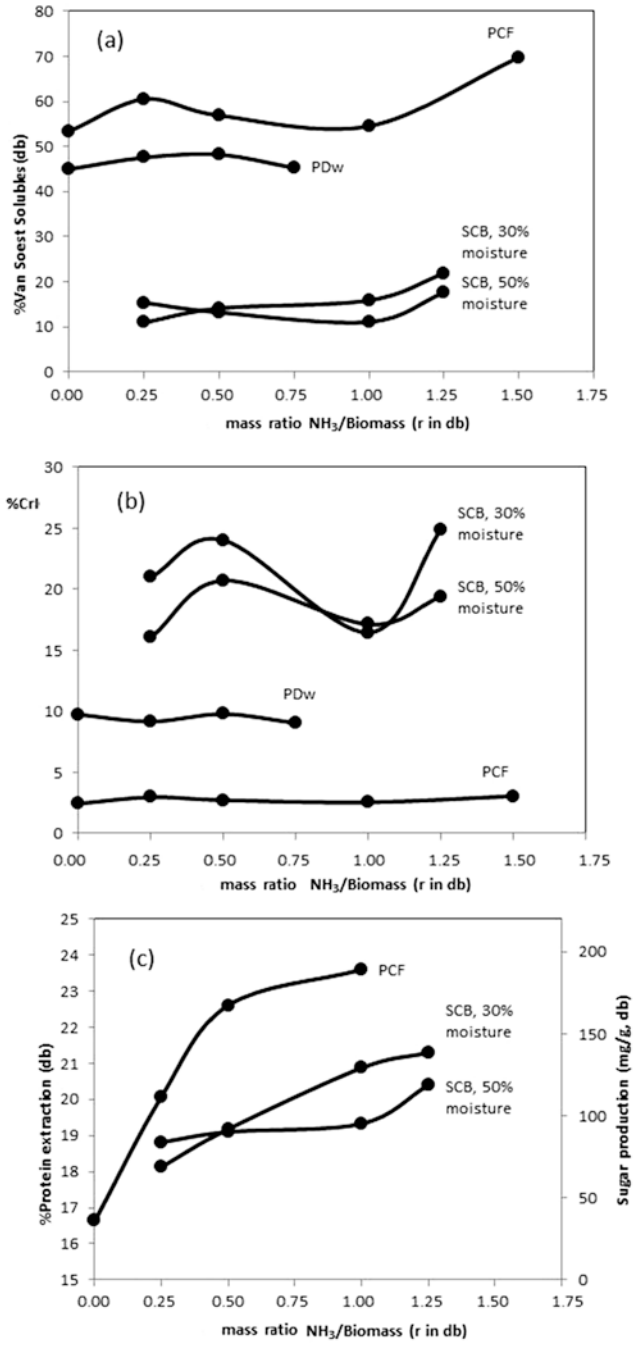

Fig. 3.10 Effect of PDA treatment, varying the ammonia/biomass ratio on (**a**) the percentage of Van Soest solubles in duckweed (Ríos 2009), cassava foliage (Montiel and Rodriguez 2008), and bagasse with two moisture contents obtained by rehydration (Urribarrí 2011); (**b**) the percentage crystallinity index of the aforementioned samples; and (**c**) the protein extraction yield for cassava foliage (Urribarrí et al. 2009), and the production of sugars from sugarcane bagasse at two moisture contents obtained by rehydration (Urribarrí 2011)

grass. The peaks of the plane 002 are at an angle of 2θ near the boundary between both types of cellulose (I and II), which is 22°, and it is possible that the PDA treatment produces a small crystallization to cellulose II, due to the plasticizing of cellulose chains that in addition may produce ordered arrays with amorphous cellulose.

Protein extraction from PDA-treated materials does not seem to be influenced by the crystallinity of the samples (Fig. 3.10c). As cassava leaves are treated with a higher ammonia loading, protein yield steadily increases (Urribarrí et al. 2009), behavior also found in PDA-treated duckweed (Ferrer et al. 2013). However, crystallinity remains very similar. On the other hand, increasing ammonia loading in sugarcane bagasse increases the susceptibility of cellulose to enzymatic hydrolysis measured by sugar production in spite of the fact that crystallinity also increased. This means that crystallinity of cellulose was not the determinant factor but its overall availability taking into account that it is more exposed to enzymes since part of the hemicellulose and lignin has been removed (Urribarrí et al. 2013). It should be also noted that the increase was only 5 %.

For an ammonia/biomass ratio in the range between 0.25 and 0.5, a maximum in the crystallinity as well as in Van Soest solubles content is observed which obeys the molecular thermodynamics of the ammonia/water mixture (Faneite 2010), for all the materials. They also decreased until an r of 1.00, which matches the behavior of the final temperature of the ammonia/water mixture calculated with a commercial simulator at the same reaction conditions but without biomass (Faneite 2010). Above an r of 1.0 crystallinity increases, which can be a response rather physical than chemical, associated with a greater penetration of ions in the lignocellulosic matrix due to higher ion concentration, greater pressure during the reaction, and a greater pressure difference during depressurization (Faneite 2010). This could separate and brake amorphous regions which would increase crystallinity and enhance hydrolysis. In addition, high pressure may help crystallize cellulose.

In the PDA treatment, unlike other ammonia treatments it is very important to moisten the sample prior to introducing it in the ammonia reactor and this generates additional phenomena which have to do with the thermodynamics of the ammonia/water mixture. This mixture is exothermic and generates heat. Indeed, making a scan by ASPEN (Faneite 2010) through the heats of solution of the ammonia/water mixture at different solid/solvent ratios, it is found that mixtures corresponding to PDw3, PCF2, SCB1.2, and SCB2.2 have the highest dissolution temperature. As the PDA reaction is carried out at constant temperature, the increase in heat is displayed as an increase in activity of the ions present in the solution (including OH^-), generating a greater penetration into the material, a higher breaking of ester bonds between lignin and hemicellulose, and higher plasticization of cellulose chains due to the repulsive negative forces between the molecules both when the ions penetrate into the material as when they are desorbed violently with depressurization.

3.3 Fourier Transform Infrared Spectroscopy

3.3.1 Theory

The regions most used by chemists are as follows: middle infrared (MIR), 4000–400 cm^{-1} (2500–25,000 nm) and near infrared (NIR), 12,820–4000 cm^{-1} (780–2500 nm).

The absorption of a photon by matter produces a transition to a higher energy level. Thus, the energy of the MIR photons (4000–400 cm^{-1}) is used to study the fundamental vibrations and rotational vibrational structure. The molecular rotation and vibration have discrete energy levels (vibrational normal modes). For a molecular vibrational mode be activated by IR, it must be associated with changes in the permanent dipole. This is known as the selection rule. The resonant frequencies may be in a first approximation related to the bond strength and the masses of the atoms involved. Thus, the frequency of vibration may be associated with a particular type of chemical bond, and tables are available which assign vibrational frequencies to types of chemical bond. The transitions related to NIR are overtones and combination bands of fundamental vibrations. In organic molecules, these vibrations involve groups of hydrogen with heteroatoms, mainly C–H, O–H, and N-H. The combination bands are much weaker and less-resolved than the fundamental absorption bands.

The most used representations of infrared spectra are percent transmittance and absorbance. Percent transmittance is defined as:

$$\%T = \left(I / I_0 \right) \times 100 \tag{3.4}$$

where I/I_0 is the incident light intensity, and I the transmitted light intensity. $\%T$ varies between 100 (no absorption) and 0 (total absorption).

Absorbance is defined as:

$$A = \log_{10} \left(I_0 / I \right) \tag{3.5}$$

The values of absorbance may vary between 0 (no absorption) and infinity ($I=0$). An absorbance of 1 means 1/10 of the energy is transmitted.

3.3.1.1 The Fourier Transform Infrared Spectrometer

The technique for infrared spectra acquisition was revolutionized by the development of Fourier Transform instruments (FTIR, usually referring to MIR; and FT-NIR) that present several advantages with respect to dispersive instruments: better optical yield, better signal-to-noise ratio, faster acquisition of spectra, and more precise wavelength determination. This last advantage makes it easier to apply averaging and subtraction of spectra. Also, spectra may be averaged, which reduces random noise.

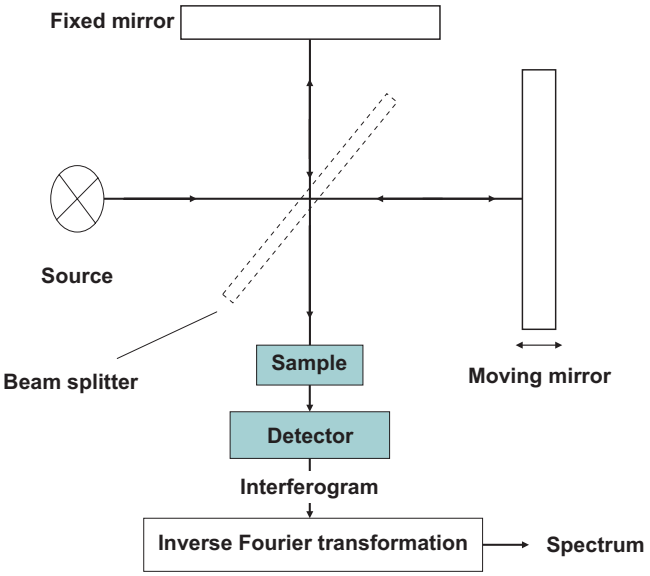

Fig. 3.11 Scheme of an FT-IR spectrometer

However, advances in technology were necessary for Fourier transform-based instruments to become of general use. The discovery of the Fast Fourier transformation (FFT) by Cooley and Tukey (Cooley and Tukey 1965) permitted to do calculations several orders of magnitude faster than with previous algorithms. Also, the development of desktop computers and graphic interfaces provided the means for efficiently generating and processing spectra. The processing of spectra includes smoothing, derivation, integration, baseline correction, peak finding, averaging, and subtraction. Also, the computers do chemometric calculations (multivariate statistical analysis applied to chemical problems), for example partial least squares (PLS) and principal components analysis (PCA), allowing for exploratory data analysis, prediction of properties, and classification of samples from the FT-IR spectra. Chemometric programs are commercially available and offered by most equipment vendors. Ozaki (2012) recently wrote a review article about the history, principles, and recent advances in NIR spectroscopy, including instrumentation and chemometrics. Figure 3.11 displays the scheme of a modern FT-IR spectrometer.

3.3.1.2 The Development of Effective Sample Analysis Techniques

The new sampling techniques have been essential for the ample applications of infrared spectroscopy to characterization, quantitative analysis, and quality control of materials. Water is an important interference in infrared spectroscopy, so samples must be carefully dried before analyzed. Also the amount of sample required is very small (in the order of milligrams), so special care is to be taken to assure that the sample properly represents the lot analyzed.

The main techniques used are: the traditional KBr pellet, diffuse reflectance infrared spectroscopy (DRIFTS), and attenuated total reflection (ATR). The KBr pellet technique produces the highest energy and signal-to-noise ratio, but it is slower, costlier, and more laborious. DRIFTS measures the light dispersed, so it requires the material be finely divided, and most of the time the samples are mixed with KBr. Certain materials, like coal, may be analyzed neat (Alciaturi et al. 1996). While the energy is low, the samples require minimal preparation. ATR needs the sample to have intimate contact with a highly refractive transparent material. Thus, liquids, powders, and sheets may be analyzed. However, limitations exist for example for hard solids, which do not make good contact with the refractive material.

A detailed explanation of these and other techniques is found in the book of Griffiths and De Haseth (2007).

3.3.1.3 Spectral Interpretation

Since functional groups absorb at certain wavenumbers, it is possible to do an interpretation of spectra from first principles (Coates 2000). Thus, the presence (or absence) of a particular group may be inferred from the peaks in an infrared spectrum (Socrates 2001; Kemp 1991). The region between 4000 and 1450 cm^{-1} is known as the *functional group region*; between 1450 and 500 cm^{-1} there is a complicated set of absorptions, and is called the *fingerprint region*. These last absorptions are (mainly) due to bending vibrations.

Thus, the mid-infrared spectrum of a molecule is a characteristic that can be used for identification of pure compounds by comparison of the spectrum of an unknown sample with previously recorded reference spectra. The comparison is done in an efficient manner by computer programs.

However, the determination of the detailed structure of an unknown necessitates information from other techniques, especially nuclear magnetic resonance (NMR) and mass spectrometry (MS) (Kemp 1991).

For quantitative analysis of biomass components, the peaks in the absorbance spectra may be used, because in some cases the absorbance is proportional to the concentration (Lambert–Beer's Law). However, deviations of linearity are common, and more effective models for quantitative analysis are created by Multivariate Analysis, mostly with the Partial Least Squares (PLS) method. These methods will be discussed in the NIR section.

FT-IR is already recognized as a great tool to study the composition of the lignocellulosic biomass (Xu et al. 2013). It can be used to distinguish among plant leaves and among different types of wood, which is useful to prepare appropriate blends for several applications, including biofuels. When fractionation is a major step in processing, FT-IR can also be used to confirm the presence or absence of cellulose, hemicelluloses, and lignin. When biofuels are the target, materials need physicochemical pretreatments to enhance the susceptibility of the fibers to enzymatic hydrolysis. The most common pretreatments are dilute acid, steam explosion, autohydrolysis, alkaline peroxide, organosolv, and alkaline pretreatments such as AFEX,

pressurization-depressurization with ammonia, liquid ammonia, sodium hydroxide, and lime, among others. Each pretreatment has their chemical properties, which may be followed by FTIR. On the other hand, hemicellulose and lignin are the target in many biorefineries as final or intermediate materials. Changes in lignin structure may be easily followed by FTIR.

3.3.2 Spectra of Cellulose, Hemicellulose, and Lignin

One approach for studying biomass by FT-IR is obtaining the spectra of cellulose, hemicelluloses, and lignin extracted from different materials. However, band positions frequently shift in the spectra according to the chemical environment of the groups.

3.3.2.1 Cellulose

Cellulose, the major constituent of all plant materials, forms about half to one-third of plant tissues and is constantly replenished by photosynthesis, with estimates of annual world biosynthesis of 10^{11} tonnes (Sun et al. 2004b).

Chemically, cellulose is a linear natural homopolymer of anhydroglucose units linked at the first and fourth carbon atoms by β-glycosidic bonds. This is confirmed by the presence of three hydroxyl groups with different acidity/reactivity, secondary OH at the C-2, secondary OH at the C-3, and primary OH at the C-6 position, and, accordingly, by the formation of strong various intermolecular and intramolecular hydrogen bonds. It is organized into fibrils, which are surrounded by a matrix of lignin and hemicelluloses. Its degree of polymerization is very high (10,000–14,000) (Xiao et al. 2001). By the use of XRD patterns and solid-state cross-polarization magic-angle spinning ^{13}C nuclear magnetic resonance (CP/MAS ^{13}C-NMR) spectroscopy, four major polymorphs of cellulose have been reported, namely celluloses I, II, III, and IV. Cellulose I is the native and predominate crystalline structure in algae, bacteria, some animals and higher plants, and can be converted into other polymorphs through a variety of treatments. The cellulose fibril is partly crystalline, with two different crystal forms, cellulose Iα and cellulose Iβ. Cellulose Iα has one-chain triclinic structure and cellulose Iβ has two-chain monoclinic structure, and they differ in hydrogen bonding. In addition, cellulose Iα is reported as the dominant polymorph in bacterial and algae celluloses, while cellulose Ib is predominant in higher plants such as cotton, wood, and sugarcane bagasse. It is also known that cellulose Iα can be irreversibly converted to cellulose Iβ by the application of heat. It can be seen from the NMR spectra of cellulose I that the broad single at 110 ppm has two shoulders, which are due to a mixture of two sub-polymorphs Iα and Iβ. This has also been noticed to happen during pulping. Non-crystalline cellulose forms are also present in the fibril: para-crystalline cellulose and cellulose at inaccessible and accessible fibril surfaces (Duchesne et al. 2001). At present, it seems

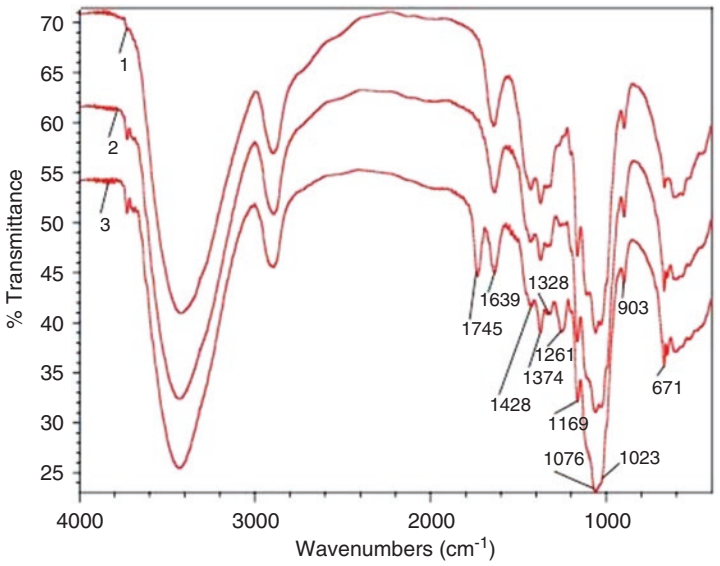

Fig. 3.12 Spectra of cellulose extracted from dewaxed sugarcane bagasse under different fractioning conditions. Spectrum 1: alkaline peroxide. Spectrum 2: acidified sodium chlorite and alkaline extraction. Spectrum 3: acetic and nitric acid (Reproduced from Sun et al. 2004a with permission. Copyright Elsevier)

generally accepted that cellulose I has a parallel chain orientation, while in cellulose II, the chains are anti-parallel (Sun et al. 2004b; Lennholm and Iversen 1995).

The spectra of native cellulose have been extensively studied by different authors, for different materials. Figure 3.12 shows three spectra corresponding to the extracted cellulose from sugarcane bagasse under different fractionation conditions (Sun et al. 2004b). The basic signals found in samples of native cellulose are presented in Fig. 3.12 and described as follows: the removal of lignin is observed with a decreasing band at 1600 and 1510 cm^{-1}. The absorbance at 3420 cm^{-1} is due to stretching of the O–H group and the signal at 2910 cm^{-1} corresponds to the stretching of the C–H group. The band at 1639 cm^{-1} corresponds to bending caused by absorbed water. A peak at 1428 cm^{-1} is attributed to CH_2 bending and at 1374 cm^{-1} to O–H bending. The absorbance at 1328 cm^{-1} arises from the skeletal C–C and C–O vibrations. The peak at 1261 cm^{-1} is indicative of the in-plane O–H bending. The absorption band at 1169 cm^{-1} refers to the stretching of antisymmetric C–O bond. Skeletal vibration of the C–O–C pyranose ring occurs between 1076 and 1023 cm^{-1}. The peak at 903 cm^{-1} is caused by β-glycosidic bonds between glucose units of cellulose. Spectrum 3 has one sharp atypical acetyl ester band at 1745 cm^{-1} (C=O ester) indicating an acetylation reaction caused by the severe acid treatment. Sun et al. (2004a) also reported this peak but shifted to 1732 cm^{-1} in cellulose extracted from wheat straw caused by an acid treatment prior to an organosolv extraction.

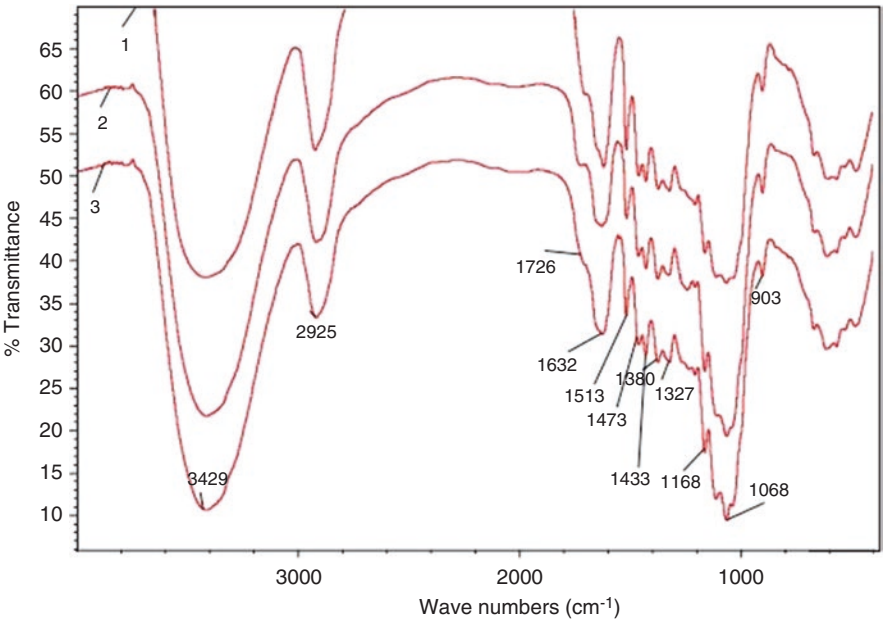

Fig. 3.13 FT-IR spectra from steam-exploded wheat straw residue (degraded cellulose) C2a (spectrum 1), C3a (spectrum 2), and C5a (spectrum 3). Shoulder at 1726 cm^{-1} almost disappeared in the more severe treatment (spectrum 3). C2a, C3a, and C5a represent the steam-exploded residues obtained at 200 °C, 15 bar with water to straw ratio (mL/g) 2:1 for 33 min (C2a); at 220 °C, 22 bar with water to straw ratio (mL/g) 2:1 for 3 min (C3a), and 8 min (C5a) (Reproduced from Sun et al. 2005 with permission. Copyright Elsevier)

Poletto et al. (2011) confirmed most of the aforementioned bands for the composition of cellulose fibers from pulping processed wood (Eucaliptus and Pinus). Differences were found just in the lower region of the range (1300–900 cm^{-1}). If hemicellulose is present in the cellulose preparation, bands will appear in the 1730–1600 cm^{-1}, typical of xylan signals from uronic acids (Poletto et al. 2012).

Sun et al. (2005) working with degraded cellulose (residues) obtained from steam-exploded wheat straw and alkaline peroxide also confirmed the typical bands and added that if lignin is present, a shoulder appears at 1726 cm^{-1} (Fig. 3.13) which can be ascribed to the ester linkage of carboxylic group of the ferulic and *p*-coumaric acids of lignin and/or hemicelluloses as well as acetyl and uronic ester groups of the hemicelluloses. Bands at 1513 and 1433 cm^{-1} may also be seen due to C=C stretch from aromatic rings of lignin. Lee et al. (2010) also showed these bands working with coastal bermuda grass subjected to autohydrolysis and AFEX pretreatments. Moreover, Mandal and Chakrabarty (2011) showed that spectra from cellulose extracted from alkaline treated sugarcane bagasse and nanocellulose obtained from acid hydrolysis of the cellulose were similar.

A summary of FT-IR bands typical of cellulose is shown in Table 3.3.

Table 3.3 Typical frequencies and vibrational modes of the spectra for cellulose

FT-IR frequencies, cm^{-1}	Vibrational modes
3600–3200 (3420)	Stretching of O–H groups
3000–2800 (2920)	C–H stretching
1700–1550 (1642–1639)	H_2O absorbed
1430–1428	CH_2 bending
1374–1365	In-plane C–H deformation
1335	In-plane O–H bending
1315	CH_2 wagging
1245	C–C plus C–O plus C=O stretch; glucose condensed > glucose etherified
1169–1160	Asymmetric C–O–C bridge stretching
1110	Anhydroglucose ring
1052	C–OR stretching
1076–1023 (1028)	C–O–C pyranose ring skeletal vibration
903–895	Glycosidic C–H deformation with ring vibrations and O–H bending, typical of β-glycosidic bonds
670	Out-of-plane O–H bending

Most likely frequencies appear between brackets (Poletto et al. 2011, 2012; Sun et al. 2005; Fan et al. 2012)

3.3.2.2 Hemicellulose

Hemicelluloses are one of the most abundant natural polysaccharides although below cellulose and lignin and have a wide range of concentration of the dry mater of lignocellulosic materials. It is very heterogeneous and is generally solubilized in alkali from the material, due to the presence of uronic acids. Pectic substances are also solubilized in alkali (Kacurákova et al. 2000). Its isolation involves alkaline hydrolysis of ester linkages with lignin substances and phenolic acids. Most of the hemicelluloses in graminae (straws, sugarcane bagasse, common grasses), legumes, and woods have a xylan backbone with branches comprised of L-arabinose, D-galactose, D-glucose, D-mannose, D-glucuronic acid, 4-*O*-methyl-D-glucuronic acid, D-galacturonic acid, and to a lesser extent, L-rhamnose, L-fucose, and various *O*-methylated neutral sugars. The degree of polymerization is around 80–200. Hemicelluloses are found in the primary and secondary cell walls in all land and freshwater plants. Some hemicelluloses have a glucose backbone such as in grains and some straws (xyloglucans).

Among chemicals that may be produced from hemicelluloses are adhesives, thickeners, stabilizers, film formers, and emulsifiers (Doner and Hicks 1997).

Xiao et al. (2001) made hemicellulosic preparations, extracted with 1 mol L^{-1} NaOH at 30 °C for 18 h from maize stems, rye straw, and rice straw. Table 3.4 shows the relevant frequencies and vibrational modes of the spectra.

Table 3.4 and Fig. 3.14 indicate that FT-IR can be used to monitor the fractionation of hemicellulose, with a strong signal for β-linkages, a very well noticeable fingerprint region (1200–1000 cm^{-1}), identify the presence of arabinosyl side groups (at 1168 cm^{-1}) and the possibility to detect the presence of residual lignin with the

Table 3.4 Frequencies and vibrational modes of the spectra obtained from the hemicellulosic preparations shown in Fig. 3.14

FT-IR frequencies, cm^{-1}	Vibrational modes
1645	Absorbed water
1125–1000	Typical of xylans
1042	C–O, C–C stretching or C–OH bending in hemicellulose
Small band at 838	For α-linkage
Sharp band at 903	For β-linkage
Low intensity shoulder at 1168	C–O–C vibrations in the anomeric region of hemicelluloses
Very small band at 1519 in spectrum b, and a shoulder in spectra a and c	Largely due to the presence of small amounts of associated lignin
3600–2800	Stretching vibrations of C–H and O–H
1200–950	C–O stretching region
950–700	Anomeric region with just a 903 band
1645	Carbonyl stretching region: water

The last four groups of frequencies refer to signals found in the residues after extraction (Xiao et al. 2001)

signal at 1519 cm^{-1}, with an intensity proportional to the lignin content, and the presence of cellulose mainly for the band at 903 cm^{-1}.

Sun et al. (2004b) studying hemicellulosic preparations extracted by alkali and alkaline peroxide from sugarcane bagasse confirmed that the intensity changes of the band (shoulders) at 1175 cm^{-1} (1168 cm^{-1} for maize stems, rye and rice straws from Xiao et al. (2001)) and that of the band at 990 cm^{-1} might reflect the arabinosyl substituent contribution and therefore, used for the identification of arabinoxylan structures. This band varies depending upon the branches at the O-2 and O-3 positions. As the number of branches increases, the intensity at 1175–990 cm^{-1} decreases. Sun et al (2000) also reported the pyranosyl band at 1162 cm^{-1} for hemicellulosic preparations from rice straw, among the bands of the 1125–1000 cm^{-1} region, typical of xylan. The presence of lignin was associated with a small signal at 1512 cm^{-1} of aromatic skeletal vibrations (Sills and Gossett 2012). The presence of cellulose was associated with bands at 1441, 1388, 1321, 1169, 1056, 1049, and 897 cm^{-1}.

3.3.2.3 Lignin

Lignin is an aromatic heterobiopolymer, the second most abundant biopolymer, found in the secondary walls and middle lamella in all vascular plants. Lignin is highly hydrophobic and its primary structure is not ordered, but with random gathering of different monomeric units. The three major units are comprised by phenyl propanoid units, namely, syringyl alcohol, guaiacyl alcohol, and *p*-coumaryl alcohol, which form a tri-dimensional network inside the cell walls (Boerjan et al. 2003). The relative abundance of these units depends on the type of plants and species. FT-IR is able to identify some of these units. The major interunit linkages are an

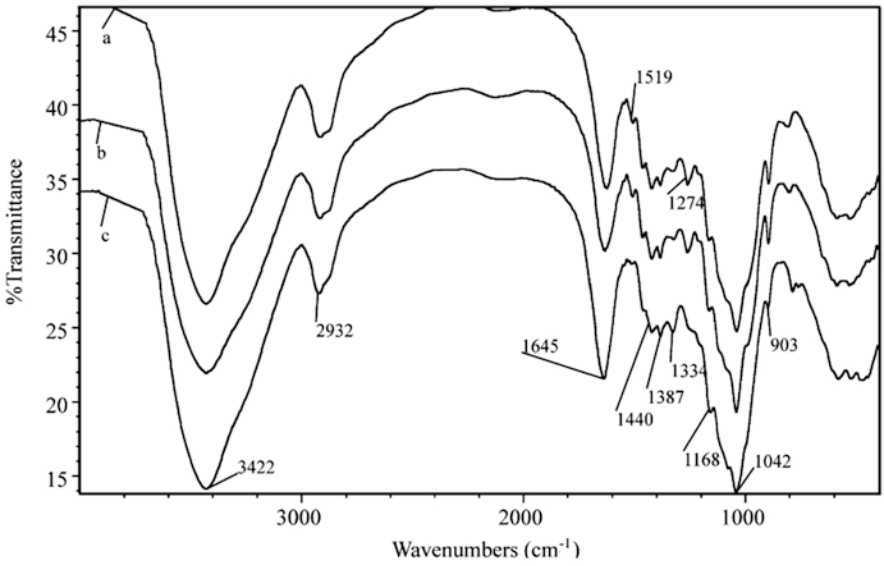

Fig. 3.14 FT-IR spectra of hemicellulosic preparations extracted with 1 mol L^{-1} NaOH at 30 °C for 18 h from maize stems (*spectrum a*), rye straw (*spectrum b*), and rice straw (*spectrum c*) (Reproduced from Xiao et al. 2001 with permission. Copyright Elsevier)

aryl–aryl ether type and a *β-O*-4 between adjacent aryl and propanoid units, although more than 20 different types of bonds have been reported within the lignin itself. However, it is widely recognized that lignin seems to be particularly associated with the hemicellulosic polysaccharides. Great variability is also a characteristic of lignin between different plants as well as in the same plant, according to the tissue.

There is a great deal of research going on lignin since it may be a feedstock for a great number of chemicals such as phenol. The applications depend on lignin physicochemical properties and therefore lignins are being extracted by several processes, although generally the products are not homogeneous, including variations in molecular weight. Applications in the oil industry include its use as asphalten dispersant, emulsifiers, demulsifiers, dispersants in drilling muds and lignosulfonates. It is also used for the production of activated fibers (Uraki and Koda 2015).

When studying lignin, it is important to point out that sometimes due to the high temperature pretreatments (hydrothermal, steam explosion, dilute acid) and oxidative pretreatments such as wet oxidation lignin is fluidized and upon cooling it solidifies and cover the biomass surface as discrete spherical, granular, or globular structures (Donohoe et al. 2007). The re-allocation of lignin (Kristensen et al. 2008) is easily seen by SEM, and FT-IR lignin bands become more intense.

There are two main reasons to work on lignin. First, it is necessary to remove it or change it to increase the susceptibility of cellulose to enzymatic hydrolysis. Second, if lignin can be separated, oxidative treatments may be applied to convert it to low-molecular-weight carboxylic acids, carbon dioxide, and water (Schmidt and Thomsen 1998). Hemicelluloses are oxidized as well.

Table 3.5 Frequencies of ATR-FT-IR spectra of organosolv lignin from dewaxed barley straw and maize stems (Sun et al. 2002) and acid-insoluble lignin extracted with NaOH from maize stems and rye straw (Xiao et al. 2001)

FT-IR frequencies, cm^{-1}	Vibrational modes
1169	C–O in ester groups as esterified *p*-coumaric acid (PCA) and ferulic acid (FA)
1712–1705	Unconjugated ketone or unconjugated carbonyl stretching
1660–1638	Conjugated carbonyl stretching in lignin
1606–1600, 1513, 1427	Aromatic skeleton vibrations in lignin
1467	C–H deformations and aromatic ring vibrations
1328, 1282, 1230	Ring breathing with C–O stretching
1135	Aromatic C–H in-plain deformation for syringyl type
1043	Aromatic C–H in-plain deformation for guaiacyl type
843–837	Aromatic C–H out of plane bending

Spectra presented so far were mainly obtained by ATR-FT-IR (Xiao et al. 2001). However, in the case of lignin, both ATR-FT-IR and DRIFT have been used. However, intents of correlating DRIFT results with digestibility have failed (Gollapalli et al. 2002), although others have found good correlations with sugar production by using PLS techniques.

Sun et al. (2002) isolated lignin solvent extracted from wheat, rice, rye, and barley straws, maize stems, and fast-growing poplar wood. Lignin was characterized by ATR-FTIR. On the other hand, Xiao et al. (2001) studied acid-insoluble lignin extracted with NaOH from maize stems and rye straw by ATR-FT-IR as well. Even though they were different materials and different extraction processes were used, the frequencies for the most important signals are very similar. The results for some of the biomasses are shown in Table 3.5.

It is possible looking at the 1135 and 1043 cm^{-1} bands to estimate relative differences in amount of PCA and FA present in lignin. In addition, since ester linkages can be seen, it is possible to assess whether those acids are linked to the main structure. Appearance, blurring, and disappearance of certain bands (shoulders, peaks), make it possible to identify type of changes caused by physicochemical pretreatments. Li et al. (2009), for instance, working with steam exploded lignin from soft and hard wood (Aspen) for biodiesel and chemicals reported the appearance of a band at 1700 cm^{-1} characteristic of keto groups, and the reduction of a signal at 1725 cm^{-1} indicating disappearance of ester structures, also reported by Sun et al. (2005) when lignin is present.

3.3.3 Comparing Compositions of Different Materials by FT-IR

Faneite et al. (2011) published the FT-IR spectra of a great variety of samples (Fig. 3.15). Some differences are pointed out. The band at 1156 cm^{-1}, corresponding to the asymmetric C–O–C bridge stretching vibration of the skeletal pyranose ring,

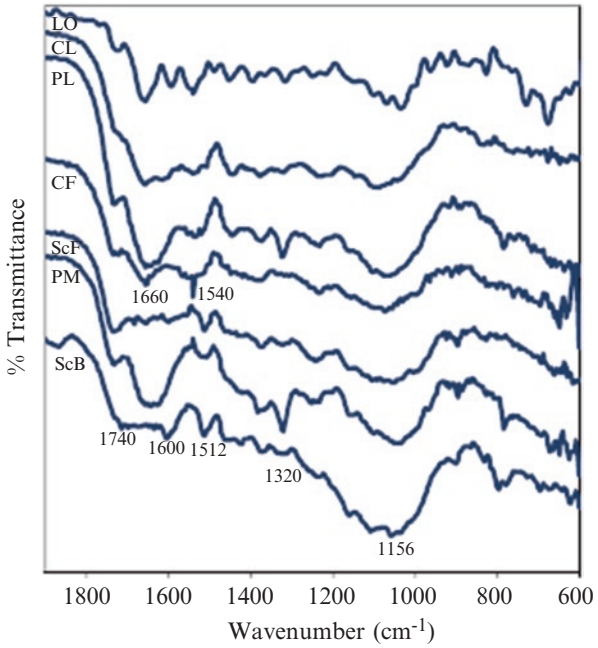

Fig. 3.15 Spectra of duckweed (LO), sugarcane bagasse (ScB), cassava leaves (CL), sugarcane foliage (ScF), hybrid yellow corn foliage (CF), plantain leaves (PL), and plantain midrib (PM) (Reproduced from Faneite et al. 2011)

was preferably absorbed in samples with greater cellulose content. The band at 1720 cm^{-1}, corresponding to the vibration of the ester bond between hemicellulose and lignin, was well defined for all samples except for CL (cassava leaves) and ScB (sugarcane bagasse), which are the samples containing less hemicellulose. The band at 1512 cm^{-1} of the C=C aromatic skeletal vibration, characteristic of lignin, was greater in the more rigid materials, which were the ones presenting also the highest cellulose content (sugarcane bagasse, plantain midrib, and sugarcane foliage). In contrast, in the softer samples the band was displaced to 1540 cm^{-1}. The band at 1316 cm^{-1}, representing C–C and C–O skeletal vibrations, characteristic of lignin, was greater in plantain leaves and plantain midrib, which are the samples with greater lignin content.

3.3.4 Monitoring Changes in Fiber Structure by FT-IR Due to Pretreatments

FT-IR is greatly useful to detect changes in fiber components when a pretreatment is applied to the biomass. Some typical and different cases will be presented. Most of them coincide in the bands already indicated for cellulose, hemicelluloses, and lignin. Only important features of the researches will be indicated.

Ibrahim et al. (2011) studying alkaline pulping and steam explosion of rice straw with infrared spectra in the 400–4000 cm^{-1} region noticed that wax removal can be detected by FT-IR since CH_2– stretching bands at approximately 2850 and 2920 cm^{-1} were reduced for the pretreated sample as Kristensen et al. (2008) have pointed out for the aliphatic fractions of waxes. Bands typical of cellulose and lignin were found. Changes in the lignin bands at approximately 1595 and, in particular, 1510 cm^{-1} (aromatic ring stretch) clearly suggested a relative increase in the amount of lignin in the steam explosion pretreatment due to the removal of hemicelluloses or by re-deposition of lignin on the surface. On the other hand, Lee et al. (2010) did not find any wax removal in AFEX-treated coastal bermuda grass (no change in the CH_2 stretching of aliphatic fractions). They also stated that if there is no change in lignin composition, increase in lignin should be just assigned to re-deposition.

Kaparaju and Felby (2010) studying lignin obtained by hydrothermal and wet explosion of wheat straw and corn stover by ATR-FT-IR spectroscopy found differences between both pretreatments. Cellulose and hemicellulose could be detected by very distinct bands at 3351 and 1035 cm^{-1}, the stretching vibrations of O–H (Fig. 3.12) and C–O (band at 1042 cm^{-1}, Fig. 3.13), respectively. A sharp peak at 1735 cm^{-1} representing carboxyl groups also confirmed the presence of hemicellulose (Himmelsbach et al. 2002). The intensity of this peak indicates the degree of hemicellulose removal. Lignin is identified by marked peaks at 1045 and 1130 cm^{-1}, typical of guaiacyl and syringyl structures (C–H bending), and at 1248 and 1270 cm^{-1} representing O–H, or CH_2 bending frequencies (Himmelsbach et al. 2002). Lignin bands at approximately 1595 cm^{-1} and in particular, 1510 cm^{-1} (aromatic ring stretch) were strongly enhanced in pretreated wheat straw compared with untreated wheat straw. Also, these peaks were more prominent in hydrothermal compared with wet exploded wheat straw. Re-deposition of lignin was noted. When lignin was purified, the intensity of peaks at 1595 and 1510 cm^{-1} increased.

A strong sharp absorption at 1734 cm^{-1} for hemicelluloses isolated from prehydrolyzed wood chips (steam hydrolysis) was interpreted as more carbonyl groups from uronic acids or acetyl groups in the hemicelluloses compared to hemicelluloses isolated the same way from sugarcane bagasse (Liu et al. 2011; Ren et al. 2007).

Rezende et al. (2011) followed lignin removal from sugarcane bagasse treated with sodium hydroxide with DRIFT. At higher alkali concentration, bands corresponding to cellulose were enhanced whereas those corresponding to lignin decreased in intensity. In addition, a band at 1729 cm^{-1} corresponding to C=O in polysaccharides was present in the untreated sample and disappeared in the treated one. The band at 1510 cm^{-1}, considered to be the most important for lignin, gradually disappears as NaOH concentration increases. Also, the band at 1263 cm^{-1}, a characteristic signal of softwood lignin (guaiacyl derivatives) and the major lignin component of sugarcane bagasse, decreases.

In ammonia pretreatments such as AFEX, Balan et al. (2009) working on hardwoods indicated that the important changes happened at 1664 and 1740 cm^{-1}. The first one assigned to an amide group appears when the ammonia ion breaks ester linkages to form amides, therefore, the band at 1740 cm^{-1} (carbonyl of ester linkages) is supposed to decrease or disappear. Lignin re-deposition might occur in

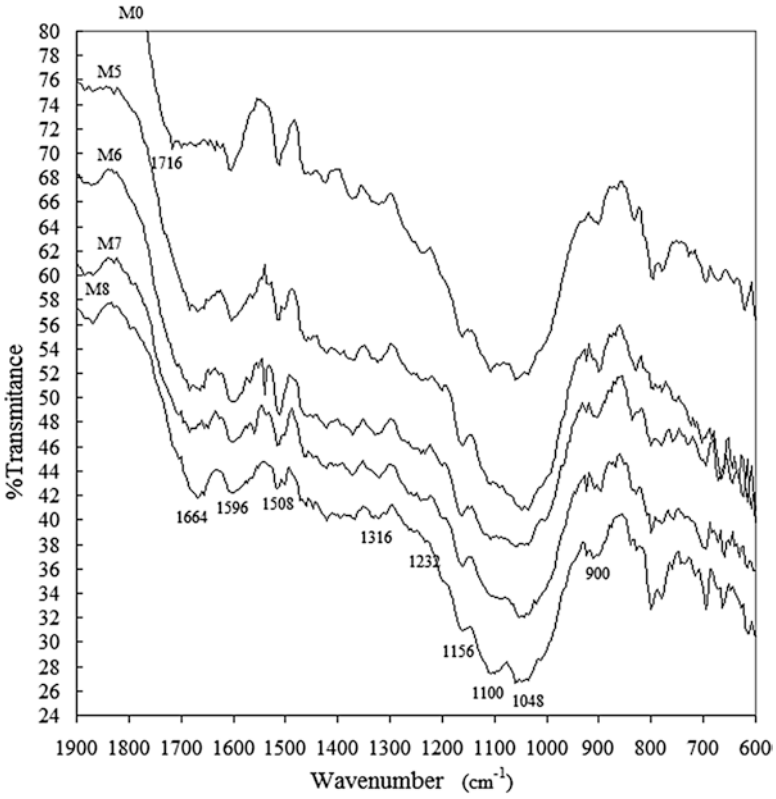

Fig. 3.16 FT-IR spectra of non-treated sugarcane bagasse (M0), and bagasse treated with ammonia. Processing conditions were: 100 °C for 5 min, 50 % moisture content, ammonia loadings of 0.25; 0.50; 1 and 1.25 kg ammonia/kg dry biomass, for M5, M6, M7, and M8, respectively (Reproduced from Urribarrí 2011)

AFEX-treated materials as well, which means an increase in the intensity of bands at 1595 and 1510 cm^{-1}, as was found in AFEX-treated coastal bermuda grass (Lee et al. 2009). For AFEX-treated oil palm empty fruit bunch fiber (Abdul et al. 2016), the changes were detected at 1606 and 1738 cm^{-1}. A band at 1241 cm^{-1} also related to carbonyl groups (Fan et al. 2012) disappeared with the treatment as well.

Urribarrí (2011) treated sugarcane bagasse with liquid ammonia at PDA treatment conditions with increasing ammonia loading. Figure 3.16 shows the FT-IR spectra.

The signal at 1716 cm^{-1} (carbonyl) is blurring as the ammonia/biomass ratio increases indicating the nucleophilic attack by the OH^- ion to the ester linkages between hemicellulose and lignin during the PDA treatment. As a consequence, a band at 1664 cm^{-1} assigned to the carboxylate ion appeared and increased accordingly with the increase in ammonia loading. Results were confirmed by chemical analyses. Little definition of bands at 1420, 1364, and 1316 cm^{-1} indicated the predominance of

cellulose I both in non-treated and in ammonia-treated sugarcane bagasse. This is also confirmed by the fact that the band at 900 cm^{-1} corresponding to the glucosidic C–H deformation with the vibrational contribution of the ring and –OH bending, is not sharp, as it is usually observed for cellulose II (Baldinger et al. 2000).

Sindhu et al. (2011) worked on characterizing FT-IR spectra of native and acid pretreated sugarcane tops. Structural changes in the biomass on acid pretreatment could be detected. After pretreatment with sulfuric acid, the hemicellulose fraction is removed from the raw material and therefore the cellulose content increases. Intensity of the band at 1045 cm^{-1} in the FT-IR spectrum originated from typical absorbance of xylan decreased in the acid pretreated material, which was also reported by Qi et al. (2009) for wheat straw pretreated with alkaline peroxide. On the other hand, absorption peaks at 1122 cm^{-1} were enhanced and band widening occurred at 1316 cm^{-1} (related to CH_2– wagging vibrations in the cellulose and hemicelluloses) and at 3302 cm^{-1} (stretching of H-bonded OH groups).

Table 3.6 shows a summary of the frequencies more relevant to study the effect of pretreatments on the biomass.

3.4 Near Infrared Spectroscopy

3.4.1 Theory

Near infrared spectroscopy (NIR) has been used for the characterization of different forms of agricultural products for more than 30 years (Marten et al. 1989). The advantages are: fast prediction of several parameters, low cost, little or no pretreatment of the samples, and no use of reactants. However, calibration needs to be done using reference methods, with a careful selection of samples (Pasquini 2003; Davies 2005). The calibration samples should cover the variability of the samples to be analyzed.

The boundaries for NIR are: 780–2500 nm (or 12,800–4000 cm^{-1}). A general explanation of this radiation and its interaction with matter is given in Pasquini (2003) and Davies (2005). The spectra of organic molecules in this region are dominated by overtones and combinations of fundamental vibrations involving hydrogen atoms (molecules containing C–H, O–H, N–H, or S–H bonds). The fundamental vibrations produce absorptions in the mid-infrared region (MIR, commonly referred to as FTIR), so the overtones and combinations in the NIR region give qualitative and quantitative information about the composition of a sample. The NIR spectra of organic materials, however, consist of many overlapping bands. Thus, to be able to predict properties of biomass, it is necessary to use multivariate statistics (chemometrics) where the absorbance at several wavelengths is taken into account (Marten et al. 1989; Pasquini 2003; Fearn 2005; Hames et al. 2003). Also, several numerical methods for conversion of spectra are applied, such as first and second derivatives (Varmuza and Filzmoser 2009). A model is thus created from the spectra (or converted spectra) and from properties determined by reference methods, mostly wet chemical analysis (Hames et al. 2003; Stark and Luchter 2005). The most popular

Table 3.6 Frequencies more relevant to observe the changes caused by physicochemical pretreatments

Pretreatment	Biomass	Frequency, cm^{-1}	Interpretation	Reference
Steam explosion	Rice straw	1595, 1510	Increase in lignin due to hemicellulose removal or lignin re-deposition	Ibrahim et al. (2011)
Hydrothermal and wet explosion	Wheat straw	1735	Intensity of the peak (carboxyl groups from uronic acids) is a measure of hemicellulose removal. It decreases.	Kaparaju and Felby (2010)
		1595, 1510	Increase in lignin due to hemicellulose removal. Hydrothermal greater than wet explosion	
Steam hydrolysis (pre-hydrolysis)	Wood chips and sugarcane bagasse	1734	Intensity and sharpness is a measure of carbonyl groups from uronic acids or acetyl groups in the hemicelluloses	Liu et al. (2011); Ren et al. (2007)
Alkaline peroxide	Wheat straw	1045	Intensity decreases due to xylan removal (C–O, C–C stretching or C–OH bending in hemicellulose)	Qi et al. (2009)
Sodium hydroxide	Sugarcane bagasse	1729	Disappeared in treated sample due to hemicellulose removal (carboxyl groups from acetyl and uronic esters)	Rezende et al. (2011)
		1510	Decreased as concentration of the alkali increased due to removal of lignin	
		1263	Decreased due to removal of lignin (guaiacyl derivatives)	
AFEX	Hardwoods and corn stover	1664	Appearance of this band is due to amide groups formed when the ammonia ion breaks ester linkages	Balan et al. (2009)
		1740	Decrease or disappearance with treatment (cleavage of ester linkages)	
	Coastal bermuda grass	1595 and 1510	Increase in intensity due to lignin re-deposition	Lee et al. (2009)
	Oil palm empty fruit bunch fiber	1606	Appearance of this band is due to amide groups formed when the ammonia ion breaks ester linkages	Abdul et al. (2016)

(continued)

Table 3.6 (continued)

Pretreatment	Biomass	Frequency, cm^{-1}	Interpretation	Reference
		1738	Decrease or disappearance with treatment (cleavage of ester linkages)	
		1241	Disappearance with treatment (cleavage of ester linkages)	
PDA ammonia treatment	Sugarcane bagasse	1716	Carbonyl band blurs as the ammonia/biomass ratio increases indicating the nucleophilic attack by the OH^- ion to the ester linkages between hemicellulose and lignin	Urribarrí (2011)
		1664	Appearance and increase with the increase in ammonia loading	
		1420, 1364 and 1316	Little definition of these bands indicates predominance of cellulose I	
		900	If band is not sharp cellulose I predominates	
Dilute acid	Sugarcane tops	1045	Intensity decreases due to xylan removal (C–O, C–C stretching or C–OH bending in hemicellulose)	Sindhu et al. (2011)
		1122	Enhancement of band due to increase in cellulose concentration caused by hemicellulose removal	
		1316 and 3302	Widening due to increase in cellulose concentration caused by hemicellulose removal	

algorithm is known as Partial Least Squares (PLS). PLS is able to use the information from the whole spectrum (Varmuza and Filzmoser 2009). Thus, rapid data acquisition with spectrometers, combined with data processing with computers, is able to give information in real time about the composition of biomass materials.

The main multivariate statistical methods used in Chemometrics are Principal Component Analysis (PCA) and Partial Least Squares (PLS). PCA is considered "the mother of all methods in multivariate data analysis" (Varmuza and Filzmoser 2009). It is a method useful for exploratory data analysis. The main purpose of PCA is dimensionality reduction. Given a matrix of data (usually with objects in rows and parameters in columns), a new set of coordinates is computed which are orthogonal and where most of the variance of the data is explained with a few "components" that are orthog-

onal. Thus, a graphic representation is frequently possible with only two or three components, and objects (samples) may be separated into classes. PLS, also known as *projection to latent structures*, is a method to relate a matrix X to a vector y (Varmuza and Filzmoser 2009; Geladi and Kowalski 1986). It is used for the creation of predictive models. Thus, if X is, for example, a set of infrared spectra, and y contains the values of a parameter (for example, concentration of a component) for the objects (samples) a PLS model may be created by calculation of a regression vector β.

$$X\beta = y \tag{3.6}$$

Thus, the values of the parameter y may be predicted for new samples from their infrared spectra. Details of the algorithms are given in Varmuza and Filzmoser (2009) and Geladi and Kowalski (1986). Biomass variation and number of samples are key components and play an important part.

There is a variety of instrument types available for NIR spectroscopy, including dispersive and Fourier transform spectrometers and also, different modes of measurement, including transmittance and diffuse reflectance, are available (Hames et al. 2003; Pasquini 2003). Reflectance is the most useful method for solid biomass analysis (Liu et al. 2010; Xu et al. 2013).

The use of fiber optics probes (certain quartz and glasses are transparent in the NIR region) gives an important technological advantage to NIR spectroscopy, since the probes might be situated on-line at several points in the production process (Hames et al. 2003).

3.4.2 NIR Applications

New methods based on dispersive NIR spectroscopy and PLS were developed by Hames et al. (2003) for the rapid analysis of corn stover and intermediates derived from a dilute-acid pretreatment process—corn stover was selected as a model feedstock for the U.S. Dept. of Energy's enzyme sugar platform work. NIR spectra from 400 to 2500 nm were obtained. Hundreds of samples may be analyzed in 1 day by the NIR/PLS methods. Several components: glucan, xylan, lignin, protein, acetyl, and arabinan could be determined for corn stover; and glucan, xylan, lignin, protein, and ash for pretreated corn stover. Thus, the potential value of bulk feedstocks for ethanol production may be determined and process conditions optimized, by these fast, economical methods.

A model for analyzing both of the two most important biomass feedstocks, corn stover and switchgrass, was developed by Liu et al. (2010) using FT-NIR and reference wet chemistry procedures. The entire spectrum from 10,000 to 4000 cm^{-1} was utilized for the calibration. Thus, glucan, xylan, galactan, arabinan, mannan, lignin, and ash contents may be predicted using FT-NIR. The broad-based model was checked by cross-validation. An independent validation was performed with corn stover, switchgrass, and wheat straw samples. The authors concluded that this "broad-based" model is promising for future chemical composition prediction of biomass species.

A mini-review of FT-IR and NIR methods for analysis of lignocellulosic biomass was published by Xu et al. (2013). Most of the work summarized refers to compositional analysis using the NIR region and chemometric methods, mainly PLS. References to determinations of lignin, glucan, and xylan in various types of biomass and with different wavelength intervals are given.

Naik et al. (2010) characterized various types of Canadian biomass (wheat straw, barley straw, flax straw, timothy grass, and pinewood) by several techniques (static bomb calorimeter, XRD, TGA, ICP-MS, CHNSO, FT-IR, and FT-NIR). The proportions of extractives (hexane, ethanol, and water extracts), cellulose, hemicelluloses, and lignin were determined. The FT-NIR spectra between 10,000 and 4000 cm^{-1} were shown and bands assigned. The authors concluded that these biomasses may meet the demands of second-generation biofuels.

Cozzolino et al. (2000) used dispersive visible-NIR spectroscopy for prediction of properties of whole maize plants, for use in breeding programs and for farmer advice. Good predictions were obtained for crude protein, acid detergent fiber, neutral detergent fiber, in vitro organic matter digestibility, and ash. The authors concluded that NIR spectroscopy may be an alternative technique when a large number of samples must be analyzed.

Jin and Chen (2007) studied the prediction of properties of rice straw from NIR spectra, 7500–4100 cm^{-1}. Total ash, insoluble ash, moisture, cellulose, hemicelluloses, and Klason lignin content were studied. Cellulose and hemicellulose were predicted more successfully than total ash and insoluble ash contents. The authors concluded that NIR calibration models might be useful for the quality determination of rice straw samples.

Fitoussi et al. (2011) demonstrated the feasibility of using NIR and MIR to estimate the composition of biomass residues. Prediction models were constructed for ammonia-pretreated sugarcane bagasse, cassava leaves, and cassava stems. Moisture, cellulose, hemicellulose, lignin, extractives, and ash contents were determined.

Kelley et al. (2004) analyzed a wide variety of agricultural samples (Agava, banana, cotton, hemp, kenaf, sugarcane, and others, with various pretreatments) using visible/near infrared spectroscopy (500–2400 nm) and pyrolysis molecular beam mass spectroscopy. It was found that good predictions for three major components, lignin, glucose, and xylose, could be obtained with both spectroscopic techniques.

Table 3.7 summarizes selected applications of NIR with chemometrics on lignocellulosic materials. It can be observed that very high correlations have been found for key compositional variables of biomass.

3.4.3 Recent Advances

One the most recent developments are the use of a high-throughput technique for NIR. High-throughput analytical techniques are necessary for the fast screening of biomass feedstocks. Lupoi et al. (2014b) reviewed the use of various analytical techniques, including near infrared, mid-infrared, and Raman spectroscopy, for the

Table 3.7 Selected applications of NIR with chemometrics on biomass

Biomass	Wavelength region (λ, nm)	R^2 of cross-validation	Modeling method	Reference
Whole maize plants	–	–	–	Cozzolino et al. (2000)
CP	400–2500	0.96	Modified PLS	–
Hem	400–2500	0.72	Modified PLS	–
ADF	400–2500	0.98	Modified PLS	–
NDF	400–2500	0.96	Modified PLS	–
Various agricultural fibers	–	–	–	Kelley et al. (2004)
Lignin	500–2400	0.77	PLS	–
Glucose	500–2400	0.88	PLS	–
Xylose	500–2400	0.76	PLS	–
Rice straw	–	–	–	Jin and Chen (2007)
Klason lignin	1333–2439	0.89	PLS	–
Cellulose	1299–2439	0.93	PLS	–
Hemicellulose	1299–2439	0.91	PLS	–
Switchgrass + corn stover	–	–	–	Liu et al. (2010)
Glucan	1000–2500	0.94	PLS	–
Xylan	1000–2500	0.88	PLS	–
Galactan	1000–2500	0.77	PLS	–
Eucalypt and Acacia	–	–	–	Lupoi et al. (2014a)
Lignin S/G	1100–2235	0.74	PLS	

The respective wavenumber (cm^{-1}) can be determined by $1\times10^7/\lambda$

high-throughput assessment of lignocellulosic biomass as a renewable source of fuel. The authors remarked that these techniques depend on the calibration with standard methods to produce chemometric models, and concluded that spectroscopic applications show promise for attaining large reductions in time and costs of analysis.

Xiao et al. (2014) reviewed the use of two high-throughput techniques: near-infrared spectroscopy and pyrolysis molecular beam mass spectrometry, for classification and prediction of chemical properties of biomass samples. The multivariate statistical techniques PCA and PLS were applied. The authors concluded that NIR and Py-mbms were efficient tools for studying the characteristics of biomass samples with minimal sample preparation.

The lignin syringyl/guaiacyl (S/G) ratio is important for understanding the role of lignin structure in depolymerization of biomass. Thus, Lupoi et al. (2014a) compared mid-infrared, near-infrared, and Raman spectroscopies for prediction of S/G ratios using pyrolysis molecular beam mass spectrometry as the reference method. Robust models could be constructed with PLS (partial least squares).

Corgié et al. (2011) studied the enzymatic hydrolysis of bacterial microcrystalline cellulose by quantitative high-throughput FT-IR spectroscopy (QHTFTIR). The concentration of cellulose was directly correlated to the absorbance of the cellulose signals. Crystallinity indexes (Lateral Order Index (LOI), Total Crystallinity Index, Hydrogen Bonding Index), allomorphic composition, and conversion of specific atomic bonds were extracted from the spectral data. Thus, a dynamic picture of the role of the cellulases in the hydrolysis was shown.

References

Abdul PM, Jahim JM, Harun S, Markom M, Lutpi NA, Hassan O, Balan V, Dale BE, Mohd MT (2016) Effects of changes in chemical and structural characteristic of ammonia fibre expansion (AFEX) pretreated oil palm empty fruit bunch fibre on enzymatic saccharification and fermentability for biohydrogen. Bioresource Technol 211:200–208

Alciaturi C, Escobar ME, Vallejo R (1996) Prediction of coal properties by derivative DRIFT spectroscopy. Fuel 75(4):491–499

Balan V, Sousa LC, Chundawat SPS, Marshall D, Sharma LN, Chambliss CK, Dale BE (2009) Enzymatic digestibility and pretreatment degradation products of AFEX-treated hardwoods (Populus nigra). Biotechnol Prog 25(2):365–375

Baldinger T, Moosbauer J, Sixta H (2000) Supermolecular structure of cellulosic materials by Fourier transform infrared spectroscopy (FT-IR) calibrated by WAXS and ^{13}C-NMR. Lenzing Berichte 79:15–17

Boerjan W, Ralph J, Baucher M (2003) Lignin biosynthesis. Annu Rev Plant Biol 54:519–546

Coates J (2000) Interpretation of infrared spectra, a practical approach. In: Meyers RA (ed) Encyclopedia of Analytical Chemistry. John Wiley & Sons, New York, pp 10815–10837

Cooley TW, Tukey TW (1965) An algorithm for the machine calculation of complex Fourier series. Mathematics of Computation 19:297–306

Corgié SC, Smith HM, Walker LP (2011) Enzymatic transformations of cellulose assessed by quantitative high throughput fourier transform infrared spectroscopy (QHTFTIR). Biotechnol Bioeng 108(7):1509–1520

Cozzolino D, Fassio A, Gimenez A (2000) The use of near-infrared reflectance spectroscopy (NIRS) to predict the composition of whole maize plants. J Sci Food Agric 81:142–146

Davies AMC (2005) An introduction to near infrared spectroscopy. NIR News 16(7):9–11

Doner LM, Hicks K (1997) Isolation of hemicellulose from corn fibre by alkaline hydrogen peroxide extraction. Cereal Chem 74:176–181

Donohoe BS, Tucker MP, Davis M, Decker SR, Himmel ME, Vinzant TB (2007) Tracking lignin coalescence and migration through plant cell walls during pretreatment. Abstracts of the 29th symposium on biotechnology for fuels and chemicals. Denver, CO, 29 Apr–2 May. 5B-01, p 67

Duchesne I, Hult EL, Molin U, Daniel G, Iversen T, Lennholm H (2001) The influence of hemicellulose on fibril aggregation of kraft pulp fibres as revealed by FE-SEM and CP/MAS ^{13}C-NMR. Cellulose 8:103–111

Fan M, Dai D, Huang B (2012) Fourier transform infrared spectroscopy for natural fibres. In: Salih S (ed) Fourier transform – materials analysis. InTech, Dublin, http://www.intechopen.com/books/fourier-transform-materials-analysis/fourier-transform-infrared-spectroscopy-for-natural-fibres

Faneite A (2010) Cinética del secado de materiales lignocelulósicos tratados y no tratados con presurización y despresurización (PDA) (Drying kinetics of lignocellulosic materials untreated and treated with pressurization and depressurization with ammonia (PDA)). Tesis. Magister Scientiarum en Ingeniería Química. Universidad del Zulia, Maracaibo, Venezuela

Faneite A, Ferrer A, Aiello-Mazzarri C, Villegas J, Gnansounou E (2011) Interaction between chemical composition, microcrystalline structure and morphology of the most important agricultural byproducts in the northern of South America, and drying kinetics. In: Proceedings of the XIX international symposium of alcohol fuels, Verona, Italy, Oct 2011, p 1–6

Fearn T (2005) Chemometrics: an enabling tool for NIR. NIR News 16(7):17–19

Ferrer A, Sulbarán-de-Ferrer B, Byers FM, Dale BE, Aiello C (1997) Aumento y aprovechamiento del potencial nutritivo de forrajes y residuos mediante procesos amoniacales y enzimáticos para alimentación de animales rumiantes y monogástricos (Enhancing the nutritional potential of forages and residues by ammonia and enzymatic processes to produce feeds for ruminant and monogastric animals). In: Primer Encuentro de Productores Agrícolas con la Biotecnología. Fundacite-Zulia. J. B. Editores. Maracaibo. p 171–194

Ferrer A, Byers FM, Sulbarán-de-Ferrer B, Dale BE, Aiello C (2000) Optimizing ammonia pressurization/depressurization processing conditions to enhance enzymatic susceptibility of dwarf elephant grass. Appl Biochem Biotechnol 84(86):163–179

Ferrer A, Ríos J, Urribarrí L (2013) Biorefinación de la *Lemna obscura* del Lago de Maracaibo. Parte II Producción de alimentos para animales y bioetanol (Biorefining of *Lemna obscura* from Lake Maracaibo. Part II. Production of animal feeds and bioethanol. In: Boves M, Rincón JE (eds) Eutrofización del Lago de Maracaibo: Pasado. Presente y perspectivas. Universidad del Zulia, Zulia, pp 257–286

Festucci-Buselli R, Otoni W, Joshi C (2007) Structure, organization, and functions of cellulose synthase complexes in higher plants. Review. Braz J Plant Physiol 19(1):1–13

Fitoussi C, Chiesa S, Villegas J, Gnansounou E, Alciaturi C, Ferrer A (2011) Compositional analysis of biomass feedstocks via near infrared spectroscopy for second-generation bioethanol production. Paper presented at the 33rd symposium of biotechnology for fuels and chemicals. Seattle, 2–5 May

Gallezot P (2012) Conversion of biomass to selected chemical products. Chem Soc Rev 41:1538–1558

Geladi P, Kowalski BR (1986) Partial least squares regression: a tutorial. Anal Chim Acta 185:1–17

Goering H, Van Soest P (1970) Forage fiber analyses (apparatus, reactants, procedures, and some applications), Agriculture handbook n° 379. ARS-USDA, Washington, DC

Gollapalli LE, Dale BE, Rivers DM (2002) Predicting digestibility of ammonia fiber explosion (AFEX)-treated rice straw. Appl Biochem Biotechnol 98(100):23–35

Griffiths PR, De Haseth JA (2007) Fourier transform infrared spectrometry, 2nd edn. John Wiley & Sons, New York

Hames BR, Thomas SR, Sluiter AD, Roth CJ, Templeton DW (2003) Rapid biomass analysis. Appl Biochem Biotechnol 105(108):5–16

Hegde RR, Kamath MG, Dahiya A (2004) Polymer crystallinity Nonwovens science and technology II. Department of Materials Science and Engineering, University of Tennessee, Knoxville, TN, http://www.engr.utk.edu/mse/Textiles/Polymer%20Crystallinity.htm. Accessed 30 Mar 2016

Himmelsbach DS, Khalili S, Akin DE (2002) The use of FT-IR microspectroscopic mapping to study the effects of enzymatic retting of flax (*Linum usitatissium* L.) stems. J Sci Food Agric 82:685–696

Ibrahim MM, El-Zawawy WK, Abdel-Fattah YR, Soliman NA, Agblevor FA (2011) Comparison of alkaline pulping with steam explosion for glucose production from rice straw. Carbohyd Polym 83:720–726

Jayme V, Knolle H (1964) The empirical x-ray determination of the degree of crystallinity of cellulosic material. Papier 18:249–255

Jin S, Chen H (2007) Near-infrared analysis of the chemical composition of rice straw. Ind Crop Prod 26:207–211

Kacurákova M, Capeka P, Sasinkova V, Wellnerb N, Ebringerova A (2000) FT-IR study of plant cell wall model compounds: pectic polysaccharides and hemicelluloses. Carbohyd Polym 43:195–203

Kaparaju P, Felby C (2010) Characterization of lignin during oxidative and hydrothermal pretreatment processes of wheat straw and corn stover. Bioresource Technol 101:175–3181

Kelley SS, Rowell RM, Davis M, Jurich CK, Ibach R (2004) Rapid analysis of the chemical composition of agricultural fibers using near infrared spectroscopy and pyrolysis molecular beam mass spectrometry". Biomass Bioenerg 27:77–88

Kemp W (1991) Organic Spectroscopy, 3rd edn. Palgrave Macmillan, London

Klemm D, Philipp B, Heinze T, Heinze U, Wagenknecht W (1998) Comprehensive cellulose chemistry, vol l. Fundamentals and analytical methods. Weinheim, Wiley-VCH Verlag GmbH, pp 14–18, 48–50

Krässig H (1993) Cellulose structure, accessibility and reactivity. Polymer monographs, vol 11. Gordon and Breach Science Publishers, Amsterdam, pp 12–16, 45–48

Kristensen JB, Thygesen LG, Felby C, Jørgensen H, Elder T (2008) Cell wall structural changes in wheat straw pretreated for bioethanol production. Biotechnology Biofuels 1(5):1–9

Landis C (1971) Graphitization of dispersed carbonaceous materials in metamorphic rocks. Lithos 14:215–224

Langan P, Nishiyama Y, Chanzy H (2001) X-ray structure of mercerized cellulose II at 1 Å resolution. Biomacromolecules 2:410–416

Lee JM, Shi J, Venditti RA, Jameel H (2009) Autohydrolysis pretreatment of coastal Bermuda grass for increased enzyme hydrolysis. Bioresource Technol 100:6434–6441

Lee JM, Hasan J, Venditti RA (2010) A comparison of the autohydrolysis and ammonia fiber explosion (AFEX) pretreatments on the subsequent enzymatic hydrolysis of coastal Bermuda grass. Bioresource Technol 101:5449–5458

Lennholm H, Iversen T (1995) The effects of laboratory beating on cellulose structure. Nordic Pulp Paper Res J 10:104–109

Li J, Gellerstedt G, Toven K (2009) Steam explosion lignins: their extraction, structure and potential as feedstock for biodiesel and chemicals. Bioresource Technol 100:2556–2561

Liu L, Ye XP, Womac AR, Sokhansanj S (2010) Variability of biomass chemical composition and rapid analysis using FT-NIR techniques. Carbohyd Polym 81:820–829

Liu Z, Fatehi P, Jahan MS, Ni Y (2011) Separation of lignocellulosic materials by combined processes of pre-hydrolysis and ethanol extraction. Bioresource Technol 102:1264–1269

Lupoi JS, Singh S, Davis M, Lee DJ, Shepherd M, Simmons BA, Henry RJ (2014a) High-throughput prediction of eucalypt lignin syringyl/guaiacyl content using multivariate analysis: a comparison between mid-infrared, near-infrared, and Raman spectroscopies for model development. Biotechnol Biofuels 7:93 (open Access number)

Lupoi JS, Singh S, Simmons BA, Henry RJ (2014b) Assessment of lignocellulosic biomass using analytical spectroscopy: an evolution to high throughput techniques. Bioenerg Res 7:1–23

Mandal A, Chakrabarty D (2011) Isolation of nanocellulose from waste sugarcane bagasse (SCB) and its characterization. Carbohyd Polyms 86:1291–1299

Marchessault R, Sarko A (1968) X-Ray structure of polysaccharides. Adv Carbohyd Chem Biochem 22:429–449

Marten G, Shenk J, Barton III F (1989) Editors "near infrared reflectance spectroscopy (NIRS): analysis of forage quality". USDA Agriculture research service handbook, n° 643

Miao CW, Hamad WY (2013) Cellulose reinforced polymer composites and nanocomposites: a critical review. Cellulose 20:2221–2262

Montiel M, Rodriguez D (2008) Optimización de las condiciones de tratamiento PDA del follaje de yuca para la obtención de concentrados protéicos (Optimizing conditions of PDA treatment of cassava foliage to obtain protein concentrates). Tesis. Ingeniería Química. Universidad Rafael Urdaneta, Maracaibo, Venezuela

Naik S, Goud VV, Rout PK, Jacobson K, Dalai AK (2010) Characterization of Canadian biomass for alternative renewable biofuel. Renew Energ 35:1624–1631

Nelson M, O'Connor R (1964) Relation of certain infrared bands to cellulose crystallinity and crystal lattice type. Part I. Spectra of lattice type I, II, III and amorphus cellulose. J Appl Polym Sci 9:1311–1324

Ozaki Y (2012) Near-infrared spectroscopy—its versatility in analytical chemistry. Anal Sci 28:545–563

Pasquini C (2003) Near infrared spectroscopy: fundamentals, practical aspects and analytical applications. J Braz Chem Soc 14(2):198–219

Peters J (2003) Caracterización de las fracciones protéicas de pasto elefante enano tratado con amoníaco (*Pennisetum pupureum Schum. cv. Mott*) (Characterization of the protein fractions of dwarf elephant grass treated with ammonia (*Pennisetum pupureum* Schum. Cv. Mott). Tesis. Licenciado en Química, Universidad del Zulia, Maracaibo

Poletto M, Pistor V, Zeni M, Zattera AJ (2011) Crystalline properties and decomposition kinetics of cellulose fibers in wood pulp obtained by two pulping processes. Polym Degrad Stabil 96:679–685

Poletto M, Pistor V, Campomanes RM, Zattera AJ (2012) Materials produced from plant biomass. Part II: evaluation of crystallinity and degradation kinetics of cellulose. Mater Res 15(3):421–427

Qi B, Chen X, Shen F, Su Y, Wan Y (2009) Optimization of enzymatic hydrolysis of wheat straw pretreated by alkaline peroxide using response surface methodology. Ind Eng Chem Res 48:7346–7353

Ren JL, Sun RC, Liu CF, Lin L, He BH (2007) Synthesis and characterization of novel cationic SCB hemicelluloses with a low degree of substitution. Carbohyd Polym 67:347–357

Rezende CA, de Lima MA, Maziero P, deAzevedo ER, Garcia W, Polikarpov I (2011) Chemical and morphological characterization of sugarcane bagasse submitted to a delignification process for enhanced enzymatic digestibility. Biotechnol Biofuels 4:54. doi:10.1186/17546834454

Ríos J (2009) Extracción, precipitación y caracterización de las proteínas de la lenteja acuática (*Lemna obscura*) tratada con amoníaco (Extraction, precipitation and characterization of proteins from duckweed (*Lemna obscura*) treated with ammonia). Tesis. Licenciado en Química. Universidad del Zulia, Maracaibo, Venezuela

Roncero M (2001) Obtención de una secuencia "TCF" con la aplicación de ozono y enzimas, para el blanqueo de pastas madereras y de origen agrícola. Optimización de la etapa Z. Análisis de los efectos en la fibra celulósica y sus componentes (Getting a sequence "TCF" with the application of ozone and enzymes for bleaching wood and agricultural pulps. Optimization of stage Z. Analysis of the effects on the cellulosic fiber and its components). Tesis doctoral, Departamento de Ingeniería Textil y Papelera, Universidad Politécnica de Cataluña, España

Sannigrahi P, Miller SJ, Rgawskas AJ (2010) Effects of organosolv pretreatment and enzymatic hydrolysis on cellulose structure and crystallinity in Loblolly pine. Carbohydr Res 345:965–970

Schmidt AS, Thomsen AB (1998) Optimization of wet oxidation pre-treatment of wheat straw. Bioresource Technol 64:139–151

Segal L, Creely J, Martin A, Conrad C (1959) An empirical method for estimating the degree of crystallinity of native cellulose using the X-ray diffractometer. Text Res J 29:786–794

Sills DL, Gossett JM (2012) Using FT-IR to predict saccharification from enzymatic hydrolysis of alkali-pretreated biomasses. Biotechnol Bioeng 109:353–362

Sindhu R, Kuttiraja M, Binod P, Janu KU, Sukumaran RK, Pandey A (2011) Dilute acid pretreatment and enzymatic saccharification of sugarcane tops for bioethanol production. Bioresource Technol 102:10915–10921

Siqueira G, Bras J, Dufresne A (2010) Cellulosic bionanocomposites: a review of preparation, properties and applications. Polymers 2:728–765

Socrates G (2001) Infrared and Raman characteristic group frequencies: tables and charts. John Wiley & Sons, New York

Stark E, Luchter K (2005) NIR instrumentation technology. NIR News 16(7):13–16
Sun RC, Tomkinson J, Ma PL, Liang SF (2000) Comparative study of hemicelluloses from rice straw by alkali and hydrogen peroxide treatments. Carbohyd Polym 42:111–122
Sun RC, Sun XF, Wang SQ, Zhu W, Wang XW (2002) Ester and ether linkages between hydroxycinnamic acids and lignins from wheat, rice, rye, and barley straws, maize stems, and fast-growing poplar wood. Ind Crop Prod 15:179–188
Sun XF, Sun RC, Fowler P, Baird MS (2004a) Isolation and characterization of cellulose obtained by a two-stage treatment with organosolv and cyanamide activated hydrogen peroxide from wheat straw. Carbohyd Polym 55:379–391
Sun JX, Sun XF, Zhao H, Sun RC (2004b) Isolation and characterization of cellulose from sugarcane bagasse. Polym Degrad Stabil 84:331–339
Sun XF, Xu F, Sun RC, Fowler P, Baird MS (2005) Characteristics of degraded cellulose obtained from steam-exploded wheat straw. Carbohyd Res 340:97–106
Therdthai N, Zhou W (2009) Characterization of microwave vacuum drying and hot air drying of mint leaves (*Mentha cordifolia* Opiz ex Fresen). J Food Eng 91(3):482–489
Uraki Y, Koda K (2015) Utilization of wood cell wall components. Review. J Wood Sci 61(5):447–454
Urribarrí L (2011) Sacarificación y fermentación simultánea de bagazo de caña de azúcar tratado con amoníaco (Simultaneous saccharification and fermentation of sugarcane bagasse treated with ammonia). PhD Dissertation in Chemistry. University of Zulia, Maracaibo, Venezuela
Urribarrí L, Chacón D, González O, Ferrer A (2009) Protein extraction and enzymatic hydrolysis of ammonia-treated cassava leaves (*Manihot esculenta* Crantz). Appl Biochem Biotechnol 153:94–103
Urribarrí L, Ferrer A, Aiello C, Rivera J (2013) Bioethanol from sugarcane bagasse. In: Proceedings of the 2nd Iberoamerican congress on biorefineries, Jaén, España, Apr 2013, p 1–6
Varmuza K, Filzmoser P (2009) Introduction to multivariate statistical analysis in chemometrics. CRC Press, Boca Raton, FL
Weise U (1998) Hornification – mechanisms and a terminology. Paper Timber 80(2):110–114
Xiao B, Sun XF, Sun RC (2001) Chemical, structural, and thermal characterizations of alkali-soluble lignins and hemicelluloses, and cellulose from maize stems, rye straw, and rice straw. Polym Degrad Stabil 74:307–319
Xiao L, Wei H, Himmel ME, Jameel H, Kelley SS (2014) NIR and Py-mbms coupled with multivariate data analysis as a high-throughput biomass characterization technique: a review. Front Plant Sci 5:388, (open access number) http://journal.frontiersin.org/article/10.3389/fpls.2014.00388/full
Xu F, Yu J, Tesso T, Dowell F, Wang D (2013) Qualitative and quantitative analysis of lignocellulosic biomass using infrared techniques: a mini-review. Appl Energ 104:801–809
Yue Y, Han J, Han G, Zhang Q, French AD, Wu Q (2015) Characterization of cellulose I/II hybrid fibers isolated from energycane bagasse during the delignification process: morphology, crystallinity and percentage estimation. Carbohyd Polyms 133:438–447

Chapter 4
Molecular Properties and Functions of Humic Substances and Humic-Like Substances (HULIS) from Biomass and Their Transformation Products

Davide Savy, Pierluigi Mazzei, Antonio Nebbioso, Marios Drosos, Assunta Nuzzo, Vincenza Cozzolino, Riccardo Spaccini, and Alessandro Piccolo

Abstract Agricultural and biorefinery byproducts should be regarded as important sources of chemicals and materials, instead of being disposed or burnt. Humic substances (HS) and humic-like substances (HULIS) isolated by such materials may be employed as plant biostimulants, due to their surprising bioactivity on plant development, either after their direct extraction from such byproducts or after composting them. In order to shed light on both the biological activity of HS and HULIS on plant physiology and on soil carbon dynamics, a number of analytical chemical techniques have been employed, thus, providing a detailed insight on their molecular nature. This chapter is intended to provide a comprehensive overview of the more advanced chemical techniques applied in the chemical characterization of HS and HULIS structure, such as GC-MS, NMR, HPSEC, EPR and thermal analyses. Each of these tools provides different but incomplete information on HS and HULIS molecular composition, due to both the intrinsic limitation of each technique and the large molecular heterogeneity and structural complexity of HS and HULIS. Thus, in order to elucidate the chemical nature of such substrates, the various analytical tools should be always exploited concomitantly and critically discussed, thus, offering a comprehensive understanding of HS and HULIS at a molecular level. Achieving this purpose will also allow to efficaciously exploit HS and HULIS as plant biostimulants in sustainable agriculture and/or biomass-based material chemistry.

Keywords Biomass for energy • Lignocellulosic residues • Humic substances • Humic-like lignins • Molecular and spectroscopic characterization

D. Savy • P. Mazzei • A. Nebbioso • M. Drosos • A. Nuzzo • V. Cozzolino
R. Spaccini • A. Piccolo (✉)
Centro Interdipartimentale di Ricerca sulla Risonanza Magnetica Nucleare per l'Ambiente, l'Agro-Alimentare ed i Nuovi Materiali (CERMANU),
Via Università 100, 80055 Portici, Italy
e-mail: alessandro.piccolo@unina.it

S. Vaz Jr. (ed.), *Analytical Techniques and Methods for Biomass*,
DOI 10.1007/978-3-319-41414-0_4

4.1 Introduction

Wastes and byproducts from agricultural and biorefinery productions may act as important sources of chemicals and materials. Large scientific efforts are devoted to find more economically convenient and environmentally friendly methods to produce fine chemicals from these heterogeneous substrates (Lin et al. 2013). The alternative is the disposal of wastes, often resulting in serious environmental concerns (Abu-Rukah and Al-Kofahi 2001). Biorefinery wastes may be employed as starters for the synthesis of a variety of products, such as biopolymers, antioxidants, or various fine chemicals (Lin et al. 2013 and reference therein). Moreover, such substrates may be either exploited directly as plant biostimulants (Popa et al. 2008) or composted (Spaccini and Piccolo 2009), and their humic-like substances (HULIS) extracted and used as biostimulants. Humic substances (HS), as commonly found in the environment, are defined as supramolecular associations of relatively small and heterogeneous molecules, which are held together by hydrophobic forces (van der Waals, π-π, C-π) and/or hydrogen bonds (Piccolo et al. 1996; Piccolo 2002). Despite the complexity of the humic superstructures, their molecular composition can be reached by applying the recently developed Humeomics (Nebbioso and Piccolo 2011, 2012; Nebbioso et al. 2015). Both HS and HULIS are extracted from environmental samples or composted lignocellulosic biomasses, respectively, by alkaline solution and then precipitated at acidic pH (Piccolo 1988). However, HS and HULIS may not have the same molecular composition due to the different time scale of their formation, being the latter rapidly stabilized in composting piles (Spaccini and Piccolo 2007) or poorly transformed in biorefinery and paper mills (Savy et al. 2015b).

Biostimulations by HS and HULIS provide benefits to plant growth, development and/or stress response (Canellas and Olivares 2014), while adding composted biomass to soil may result in increased soil fertility and crop production (Marchesini et al. 1988; Abbasi et al. 2002), enhanced availability of macronutrients (Weber et al. 2007), and improved soil structural stability and porosity (Bronick and Lal 2005; Spaccini and Piccolo 2013). The comprehension of the still unclear physiological mechanisms through which HS and HULIS affect plant development and soil organic matter stabilization needs to ensure an advanced knowledge of the chemical and structural compositions of these substrates. A number of analytical techniques have been employed to reach this purpose, the most useful are: nuclear magnetic resonance (NMR) spectroscopy, electron paramagnetic resonance (EPR) spectroscopy, gas-chromatography-mass spectrometry (GC-MS), high-performance liquid chromatography (HPLC) and thermal analyses. Owing to the intrinsic molecular heterogeneity and structural complexity of HS and HULIS, and the different information provided by a single technique, these analytical tools should be applied in combination. For example, GC-MS is essential to characterize humic matter at molecular level, while HPSEC provides information on its aggregation state and molecular size. Thermodynamic stability may be studied only by thermal analyses, while the content of paramagnetic species (free electrons, free radicals) can only be quantified by ESR spectroscopy. The molecular structure and reactivity of HS and

HULIS can be successfully studied through various NMR experiments. Hence, the multiple use of the techniques may help to unravel the molecular nature of HS and HULIS and their results critically combined. In this chapter, we will illustrate how the analytical techniques can be applied to study the chemical and structural composition of humic matter from different lignocellulosic biomasses.

4.2 Gas Chromatography–Mass Spectrometry

The HS and HULIS have been unsuccessfully characterized by direct gas chromatography techniques coupled to mass spectrometry, since the heterogeneity and complexity of their molecular composition allow detection by GC-MS of only a small percentage. More information on their molecular structure was obtained by applying degradative reactions (Hayes et al. 1972), but at the cost of loosing the pristine structure of humic molecules. More profitable for the study of HS and HULIS was the pyrolysis and thermochemolysis techniques followed by GC-MS, that has been largely employed in recent times (Challinor 2001). GC-MS was also employed to characterize lignins alone or in biomasses following a degradative technique called derivatization followed by reductive cleavage (DFRC) (Lu and Ralph 1997a).

4.2.1 Pyrolysis and Thermochemolysis

Pyrolysis is the thermochemical degradation of an organic material in the absence of oxygen. Due to easiness of execution and modesty of sample requirement (Amir et al. 2006), pyrolysis is applied not only to characterize the molecular structure of HS (Spaccini and Piccolo 2009), but also in forensic science (DeForest et al. 1994), petroleum geochemistry (Larter and Horsfield 1993), or natural organic polymers chemistry (Moldoveanu 1998). Pyrolysis-GC-MS (Py-GC-MS) allowed to identify up to 322 compounds in different soil humic fractions and recognize that aliphatic biopolymers similar to those in plant cuticles were present in a purified humic acid (HA) (Saiz-Jimenez 1996). The type and amount of identified compounds in HA depend on the pyrolysis temperature. In fact, at 358 °C, only carbohydrates, polysaccharides, and, to a lower extent, lignin molecules are pyrolysed, while phenols, dialkylphtalates, fatty acids and alkanes simply evaporate. Conversely, polysaccharide and lignin-rich HS may be successfully pyrolysed at 510 °C (Saiz-Jimenez 1996). Higher temperatures may be needed in order to obtain more in-depth information, such as those required from purified HA fractions containing refractory materials (Janoš 2003). In spite of the large diffusion and usefulness of pyrolysis in humus chemistry, Py-GC-MS is considered a "two-edge sword", since the resulting pyrograms are easily subjected to misinterpretation and/or errors when analysing the fragmentation pattern. Moreover, analytical pyrolysis often induces dramatic changes in the chemical structure of pyrolysed molecules, due to secondary reactions, such as dehydration and cyclization in

the case of polysaccharides and proteins. Another pitfall of this technique regards the decarboxylation reactions of fatty acids, that leads to formation of alkanes and alkenes (Saiz-Jimenez 1996). This explains the significantly lower amount of acidic compounds found by Py-GC-MS than by integration of signals in NMR spectra of the same humic matter (Spaccini and Piccolo 2007).

The above limitations were overcome by employing a combined pyrolysis/methylation technique with tetramethylammonium hydroxide (TMAH) (Challinor 1989). This technique involves the in situ methylation of acids and alcohols under pyrolysis into their GC-MS detectable methyl ethers and esters. However, this pyrolysis/methylation should be regarded more as a thermally assisted chemolysis, rather than a proper pyrolysis (Challinor 2001). The methylation of pre-existing carboxyl and hydroxyl groups follows the pathway illustrated in Scheme 4.1a, with hydroxide anions (OH^-) extracting a hydrogen from alcoholic or carboxyl groups, with the consequent formation of an organic tetramethylammonium salt and water. Then, after salt disproportion, a methylated compound and a trimethylamine are formed (Kossa et al. 1979). The alkylation of ether and ester bonds proceeds via their hydrolysis by the OH^- ion, with the production of an alcohol and an anion (Scheme 4.1b—reaction I). Both these two compounds react with the alkyl ammonium ion yielding the corresponding salts, which then dissociate into the methyl derivatives and the alkylamine (Scheme 4.1b—reactions II and III). However, homolytic cleavage of C-C bonds is also likely to occur in the TMAH-assisted pyrolysis (Challinor 2001).

A

$$\text{R-OH} + (CH_3)_4N^+OH^- \xrightarrow{-H_2O} (CH_3)_4N^+OR^- \xrightarrow{\text{Heat}} ROCH_3 + (CH_3)_3N$$

B

Hydrolysis

$$\text{R-O-R}_1 + OH^- \longrightarrow RO^- + R_1OH \qquad \text{I}$$

Formation of TMAH salts amd thermal dissociation to methyl derivatives

$$RO^- + (CH_3)_4N^+OH^- \longrightarrow (CH_3)_4N^+RO^- + OH^- \longrightarrow ROCH_3 + (CH_3)_3N \qquad \text{II}$$

$$R_1OH + (CH_3)_4N^+OH^- \xrightarrow{-H_2O} (CH_3)_4N^+OR_1^- \longrightarrow R_1OCH_3 + (CH_3)_3N \qquad \text{III}$$

R: alkyl or carbonyl group
R_1: alkyl group

Scheme 4.1 Reaction mechanims for derivatization of free hydroxyl or carboxyl groups (**a**) and ether- and ester-containing compounds (**b**) under pyrolysis/methylation with tetramethylammonium hydroxide

The pyrolysis/methylation has been largely employed in HS studies. Hatcher and Clifford (1994), for example, have applied either conventional or TMAH pyrolysis to three HA of different origin and reported that the TMAH technique was much more efficient. Moreover, they found both benzenedicarboxylic acids and long-chain aliphatic acids as the most abundant constituents in the three HA, suggesting that the previously proposed structural models of HS molecular nature, based upon canonical pyrolysis studies, should have been reconsidered. Other humic compounds, such as aromatic acids, long-chain fatty acid methyl esters (FAMEs) and homologous series of α,ω-dicarboxylic acid methyl esters, were identified only by TMAH treatments and were indicated as possible diagnostic indicators of origin or degree of decomposition of HS (Pöerschmann 2000). The occurrence of 3,4,5-trimethoxybenzoic acid, for example, is considered as indicative of the complete oxidation of lignin side chains and it has been related to the state of decomposition of HS (Abbt-Braun et al. 1989). Instead, long-chain FAMEs may provide information on the origin of organic matter. In fact, while biogenic inputs produce FAMEs with a majority of even-carbon atoms, a balanced even-odd forms indicate anthropogenic FAMEs (Peacock et al. 2001). Furthermore, FAMEs may inform on the kind of bacterial population providing metabolites to humic suprastructures. Proliferation of Gram-positive bacteria is suggested by the occurrence of iso- and anteiso FAMEs (frequently C_{15} and C_{17}), whereas Gram-negative communities are indicated by the presence of *cis*-vaccenic acid ($C_{18:1}$, double bond in $\Delta 11$ position) (Pöerschmann 2000).

The TMAH technique has been also exploited to study HULIS extracted from compost (Fukushima et al. 2009; Spaccini and Piccolo 2009) or the compost itself at various maturity stages (Spaccini and Piccolo 2007). The composting process involves the stabilization of fresh organic matter into humified HS, thereby increasing compost quality, in terms of greater stability (low degradation rate of the intrinsic organic matter) and reduced bioaccessibility (lack of phytotoxicity) (Fuentes et al. 2010). The stable incorporation of bio-labile compounds, such as peptides or oligosaccharides, into the hydrophobic domains of the progressively humified matter, as well as the oxidation of lignin side-chains, are key processes in compost stabilization (Zang et al. 2000; Amir et al. 2006; Spaccini and Piccolo 2009). The occurrence of oxidized lignin molecules (in both aldehydic and acidic forms) is a good indicator of the bio-oxidative transformation of lignin polymers (Vane et al. 2001), and determines the general redox state of a compost and, therefore, its maturity (Spaccini and Piccolo 2007). Finally, Spaccini and Piccolo (2009) characterized compost HULIS during the course of a composting process by TMAH and reported a progressive decrease in carbohydrate content, and a concomitant significant increase of hydrophobic alkyl molecules, thus showing the usefulness of TMAH pyrolysis-GC-MS in distinguishing different HULIS from compost.

Reagents other than TMAH have also been employed for the alkylation of HS, such as tetraethylammonium hydroxide (TEAH) and tetrabutylammonium hydroxide (TBAH) (Lehtonen et al. 2003). However, only TMAH provided the quantitative methylation of all the phenolic hydroxyl groups while TEAH and TBAH only partially alkylated phenols and polycarboxylic acids. Recently, the derivatization

efficiency of another reagent, the trimethylsulfonium hydroxide (TMSH), has been compared to that of TMAH in the reaction with various classes of lipids (Ishida et al. 2009). Results showed that TMSH allowed a greater detection sensitivity for polyunsaturated fatty acids as well as the other fatty acid components in various lipid classes (except cholesteryl esters), whereas TMAH provided the quantitative derivatization of saturated and monounsaturated fatty acid, although the use of TMAH resulted in isomerization and partial degradation of polyunsaturated fatty acids.

Even though the TMAH tool is considered to be less error-prone if compared to the conventional pyrolysis, it should be reminded that some secondary, unwanted reaction may occur. The decarboxylation of some phenolic acids (Saiz-Jimenez 1996), but also decarboxylation and isomerization of unsaturated fatty acids cannot be completely ruled out (Pöerschmann 2000). Furthermore, Tanczos et al. (1997) showed that the reaction of aldehydes with the TMAH could produce aldehydes alcohol, methoxy aldehydes or carboxylic acid aldehydes in different amount depending on aldehydes types via a Cannizzaro-like reaction.

4.2.2 Derivatization Followed by Reductive Cleavage

Residues from paper mills and biorefineries are rich in lignin-derived compounds, and the corresponding humic-like substances may be isolated from such wastes (Ertani et al. 2011). Lignin is the most abundant organic polymer on earth, immediately after cellulose, and it is composed of phenyl propanoid monomers (Fig. 4.1a): the *p*-hydroxyphenyl (H), the guaiacyl (G) and the syringyl (S) units. The amount of these monomers in plants varies according to the plant nature, with lignin from softwood being essentially composed of guaiacyl units (G), whereas that from hardwood contains both guaiacyl (G) and syringyl (S) monomers. Finally, in grass lignin all the three monolignols (H, G and S) are present (Goñi and Hedges 1992). The three monolignols may couple by forming a variety of dimers, the most abundant of which is the arylglycerol β-O-4′ (Fig. 4.1b), accounting for up to the 60 % of all the intermolecular linkages in such aromatic polymer (Zakzeski et al. 2010). Thus, in order to study lignin structure, most research focussed on the selective cleavage of such dimeric forms. In 1997, Lu and Ralph proposed a versatile manner to selectively degrade, reduce and derivatize the lignin macromolecule, in order to analyse the resulting fragments by GC-MS. The procedure is known as derivatization followed by reductive cleavage (DFRC), in order to both recall the reaction steps involved in the technique and reflect the Dairy Forage Research Centre, where the protocol was developed (Lu and Ralph 1997a). The lignin sample is firstly derivatized in acetyl bromide, thus brominating hydroxyl groups (OH) on α-carbons and acetylating both the free phenolic moieties and the OHs at the γ-position (Fig. 4.2). Then, the sample is added with zinc (Zn) powder in acidic medium for the reductive cleavage of the previously formed brominated β-O-4′ ether linkages, hence yielding lignin monomers. Finally, the newly generated OH groups are derivatized with acetic anhydride, in order to obtain GC-visible products (Fig. 4.2).

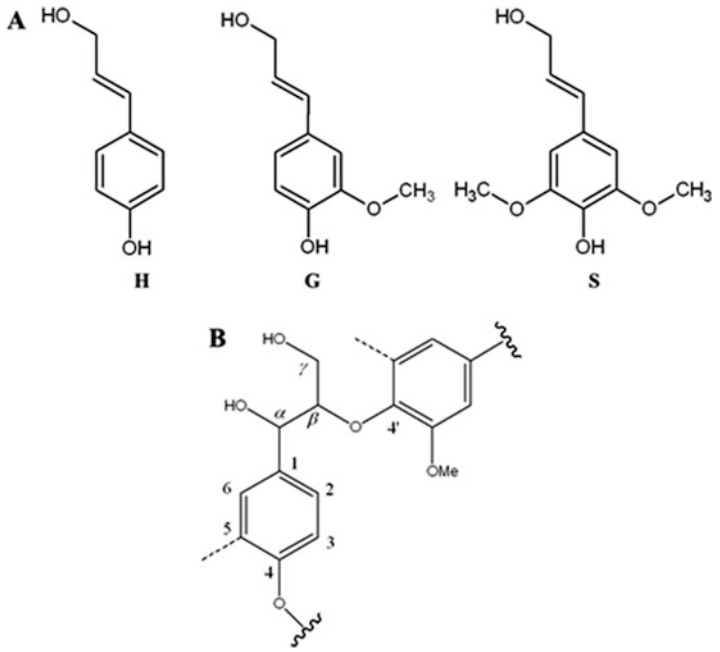

Fig. 4.1 Lignin monomers (**a**) and *β*-O-4′ lignin dimer (**b**). *H p*-hydroxyphenyl unit, *G* guaiacyl unit, *S* syringyl units

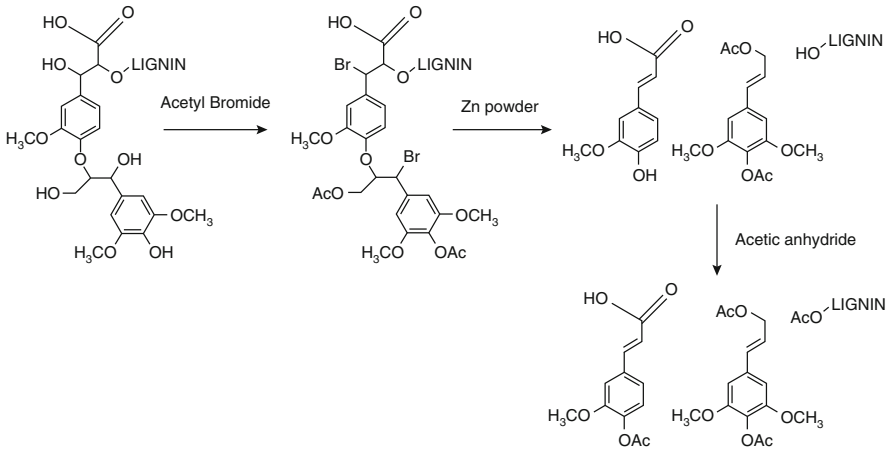

Fig. 4.2 Reaction mechanims for the derivatizaion followed by reductive cleavage (DFRC)

All steps involved in DFRC are carried out at very mild temperatures, thus making the DFRC one of the best techniques for the characterization of lignin side chain. The conditions of 50 ° C for the first step, and room temperature for the second and third steps provided stable products without undesirable secondary

condensation reactions (Lu and Ralph 1996). Furthermore, this technique is able to cleave β-O-4′ dimers almost quantitatively when applied on model compounds, with 92–97 % yields of monomers released of 92–97 %. Noticeably, such results are significantly larger than those obtained by applying other degradative techniques (Lu and Ralph 1997b and references therein). Another advantage of the DFRC procedure is that it is composed of three distinct steps, thus, making it very flexible and versatile (Ralph and Lu 1998; Tohmura and Argyropoulos 2001).

In spite of all the benefits provided by DFRC, quantitative results may be achieved only when the technique is applied on model compounds, since it fails to completely degrade all the β-O-4′ linkages in real lignin samples, as shown by NMR studies (Holtman et al. 2003). This limitation occurs when the bromide on α-carbon and oxygen in the β-O-4′ ether are not in a *cis* orientation, thus preventing the complete reduction of the β-O-4′ dimers. Ikeda and co-workers (2002) showed that, due this inconvenience, only about 20 wt% of the Klason lignin from loblolly pine (*Pinus taeda* L.) may be analysed by DFRC-GC-MS. Finally, it should be reminded that DFRC-derived fragments are acetylated only on the hydroxyl and phenolic functions, since the carboxyl moieties cannot be acetylated (Fig. 4.2), thus reducing the accurate appraisal of all the monomers released during the reductive cleavage (Savy et al. 2015a, b). However, this limitation may be overcome by derivatizing the mixture with trimethylsilydiazomethane (Grasset et al. 2010).

The DFRC technique has been often applied to assess the structure of lignin from lignocellulosic biomasses (Ralph and Lu 1998; Guerra et al. 2006; Tohmura and Argyropoulos 2001; del Río et al. 2012; Savy et al. 2015a), and it has been only recently exploited for elucidating HS and HULIS molecular structure (Grasset et al. 2010; Savy et al. 2015b). Savy et al. (2015b) extracted a humic-like lignins from both giant reed (*Arundo donax* L., AD) and miscanthus (*Miscanthus X Giganteus* Greef et Deut, MG) and elucidated their molecular structure by DFRC-GC-MS. Guaiacyls (G) were the most abundant monolignols released from both biomasses, being that obtained from MG twice as much as from AD. Conversely, the content of syringyl (S) and *p*-hydroxyphenyl (H) monomers was comparable in the two biomasses, while AD contained a significantly larger amount of S-units than MG. The main compound found in DFRC chromatograms were the *trans*-guaiacyl alcohol for both biomasses, followed by the *cis*-guaiacyl alcohol in MG and the *trans*-sinapyl alcohol in AD (Savy et al. 2015b). The molecular variations between the two Humic-Like lignins indicate the different distribution of lignin monomers in the original plant structure, thus pointing out that the DFRC is also a valuable tool for the characterization of HULIS derived from energy biomasses. The detection of some carbohydrates in DFRC products from AD and MG has shown the persistent presence of hemicellulose-derived compounds, due to incomplete lignins from plant cell sugar (Savy and Piccolo 2014; Savy et al. 2015a, b).

The DFRC protocol has been also applied on humic acids (HA) isolated from lignite ores (Grasset et al. 2010). The lignite HA mainly contained G-based molecules, with coniferyl alcohol (in both *cis*- and *trans*-isomers) as the most abundant compounds, thus suggesting that gymnosperm wood has largely contributed to the development of the original material. Interestingly, the authors modified the DFRC protocol by subjecting the final acetylated products to a methylation reaction with

trimethylsilyldiazomethane. This derivatization allowed the identification of coumarilic, coniferilic and sinapilic acids (Grasset et al. 2010), thus overcoming the limitation of the conventional DFRC protocol in characterizing carboxylated molecules (Fig. 4.2). The same lignite HA was also characterized by pyrolysis assisted with hydrolysis and methylation by TMAH (thermochemolysis), again revealing the G-type substances as the predominant compounds in the humic structure. However, there were significant molecular differences recognized by the two techniques. First of all, more compounds were identified by DFRC than by thermochemolysis. Nevertheless, the S/G ratios calculated by employing the two techniques were comparable, being 0.21 and 0.15 for DFRC and thermochemolysis, respectively. Another difference between the two procedures was related to the absence of H-units in mixtures obtained by thermochemolysis, whereas they were present in DFRC products, although in low amount (Grasset et al. 2010). Finally, it should be noted that DFRC allowed to recognize also lipidic compounds (fatty alcohols, fatty acids, ω-hydroxyacids, *n*-alkanes), originating by either plant or microbial communities. All these results seem to suggest that DFRC may be successfully exploited to trace lignin- and, more generally, plant-derived substances (carbohydrates, lipids) in HS. Further efforts should be made in order to verify whether this method is appropriate for studying lignin in humic materials from other sediments.

4.3 Nuclear Magnetic Resonance Spectroscopy

Nuclear magnetic resonance (NMR) spectroscopy represents a powerful analytical technique to characterize the molecular composition of complex materials such as HS and HULIS. This efficacy of this nondestructive spectroscopic is due to the versatility of its applications in the solid, semisolid and liquid state (Jacobsen 2007). Despite its relatively low sensibility, NMR offers a number of unique advantages, including the possibility to use different, complementary and multidimensional experimental strategies and pulse sequences which can be combined to evaluate specific intermolecular and intramolecular correlations (Piccolo et al. 1990; Simpson 2001a; Levitt 2008; Nuzzo et al. 2014; Mazzei and Piccolo 2015).

4.3.1 Solution-State NMR Spectroscopy

The application of NMR spectroscopy on samples totally soluble in deuterated solvents is commonly referred to as high-resolution solution-state NMR spectroscopy. This condition confers a larger mobility to nuclear spins, thereby lengthening their relaxation times and consequently improves spectral resolution. The one dimension (1D) ^{1}H-NMR spectroscopy represents a very useful tool to examine HS and HULIS due to the high sensitivity (high gyromagnetic ratio—γ) of the proton nucleus that allows a rapid achievement of structural information.

Nevertheless, in the case of HS and HULIS, the ^{1}H-NMR spectra are poorly informative due to the complexity and heterogeneity of their molecular mixtures, which diversify the relaxation times to the extent that some abundant compounds, such the aromatics, are often hardly detectable (Piccolo et al. 1990; Mazzei and Piccolo 2015). Better results may be achieved by hyphenating liquid-state NMR with other techniques. For example, natural organic matter (NOM) isolated from water and soil was studied by combining NMR analyses with liquid chromatography, which was in turn coupled to solid-phase extraction (LC-SPE-NMR). It was shown that separation and/or concentration of specific NOM components increased NMR detection, thus implying that integrated analytical approaches may help to further understand the NOM complexity (Piccolo et al. 2002; Conte et al. 2007).

Some attention has been recently devoted to the application in agriculture of biochar, the solid pyrolysis product of lignocellulosic biomasses at high temperatures, despite its resulting inherent poor abiotic and biotic reactivity (Zhang et al. 2014). Proton NMR spectra were used to characterize water extracts from biochar, obtained from sugar maple wood, and organic matter isolated from soil amended with the same biochar (Mitchell et al. 2015). Moreover, water/methanol and chloroform extracts from biochars obtained by solid olive mill pomace were also examined by ^{1}H-NMR spectroscopy (Hmid et al. 2014). None of these NMR investigations on biochars were conclusive, nor provided any evidence of the usefulness of such a "dead carbon" in agriculture (Lehmann et al. 2015).

Liquid-state ^{31}P-NMR spectroscopy has been increasingly employed to characterize the phosphorous forms in soils and HS (Busato et al. 2005; Li et al. 2015). It was found that most of phosphorous in HS are mainly in organic forms, prevalently as orthophosphate monoesters (Liptaj et al. 2005; He et al. 2011; Li et al. 2015). ^{31}P-NMR spectroscopy was also used to follow the humification process during the aerobic treatment of sewage sludge (Bartoszek et al. 2008), whereby the most relevant P compounds were orthophosphate monoesters and diesters, and pyrophosphates. This work showed that the concentration of orthophosphates increases in HS extracted from sewage sludge during the sewage treatment, while that of pyrophosphates diminished, especially in the specific mesophilic fermentation step of the process.

^{31}P-NMR spectroscopy was also used to quantify the amount of hydroxyl (OH) groups in lignin and lignin-derived HULIS, following derivatization with 2-chloro-4,4,5,5-tetramethyldioxaphospholane (CTMP), providing the corresponding phosphites (Tohmura and Argyropoulos 2001; Savy et al. 2015a, b, c, 2016). Since the CTMP reagent reacts equally with phenols, and primary and secondary OH and carboxyl groups, it is possible to reach a quantitative determination of these groups (Argyropoulos 2010). The signals of P-derivatized acidic functions are well resolved and separated (Fig. 4.3), with hydroxyalkyl groups located in the 150.8–146.3 ppm range, the phenolic molecules in the 143.7–136.9 ppm interval, and carboxyl OH signals in the 135.6–133.7 ppm range. The derivatized ^{31}P-NMR spectra also allow recognizing the different phenolic structure, due to their different chemical shift values. Thus, the signals around 143.7–142.2 ppm are attributed to the syringyl (S) molecules, while those around 140.2–138.4 ppm and those around 138.6–136.9 are

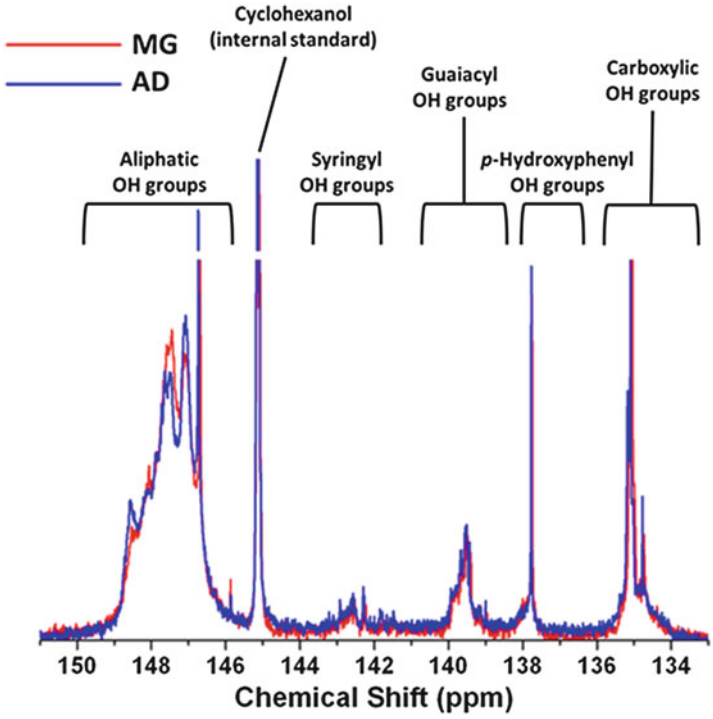

Fig. 4.3 ^{31}P-NMR spectra of HULIS isolated from giant reed (AD) and miscanthus (MG) bioenergy crops and derivatized with 2-chloro-4,4,5,5-tetramethyldioxaphospholane. Cyclohexanol was added as internal standard prior to derivatization (from Savy et al. 2016)

assigned to guaiacyl (G) and *p*-hydroxyphenyl (H) units, respectively. Finally, also some dimeric structures may be identified in the 142.8–141.7 ppm range (Guerra et al. 2006).

A number of humic-like lignins have been extracted from lignocellulosic biomasses for energy by an alkaline oxidative procedure, and then studied by ^{31}P-NMR (You et al. 2013; Savy et al. 2015a, c, 2016). The water-soluble lignin materials from giant reed (*Arundo donax* L., AD), miscanthus (*Miscanthus X Giganteus* Greef et Deut, MG), cardoon (*Cynara cardunculus* L.), two black poplars grown in different areas (*Populus nigra* L.) and eucalyptus (*Eucalyptus camaldulensis*, Dehnh., EUC) were all composed by mixture of low-molecular-weight fragmented and oxidized molecules. They contained mainly phenols, in either monomeric or oligomeric forms, as products of the isolating procedure that oxidatively depolymerizes lignin polymers in lignocellulosic biomasses (Savy and Piccolo 2014). The quantity of OH groups in the HULIS extracts was assessed with ^{31}P-NMR spectra after derivatization. While the alcoholic OH functions were most abundant in all substrates, due to lignin side chain and residual carbohydrates, the total content of phenols and carboxylic acids varied among the biomasses. The total phenolic content, for example, was larger in AD and MG, indicating a lower extractability of

these materials in the extracting solution (Savy et al. 2016). On the contrary, lignin HULIS from EUC biomasses contained a few phenolic moieties and the largest amount of COOH, suggesting a scarce resistance of the eucalyptus biomass to the strongly oxidizing conditions applied to extract the raw biomass (Savy et al. 2015c). This result is an evidence not only of the different relative amount of lignin monomers in the various plants, but also of the efficacy of the CTMP derivatization for the HULIS characterization reactivity by ^{31}P-NMR spectroscopy (Savy et al. 2015c).

Solution-state spectra can be obtained in the 2D mode which are useful to characterize the structure of molecular components and functional groups in humic matter. 2D NMR experiments may detect homo- and heteronuclear connectivities as well as intra- and intermolecular correlations among humic molecules. A further nuclear dimension may lead to a differentiation among those signals which, even though overlapped in proton domains, are correlated to neatly resolved peaks in the second dimension (Jacobsen 2007). In addition, many experiments take advantage from the transfer of magnetization (either through-bonding or through-space) from a very sensitive nucleus, such as hydrogen, to an insensitive nucleus, thus conferring to the latter an enhanced NMR response. This strategy is very profitable for the detection of magnetically active nuclei characterized by low sensitivity and low natural isotopic abundance, such as ^{13}C or ^{15}N (Jacobsen 2007). The characterization of a humic sample requires the acquisition of different and complementary 2D NMR experiments in order to achieve the maximum of information. For example, different HS are characterized by several NMR experiments, including ^{1}H-^{1}H COSY (COrrelation SpectroscopY, which detects ^{1}H-^{1}H geminal/vicinal connectivities) and ^{1}H-^{13}C HSQC (Hetero Single Quantum Correlation, which is identifies ^{1}H-^{13}C scalar connectivities) (Simpson et al. 2001, 2004). Moreover, 2D NMR connectivity pattern of a model lignin was studied as a guide to recognize lignin-derived fragments in humic matter (Simpson et al. 2004). By this comparison approach, some macroscopic differences in HS composition in two soils under different vegetation were observed by 2D-NMR spectroscopy (Kelleher and Simpson 2006). However, this only confirmed the very complex and heterogeneous nature of soil humic supramolecular associations, which are hardly resolvable by only NMR, unless the bulk humic matter is subjected to a preliminary fractionation by the Humeomics approach (Nebbioso et al. 2014) (Fig. 4.4).

Among 2D NMR experiments, ^{1}H-^{13}C HSQC represents the most useful tool to characterize lignocellulosic material and in particular humic-like lignins. HSQC experiments were employed to examine both wood gels and milled-wood lignin of a selected *Eucalyptus globulus* clone with the purpose to investigate the molecular changes occurring during plant growth (Rencoret et al. 2011). Water-soluble lignins obtained by alkaline oxidation from miscanthus and giant reed were thoroughly characterized by HSQC spectra (Savy et al. 2015a). Hedenstrom et al. (2009) detected structural and compositional changes in the ligninocellulosic material of several poplar woods by combining HSQC spectral data with Principal Component Analysis. Finally, the HMBC (heteronuclear multiple bonding correlation) technique that detects long-range ^{1}H-^{13}C connectivities was applied to characterize the molecular composition of humic-like lignins (Savy et al. 2016), and the cell wall material obtained by using either N-methylimidazole or dimethysulphoxide/tetrabutylammonium fluoride as extraction solvent (Lu and Ralph 2003).

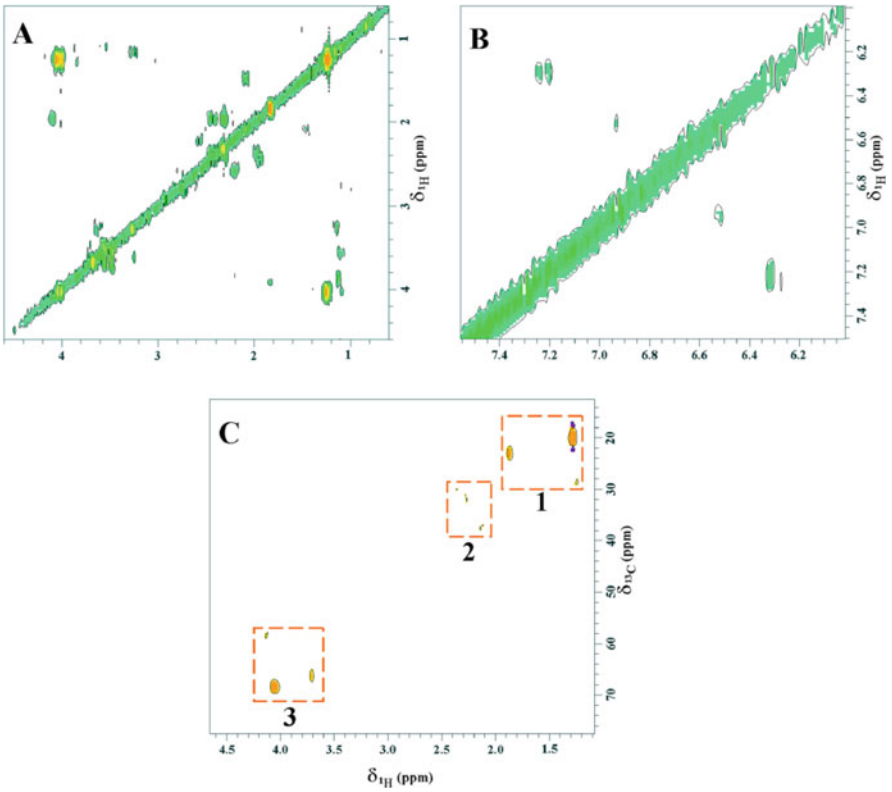

Fig. 4.4 ^{1}H-^{1}H COSY and ^{1}H-^{13}C HSQC spectra of RES4. ^{1}H-^{1}H COSY (**a**, aliphatic and hydroxyalkyl region; **b**, aromatic region) and ^{1}H-^{13}C HSQC (**c**) spectra of RES4. Rectangular regions in HSQC correspond to the following sets of proton signals: Alkyl CHn (1); CHC=O (2); CHn-X where X=electron-withdrawing group (3) (from Nebbioso et al. 2014)

The derivatization of specific functional groups in humic matter with a ^{13}C-labelled compound was exploited to enable acquisition not only of 3D but even of 4D NMR spectra (Bell et al. 2015). However, despite elegant and complex NMR techniques may provide a wide set of structural information in one single experiment, there are still drawbacks such as the requirement of both very long acquisition times and relatively powerful static field (>18.8 T), and the inherent long relaxation times of HS.

4.3.1.1 Diffusion-Ordered NMR Spectroscopy

2D Diffusion-ordered NMR spectroscopY (DOSY-NMR) is becoming an useful technique to investigate the structural features of HS and HULIS in solution state (Smejkalova and Piccolo 2008; Mazzei and Piccolo 2012, 2015). This NMR experiment is based on a pulsed field gradient sequence that enables the measurement of translational diffusion (conventionally defined as self-diffusion) of dissolved

molecules and provides direct information on their structure, molecular dynamics and conformational changes. As dictated by the Einstein–Stokes theory, the diffusivity of a molecule decreases when its hydrodynamic radius increases and vice versa. Therefore, the molecular rigidity as well as intramolecular associations of humic components can be evaluated by measuring the NMR-based diffusion coefficients of humic functional groups (Levitt 2008; Morris et al., 1999). For example, Smejkalova and Piccolo (2008) used ^{1}H DOSY-NMR spectroscopy to explore the diffusivity of a number of fulvic and humic acids of different origin. They showed the supramolecular nature of humic associations by detecting relevant conformational variations depending on solution pH value and used DOSY spectra to measure the occurrence of the critical micelle concentration (CMC) in humic solutions. The aggregation state of bulk HS and their size fractions were assessed by ^{1}H DOSY and used for a correlation to a possible auxin-like bioactivity of humic materials (Canellas et al. 2010). ^{1}H DOSY spectra were also applied to evaluate the effect of metal complexation on the aggregation of different molecular components in the same humic solutions (Nebbioso and Piccolo 2009).

1D diffusion-edited techniques are used as NMR filters to simplify the spectra of complex molecular mixtures. Diffusion-based filters exploit the rapid diffusion of small molecules, thus enabling the isolation and characterization of signals due only to real large molecules, or molecular aggregate, such as humic matter. The application of a diffusion-edited filter to ^{1}H spectra of organic matter from A horizon of a brown chernozem soil enabled the spectral isolation of those signals prevalently attributable to microbial biomass and microbial-derived proteins (Simpson et al. 2007). However, DOSY NMR may be also applied to other relatively sensitive nuclei, such as the phosphorous (Mazzei and Piccolo 2012). ^{31}P-DOSY NMR spectra were recently applied to explore the diffusivity of lignin samples isolated with subcritical water:ethanol:CO_2 from biomasses for energy and derivatized by the ^{31}P derivatization agent 2-chloro-4,4,5,5-tetramethyl-1,3,2-dioxa-phospholane (Savy et al. 2015b).

4.3.2 Solid-State NMR Spectroscopy

The magic angle spinning (MAS) NMR technique enables the analysis of crystalline or amorphous solids by minimizing the processes (strong homonuclear dipolar interactions, chemical shift anisotropy, quadrupolar interactions, and enhanced magnetic susceptibility) that prevent the acquisition of meaningful NMR spectra in the solid state (Duer 2002). Despite the low resolution of solid-state MAS spectroscopy, this NMR technique represents the best choice to appreciate the molecular distribution of solid or poorly soluble samples such as HS and HULIS (Maunu 2002). Moreover, the dipolar heteronuclear interactions (typically strong for solid samples) can be exploited to produce efficient through-space magnetization transfers (referred to as cross-polarization, CP) which are capable to induce a significant signals enhancement. Consequently, it may be profitably employed to increase the response of less abundant nuclei with low gyromagnetic ratio γ (such as ^{13}C, ^{15}N and ^{29}Si), via polarization transfer from the large γ and most abundant ^{1}H nucleus.

The advantages of the CPMAS technique make it mostly appropriate for the study of the composition of heterogeneous and complex materials such as HS and HULIS (Deiana et al. 1990; Keeler et al. 2006; Preston et al. 2009; Mao et al. 2011; Mazzei and Piccolo 2015). The variation in molecular content of HS in different world soils was revealed by this solid-state NMR technique and elaborated by multivariate statistical analyses to provide an innovative tool for differentiation of soil properties (Šmejkalová et al. 2008). ^{13}C CPMAS spectra were used to follow the molecular changes in HA extracted from composts at increasing maturity stages (Blanco and Almendros 1997; Spaccini and Piccolo 2009; Amir et al. 2010). Moreover, the molecular changes of fulvic acids extracted from the sludge/plant mixture as a function of maturation time were evaluated by this NMR technique (Jouraiphy et al. 2008), while Jindo et al. (2012) also employed CPMAS-NMR spectroscopy to investigate on the role of HS from sewage sludge as plant root promoter.

A highly bioactive HULIS is commonly extracted from the vermicomposting process, that recycles different organic wastes into stable humus through the action of earthworms (Fernández-Gómez et al. 2015). The molecular properties of HA from several vermicomposts produced from different ratio of tomato residues and paper-mill sludge in a vermireactor were assessed by CPMAS-NMR spectroscopy (Fernández-Gómez et al. 2015). Moreover, solid-state NMR technique was used to characterize several HA isolated from vermicompost and subsequently subjected to controlled chemical modifications to modulate their auxin-like bioactivity as promoter of both plant root growth and proton pump activation (Dobbss et al. 2010). The molecular properties of a fermented manure preparation used as field spray in biodynamic agriculture were shown by CPMAS-NMR spectroscopy to be different from those of common aerobic compost (Spaccini et al. 2012).

As in the case of solution-state NMR, the complexity of solid-state NMR spectra may be reduced by applying specific spectral filters. Dipolar dephasing (DD) and chemical shift anisotropy (CSA) techniques represent the most employed filters to characterize HS and HULIS. The DD filter allows to selectively suppress CH- and CH_2-carbon signals from ^{13}C spectra as a function of their protonation extent (Liitia et al. 2002; Spaccini and Piccolo 2009). The molecular composition of several biochars produced from different feedstocks and obtained at different pyrolysis temperatures were investigated by DD-CPMAS NMR (McBeath et al. 2014). The chemical shift anisotropy (CSA) filter only show only sp^3-hybridized carbons due to the selective removal of anisotropic signals, such as those for aromatic or carbonyl carbons, while increasing the detection of anomeric carbons. Mao and Schmidt-Rohr (2004) applied the symmetry-based CSA filter to efficiently select alkyl carbon signals, and concomitantly suppress aromatic carbon signals from a peat humic acid.

Diagnostic and structural information of HS and HULIS can be obtained by evaluating changes in spin relaxation times of visible nuclei. In fact, NMR relaxation is the process by which the total energy of a nuclear system acquired after radiofrequency excitation is progressively lost and the equilibrium recovered (Bakhmutov 2004). The measurement of nuclear relaxation rate in molecules is important since it is related to either structural or conformational variations of the studied nucleus (Bakhmutov 2004; Mazzei and Piccolo 2015). Savy and Piccolo (2014) employed NMR spectroscopy to characterize the chemical properties of

water-soluble lignin samples isolated from different biomasses. Humic-like lignins not only differentiated based on molecular distribution by 13C-CPMAS spectra, but their molecular mobility and flexibility are also inferred by proton NMR relaxation times in the rotating frame (referred to as T1 ρH) (Savy and Piccolo 2014). A refined NMR pulse technique such as ultrafast magic angle spinning (30 kHz) in tandem with delayed echo acquisition was also applied to obtain high-resolution ^{1}H spectra in the solid state of complex natural organic materials, such as cork and wood components (Gil et al. 1999).

Due to the intrinsic limitations of the solid-state NMR conditions (i.e., excessively short spin nuclear relaxation times, strong ^{1}H-^{1}H dipolar couplings), the number of 2D NMR experiments applicable to HS and HULIS in their natural isotopic abundance is more restricted than for solution-state NMR. Nevertheless, the ^{1}H-^{13}C HETCOR (HETeronuclear CORrelation) pulse sequence represents an useful 2D NMR technique for an advanced solid-state NMR investigation on HS and HULIS. Through this technique it is possible to detect through-space (<10 Å) correlations among different humic molecular domains thereby revealing structural and conformational information on the materials (Mao et al. 2011). Up to date, few works have yet showed that the HETCOR technique improves understanding of HS composition by resolving overlapped carbon signals along the proton dimension and identifying intermolecular correlations (Mao et al. 2001, 2011; Lattao et al. 2008; Le Brech et al. 2015).

The versatility of NMR spectroscopy provides an additional technique to be exploited in the analysis of the molecular composition of HS and HULIS. The high-resolution MAS (HR-MAS) technique enables to apply the NMR spectroscopy also to semisolid or gel-phase samples (Doty et al. 1998). The sample is placed in a locked-up rotor and added with a small amount of a deuterated solvent that helps to reduce dipolar interactions, which are further minimized by spinning the rotor at the magic angle. Simpson and coworkers (Simpson et al. 2001) were first to apply the HR-MAS NMR technique to study materials of environmental interest. They showed that the molecular composition of the organic matter in a whole soil may be characterized at the solid–aqueous interface by HR-MAS by combining one-dimensional and two-dimensional solution-like experiments, including T_2-based filters, when necessary. They also reported spectral variations as a function of specific solvents. While deuterated water produced broad signals, dimethylsulphoxide-d6 improved signals resolution, prevalently because it induced displacement of H-bonds (Simpson et al. 2001). Later, they again exploited the versatility of HR-MAS by examining the molecular composition of a humin fraction isolated from an eluviated chernozem soil (Simpson et al. 2007).

4.4 Thermal Analyses

Thermal experiments (thermogravimetric analysis—TGA, differential thermal analysis—DTA and differential scanning calorimetry—DSC) are based on programmed heating of solid samples under either oxidizing or pyrolytic conditions is

in order to relate their progressive alteration with increasing temperature to chemical composition, transition temperatures, moisture and ash content (Plant et al. 2009).

Sample mass losses are related to thermal reactions and may be measured between the inflection points of the thermal curve. TGA interpretation is simplified by calculating its first derivative (DTG) of the thermal curve that can provide information on sample's chemical nature (Francioso et al. 2007; Martin et al. 2010). In DTA experiments, a sample and a reference material are placed in two different crucibles and subjected to the same temperature regime. The temperature difference between the two materials is calculated, thus allowing to detect the endothermic (if sample temperature is smaller than that of the reference) or exothermic (when sample temperature is larger than that of the reference) processes. Finally, DSC measures changes in the sample heat capacity as a function of temperature, and provides information on sample's heat capacity as well as its inherent exo- and endothermic reactions (reported as change in heat flux). Contrary to DTA, the signal detected by DSC is independent of the substance thermal properties (Plant et al. 2009).

Thermal techniques have been widely employed for studying the molecular nature of HS from soils and lignocellulosic biomasses and for tracing compost stabilization processes (Campanella et al. 1990). Thermal analyses provide information at the whole-matrix level, since thermal stability strongly depends on sample macrostructure and physical arrangement of molecules. Hence, size and packing of particles may influence the sample's heat capacity and thus the resulting reaction products (Plant et al. 2009). The DTG of HS showed typical pattern in thermal degradation, with the first endothermic peak within 105–200 °C, related to dehydration of free and bound water. Then, two exothermic signals are usually detected and ascribed to humic components with different thermal stabilities. The first peak (300–350 °C) is related to the degradation of carbohydrates and other aliphatic moieties, whereas the second signal represents the decomposition of aromatic molecules, long-chained hydrocarbons and nitrogen compounds (Leinweber et al. 1992). Similar patterns were reported for the thermal behaviour of HULIS from several lignocellulosic biomasses for energy (giant reed, miscanthus, eucalyptus, cardoon and two different black poplars) (Savy et al., 2014; 2015c). In these materials, the signals below 350 °C were related to the degradation of either lignin side-chain or hemicellulose, while those at temperatures larger than 400 °C were attributed to char volatilization (Fig. 4.5) (Martin et al. 2010).

4.5 Electron Paramagnetic Resonance Spectroscopy

Humic substances (HS) contain stable organic radical species due to phenolic groups that can be photoexcited (Sunda and Kieber 1994). The first observation of stable-free radicals in HS was made by Rex (1960). By the term 'free radical', it is assumed an atom or a group of atoms containing one unpaired electron. These free radicals are involved in a number of environmental processes, including transformation of HS (Sunda and Kieber 1994) and degradation of organic compounds

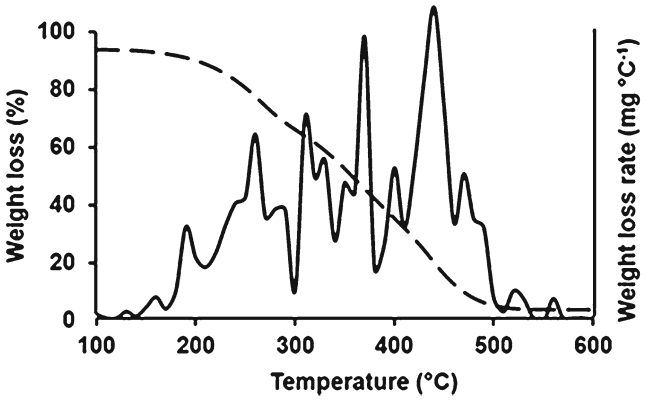

Fig. 4.5 Thermogravimetric and derivative thermogravimetric curves for HULIS isolated by giant reed bioenergy crops (from Savy and Piccolo 2014)

(Kamiya and Kameyama 1998). Moreover, HS may act as electron acceptors from soil microorganisms during the anaerobic oxidation of organic compounds (Lovley et al. 1996), and efficiently mediate the formation of elemental mercury via radical reactions (Alberts et al. 1974).

Free radicals in HS are affected by the magnetic field and can be assessed using electron spin resonance (ESR) Spectroscopy. Each electron possesses a magnetic moment and a spin quantum number, and when two electrons are present in the same orbital, they have opposite spins, resulting in a neutralization of their magnetic field (Hon 1992). Conversely, the spin of the unpaired electron is not neutralized and thus the free radical develops a magnetic field due to the paramagnetic phenomenon. When a molecule with one or more unpaired electrons enters a magnetic field, and an electromagnetic radiation in the radio frequency region is applied, energy is being adsorbed and an adsorption signal can be recorded (Shindo and Huang 1982). From known values of the magnetic field intensity and from the frequency required to induce resonance, it is possible to calculate the so-called g tensor that provides information on the orbital status of the unpaired electron and the related chemical bonds. For an unpaired electron, the g tensor is 2.0023. The deviation from this value describes the electron interactions with its surrounding environment (Hon 1992). Other information may be obtained from an ESR signal: (1) the number of the unpaired electrons, which is given in spins g^{-1}, (2) the width of the adsorption line (Gauss), which is affected from the free radicals concentration, the temperature, and the coiling status of the sample molecules, and (3) the hyperfine structure, that indicates the number and the type of nuclei that are interacting with the unpaired electron, depicting the chemical structure of the free radical (Giannakopoulos et al. 2005).

All the ESR data on HS published within the past 50 years are based on conventional X-band ESR spectrometers (Steelink and Tollin 1962; Paul et al. 2006) operating at ~9 GHz, where the radicals are detected for magnetic fields around 3400 G, providing a spectrum such as the one reported in Fig. 4.6. The X-band ESR spectra

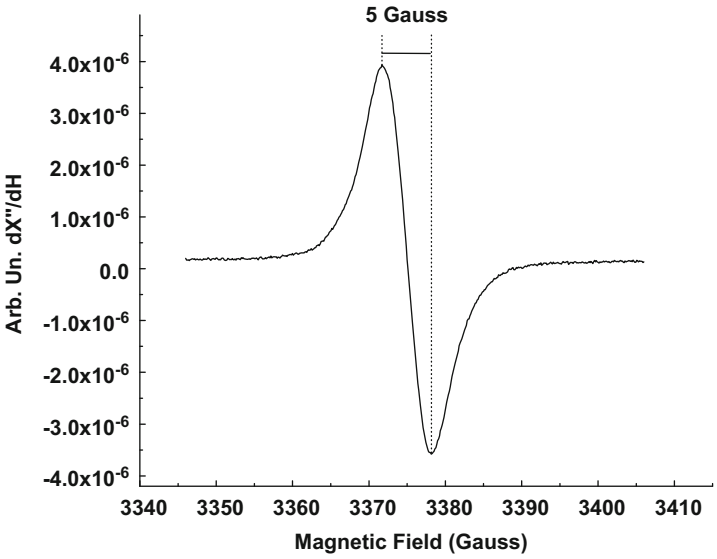

Fig. 4.6 ESR signal of humic acid

provide a *g* value, the line width and the spin concentration per gram of HS. Christoforidis et al. (2007) used high-field ESR spectrometers to study the HS radicals content and reported that all samples, regardless of their origin, contained two limiting types of stable radicals, types I and II, with distinct electronic structure. The type I prevailed at pH 5 value, while type II was predominant at alkaline pH 12 value, and both had different *g* values. The two limiting types are correlated in a unified reversible manner with pH value. Both types of radical centres are consistent with π-type radicals and they persist not only in liquid solutions, but also in solid-state forms (Drosos 2009).

Due to the structural complexity and heterogeneity of natural HA (Piccolo 2002), it was attempted to produce synthetic HULIS (Martin et al. 1974; Wang et al. 1980; Wang and Huang 1989, 2003). HS-like polycondensates (HSLP) can be synthetized from simple phenols and phenolic acids (Haider and Martin 1967; Martin et al. 1972), by employing either biotic or abiotic (oxide, clay or soil) catalysts. Biotic processes may provide satisfactory yields (3–80 %), but the transformation rates are low with typical reaction times >40 days (Haider and Martin 1967; Martin et al. 1972, 1974; Bollag 1992). Conversely, larger transformation rates and yields can be achieved using abiotic catalysts (Wang and Huang 1986). Giannakopoulos and co-workers (2005, 2006) have shown that gallic acid is an appropriate model for the radical properties of HS. Moreover, they have recently produced a HSLP by oxidative co-polymerization of gallic and protocatechuic acids without using a catalyst (Giannakopoulos et al. 2009). This material contained phenolic π-type radicals which strongly resembled the indigenous radicals found in HS (Shindo and Huang 1982; Christoforidis et al. 2007). The ESR signal for this HSLP gave a high radical

concentration of 8.9×10^{18} spins g^{-1} vs 4.4×10^{18} spins g^{-1} for Leonardite at pH 12. Moreover, the radical content of HSLP was found to be pH-dependent, and such pH-dependence was reversible. In fact, when the pH value was decreased from 12 to 5, a severe signal decrease occurred, and the ESR signal could be 100 % recovered if the pH was raised again to 12 and kept constant for 20 min. While such a reversibility was not observed for gallic acid solutions (Giannakopoulos et al. 2005), it represents a hallmark of the radical properties of natural HS (Shindo and Huang 1982; Giannakopoulos et al. 2005). Local effects such as π-stacking and hydrophobic sequestration modulated the stability of the radicals in HS, and the great aromatic and phenolic character of HASP concurred to provide a large radical content. In fact, the unusual stability of free radicals in natural HA, even in aqueous solutions under various pH values and redox conditions, is attributed to the combined effects due to phenolic and aromatic groups. A recent update of previous HSLP studies was conducted by altering the redox potential (Eh) during the polymerization reaction (Drosos et al. 2011). Mass yield of HSLP was significantly reduced by Eh increase. Furthermore, when HSLP was produced at high Eh, aliphatic structures were more abundant, and ionic strength had a significant impact on both charge and H-binding properties. Indeed, the estimated Donnan volume revealed a much more expanded structure and HSLP gave only 4.0×10^{17} spins g^{-1} at pH 12 value, behaving more like a compost or soil HA or FA (Jezierski et al. 2000a). Conversely, when HSLP was produced at low Eh, its characteristics resembled more those of a lignite HA. These results indicated that redox potential may play a significant role in the stability of free radicals in HS and might be a primary factor in the stabilization of HS and HULIS. Finally, the reactions occurring during oxidative polymerization of HS may lead to an increase in the organic free radical content (Cozzolino and Piccolo 2002; Piccolo et al. 2000, 2005).

ESR can be also a useful tool to obtain information on certain transition metals and their interactions with HS (Jezierski et al. 2000b; Giannakopoulos et al. 2005, 2006), or on the hydrophobic properties of HS (Ferreira et al. 2001). However, during the first stages of biotic and abiotic transformation, like the composting of plant litter and lignin materials, the formation of the radicals is not stable, thus requiring the monitoring by special molecules that act as spin traps (Blodig et al. 1999; Garbin et al. 2007).

4.6 High-Performance Size-Exclusion Chromatography

The high-performance size-exclusion chromatography (HPSEC) is a chromatographic technique aimed to assess the molecular size (or dimension) of an analyte. Unlike other chromatographic methods, the interactions between the column stationary phase and the analyte should be minimized in HPSEC and the analyte retention time (RT) be only determined by its flowing through pores of different *radii*. A molecule with a large hydration size cannot penetrate the micropores of smaller radius, and it is eluted rapidly out of the column. Conversely, smaller molecules can

diffuse through the micropores of the stationary phase and, consequently, are eluted later (Striegel et al. 2009). Hence, the largest the apparent molecular dimension of a molecule or an association of molecules, the lower will be its elution volume and vice versa. Nevertheless, the elution behaviour in HPSEC will bring along some interferences due to some unavoidable enthalpic interactions between analyte and stationary phase (Striegel et al. 2009).

Size-exclusion chromatography has been instrumental to the development of the new paradigmatic understanding of the chemical nature of natural organic matter (Piccolo et al. 2001; 2002). From the first size-exclusion chromatography experiment at low pressure in which it was shown that humic substances varied dramatically in molecular size with addition of acetic acid (Piccolo et al. 1996), to those at high pressure, whereby other organic acids were added either directly to sample solutions before injections (Piccolo et al. 1999, 2002, 2003; Cozzolino et al. 2001) or to elution solutions to modify their pH (Conte and Piccolo 1999), it was revealed the fragility of the conformational structure of HS within a dynamic HPSEC elution (Fig. 4.7). These findings showed that dissolved HS could not behave as macropolymers, as for the traditional description of their chemistry, but they rather should be regarded as supramolecular associations of heterogeneous molecules self-assembling in only apparent high molecular size materials by non-covalent interactions such as dispersive forces (van der Waals, π-π, CH-π) at neutral pH, and classical hydrogen bonds at lower pH. As a confirmation of the supramolecular structure of HS, a final HPSEC experiment showed the dramatic difference in elution profiles upon addition of organic acids between real covalently bound polymers and humic supramolecular associations stabilized only by hydrophobic and hydrogen bonds (Piccolo et al. 2001).

In the quest to determine the absolute molecular weight of humic molecules, the electrospray ionization mass-spectrometry (ESI-MS) technique has recently received great attention among the soft ionization methods, when applied to humic substances in either single (MS) or tandem (MS/MS) mode (Pfeifer et al. 2001; McIntyre et al. 2001; Reemtsma and These 2003; Reemtsma et al. 2006). The interest in electrospray

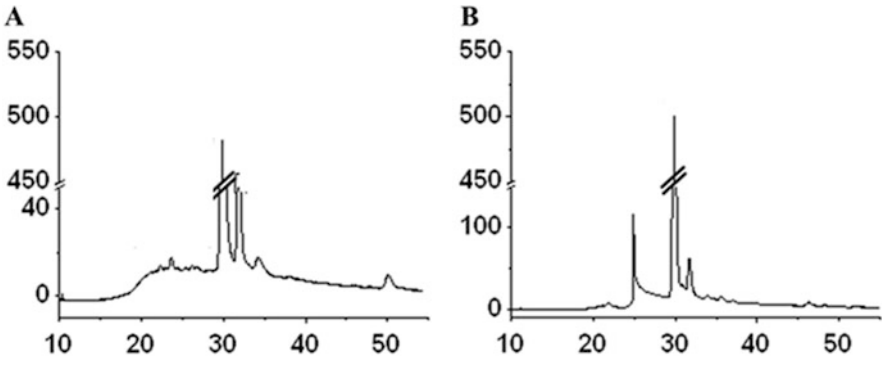

Fig. 4.7 HPSEC profiles of HULIS extracted by giant reed before (**a**) and after (**b**) the addition of acetic acid (from Savy et al. 2016)

ionisation is due to its advantage in being an extremely soft ionization process and therefore providing unfragmented ions, from which not only the absolute molecular weight (ESI/MS) but also unequivocal structural information (MS/MS) can be obtained (Cole 1997).

These features were proved for ESI of humic molecules in combination with high-resolution instrumentation such as Fourier transform ion cyclotron resonance mass spectrometry (FT IRC-MS) providing a resolving power up to 120,000 for low-mass molecules (Stenson et al. 2002; Ohno et al. 2010). Plancque and coworkers (2001), using quadrupole time-of-flight (Q-TOF) ESI-MS, showed that singly charged ions were by far the most abundant ions generated from a fulvic acid. Their MS/MS experiments revealed that humic ions were fragmented by loosing *m/z* 44 or 18, corresponding to the neutral masses of CO_2 and H_2O from singly charged ions, whereas doubly charged ions would loose *m/z* 22 and 9 fragments, respectively. The predominance of singly charged ions in humic materials was definitively confirmed by high-resolution mass spectra (McIntyre et al. 2001) and ESI-FTIRC mass spectrometry in both positive and negative modes (Stenson et al. 2003; Ohno et al. 2010), thereby eliminating inadequate accounting for multiply charged ions as a cause of any low molecular weight bias. These findings are consistent with the reported formation of mainly monocharged ions from small (<1000 Da) molecules (Ohno et al. 2010; Piccolo et al. 2010) and with the supramolecular concept of humic substances that involves self-assembling non-covalent association of small molecules (Piccolo et al. 2001; Piccolo 2002). However, while it was proved by ESI-MS that the average molecular weight of humic molecules is not larger than 800–900 Da (Piccolo and Spiteller 2003), the intrinsic ESI procedure to reduce hydration of molecules before entering the mass spectrometer, forced humic mixtures to present always hydrophobic molecules at the gas–water interface. This limitation was hence recognized to prevent ESI-MS to enable the uniform ionization of all heterogeneous molecules present in humic complex mixtures, thereby reducing the capacity of the technique to truly indicate the mass of all humic molecules in a sample (Nebbioso et al. 2010).

Humic-like lignins from lignocellulosic biomasses for energy have been also studied by HPSEC, and revealed slightly different apparent molecular dimensions as a function of the plant biomass from which they were isolated (Savy and Piccolo 2014). It has been also suggested that these lignins, rather than being still polymers or oligomers, were actually composed by a variety of small molecules with a confirmation that resembled that of supramolecular humic associations (Savy et al. 2016). The small lignin-derived molecules were shown to be held in larger associations by weak dispersive forces (van der Waals, π-π, π-CH) and/or hydrogen bonds (Piccolo 2002), inasmuch as HS. In fact, similarly to soil humic fractions, the addition of acetic acid to the lignin solutions resulted in a decrease in the molecular size distribution, due to the disruption of cohesive forces occurring in the meta-stable aggregates (Piccolo et al. 2003; Savy et al. 2016). Such an alteration in the conformational arrangement of dissolved HS and HULIS upon interactions with organic acids exuded by plants has been proposed as a mechanism of bioactivity toward plant growth and development (Canellas et al. 2010; Savy et al. 2016).

4.7 Conclusions

The rapid development of the advanced analytical techniques described in this chapter enabled the accumulation of a large body of data on HS and HULIS chemical nature and molecular composition. Moreover, the recent understanding of HS as supramolecular associations of small heterogeneous molecules has opened the way to the rationale evaluation of the molecular composition of the organic matter isolated from plant-derived biomass. These molecules of natural origin can then be re-employed in profitable economic sector such as agriculture or material chemistry, thereby enhancing the sustainability of these activities.

References

Abbasi PA, Al-Dahmani J, Sahin F et al (2002) Effect of compost amendments on disease severity and yield of tomato in conventional and organic production systems. Plant Dis 86:156–161

Abbt-Braun G, Frimmel FH, Schulten HR (1989) Structural investigations of aquatic humic substances by pyrolysis-field ionisation mass spectrometry and pyrolysis-gas chromatography/mass spectrometry. Water Res 23:1579–1591

Abu-Rukah Y, Al-Kofahi O (2001) The assessment of the effect of landfill leachate on groundwater quality — a case study El-Akader landfill site-north Jordan. J Arid Environ 49:615–630

Alberts JJ, Schindler JE, Miller RW (1974) Elemental mercury evolution mediated by humic acid. Science 184:895–896

Amir S, Hafidi M, Lemee L et al (2006) Structural characterization of humic acids, extracted from sewage sludge during composting, by thermochemolysis–gas chromatography–mass spectrometry. Process Biochem 41:410–422

Amir S, Jouraiphy A, Meddich A et al (2010) Structural study of humic acids during composting of activated sludge-green waste: Elemental analysis, FTIR and ^{13}C NMR. J Hazard Mater 177:524–529

Argyropoulos DS (2010) Heteronuclear NMR Spectroscopy of Lignins. In: Heitner C, Dimmel DR, Schmidt JA (eds) Lignin and lignans: advances in chemistry. Taylor and Francis Group LLC, Boca Raton, FL, pp 245–265

Bakhmutov VI (2004) Practical NMR relaxation for chemists. Wiley & Sons Chichester, West Sussex, England

Bartoszek M, Polak J, Sułkowski WW (2008) NMR study of the humification process during sewage sludge treatment. Chemosphere 73:1465–1470

Bell NGA, Michalchuk AAL, Blackburn JWT et al (2015) Isotope-filtered 4D NMR spectroscopy for structure determination of humic substances. Angew Chem Int Ed Engl 54:8382–8385

Blanco MJ, Almendros G (1997) Chemical transformation, phytotoxicity and nutrient availability in progressive composting stages of wheat straw. Plant Soil 196:15–25

Blodig W, Smith AT, Winterhalter K et al (1999) Evidence from spin-trapping for a transient radical on tryptophan residue 171 of lignin peroxidase. Arch Biochem Biophys 370:86–92

Bollag JM (1992) Enzymes catalyzing oxidative coupling reactions of pollutants. In: Sigel H, Sigel A (eds) Metal ions in biological systems. Marcel-Dekker, New York, pp 205–217

Bronick CJ, Lal R (2005) Soil structure and management: a review. Geoderma 124:3–22

Busato JG, Canellas LP, Rumjanek VM et al (2005) Rev Bras Ciênc Solo 29:945–953

Campanella L, Tomasetti M, Piccolo A (1990) TG and IR analysis of different extracts of soil humic acids. Termochim Acta 170:67–80

Canellas LP, Olivares FL (2014) Physiological responses to humic substances as plant growth promoter. Chem Biol Technol Agric 1:3

Canellas LP, Piccolo A, Dobbss LB et al (2010) Chemical composition and bioactivity properties of size-fractions separated from a vermicompost humic acid. Chemosphere 78:457–466
Challinor JM (1989) A pyrolysis-derivatisation-gas chromatography technique for the structural elucidation of some synthetic polymers. J Anal Appl Pyrol 16:323–333
Challinor JM (2001) Review: the development and applications of thermally assisted hydrolysis and methylation reactions. J Anal Appl Pyrol 61:3–34
Christoforidis KC, Un S, Deligiannakis Y (2007) High-field 285 GHz electron paramagnetic resonance study of indigenous radicals of humic acids. J Phys Chem A 111:11860–11866
Cole EB (1997) Electrospray ionization mass spectrometry. In: Wiley & Sons (ed) Fundamentals, instrumentation and applications. Wiley & Sons, New York, NY
Conte P, Piccolo A (1999) Conformational arrangement of dissolved humic substances. Influence of solution composition on the association of humic molecules. Environ Sci Technol 33:1682–1690
Conte P, Spaccini R, Smejkalova D, Nebbioso A, Piccolo A (2007) Spectroscopic and conformational properties of size-fractions separated from a lignite humic acid. Chemosphere 69:1032–1039
Cozzolino A, Piccolo A (2002) Polymerization of dissolved humic substances catalyzed by peroxidase. Effects of pH and humic composition. Org Geochem 33:281–294
Cozzolino A, Conte P, Piccolo A (2001) Conformational changes of soil humic substances induced by some hydroxy-, cheto-, and sulphonic acids. Soil Biol Biochem 33:563–571
DeForest PR, Tebbet IR, Larsen AK (1994) Pyrolisys Gas Chromatography in Forensic Science. In: Tebbett I (ed) Gas chromatography in forensic science. Prentice Hall, Oltd Tappan, NJ, pp 165–1850
Deiana S, Gessa C, Manunza B et al (1990) Analytical and spectroscopic characterization of humic acids extracted from sewage sludge, manure, and worm compost. Soil Sci 150:419–424
del Río JC, Rencoret J, Prinsen P et al (2012) Structural characterization of wheat straw lignin as revealed by analytical pyrolysis, 2D-NMR, and reductive cleavage methods. J Agric Food Chem 60:5922–59350
Dobbss LB, Canellas LP, Olivares FL et al (2010) Bioactivity of chemically transformed humic matter from vermicompost on plant root growth. J Agric Food Chem 58:3681–3688
Doty FD, Entzminger G, Yang AY (1998) Magnetism in high-resolution NMR probe design: HR MAS. Concept Magnetic Res 10:239–260
Drosos M (2009) Isolation and physical-chemical characterization of humic and fulvic acids from Greek soils/lignite/compost. Ph.D. thesis, University of Ioannina, Greece, p 116
Drosos M, Jerzykiewicz M, Louloudi M (2011) Progress towards synthetic modelling of humic acid: peering into the physicochemical polymerization mechanism. Colloids Surf A Physicochem Eng Asp 389:254–265
Duer MJ (2002) Solid-state NMR Spectroscopy: Principles and Applications, first ed., Blackwell Science, Oxford
Ertani A, Francioso O, Tugnoli V et al (2011) Effect of commercial lignosulfonate-humate on *Zea mays* metabolism. J Agric Food Chem 59:11940–11948
Fernández-Gómez MJ, Nogales R, Plante A et al (2015) Application of a set of complementary techniques to understand how varying the proportion of two wastes affects humic acids produced by vermicomposting. Waste Manage 35:81–88
Ferreira AJ, Nascimento RO, Martin-Neto L (2001) Hydrophobic interactions between spin-label 5-SASL and humic acid as revealed by ESR spectroscopy. Environ Sci Technol 35:761–765
Francioso O, Ferrari E, Saladini M, Montecchio D, Gioacchini P, Ciavatta C (2007) TG–DTA, DRIFT and NMR characterisation of humic-like fractions from olive wastes and amended soil. J Hazard Mat 149:408–417
Fuentes M, Baigorri R, González-Vila FJ et al (2010) Pyrolysis–gas chromatography/mass spectrometry identification of distinctive structures providing humic character to organic materials. J Environ Qual 39:1486–1497
Fukushima M, Yamamoto M, Komani T et al (2009) Studies of structural alterations of humic acids from conifer bark residue during composting by pyrolysis-gas chromatography/mass spectrometry using tetramethylammonium hydroxide (TMAH-py-GC/MS). J Anal Appl Pyrol 86:200–206

Garbin JR, Milori DMBP, Simões ML et al (2007) Influence of humic substances on the photolysis of aqueous pesticide residues. Chemosphere 66:1692–1698
Giannakopoulos E, Christoforidis KC, Tsipis A et al (2005) Influence of Pb(II) on the radical properties of humic substances and model compounds. J Phys Chem A 109:2223–2232
Giannakopoulos E, Stathi P, Dimos K et al (2006) Adsorption and radical stabilization of humic-acid analogues and Pb^{2+} on restricted phylomorphous clay. Langmuir 22:6863–6873
Giannakopoulos E, Drosos M, Deligiannakis Y (2009) A humic-acid-like polycondensate produced with no use of catalyst. J Colloid Interface Sci 336:59–66
Gil AM, Lopes MH, Pascoal Neto C et al (1999) Very high-resolution 1H MAS NMR of a natural polymeric material. Solid State Nucl Mag 15:59–67
Goñi MA, Hedges JI (1992) Lignin dimers: structures, distribution, and potential geochemical applications. Geochim Cosmochim Acta 56:4025–4043
Grasset L, Vlčková Z, Kučerík J et al (2010) Characterization of lignin monomers in low rank coal humic acids using the derivatization/reductive cleavage method. Org Geochem 41:905–909
Guerra A, Filipponen I, Lucia L et al (2006) Comparative evaluation of three lignin isolation protocols for various wood species. J Agric Food Chem 54:9705
Haider K, Martin JP (1967) Synthesis and transformation of phenolic compounds by *Epicoccum nigrum* in relation to humic acid formation. Soil Sci Soc Am Proc 31:766–772
Hatcher PG, Clifford DJ (1994) Flash pyrolysis and in situ methylation of humic acids from soil. Org Geochem 21:1081–1092
Hayes MHB, Stacey M, Swift RS (1972) Degradation of humic acid in a sodium sulphide solution. Fuel 51:211–213
He Z, Olk DC, Cade-Menum BJ (2011) Forms and lability of phosphorus in humic acid fractions of hord silt loam soil. Soil Sci Soc Am J 75:1712–1722
Hedenstrom M, Wiklund-Lindstrom S, Oman T et al (2009) Identification of lignin and polysaccharide modifications in populus wood by chemometric analysis of 2D NMR spectra from dissolved cell walls. Mol Plant 2:933–942
Hmid A, Mondelli D, Fiore S, Dumontet S (2014) Production and characterization of biochar from three-phase olive mill waste through slow pyrolysis. Biomass Bioenerg 71:330–339
Holtman K, Chang H-M, Jameel H et al (2003) Elucidation of lignin structure through degradative methods: comparison of modified DFRC and thioacidolysis. J Agric Food Chem 51: 3535–3540
Hon DNS (1992) Electron Spin Resonance (ESR) Spectroscopy. In: Lin SY, Dence CW (eds) Methods in lignin chemistry. Springer, Berlin, pp 274–287
Ikeda T, Holtman K, Kadla JF et al (2002) Studies on the effect of ball milling on lignin structure using a modified DFRC method. J Agric Food Chem 50:129–135
Ishida Y, Katagiri M, Ohtani H (2009) Reaction efficiency of organic alkalis with various classes of lipids during thermally assisted hydrolysis and methylation. J Chromatogr A 1216:3296–3299
Jacobsen NE (2007) NMR spectroscopy explained – simplified theory, applications and examples for organic chemistry and structural biology. Wiley & Sons, Hoboken, NJ
Janoš P (2003) Separation methods in the chemistry of humic substances. J Chromatogr A 983:1–18
Jezierski A, Czechowski F, Jerzykiewicz M et al (2000a) Electron paramagnetic resonance (EPR) studies on stable and transient radicals in humic acids from compost, soil, peat and brown coal. Spectrochim Acta Mol Biomol Spectrosc 56:379–385
Jezierski A, Czechowski F, Jerzykiewicz M et al (2000b) EPR investigations of structure of humic acids from compost, soil, peat and soft brown coal upon oxidation and metal uptake. Appl Magn Res 18:127–136
Jindo K, Martim SA, Navarro EC et al (2012) Root growth promotion by humic acids from composted and non-composted urban organic wastes. Plant Soil 353:209–220
Jouraiphy A, Amir S, Winterton P et al (2008) Structural study of the fulvic fraction during composting of activated sludge-plant matter: elemental analysis, FTIR and 13C NMR. Bioresource Technol 99:1066–1077
Kamiya M, Kameyama K (1998) Photochemical effects of humic substances on the degradation of organophosphorus pesticides. Chemosphere 36:2337–2344

Keeler C, Kelly EF, Maciel GE (2006) Chemical–structural information from solid-state 13C NMR studies of a suite of humic materials from a lower montane forest soil, Colorado, USA. Geoderma 130:124–140

Kelleher BP, Simpson AJ (2006) Humic substances in soils: are they really chemically distinct? Environ Sci Technol 40:4605–4611

Kossa WC, MacGee J, Ramachandran JS, Webber AJ (1979) Pyrolytic methylation/gas chromatography. A short review. J Chromatogr Sci 17:177–187

Larter SR, Horsfield B (1993) Determination of structural components of kerogens by the use of analytical pyrolysis methods. In: Engel MH, Macko SA (eds) Organic geochemistry. Principles and applications. Plenum, New York, NY, pp 271–288

Lattao C, Birdwell J, Wang JJ, Cook RL (2008) Studying organic matter molecular assemblage within a whole organic soil by nuclear magnetic resonance. J Environ Qual 37:1501–1509

Le Brech Y, Delmotte L, Raya J et al (2015) High resolution solid state 2D NMR analysis of biomass and biochar. Anal Chem 87:843–847

Lehmann J, Kuzyakov Y, Pan G, Ok Y-S (2015) Biochars and the plant-soil interface. Plant Soil 395:1–5

Lehtonen T, Peuravuori J, Pihlaja K (2003) Comparison of quaternary methyl-, ethyl- and butylammonium hydroxides as alkylating reagents in pyrolysis-GC/MS studies of aquatic fulvic acid. J Anal Appl Pyrol 68–69:315–329

Leinweber P, Schulten HR, Horte C (1992) Differential thermal analysis, thermogravimetry and pyrolysis-field ionisation mass spectrometry of soil organic matter in particle-size fractions and bulk soil sample. Thermochim Acta 194:175–187

Levitt M (2008) Spin dynamics: basics of nuclear magnetic resonance, 2nd edn. Wiley & Sons, Chichester

Li M, Mazzei P, Cozzolino V et al (2015) Optimized procedure for the determination of P species in soil by liquid-state 31P-NMR spectroscopy. Chem Biol Technol Agric 2:7

Liitia T, Maunu SL, Sipil J, Hortling B (2002) Application of solid-state 13CNMR spectroscopy and dipolar dephasing technique to determine the extent of condensation in technical lignins. Solid State Nucl Mag 21:171–186

Lin CSK, Pfaltzfraff LA, Herrero-Davila L et al (2013) Food waste as a valuable resource for the production of chemicals, materials and fuels. Current situation and global perspective. Energ Environ Sci 6:426–464

Liptaj T, Barancikova G, Pronayova N (2005) Application of 31P nuclear magnetic resonance for study of phosphorus structural types in humic acids. Agriculture (Bratislava, Slovakia) 51:423–428

Lovley DR, Coates JD, Blunt-Harris EL et al (1996) Humic substances as electron acceptors for microbial respiration. Nature 382:445–448

Lu F, Ralph J (1996) Reactions of lignin model β-aryl ethers with acetyl bromide. Holzforschung 50:360–364

Lu F, Ralph J (1997a) Derivatization followed by reductive cleavage (DFRC method), a new method for lignin analysis: protocol for analysis of DFRC monomers. J Agric Food Chem 45:2590–2592

Lu F, Ralph J (1997b) The DFRC method for lignin analysis. Part 1. A new method for β-aryl ether cleavage: lignin model studies. J Agric Food Chem 45:4655–4660

Lu F, Ralph J (2003) Non-degradative dissolution and acetylation of ball-milled plant cell walls: high-resolution solution-state NMR. Plant J 35:535–544

Mao JD, Schmidt-Rohr K (2004) Separation of aromatic-carbon ^{13}C NMR signals from di-oxygenated alkyl bands by a chemical-shift-anisotropy filter. Solid State Nucl Mag 26:36–45

Mao JD, Xing B, Schmidt-Rohr K (2001) New structural information on a humic acid from two-dimensional 1H-13C correlation solid-state nuclear magnetic resonance. Environ Sci Technol 35:1928–1934

Mao JD, Chen N, Cao X (2011) Characterization of humic substances by advanced solid state NMR spectroscopy: demonstration of a systematic approach. Org Geochem 42:891–902

Marchesini A, Allievi L, Comotti E, Ferrari A (1988) Long-term effects of quality-compost treatment on soil. Plant Soil 106:253–261
Martin JP, Haider K, Wolf D (1972) Synthesis of phenols and phenolic polymers by Hendersonula toruloidea in relation to humic acid formation. Soil Sci Am Proc 36:311–315
Martin JP, Haider K, Saiz-Jimenez C (1974) Sodium amalgam reductive degradation of fungal and model phenolic polymers soil humic acids and simple phenolic compounds. Soil Sci Am Proc 38:760–765
Martin AR, Martins MA, da Silva ORRF, Mattoso LHC (2010) Studies on the thermal properties of sisal fiber and its constituents. Thermochim Acta 506:14–19
Maunu SL (2002) NMR studies of wood and wood products. Prog Nucl Magn Reson Spectrosc 40:151–174
Mazzei P, Piccolo A (2012) Quantitative evaluation of noncovalent interactions between glyphosate and dissolved humic substances by NMR spectroscopy. Environ Sci Technol 46:5939–5946
Mazzei P, Piccolo A (2015) Interactions between natural organic matter and organic pollutants as revealed by NMR spectroscopy. Magn Reson Chem 53:667–678
McBeath AV, Smernik RJ, Krull ES, Lehmann J (2014) The influence of feedstock and production temperature on biochar carbon chemistry: a solid-state 13C NMR study. Biomass Bioenerg 60:121–129
McIntyre C, Jardine DR, McRae C (2001) Electrospray mass spectrometry of aquatic fulvic acids. Rapid Commun Mass Spectrom 15:1974–1975
Mitchell PJ, Simpson AJ, Soong R, Simpson MJ (2015) Shifts in microbial community and water-extractable organic matter composition with biochar amendment in a temperate forest soil. Soil Biol Biochem 81:244–254
Moldoveanu SC (ed) (1998) Analytical pyrolysis of natural organic polymers. Elsevier, Amsterdam, NL
Morris KF, Cutak BJ, Dixon AM, Larive CK (1999) Analysis of diffusion coefficient distributions in humic and fulvic acids by means of diffusion ordered NMR spectroscopy. Anal Chem 71:5315–5321
Nebbioso A, Piccolo A (2009) Molecular rigidity and diffusivity of Al^{3+} and Ca^{2+} humates as revealed by NMR spectroscopy. Environ Sci Technol 43:2417–2424
Nebbioso A, Piccolo A (2011) Basis of a humeomics science: chemical fractionation and molecular characterization of humic biosuprastructures. Biomacromolecules 12:1187–1199
Nebbioso A, Piccolo A (2012) Advances in humeomic: enhanced structural identification of humic molecules after size fractionation of a soil humic acid. Anal Chim Acta 720:77–90
Nebbioso A, Piccolo A, Spiteller M (2010) Limitations of electrospray ionization in the analysis of a heterogeneous mixture of naturally occurring hydrophilic and hydrophobic compounds. Rapid Commun Mass Spectrom 24:3163–3170
Nebbioso A, Mazzei P, Savy D (2014) Reduced complexity of multidimensional and diffusion NMR spectra of soil humic fractions as simplified by humeomics. Chem Biol Technol Agr 1:24
Nebbioso A, Vinci G, Drosos M et al (2015) Unveiling the molecular composition of the unextractable soil organic fraction (humin) by humeomics. Biol Fertil Soils 51:443–451
Nuzzo A, Scherman OA, Mazzei P, Piccolo A (2014) pH-controlled release of auxin plant hormones from cucurbit[7]uril macrocycle. Chem Biol Technol Agr 1:2
Ohno T, He Z, Sleighter RL, Honeycutt CW, Hatcher PG (2010) Ultrahigh resolution mass spectrometry and indicator species analysis to identify marker components of soil- and plant biomass-derived organic matter fractions. Environ Sci Technol 44:8594–8600
Paul A, Stösser R, Zehl A et al (2006) Nature and abundance of organic radicals in natural organic matter: effect of pH and irradiation. Environ Sci Technol 40:5897–5903
Peacock AD, Macnaughton SJ, Cantu J et al (2001) Soil microbial biomass and community composition along an anthropogenic disturbance gradient within a long-leaf pine habitat. Ecol Indic 1:113–121
Pfeifer T, Uwe K, Hoffmann R, Spiteller M (2001) Characterisation of humic substances using atmospheric pressure chemical ionisation and electrospray ionisation mass spectrometry combined with size-exclusion chromatography. J Chromatogr A 926:151–159

Piccolo A (1988) Characteristics of soil humic substances extracted with some organic and inorganic solvents and purified by the HCl-HF treatment. Soil Sci 146:418–426
Piccolo A (2002) The supramolecular structure of humic substances. A novel understanding of humus chemistry and implications in soil science. Adv Agron 75:57–134
Piccolo A, Spiteller M (2003) Electrospray ionization mass spectrometry of terrestrial humic substances and their size-fractions. Anal Bioanal Chem 377:1047–1059
Piccolo A, Campanella L, Petronio BM (1990) ^{13}C-NMR spectra of humic substances extracted with different mechanisms. Soil Sci Soc Am J 54:750–755
Piccolo A, Nardi S, Concheri G (1996) Macromolecular changes of soil humic substances induced by interactions with organic acids. Eur J Soil Sci 47:319–328
Piccolo A, Conte P, Cozzolino A (1999) Effects of mineral and monocarboxylic acids on the molecular association of dissolved humic substances. Eur J Soil Sci 50:687–694
Piccolo A, Cozzolino A, Conte P, Spaccini R (2000) Polymerization of humic substances by an enzyme-catalyzed oxidative coupling. Naturwissenschaften 87:391–394
Piccolo A, Conte P, Cozzolino A (2001) Chromatographic and spectrophotometric properties of dissolved humic substances compared with macromolecular polymers. Soil Sci 166:174–185
Piccolo A, Conte P, Trivellone E et al (2002) Reduced heterogeneity of a lignite humic acid by preparative HPSEC following interaction with an organic acid. Characterization of size-separates by PYR-GC-MS and ^{1}H-NMR spectroscopy. Environ Sci Technol 36:76–84
Piccolo A, Conte P, Spaccini R, Chiarella M (2003) Effects of some dicarboxylic acids on the association of dissolved humic substances. Biol Fertil Soils 37:255–259
Piccolo A, Conte P, Tagliatesta P (2005) Increased conformational rigidity of humic substances by oxidative biomimetic catalysis. Biomacromolecules 6:351–358
Piccolo A, Spiteller M, Nebbioso A (2010) Effects of sample properties and mass spectroscopic parameters on electrospray ionization mass spectra of size-fractions from a soil humic acid. Anal Bioanal Chem 397:3071–3078
Plancque G, Amekraz B, Moulin V et al (2001) Molecular structure of fulvic acids by electrospray with quadrupole time-of-flight mass spectrometry. Rapid Commun Mass Spectrom 15:827–835
Plant AF, Fernández JM, Leifeld J (2009) Application of thermal analysis techniques in soil science. Geoderma 153:1–10
Pöerschmann J (2000) Gas Chromatography. In: Wilson ID (ed) Encyclopedia of separation science. Elsevier, Amsterdam, pp 3026–3032
Popa VI, Dumitru M, Volfa I, Anghel N (2008) Lignin and polyphenols as allelochemicals. Ind Crops Prod 27:144–149
Preston CM, Nault JR, Trofymow JA (2009) Chemical changes during 6 years of decomposition of 11 litters in some Canadian forest sites. Part 2. 13C abundance, solid-state 13C NMR spectroscopy and the meaning of "lignin". Ecosystems 12:1078–1102
Ralph J, Lu F (1998) The DFRC method for lignin analysis. 6. A simple modification for identifying natural acetates on lignins. J Agric Food Chem 46:4616–4619
Reemtsma T, These A (2003) On-line coupling of size exclusion chromatography with electrospray ionization-tandem mass spectrometry for the analysis of aquatic fulvic and humic acids. Anal Chem 75:1500–1507
Reemtsma T, These A, Venkatachari P et al (2006) Identification of fulvic acids and sulfated and nitrated analogues in atmospheric aerosol by electrospray ionization Fourier transform ion cyclotron resonance mass spectrometry. Anal Chem 78:8299–8304
Rencoret J, Gutierrez A, Nieto L et al (2011) Lignin composition and structure in young versus adult *Eucalyptus globulus* plants. Plant Physiol 155:667–682
Rex RW (1960) Electron paramagnetic resonance studies of stable free radicals in lignins and humic acids. Nature 188:1185–1186
Saiz-Jimenez C (1996) The chemical structure of humic substances. Recent advances. In: Picco A (ed) Humic substances in terrestrial ecosystems. Elsevier, Amsterdam
Savy D, Piccolo A (2014) Physical–chemical characteristics of lignins separated from biomasses for second-generation ethanol. Biomass Bioenerg 62:58–67

Savy D, Mazzei P, Drosos M et al (2015a) Molecular composition of water-soluble lignins separated from different non-food biomasses. Fuel Process Technol 131:175–181
Savy D, Mazzei P, Roque R et al (2015b) Structural recognition of lignin isolated from bioenergy crops by subcritical water:ethanol extraction. Fuel Process Technol 138:637–644
Savy D, Cozzolino V, Nebbioso A et al (2015c) Water-soluble lignins from different biomasses for energy stimulate the early development of maize (*Zea mays*, L.). Molecules 20:19958–19970
Savy D, Cozzolino V, Nebbioso A et al (2016) Humic-like bioactivity on emergence and early growth of maize (*Zea mays* L) of water-soluble lignins isolated from biomass for energy. Plant Soil 402:221–233. doi:10.1007/s11104-015-2780-2
Shindo H, Huang PM (1982) Role of Mn(IV) oxide in abiotic formation of humic substances in the environment. Nature 298:363–365
Simpson AJ (2001) Multidimensional solution state NMR of humic substances: a practical guide and review. Soil Sci 166:795–809
Simpson AJ, Kingery WL, Shaw D et al (2001) The application of 1H HR-MAS NMR spectroscopy for the study of structures and associations of organic components at the solid-aqueous interface of a whole soil. Environ Sci Technol 35:3321–3325
Simpson AJ, Tseng LH, Simpson MJ et al (2004) The application of LC-NMR and LC-SPE-NMR to compositional studies of natural organic matter. Analyst 129:1216–1222
Simpson AJ, Simpson MJ, Smith E, Kelleher BP (2007) Microbially derived inputs to soil organic matter: are current estimates too low? Environ Sci Technol 41:8070–8076
Simpson AJ, McNally DJ, Simpson MJ (2011) NMR spectroscopy in environmental research: From molecular interactions to global processes. Prog Nucl Magn Reson Spectrosc 58:97–175
Smejkalova D, Piccolo A. (2008) Aggregation and disaggregation of humic supramolecular assemblies by nmr diffusion ordered spectroscopy (DOSY-NMR). Environ Sci Technol 42: 699–706.
Šmejkalová D, Spaccini R, Piccolo A (2008) Multivariate analysis of CPMAS 13C-NMR spectra of soils and humic matter as a tool to evaluate organic carbon quality in natural systems. Eur J Soil Sci 59:496–504
Spaccini R, Piccolo A (2007) Molecular characterization of compost at increasing stages of maturity. 1. Chemical fractionation and infrared spectroscopy. J Agric Food Chem 55:2293–2302
Spaccini R, Piccolo A (2009) Molecular characteristics of humic acids extracted from compost at increasing maturity stages. Soil Biol Biochem 41:1164–1172
Spaccini R, Piccolo A (2013) Effects of field managements for soil organic matter stabilization on water-stable aggregates distribution and aggregate stability in three agricultural soils. J Geochem Explor 129:45–51
Spaccini R, Mazzei P, Squartini A, Giannattasio M, Piccolo A (2012) Molecular properties of a fermented manure preparation used as field spray in biodynamic agriculture. Environ Sci Pollut Res 19:4214–4225
Steelink C, Tollin G (1962) Stable free radicals in soil humic acid. Biochim Biophys Acta 59:25–34
Stenson AC, Landing WM, Marshall AG, Cooper WT (2002) Ionization and fragmentation of humic substances in electrospray ionization Fourier transform-ion cyclotron resonance mass spectrometry. Anal Chem 74:4397–4409
Stenson AC, Marshall AG, Cooper WT (2003) Exact masses and chemical formulas of individual Suwannee River fulvic acids from ultrahigh resolution electrospray ionization Fourier transform ion cyclotron resonance mass spectra. Anal Chem 75:1275–1284
Striegel A, Yau WW, Kirkland JJ, Bly DD (eds) (2009) Modern size exclusion chromatography: practice of gel permeation and gel filtration chromatography, 2nd edn. Wiley, New York, NY
Sunda WG, Kieber DJ (1994) Oxidation of humic substances by manganese oxides yields low-molecular-weight organic substrates. Nature 367:62–65
Tanczos I, Schoflinger M, Schmidt H, Balla J (1997) Cannizzaro reaction of aldehydes in TMAH thermochemolysis. J Anal Appl Pyrol 42:21–31

Tohmura S, Argyropoulos DS (2001) Determination of arylglycerol-β-aryl ethers and other linkages in lignins using DFRC/31P NMR. J Agric Food Chem 49:536–542

Vane CH, Martin SC, Snape CE, Abbott GD (2001) Degradation of lignin in wheat straw during growth of the oyster mushroom (*Pleurotus ostreatus*) using off-line thermochemolysis with tetramethylammonium hydroxyde and solid state ^{13}C NMR. J Agric Food Chem 49:709–2716

Wang MC, Huang PM (1986) Humic macromolecule Interlayering in nontronite through interaction with phenol monomers. Nature 323:529–531

Wang MC, Huang PM (1989) Abiotic ring cleavage of pyrogallol and the associated reactions as catalyzed by a natural soil. Sci Total Environ 81:501–510

Wang MC, Huang PM (2003) Cleavage and polycondensation of pyrogallol and glycine catalyzed by natural soil clays. Geoderma 112:31–50

Wang TSC, Kao MM, Huang PM (1980) The effect of pH on the catalytic synthesis of humic substances by illite. Soil Sci 129:333–338

Weber J, Karczewska A, Drozd J et al (2007) Agricultural and ecological aspects of a sandy soil as affected by the application of municipal solid waste composts. Soil Biol Biochem 39: 1294–1302

You TT, Mao J, Yuan T et al (2013) Structural elucidation of the lignins from stems and foliage of *Arundo donax* Linn. J Agric Food Chem 61:5361–5370

Zakzeski J, Bruijnincx PCA, Jongerius AL et al (2010) The catalytic valorization of lignin for the production of renewable chemicals. Chem Rev 110:3552–3599

Zang X, van Heemst JDH, Dria KJ et al (2000) Encapsulation of protein in humic acid from a histosol as an explanation for the occurrence of organic nitrogen in soil and sediment. Org Geochem 31:679–695

Zhang D, Pan G, Wu G et al (2014) Biochar helps enhance maize productivity and reduce greenhouse gas emissions under balanced fertilization in a rainfed low fertility inceptisol. Chemosphere 142:106–113

Chapter 5
Mass Spectrometry for Metabolomics and Biomass Composition Analyses

Maria Esther Ricci-Silva, Boniek Gontijo Vaz, Géssica Adriana Vasconcelos, Wanderson Romão, Juliana A. Aricetti, Camila Caldana, and Patrícia Verardi Abdelnur

Abstract Mass spectrometry (MS) is a versatile technique used to analyze a broad range of compounds originated from different species with high accuracy, resolution, sensibility, selectivity, and fast scan speed. MS has been widely used in various areas, from theoretical chemistry studies to the discovery of disease

M.E. Ricci-Silva
EMBRAPA Agroenergy, Brazilian Agricultural Research Corporation, National Center for Agroenergy Research, Parque Estação Biológica, PqEB s/n, Av. W3 Norte (final), 70770-901 Brasília, DF, Brazil

B.G. Vaz • G.A. Vasconcelos
Institute of Chemistry, Mass Spectrometry and Chromatography Laboratory, Federal University of Goiás, Avenida Esperança s/n, 74690-900 Goiânia, GO, Brazil

W. Romão
Department of Chemistry, Petroleomic and Forensic Laboratory, Federal University of Espírito Santo, Av. Fernando Ferrari, 514, 29075-910 Vitoria, ES, Brazil

J.A. Aricetti
Brazilian Bioethanol Science and Technology Laboratory at Brazilian Center for Research in Energy and Materials, Rua Giuseppe Máximo Scolfaro 10000, CP 6192, 13083-970 Campinas, SP, Brazil

C. Caldana
Brazilian Bioethanol Science and Technology Laboratory at Brazilian Center for Research in Energy and Materials, Rua Giuseppe Máximo Scolfaro 10000, CP 6192, 13083-970 Campinas, SP, Brazil

Max Planck Partner Group at Brazilian Bioethanol Science and Technology Laboratory/CNPEM, Campinas, SP, Brazil

P.V. Abdelnur (✉)
EMBRAPA Agroenergy, Brazilian Agricultural Research Corporation, National Center for Agroenergy Research, Parque Estação Biológica, PqEB s/n, Av. W3 Norte (final), 70770-901 Brasília, DF, Brazil

Institute of Chemistry, Mass Spectrometry and Chromatography Laboratory, Federal University of Goiás, Avenida Esperança s/n, 74690-900 Goiânia, GO, Brazil
e-mail: patricia.abdelnur@embrapa.br

S. Vaz Jr. (ed.), *Analytical Techniques and Methods for Biomass*,
DOI 10.1007/978-3-319-41414-0_5

biomarkers. In this chapter, we will focus on the use of MS in bioenergy, describing new developed technologies that can perform a full metabolite characterization of a biological system. The chapter is presented in three topics: (1) Mass spectrometry; (2) Mass spectrometry-based metabolomics; and (3) Mass spectrometry for biomass composition analyses. The first topic (Section 1), is about the fundamentals of MS, including some advanced applications in instrumentation that greatly contribute to chemical compound identification and characterization. The next two other topics describe the applications of MS in two important areas related to metabolite characterization that are used in the bioenergy scenario. A general description of metabolomics principles and approaches, such as targeted and untargeted analyses, was discussed, including some applications in the system biology (Section 2). Finally, an overview of agricultural biomass composition for biofuel and chemicals production, based on MS approaches, is presented in Section 3.

Keywords Metabolomics for bioenergy • Metabolomics-assisted synthetic biology • Metabolite characterization • Biomass characterization

5.1 Mass Spectrometry

Mass spectrometry (MS) has emerged as a powerful technique to analyze qualitatively and quantitatively a wide range of compounds and materials, from small molecules to large polymers, including inorganic and organic compounds, peptides, proteins, nucleic acids, and molecule interactions. The analytical applications are selected based on the MS instrumentation features, such as dynamic range, resolution, accuracy, sensitivity, specificity, and speed of scan rate (Hoffmann and Stroobant 2007). MS applications can be used to determine the molecular weight of compounds, structure elucidation (mono- or multimers) or to provide a complete profile of a sample using the full-scan mode (Silverstein et al. 2005). Due to the advances in MS technology, nowadays, it has become a multidisciplinary area, requiring a combination of expertises in chemistry, bioinformatics, biochemistry, and informatics.

Typically, a mass spectrometer consists of five main parts: (a) sample inlet, (b) ion source, (c) mass analyser, (d) detector, and (e) data processing (Fig. 5.1). Analytes generally are ionized in the ion source, isolated based on their mass/charge ratio (*m/z*) in the mass analyser, detected and, finally, a spectrum is generated for data interpretation. In addition, tandem MS (MS/MS or MS^n) provides structural characterization. Usually, this approach is based on collision-induced dissociation (CID), which involves an inert gas that collides with a selected precursor ion resulting in product ions (Williams and Scrivens 2005).

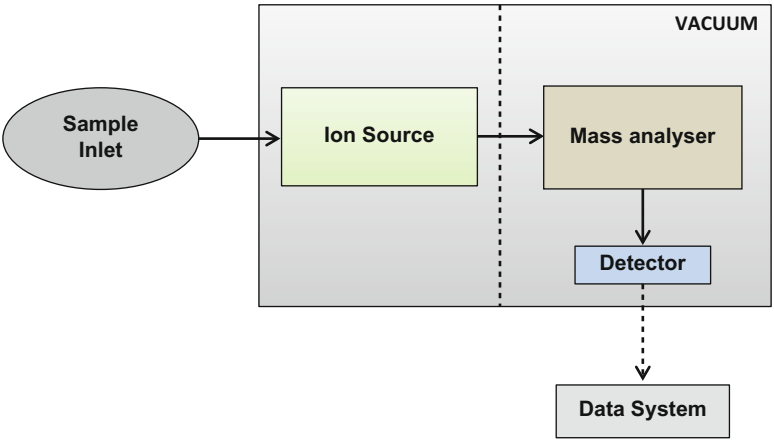

Fig. 5.1 General schematic diagram of a mass spectrometer

5.1.1 Sample Inlet

The choice of inlet to be used is always dependent of the sample composition. Analytes in solution can be directly injected into the mass spectrometer through a syringe (direct infusion) or after a pre-separation step, as liquid chromatographic columns, whereas volatile and thermo-stable samples use gas chromatography as sample inlet. Capillary electrophoresis (CE) is a powerful technique for the separation of charged metabolites, offering high-analyte resolution. The combination with mass spectrometry makes CE-MS an ideal tool for the analysis of the metabolome. However, only a few applications have been published to date.

5.1.1.1 Gas Chromatography (GC)

GC is a standard technique used to analyze volatile, thermo-stable, and apolar compounds (Van Bramer 1998). Derivatization is a pre-treatment process required for studies involving polar molecules to reduce their polarity or enhance the detection of some compounds (Koek et al. 2011). In general, this method is robust and reproducible, however, it is a time-consuming step (Covey et al. 1991). Complex mixtures are routinely separated by GC-MS to identify and quantify individual compounds.

5.1.1.2 Liquid Chromatography (LC)

LC is used to analyze a broad range of molecules, varying from small to high molecular weight, apolar to polar and charged or not. Analyzing different types of compounds may be performed by selecting the appropriate column and mobile

phases (Ardey 2003). Reversed phase columns such as C_8 and C_{18} are commonly used in metabolomics and biomass studies, especially for polar metabolites. However, normal phase separation can provide additional information concerning metabolome and biomass composition.

Recently, ultra-high-performance liquid chromatography–mass spectrometry (UHPLC-MS) has been widely applied in different areas as its smaller bead diameters provide higher resolution, shorter run time, and less solvent consuming (Nováková and Vlčková 2009). However, this technique is carried out in a continuous flow which means it cannot be coupled directly to some mass spectrometers that operate in a pulsed mode, like MALDI.

5.1.1.3 Direct Infusion

Samples are directly infused into the mass spectrometer from the condensed phase without chromatographic separation by using a syringe pump or Nanochip. Direct infusion mass spectrometry (DIMS) is a high-throughput method that is widely used for qualitative analyses. However, the co-elution of compounds with a broad difference in the ionization efficiency can result in ion suppression, thereby preventing the detection of low abundant ions (Mol et al. 2011). Isomers (compounds with same molecular formulae) cannot be analyzed directly by DIMS, even using high-resolution mass spectrometry (HRMS), in which case a chromatographic pre-separation is necessary.

5.1.2 Ion Sources

To handle a wide variety of atoms and molecules, matrices, and mixtures, MS needs to promote efficient ionization to generate ions. The main principles of ionization techniques in mass spectrometry used in metabolomics and biomass analysis are discussed below (Fig. 5.2).

5.1.2.1 Electron Ionization (EI)

The EI process (Fig. 5.2a) is a direct result of the energetic electrons interaction with the analytes (Bleakney 1930). Electrons are released from a metal filament (usually rhodium), producing heat of up to 200°C, which will expel the electrons from the metal toward the mass analyser. A classic EI spectrum of organic compounds is obtained when the potential difference between the filament and the source is 70 eV, maintaining a positive potential at the source. EI provides a mass spectra with high repeatability that enables the use of the spectral library for compound identification without injecting standards. There are some GC-MS commercial libraries available, such as NIST (Mass Spectrometry Data Center 2014).

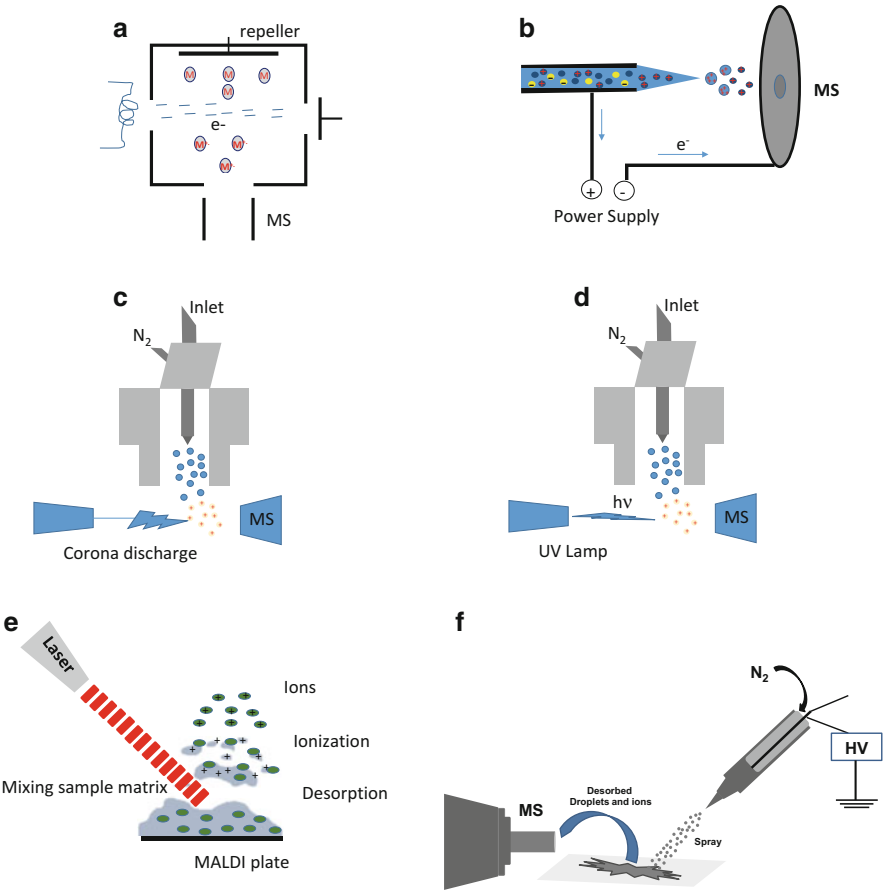

Fig. 5.2 Schematic display of ion sources: (**a**) EI, (**b**) ESI, (**c**) APCI, (**d**) APPI, (**e**) MALDI, and (**f**) DESI

5.1.2.2 Electrospray Ionization (ESI)

ESI is an atmospheric pressure ionization (API) technique (Fig. 5.2b). ESI ionization is produced by applying a high electric field on a continuous liquid flow through a capillar (1–10 μL min^{-1}) under atmospheric pressure. The electric field results from the potential difference (1–4 kV) between the capillar and the counter-electrode separated by 0.3–2 cm (Kebarle 2000). This field induces a charge accumulation on the liquid surface at the end of the capillar, forming highly charged droplets. These droplets pass through a high-temperature gas stream (desolvation gas) or a heated capillar to remove the remaining solvent molecules. An injected coaxial gas allows ion dispersion and spray formation in a limited space, resulting in multi-charged droplets through solvent evaporation and droplet fission caused by Coulombic repulsion. Gas-phase analyte ions are formed from highly charged droplets by the

charge residue or ion evaporation models (Covey et al. 1991). ESI results in high ionization efficiency of different compound classes and, therefore, is the method of choice in a wide range of LC-MS applications for metabolomics.

5.1.2.3 Atmospheric Pressure Chemical Ionization (APCI)

APCI is based on ion–molecule reactions in the gas phase under atmospheric pressure conditions (Fig. 5.2c) (Bruins 1991). The solution containing the analyte is introduced into a pneumatic nebulizer and converted into a fine spray through a high-speed nitrogen flow. The gas flow carries the droplets to a heated quartz tube (120 °C), called a desolvation/vaporization chamber, then they are directed to the corona discharge area, where the ionization process takes place by means of three ionization mechanisms: (1) penning ionization (M^+); (2) protons transfer ($[M+H]^+$ or $[M-H]^-$); and (3) formation of adduct reactant gas ($[M+NH_4]^+$). APCI is a complementary ionization method to ESI; it is applied to apolar, medium-polar, and neutral metabolites.

5.1.2.4 Atmospheric Pressure Photoionization (APPI)

APPI is a technique developed by Bruins in 2000 (Hanold et al. 2004). APPI is a complementary method to ESI and APCI, which differs from some techniques in which a wider range of compounds can be analyzed. APPI analyses apolar compounds (e.g., polycyclic aromatic hydrocarbons). The APPI ionization source consists of a heated nebulizer to desolvate and disperse the eluent, and a UV source (Fig. 5.2d). Photoionization is based on the interaction between a photon beam produced by the discharge lamp and the vapor formed by spraying a liquid solution. Initially, a photon ($E=h\nu$) is absorbed by a molecule (M), resulting in an electronically charged molecule ($M^{+\bullet}$). APPI is commonly applied in environmental (e.g., pesticides) and pharmaceutical (e.g., drugs) analyses.

5.1.2.5 Matrix-Assisted Laser Desorption/Ionization (MALDI)

MALDI is considered a soft ionization method because the mainly monocharged ions produced have low internal energy at low pressure ($\cong 10^{-6}$mbar), and the absence of extensive fragmentation is observed in the spectrum. In the MALDI analysis, the sample is embedded in a matrix (usually 100-fold molar excess), and a laser beam (ultraviolet or infrared pulsed) serves as a source of desorption and ionization. The matrix absorbs the laser energy, thereby inducing the vaporization of the sample. After atomization and ionization, the molecules are transferred to the mass analyser. MALDI has routinely been used for analyzing high-molecular-weight compounds such as protein, peptides, and polymers. However, it provides a poor quantitative performance, low reproducibility and interference on the ionization process caused by the matrix (Vaidyanathan et al. 2006). In metabolomics

studies, MALDI has been applied for lipids analyses (Araújo et al. 2014), and recently MALDI Imaging MS has been used for fast in situ lignin assessment in Eucalyptus (Araújo et al. 2014). A direct surface analysis with an extensive fragmentation of peaks combined with imaging provides a spatial resolution that allows specific chemical mapping using intact tissue. The imaging strategy can be performed by MALDI-TOF or time-of-flight-secondary ionization mass spectrometry (TOF-SIMS). MALDI matrix is applied to the sample and images are generated by scanning the laser over the sample, while, in SIMS, the sample is sputtered with ions to generate secondary ions (Yang and Gilmore 2015). MALDI Imaging MS and SIMS-TOF Imaging have been applied in biomass composition analyses (Saito et al. 2012; Araújo et al. 2014). Biomass application in MS imaging is a promising approach as it provides a unique spatial information of analytes combined to the advantage of the accurate identification by ion fragmentation.

5.1.2.6 Desorption Electrospray Ionization (DESI)

In 2004, Cooks et al. introduced ambient mass spectrometry ionization DESI, which is an atmospheric pressure ion source that ionizes compounds in open air at ambient conditions (Takats et al. 2006). In this ionization method, based on droplet pickup, a spray of charged droplets is directed into the sample, impacting on its surface and spreading secondary microdroplets containing the dissolved analytes from the solvent film. As a consequence, droplets containing analytes are generated in the open ambient and reach the mass spectrometer through a heated extended capillar. After the desorption process, ionization occurs via mechanisms that are similar to those of electrospray ionization. DESI has shown itself to be useful for chemical identification of a broad range of relevant compounds, such as metabolites, pharmaceuticals, drugs of abuse, explosives, organic and inorganic molecules at ambient conditions (Takats et al. 2006).

5.1.3 Mass Analyser

After the ions are produced in the gaseous phase, a mass analyser separates them based on the mass/charge (*m/z*) ratio. There are several mass analysers used in metabolomics approaches which mainly differ in their physical principles used to discriminate the *m/z*, and therefore, result in mass spectra with different magnitudes of resolution and accuracy (Fig. 5.3).

5.1.3.1 Quadrupole (Q)

Q mass filters operate by applying radio frequency (RF) and direct current (DC) voltages to four rods (Fig. 5.3a) (Miller and Denton 1986); its combination determines the ions' trajectories of a given *m/z* within the mass filter. Ions with stable

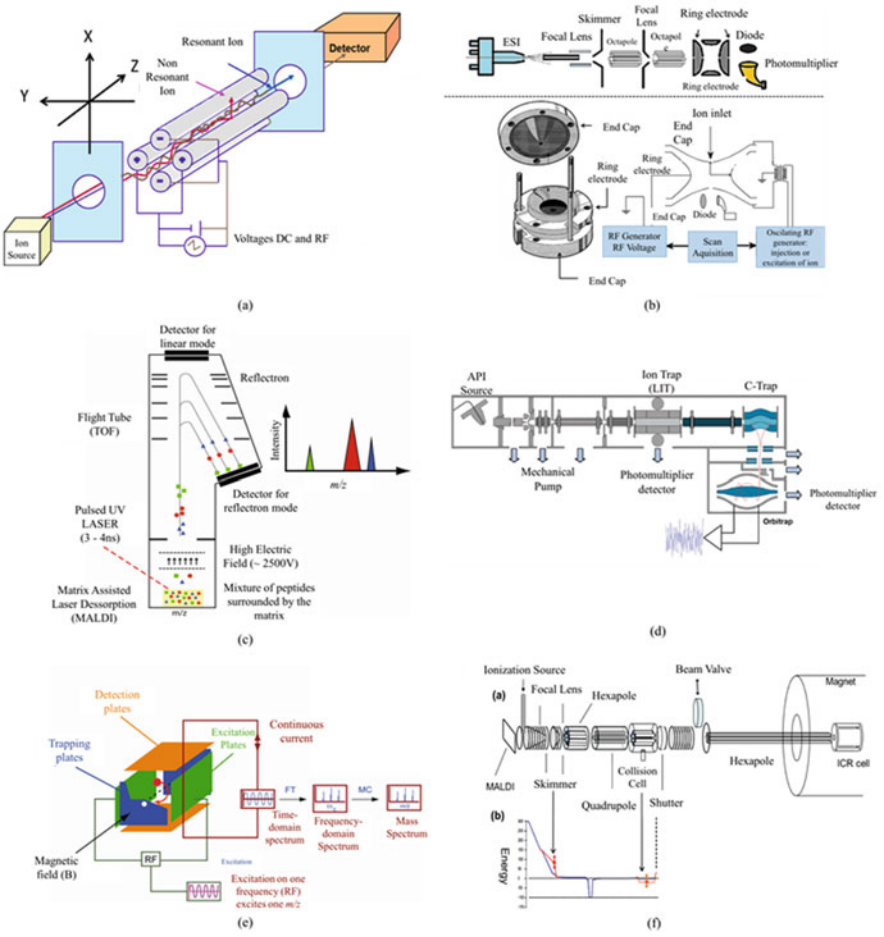

Fig. 5.3 Schematic display of mass analysers: (**a**) quadrupole, (**b**) ion trap, (**c**) TOF (**d**) Orbitrap, and (**e**) ICR. Schemes **d** and **e** were adapted from Thermo Scientific® and Brucker Daltonics®

trajectories pass through the detector, while ions with unstable trajectories are neutralized by striking on the quadrupole electrodes. Ions with different *m/z* can sequentially pass through the mass filter toward the detector by increasing the RF and DC magnitude voltages and by keeping the ratio of these parameters constant. Although Q is considered a low-performance instrument, due to its low-resolution power, accuracy, and dynamic range, it has been widely used for quantitative analysis, and MS fragmentation experiments, which is essential to compound structural elucidation. Q can also be arranged in a tandem configuration, such as a triple quadrupole mass spectrometer. In MS/MS experiments, the first quadrupole selects the precursor ion of interest, the second one works as a collision cell to fragment the precursor ion, and the third one isolates the product ion. The triple quadrupole mass spectrometer is routinely used to perform the quantitation of small molecules, since it offers

good sensitivity, reproducibility, and a broad dynamic range. Finally, the quadrupole could also be coupled to other mass analysers, such as the TOF and orbitrap, to perform MS/MS experiments.

5.1.3.2 Ion Trap (IT)

In this system, ions with different *m/z* are stored and trapped in the ring electrode by applying RF voltage to the two end-cap electrodes with variable voltage (*V*) (Fig. 5.3b) (March and Hughes 1989). The IT is filled with helium to decrease the kinetic energy of ions. During storage, each ion has a discrete orbit due to the RF voltage. The selective ejection process of *m/z* starts when the amplitude of RF voltage applied to the ring electrode is increased until smaller *m/z* ions become unstable and, as a consequence of that, they fly toward the two end-caps electrodes. The biggest advantage of IT is its capability to perform MS^n analyses and its fast screening and fingerprinting of metabolites. Besides that, MS^n spectrometric data facilitate structural identification of compounds, and semi-quantitative analyses can be carried out for a broad range of molecules.

5.1.3.3 Time-of-Flight (TOF)

This mass analyser relies on the acceleration of ions, through a fixed potential into the drift region of a tube (Fig. 5.3c) (Dawson and Guilhaus 1989). They are separated based on their *m/z* according to their flight trajectories through the tube length. Ions with different *m/z* have distinct speeds and, therefore, arrive at the detector at different times. Lighter ions reach the detector faster than the heavier ones if the kinetic energy of the ionized species is theoretically the same. When combining quadrupole with TOF, the Q-TOF mass spectrometer enables MS/MS experiments to be integrated. Q-TOF instruments are often used for identification of metabolites, due to the high resolution and good accuracy that is routinely provided by the TOF analyser.

5.1.3.4 Orbitrap

The Orbitrap analyser is composed of spindle-like central and barrel-like outer electrodes (Fig. 5.3d) (Perry et al. 2008). DC voltage is applied between the two axially symmetric electrodes, resulting in an electrostatic field (Hu et al. 2005). The electrodes are carefully shaped, producing electrostatic attractions that trap a set of ions around a central spindle electrode, while the axial field causes the ions to perform simultaneously harmonic oscillations along the axis at a frequency that is proportional to $(m/z)^{0.5}$. The oscillating ions induce image currents, and the latter is detected by the outer wall of the barrel-like chamber. In a similar manner to FT-ICR, the resultant time-domain signals obtained by ion motion are converted into

frequency-domain signals via Fourier transform, which allows a mass spectrum to be generated. Orbitraps are still capable of achieving mass resolving power of up to 150,000, which places them among the most powerful instruments available today that can perform untargeted metabolomics and biomass composition analyses.

5.1.3.5 Ion Cyclotron Resonance (ICR)

In the broad field of mass spectrometry, FT-ICR MS has unparsed ultra-high resolution and mass accuracy (Marshall et al. 2007). The ions are trapped in the ICR cell—known as the Penning trap (trap in the presence of a magnetic field), and due to an uniform magnetic field, each of the ions starts their precession at a given position (Fig. 5.3e). These trapped ions orbit with a cyclotron frequency that is inversely proportional to their *m/z*. Following the trapping of the ions, the RF voltages on excitation plates held perpendicular to the magnetic field, are swept through a range of frequencies. This action causes the sequential resonance excitation of ions into higher radius orbits. The oscillating field generated by these ion groups induces image currents in circuits connected to the detection plates. The resultant time-domain signals caused by the ion motion are converted to frequency domain signals via a Fourier transform, leading to the generation of a mass spectrum. FT-ICR MS offers superior resolution and mass accuracy, which is necessary to perform analysis of complex mixtures such as bio-oil (Abdelnur et al. 2013).

Analytical success depends on the selection of the correct instrumentation. Several hyphenated mass spectrometers are available, and the best option should be based on desired application. MALDI, ESI, APCI, and APPI are soft ionization techniques that can be associated with higher resolution devices, for instance, the TOF mass analyser. Ion trap spectrometers' main benefit is their capacity for performing MS^n analyses, which helps in structural characterization by further fragmentation of the precursor ions. Moreover, sensitive instruments are also specific, such as the triple quadrupole. Nowadays, HRMS are the best instrumentation (Orbitrap, FT-ICR MS, and Q-TOF MS) available. They can screen samples quickly and group compounds of unknown composition based on fragments.

5.2 Mass Spectrometry-Based Metabolomics

Metabolomics has emerged as a comprehensive analytical approach for profiling and quantifying (or targeting) different classes of low-molecular-weight (MW < 1500 Da) molecules or metabolites that are present in a biological system (Fiehn 2002). Currently, mass spectrometry (MS), alone or coupled with chromatographic separation, is the leading technology for generating metabolomics data (Jorge et al. 2015; Dettmer et al. 2007). The metabolome, typically defined as the quantitative collection of all structurally diverse small molecules present in a cell or organism in a particular state (Jorge et al. 2015; Patti et al. 2012; Oliver et al. 1998),

permits a global view of cellular functions since it directly reflects the physiological status of a cell. The wide range of applications cover multiple research areas such as evaluation of genetically modified organisms (Baker et al. 2006; Kusano et al. 2007, 2011), functional genomics (Watanabe et al. 2008; Hirai et al. 2005; Jung et al. 2012; Park et al. 2012; Yoshida et al. 2010), response to the environment (Caldana et al. 2011; Gibon et al. 2006; Guy et al. 2008; Kaplan et al. 2007; Bergdahl et al. 2012; Jozefczuk et al. 2010), metabolic engineering (Toya and Shimizu 2013; Hasunuma et al. 2011), and quantitative genetics (Keurentjes et al. 2006; Lisec et al. 2008, 2012; Meyer et al. 2007; Sulpice et al. 2009). Furthermore, metabolomics alongside multivariate and correlation analyses provide an excellent tool for the study of systems biology, which is recognized as the cornerstone of this emerging area (Bergdahl et al. 2012; Herrgard et al. 2008; Nielsen and Pronk 2012; Zhang et al. 2003; Hasunuma and Kondo 2012).

Advances in cutting-edge mass spectrometry, associated with the recent development of softwares and bioinformatics, have enabled accurate identification and quantification of a broad range of metabolites simultaneously from a given biological sample without bias (Patti et al. 2012). Despite the significant advances in analytical tools, the complete coverage of the metabolome will be always constrained by polarity, dynamic stability range, and biological properties of metabolites (Hall 2006). Currently, there is no single technology that is suitable to quantify accurately and detect all metabolites from an organism (Lei et al. 2011; Lisec et al. 2006; Fukushima and Kusano 2013; Griffiths et al. 2010). Consequently, the choice of the extraction methods and analytical tools will largely depend on the aim of the study and usually represent a compromise between selectivity and speed of analysis (Lei et al. 2011).

5.2.1 Targeted and Untargeted Approaches

Prior to performing any metabolomics experiments, it is crucial to determine the number and chemical composition of the metabolites to be surveyed. In some cases, a targeted approach, in which the defined groups of chemically characterized and biochemically annotated metabolites that can be measured, may be the best method of choice (Roberts et al. 2012), whereas, in other instances, it may be of interest to cover as many metabolites as possible by an untargeted approach.

Targeted metabolomics is the most advanced analytical technology and has played a significant role in the development of the metabolomics field (Patti et al. 2012). This approach is often driven by a particular biochemical question or hypothesis that prompts the inspection of specific pathways. Since the physicochemical nature of the metabolites is known, the sample preparation can be optimized, thereby reducing the dominance of high-abundance molecules and analytical artifacts (Roberts et al. 2012; Raterink et al. 2014). By contrast, untargeted metabolomics involves the analyses of the largest number of compounds without having previous information regarding their nature or identity, unraveling novel targets or previously

unexplored metabolic pathways (Patti et al. 2012; Yanes et al. 2011). In this sense, extraction should be unselective to avoid metabolite losses, whereas ionization efficiency and ideal chromatographic conditions should be maximized to cover a broad range of masses. Due to their number of features, the datasets are extremely complex, precluding manual inspection of large numbers of detected peaks. Therefore, one of the biggest challenges is to convert the detected features into metabolite identities (Zamboni et al. 2015).

5.2.2 *Fundamental Principles of Metabolomics Experiments*

Experimental design and sample preparation have a tremendous impact on the analytical techniques. In this context, several initiatives for the standardization of metabolomics have been created, which includes methods for sample extraction, storage, metabolite identification, and data processing (Bino et al. 2004; Fiehn et al. 2007; Fernie et al. 2011; Abdelnur et al. 2014) (Fig. 5.4).

1. Harvesting and quenching: an appropriate number of biological, technical, and analytical replicates are needed to reduce the biological variability and represent the population under study (Fernie et al. 2011). Since the metabolome is highly influenced by environmental changes and developmental conditions, harvesting should be done as fast as possible to prevent changes caused by diurnal variation or turnover of metabolites, remaining enzymatic activity or oxidation processes (Dettmer et al. 2007; Jorge et al. 2015; Fernie et al. 2011; Ernst et al. 2014). The most widely used quenching method is snap freezing in liquid nitrogen, whereas freeze clamping or salt containing aqueous methanol at low temperatures seems to be more efficient to inactivate the metabolism of bulky tissues or cells. After harvesting, samples should be stored in corrected conditions, depending on the stability of the metabolite class or the metabolite fraction under study (Fernie et al. 2011).

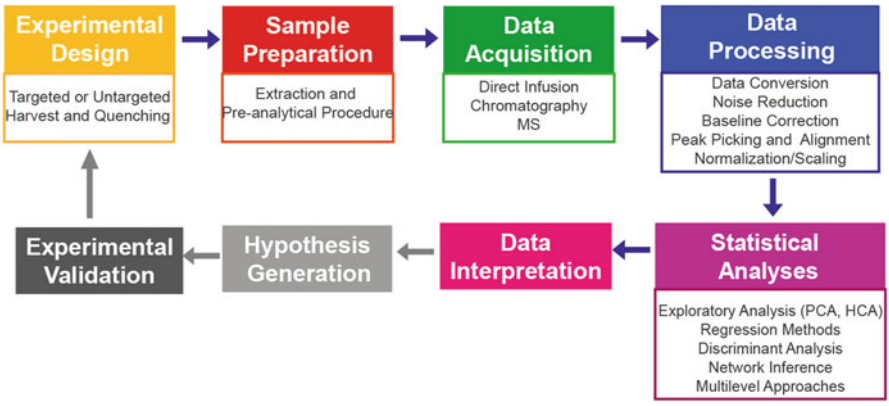

Fig. 5.4 Typical workflow used in current metabolomics studies

2. Sample extraction and pre-analytical procedures: this is one of the key steps in metabolomics as it has an enormous influence on coverage and quality of the metabolic profiles and consequently on the biological interpretation of the data (Raterink et al. 2014). The most commonly used protocols are based on solvent extraction, allowing protein precipitation and separation of polar and non-polar metabolites without degradation (Yanes et al. 2011). The nature and proportion of the solvents used in these protocols can affect the range of the metabolite coverage (Raterink et al. 2014; Yanes et al. 2011).
3. Data acquisition: the choice of the analytical method is highly dependent on the nature of the sample; often a combination of MS-based platforms are required for a comprehensive coverage of chemical compounds, since the metabolome and biomass composition are characterized by a wide range of compounds, as described in Section 1 (Mass spectrometry).
4. Data pre-processing: being a high-throughput technology, metabolomics produce extremely large datasets that requires multiple tools for data information and management. The main aim of this step is to transform any set of raw chromatograms into a matrix including the samples and metabolic features, which eliminates the variance and bias caused throughout the whole protocol (from sample preparation to MS analyses), reduces the complexity and extracts the features from the raw data (Van den Berg et al. 2006; Wehren 2011). Processing a set of raw chromatograms involves data conversion, noise reduction, baseline removal, peak alignment, peak picking, and scaling/normalization (Wehren 2011; Shulaev 2006; Johnson et al. 2015). These procedures aim to distinguish signals from the background and compounds originating from chemical or instrumental interference (Ernst et al. 2014); correct the variation and contribute for comparison among the samples; and correct the identification of the metabolites. There are a number of commercial and open source programs that automatically perform those steps that can be effectively used for each specific analytical platform ((e.g., Target Search (Cuadros-Inostroza et al. 2009) or TagFinder (Luedemann et al. 2012) for GC-MS)) or a combination of them ((e.g., Metalign (Lommen 2009); XCMS (Smith et al. 2006); Metaboanalyst (Xia et al. 2015) for GC-MS or LC-MS)). Due to the number of steps taken in the pre-processing analyses, the numbers of possible protocols are enormous and it is hard to have a general procedure (Wehren 2011). Therefore, the best way is to assess the data before/after processing and inspect whether there is still some relevant information (Wehren 2011).
5. Statistical analyses: after data processing, there are a wealth of statistical and machine-learning algorithms using unsupervised (e.g., hierarchical clustering and principal component analysis) or supervised methods (e.g., ANOVA, partial least squares, etc.) that enable the comprehensive identification of variables (metabolic features) in order to capture the dimension of variation among the entire dataset (Shulaev 2006; Fiehn et al. 2007; Kopka et al. 2011; Krastanov 2010; Sugimoto et al. 2012) and to identify the key features underlying the process under study. At this stage, visualization tools might simplify the data dimension, allowing the incorporation of metabolic data into biochemical pathways, which enables its interpretation. There are several reports on exploratory analyses (Xia et al. 2015;

Wehren 2011; Shulaev 2006; Johnson et al. 2015) and tools for metabolite identification and pathway mapping (reviewed in Fukushima and Kusano 2013). Altogether, the analyses performed here will facilitate the interpretation of data and generation of a novel hypothesis that can be validated by new experiments or different technologies, including genetic approaches.

5.2.3 Metabolomics-Assisted Synthetic Biology

Metabolomics has opened perspectives for the discovery of new compounds and unexpected pathway fluxes with significant physiological relevance, which has changed the idea of a complete cellular metabolism picture (Zamboni et al. 2015). Such features render metabolomics, among many applications, a suitable tool for synthetic biology studies. Conversion from substrates into profitable products, while reducing unwanted side-products and reducing energy costs to the cell, are the primary goal of synthetic biology (Ellis and Goodacre 2012). To this aim, important pathways can be manipulated to increase the cell production of a desired compound with the use of biochemical and genetic information. However, classical metabolic engineering strategies are unable to identify bottlenecks such as precursor depletion, accumulation of toxic reaction intermediates, excessive flux toward unwanted side products or limitation of co-factors (Nguyen et al. 2012). By identifying these constrains, metabolomics allows a fine-tuning of synthetic routes that are needed for further optimization.

Bergdahl et al. (2012) used a targeted approach to determine the metabolic status of two recombinant strains of *Saccharomyces cerevisiae* during the anaerobic batch fermentation of a glucose/xylose mixture. Depletion of NADPH and several intermediates of glycolysis, accumulation of PEP, and a reduced GTP/GDP ratio were identified as the main differences between the strains harboring either xylose isomerase or NAD(P)H-dependent xylose reductase and NAD-dependent xylitol hydrogenase. The authors concluded that the redox imbalance combined with the poor ability of xylose to suppress genes associated with respiratory pathway are unbeneficial for xylose fermentation.

Synthetic approaches using the bacteria *Escherichia coli* were performed to produce less volatile ethanol, such as isobutanol, 1-butanol, 2-methyl-1-butanol, 3-methyl-1-butanol and 2-phenylethanol from glucose, by over-activation of the amino acid biosynthetic pathway and re-directing the flux to 2-keto-acid intermediates for alcohol synthesis (Atsumi et al. 2008). 2-Keto-acids, intermediates of amino acids biosynthetic pathways, are converted by the critical enzyme 2-keto-acid decarboxylases (KDC) to aldehydes, which are further used as a substrate for alcohol dehydrogenase to produce ethanol. Out of five overexpressed KDCs enzymes obtained from different microorganisms, two, *Kivd* and *Aro10*, produced significantly higher levels of the expected alcohols, which were confirmed by GC-MS analyses (Atsumi et al. 2008). This strategy opened the possibility of exploring non-naturally occurring biofuels by metabolic engineering.

Efforts have also been made to optimize fermentative hydrogen production. Some aquatic microbial oxygenic photoautotrophs are facultative anaerobes and can use the fermentative metabolism to fulfill the need for ATP generation. Furthermore, these cyanobacteria excrete the alternative fuel precursor hydrogen (H_2), which is a renewable product derived from water (McNeely et al. 2010). A recent report used a metabolomics approach based on LC-MS and NMR to validate the manipulation of the gene encoding an enzyme involved in the NADH-dependent reduction of pyruvate to D-lactate in the cyanobacterium *Synechococcus* sp. strain PCC 7002 (McNeely et al. 2010). The metabolite profiling analyses revealed that the fermentation of the mutant resulted in a lack of lactate production and a higher concentration of excreted acetate, succinate, and hydrogen when compared to the wild-type. The results indicated that metabolic engineering can be an efficient tool to enhance H_2 production in cyanobacteria without compromising viability.

5.3 Mass Spectrometry for Biomass Composition Analyses

Plant biomass is a complex composition of polysaccharides cellulose and hemicellulose, the aromatic molecule lignin, extractives, and ash. These compounds handle the structural, stability, and pathogen resistance of plant cell walls (Taiz and Zeiger 2010). Several energy-biomass sources are available, including algae, wood, crops (such as sugarcane, corn, rice, soybean, etc.), and agricultural and animal waste. Researchers are improving analytical technologies to elucidate the chemical composition of the cell wall or are bioengineering plants to obtain given features that are suitable for biofuel production (Joyce and Stewart 2012; Vanholme et al. 2012a). Additionally, advances in analytical approaches provide further knowledge through the screening of sample compositions (known and unknown compounds), to monitor biorefinery processes and in prospecting for new valuable chemicals.

In this way, here we discuss that plant cell wall complex composition can be elucidated using modern mass spectrometry approaches. Besides this, new perspectives are to improve the new chemicals generation from plant biomass (Fig. 5.5).

5.3.1 Analyses of Cell Wall Polymers from Biomass

As the focus of this chapter is related to cell wall as biomass source, here we introduce the cell wall structure/composition. The primary cell wall surrounds and protects the inner cell that lies down the middle lamella during growth and expansion, which is composed predominantly of polysaccharides (cellulose, hemicelluloses, and pectin) and lower amounts of structural proteins (hydroxyproline-rich extensins). The secondary walls are thickened structures containing lignin and specialized cells, such as vessel elements and fiber cells. However, lignin and hemi-cellulose

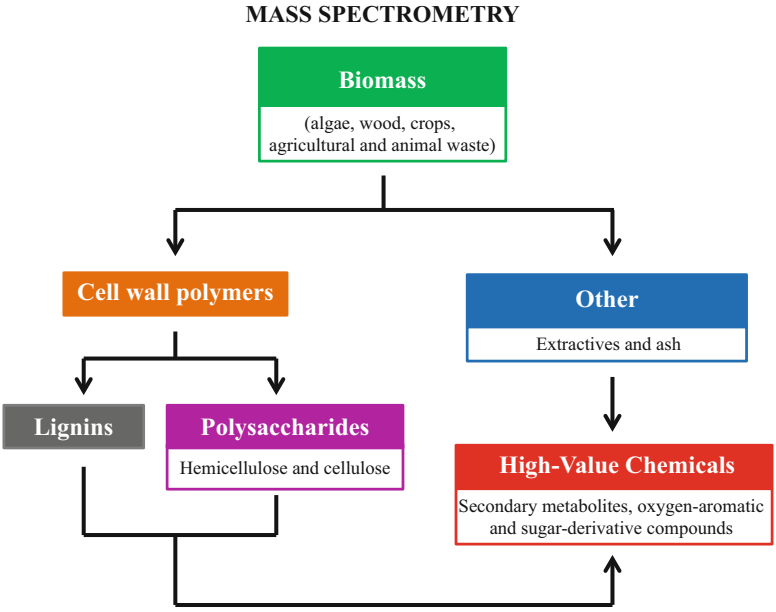

Fig. 5.5 An overview of biomass composition from major compounds to high-value chemicals. Mass spectrometry approaches are used in all steps, from biomass characterization to prospecting new compounds

greatly contribute to the cell wall's innate resistance to chemical or biological deconstruction, which consist of a mechanical barrier that limits sugar release, known as recalcitrance (Taiz and Zeiger 2010).

5.3.1.1 Lignin

Lignin is the second most abundant polymer in vascular plants, providing structural integrity, mechanical strength-rigidity, resistance to pathogen and also to oxidative stress, while also contributing to an efficient transport of water/nutrients in the xylem vessels (Taiz and Zeiger 2010; Frei 2013). Lignin is a complex aromatic polymer that is composed of three phenylpropanoid monolignols: hydroxyphenyl (H), guaiacyl (G), and syringyl (S), which are polymerized by peroxidases and laccases through oxidative coupling reactions (8-*O*-4′, 8–5′, and 8–8′) (Morreel et al. 2010).

Previous studies (Ragauskas et al. 2014; Campbell and Sederoff 1996) have demonstrated a variation in lignin composition depending on the biomass source, which varies according to the tissue morphology, developmental stage, and environmental conditions — including abiotic (climate, soil, mechanical damage) and biotic (pathogens) factors (Taiz and Zeiger 2010; Frei 2013). Considering this complex heterogeneous polymer, elucidation of the structural composition is essential for understanding plant recalcitrance.

Traditional total lignin quantitative analyses are based on gravimetric or spectrometric methods (Frei 2013; Morreel et al. 2010; Reale et al. 2004). However, undegraded lignin can be analyzed by mass spectrometry. MALDI-MS and ESI-MS have been used to estimate the molecular weight of the molecule (typical molecular weight of lignin is in the range of 1000 – 20,000 Da); although a limitation in molecular weight determination can be related to lignin isolation. Besides this, laccase polymerization could be followed by MALDI-MS (Banoub et al. 2015). It is also possible to monitor the lignification of the secondary cell walls during developmental stages by ESI-MS/MS (Reale et al. 2004; Vanholme et al. 2012b).

However, analyses of degradative lignins, by alkaline and oxidative conditions, are performed by thermal or chemical procedures, which can be coupled to mass spectrometry (Frei 2013; Reale et al. 2004). Lignin monomer composition is an important measurement, as the ratio S/G is related to the recalcitrance measurement. S/G ratio is in the range of 0.4–3.4, depending on the type of biomass. The traditional technique to measure S/G is alkaline nitrobenzene oxidation, which was developed in 1939 (Freudenberg and Lautsch 1939). Nowadays, such analysis can be coupled with HPLC, GC, GC-MS, and Py-GC-MS to provide higher sensitivity, specificity, and accuracy. Lignin, isolated from coconut coir fibers, was characterized by thioacidolysis and Py-GC-MS and showed a predominance of guaiacyl units (S/G 0.23), as expected for angiosperms (Rencoret et al. 2013). However, these chemical techniques require toxic reagents, such as nitrobenzene or boron trifluoride etherate. Another approach available for S/G ratio determination is pyrolysis molecular beam mass spectrometry (PyMBMS), as observed for sunflower biomass (S-rich lignin; S/G average 1.5); however, pyrolysis products are also toxic (Ziebell et al. 2013).

A desired characteristic for lignocellulosic material comes from enriching the syringyl monomers, since the methoxylated syringyl units are less cross-linked and more reactive to thermal and catalytic fragmentation, which enables the lignin hydrolysis (Campbell and Sederoff 1996). This feature can be achieved by transgenic approaches. Otherwise, lignin rich in G units contains more recalcitrant 8–5, 5–5, and 5-*O*-4 links. Thus, in order to reach a high yield in biomass production, lignin composed of a majority of S monomers is preferred.

Lignomics (lignin researches applying "omics" strategies) is a new term used in lignin analyses based on sequencing using ion-trap MS^n analyses. This approach characterizes the linkage unit using neutral loss and identifies the attached units (Morreel et al. 2010). In this sense, an oligomer database from soluble lignin was developed by ultra-high-performance liquid chromatography-tandem mass spectrometry (UHPLC-MS/MS) and it was validated with a sugarcane sample (Kiyota et al. 2012).

Recently, a new method based on MALDI Imaging MS was developed by Araújo et al. (2014). A total of 22 compounds were detected in *Eucalyptus* species, and a proportion between syringil and guaiacyl could be established. This simple and fast method could replace complex and laborous methods in the study of lignin composition.

The lignin analyses topic was recently covered by two reviews focused on the extensive applications using diverse approaches, including mass spectrometry (Banoub et al. 2015; Lupoi et al. 2015).

5.3.1.2 Polysaccharides

Polysaccharides constitute about 60 and 90 % of the dry weight of primary cell walls and lignified secondary walls, respectively. Cellulose, the major cell wall constituent (>100 kDa), is a linear polymer of glucopyranose linked by β-(1-4)-glucosidic bonds. Hemicelluloses are the second most abundant polysaccharides in plants (Taiz and Zeiger 2010), including a wide variety of monosaccharides and their heterogeneous sugar association, such as galactoglucomannans, arabinoglucuronoxylan, and arabinogalactan. Besides this, hemicelluloses are usually linked to other cell wall components, such as cellulose, proteins, lignin, and phenolic compounds by covalent bond, hydrogen bond, ionic, and hydrophobic interactions (Taiz and Zeiger 2010; Peng et al. 2012). Polysaccharides' conversion to monomeric units requires acidic or basic hydrolyses, usually diluted acidic pre-treatment is performed resulting in the almost total solubilization of hemicellulose and high digestibility of cellulose (Tomás-Pejó et al. 2011).

Polysaccharide characterization involves the determination of the constituent units sequence and structural characteristics, such as the linking positions of these units and the presence of branching (Fernández et al. 2003; Bauer 2012; Quéméner et al. 2015). However, the complexity of the cell wall oligosaccharides continues to be a challenging task, and a combination of methodologies are usually performed (Zaia 2010).

Mass spectrometry approaches could be employed to identify polysaccharide's molecular weight, e.g., MALDI-TOF, ESI-QTOF, or ESI-IT-MS. Further discrimination of the oligosaccharides ions by shape can be analyzed using mass spectrometry with ion mobility (IM) technology, which uses a buffer gas flow in the opposite direction of the drift tube, operating under the influence of the electric field (Zaia 2010; Plancot et al. 2014).

Usually, a chromatographic separation technique coupled to MS is required to identify sugars or sugar-derivative compounds, such as sugar acids, because some of them are isomers (Bauer 2012).

Cell wall polysaccharide's profiles can be analyzed after chemical and enzymatic treatment using high-throughput and fractionation technologies, such as anion-exchange chromatography and ESI-MS (Moore et al. 2014). This approach was used to identify the profile of grapevine leaves, that includes arabinose, rhamnose, fucose, xylose, mannose, galactose, glucose, and uronic acids: galacturonic acid and glucuronic acid (Moore et al. 2014). However, these analyses can also be applied for the identification of these sugars in other samples.

A powerful technique for the identification of different oligosaccharides in complex samples of plant cell walls is a combination of hydrophilic interaction liquid chromatography (HILIC), due to their sugar hydrophilic properties, with online ESI-

IT-MS^n and evaporative light scattering detection (ELSD), which results from the *m*/*z* separation and CID fragmentation of the sugar branches (Leijdekkers et al. 2011).

Another approach is sugar enrichment, for example using porous-graphitized-carbon (PGC), which eliminates other components from a sample that can interfere with sugar detection, followed by LC-ESI-TOF-MS. Thermochemical pretreatment of cellulosic biomass from a corn stover using this technique was used to characterize neutral oligosaccharides, such as glucans and arabinoxylans (Vismeh et al. 2013).

Combinatorial mass spectrometry approaches were applied to glycan characterization. Arabinoxylan, a high-molecular-weight sugar, derived from *Eragrostis* spp., were digested with endo-xylanase and analyzed by complementary techniques: GC-MS (alditol acetates after permethylation) (for monosaccharide composition and linkage information), MALDI-TOF-MS (for fingerprinting analysis), ESI-MS^n (for branching and sequence details), and IM-MS (for structural isomeric ions) (Plancot et al. 2014).

Structural isomers could be identified using IT-MS, through MS^n experiments. Isobaric differentiation of xylose and arabinose (both have the same molecular mass of 150.13 Da), by observing the degree and the position of branching, could be analyzed in wheat after endoxylanase A digestion by permethylation-ESI-MS/MS using the IT-MS approach (Fernández et al. 2003). This study showed that sensitivity and selectivity of mass spectrometry allowed highly heterogenous sugar sample analyses, and the technique can be extended to another biomasses.

5.3.2 Analyses of High-Value Chemicals from Biomass

The conversion of biomass to biofuels, including bio-oil, biodiesel, and second-generation ethanol (2G), is a topic for several bioenergy projects. However, the final product usually is cheap and several residual wastes are underused. A biorefinery concept has been discussed as a topic to extract new valuable chemicals from biomass, increasing the economic viability of the process. Mass spectrometry is a powerful technique for unraveling biomass composition and to prospecting new compounds in the biomass, even those unexpected.

Lignin can provide some oxygen-aromatic compounds, such as benzene, toluene, *p*-xylene, hydroxycinnamic acid, coumaric acid, ferulic acid, coumaryl alcohol, sinapyl alcohol, and coniferyl alcohol. Some potentially valuable products from lignin degradation were characterized by FT-ICR-MS (Owen et al. 2012).

Otherwise, high-value derivatives from polysaccharides can also be obtained from biomass, including ethene, acetone, lactic acid, 3-hydroxypropionic acid, itaconic acid, and glucaric acid (Cherubini and Stromman 2011). The xylans, which are monomers of hemicellulose chains, can be detected by GC-MS and have several applications. They can be used as pre-biotics in food and health products, such as surfactants, porous foams, and gels from cross-linked xylan, and in the medical applicability of pure xylan polymers (Deutschmann and Dekker 2012). Carbohydrates

can be converted to a broad range of products by fermentation (succinic acid, fumaric acid, malic acid, glutamic acid, and aspartic acid) or by chemical transformations. Sugar oxidation produces gluconic acid, which can be used for pharmaceutical applications, or levulinic acid, and furfural can be used as fuel additives. However, catalytic hydrogenation of sugars produces sugar alcohols, such as xylitol and sorbitol, which are used as food additives (Cherubini and Stromman 2011).

Some biomass has secondary metabolites in their composition, as polyketides, isoprenoids, alkaloids, phenylpropanoids and flavonoids, and they can also be identified by mass spectrometry. Flavonoids are a major class and have a diverse role as medicinal compounds (anti-tumor, anti-inflammatory, etc.) and in food nutrition (anti-oxidant). A flavonoid database composed of 624 compounds was employed for mass spectral identification, from which 104 compounds were identified in herbs (*Smilax glabra*), presenting at least 27 as new structures (Gu et al. 2015).

Figure 5.6 illustrates a LC-MS data from oil palm (*Elaeis guineensis*) leaves, a biomass used to biodiesel production. Different compounds were identified using HRMS data and database search (KEGG and CheBI), including metabolites with bioactive properties, as a luteolin derivative compound ($C_{21}H_{20}O_{11}$).

Ferula gummosa, an oleo-gum-resin, has a potential value due to its sesquiterpene composition, which was identified by GCxGC-EI-TOF-MS. Bulnesol, α-eudesmol, and α-bisabolol were the main sesquiterpenes with pharmacological potential that were identified during this study (Jalali et al. 2013). Furthermore, different hydroxycinnamates and several flavones were identified in leaves from *Miscanthus sinensis*, after SPE extraction, using reverse phase liquid chromatography

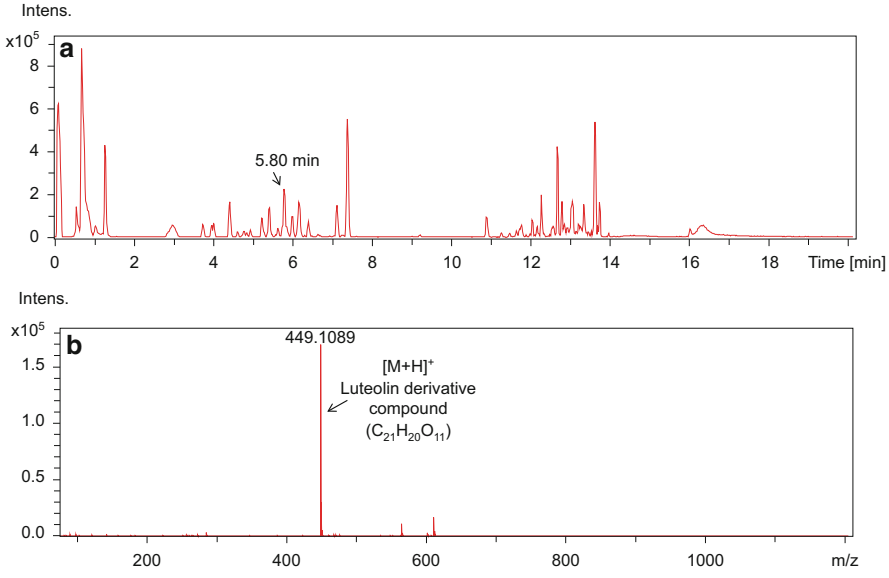

Fig. 5.6 (**a**) Base peak chromatogram (BPC) of oil palm leaves; (**b**) ESI(+)-MS mass spectrum of compound detected at 5.80 min, identified as $C_{21}H_{20}O_{11}$, a luteolin derivative compound

coupled to diode array detector / ESI-MS/MS. Another study, on the leaves and stems from *Miscanthus x giganteus* by LC-ESI-MS^n, identified 20 hydroxycinnamates, having some new caffeoyl-quinic acid-cyano conjugates that may have commercial value as a feedstock for platform chemicals and biological conversion to biofuels (Parveen et al. 2011).

Another method for screening new compounds takes advantage of the triple quadrupole analyser, using MS/MS precursor-ion analysis, product-ion analysis (isoforms can differ by their fragments), neutral-loss analysis (for example, sugar loss) and selected reaction monitoring (SRM) (specificity transition precursor-product ion) analyses. A successful example of this application is the characterization of anthocyanins and their isoforms produced by several berry species (Tian et al. 2005), demonstrating that it is a helpful approach for identifying new high-value chemicals.

A more recent identification of natural products from fermentation processes was carried out using untargeted LC-MS analysis (Q-TOF-MS) (Hoffmann et al. 2014). The study compared the MS profiles of media cultivated with or without microorganisms for the identification of key ions of potential interest (exclusively present in the strain flask). Lipothiazoles and amidated tripeptides were identified in *Sorangium cellulosum* culture and followed by NMR confirmation (Hoffmann et al. 2014).

Considering the high-accuracy, high-resolution, and specificity analyses performed on mass spectrometers, the biomass composition from any source can be estimated and quantified using DIMS. LC-MS or GC-MS approaches. However, complex samples require complementary techniques for structural characterization, using even orthogonal analyses to improve the compound separations. As it was shown, many different applications are being developed to improve biomass utilization for bioenergy conversion.

Otherwise, biorefinery industries are looking for new high-value chemicals. This is quite a new approach for mass spectrometry analyses, and thus, it seems to be a promising technique for screening metabolites, including organic acids in fermentative processes or secondary metabolites from plant extracts.

References

Abdelnur PV, Vaz BG, Rocha JD, Almeida MBB, Teixeira MAG, Pereira RCL (2013) Characterization of bio-oils from different pyrolysis process steps and biomass using high-resolution mass spectrometry. Energy Fuels 27:6646–6654

Abdelnur PV, Caldana C, Martins MCM (2014) Metabolomics applied in bioenergy. Chemical and Biological Technologies in Agriculture 1(22):1–9

Araújo P, Ferreira MS, de Oliveira DN, Pereira L, Sawaya AC, Catharino RR, Mazzafera P (2014) Mass spectrometry imaging: an expeditious and powerful technique for fast in situ lignin assessment in Eucalyptus. Anal Chem 86(7):3415–3419

Ardey RE (2003) Liquid chromatography–mass spectrometry: an introduction. John Wiley & Sons, New York

Atsumi S, Hanai T, Liao JC (2008) Non-fermentative pathways for synthesis of branched-chain higher alcohols as biofuels. Nature 451:86–89

Baker JM, Hawkins ND, Ward JL, Lovegrove A, Napier JA, Shewry PR, Beale MH (2006) A metabolomic study of substantial equivalence of field-grown genetically modified wheat. Plant Biotech J 4(4):381–392

Banoub J, Delmas G-H Jr, Joly N, Mackenzie G, Cachet N, Benjelloun-Mlayah B, Delmas M (2015) A critique on the structural analysis of lignins and application of novel tandem mass spectrometric strategies to determine lignin sequencing. J Mass Spectrom 50:5–48

Bauer S (2012) Mass spectrometry for characterizing plant cell wall polysaccharides. Front Plant Sci 3:1–6

Bergdahl B, Heer D, Sauer U, Hahn-Hagerdal B, van Niel EW (2012) Dynamic metabolomics differentiates between carbon and energy starvation in recombinant Saccharomyces cerevisiae fermenting xylose. Biotechnol for Biofuels 5:34

Bino RJ, Hall RD, Fiehn O, Kopka J, Saito K, Draper J, Nikolau BJ, Mendes P, Roessner-Tunali U, Beale MH, Trethewey RN, Lange BM, Wurtele ES, Sumner LW (2004) Potential of metabolomics as a functional genomics tool. Trends in Plant Sci 9:418–425

Bleakney W (1930) The ionization of hydrogen by single electron impact. Physical Review 35:1180–1186

Bruins AP (1991) Mass spectrometry with ion sources operating at atmospheric pressure. Mass Spectrom Rev 10:53–77

Caldana C, Degenkolbe T, Cuadros-Inostroza A, Klie S, Sulpice R, Leisse A, Steinhauser D, Fernie AR, Willmitzer L, Hannah MA (2011) High-density kinetic analysis of the metabolomic and transcriptomic response of Arabidopsis to eight environmental conditions. The Plant J 67:869–884

Campbell MM, Sederoff RR (1996) Variation in lignin content and composition. Plant Physiol 110:3–13

Cherubini F, Stromman AH (2011) Principles of biorefining. Academic, In Biofuels – Alternative feedstocks and conversion processes

Covey TR, Huang EC, Henion JD (1991) Structural characterization of protein tryptic peptides via liquid chromatography/mass spectrometry and collision–induced dissociation of their doubly charged molecular ions. Anal Chem 63:1193–2000

Cuadros-Inostroza A, Caldana C, Redestig H, Kusano M, Lisec J, Pena-Cortes H, Willmitzer L, Hannah MA (2009) TargetSearch – a bioconductor package for the efficient preprocessing of GC-MS metabolite profiling data. Bmc Bioinformatics 10:12

Dawson JHJ, Guilhaus M (1989) Orthogonal-acceleration time-of-flight mass spectrometer. Rapid Commun Mass Spectrom 3(5):155–159

Dettmer K, Aronov PA, Hammock BD (2007) Mass spectrometry-based metabolomics. Mass Spectrom Reviews 26:51–78

Deutschmann R, Dekker RF (2012) From plant biomass to bio-based chemicals: latest developments in xylan research. Biotechnol Adv 30(6):1627–1640

Ellis DI, Goodacre R (2012) Metabolomics-assisted synthetic biology. Current Opinion in Biotechnol 23:22–28

Ernst M, Silva DB, Silva RR, Vencio RZN, Lopes NP (2014) Mass spectrometry in plant metabolomics strategies: from analytical platforms to data acquisition and processing. Nat Product Reports 31:784–806

Fernández LEM, Obel N, Scheller HV, Roepstorff P (2003) Characterization of plant oligosaccharides by matrix–assisted laser desorption/ionization and electrospray mass spectrometry. J Mass Spectrom 38:427–437

Fernie AR, Aharoni A, Willmitzer L, Stitt M, Tohge T, Kopka J, Carroll AJ, Saito K, Fraser PD, DeLuca V (2011) Recommendations for reporting metabolite data. The Plant Cell 23:2477–2482

Fiehn O (2002) Metabolomics – the link between genotypes and phenotypes. Plant Mol Biol 48:155–171

Fiehn O, Robertson D, Griffin J, van der Werf M, Nikolau B, Morrison N, Sumner L, Goodacre R, Hardy N, Taylor C, Fostel J, Kristal B, Kaddurah-Daouk R, Mendes P, van Ommen B, Lindon

J, Sansone S-A (2007) The metabolomics standards initiative (MSI). Metabolomics 3:175–178
Frei M (2013) Lignin: characterization of a multifaceted crop component. Sci World J 2013:1–25
Freudenberg K, Lautsch W (1939) The constitution of pine lignin. Naturwissenschaften 27:227–228
Fukushima A, Kusano M (2013) Recent progress in the development of metabolome databases for plant systems biology. Front in Plant Sci 4:73
Gibon Y, Usadel B, Blaesing OE, Kamlage B, Hoehne M, Trethewey R, Stitt M (2006) Integration of metabolite with transcript and enzyme activity profiling during diurnal cycles in Arabidopsis rosettes. Genome Biol 7(8):R76
Griffiths WJ, Koal T, Wang Y, Kohl M, Enot DP, Deigner HP (2010) Targeted metabolomics for biomarker discovery. Angew Chem Int Ed 49:5426–5445
Gu W-Y, Li N, Leung EL-H, Zhou H, Luo G-A, Liu L, Wu J-L (2015) Metabolites software-assisted flavonoid hunting in plants using ultra-high performance liquid chromatography-quadrupole-time of flight mass spectrometry. Molecules 20:3955–3971
Guy C, Kaplan F, Kopka J, Selbig J, Hincha DK (2008) Metabolomics of temperature stress. Physiologia Plantarum 132(2):220–235
Hall RD (2006) Plant metabolomics: from holistic hope, to hype, to hot topic. New Phytologist 169:453–468
Hanold KA, Fischer SM, Cormia PH, Miller CE, Syage JA (2004) Atmospheric pressure photoionization: general properties for LC/MS. Anal Chem 76:2842–2851
Hasunuma T, Kondo A (2012) Development of yeast cell factories for consolidated bioprocessing of lignocellulose to bioethanol through cell surface engineering. Biotechnol Advances 30:1207–1218
Hasunuma T, Sanda T, Yamada R, Yoshimura K, Ishii J, Kondo A (2011) Metabolic pathway engineering based on metabolomics confers acetic and formic acid tolerance to a recombinant xylose-fermenting strain of Saccharomyces cerevisiae. Microbial Cell Factories 10(1):2
Herrgard MJ, Swainston N, Dobson P, Dunn WB, Arga KY, Arvas M, Bluthgen N, Borger S, Costenoble R, Heinemann M, Hucka M, Le Novere N, Li P, Liebermeister W, Mo ML, Oliveira AP, Petranovic D, Pettifer S, Simeonidis E, Smallbone K, Spasic I, Weichart D, Brent R, Broomhead DS, Westerhoff HV, Kirdar B, Penttila M, Klipp E, Palsson BO, Sauer U, Oliver SG, Mendes P, Nielsen J, Kell DB (2008) A consensus yeast metabolic network reconstruction obtained from a community approach to systems biology. Nat Biotechnol 26:1155–1160
Hirai MY, Klein M, Fujikawa Y, Yano M, Goodenowe DB, Yamazaki Y, Kanaya S, Nakamura Y, Kitayama M, Suzuki H, Sakurai N, Shibata D, Tokuhisa J, Reichelt M, Gershenzon J, Papenbrock J, Saito K (2005) Elucidation of gene-to-gene and metabolite-to-gene networks in Arabidopsis by integration of metabolomics and transcriptomics. J of Biol Chem 280(27):25590–25595
Hoffmann E, Stroobant V (2007) Mass spectrometry: principles and applications. Wiley, London
Hoffmann T, Krug D, Huttel S, Muller R (2014) Improving natural products identification through targeted LC–MS/MS in an untargeted secondary metabolomics workflow. Anal Chem 86:10780–10788
Hu Q, Noll RJ, Li H, Makarov A, Hardmanc M, Cooks RG (2005) The Orbitrap: a new mass spectrometer. J of Mass Spectrom 40:430–443
Jalali HT, Petronilho S, Villaverde JJ, Coimbra MA, Domingues MRM, Ebrahimian ZJ, Silvestre AJD, Rocha SM (2013) Assessment of the sesquiterpenic profile of Ferula gummosa óleo–gum–resin (galbanum) from Iran. Contributes to its valuation as a potential source of sesquiterpenic compounds. Ind Crops Prod 44:185–191
Johnson CH, Ivanisevic J, Benton HP, Siuzdak G (2015) Bioinformatics: the next frontier of metabolomics. Anal Chem 87:147–156
Jorge TF, Rodrigues JA, Caldana C, Schmidt R, van Dongen JT, Thomas-Oates J, António C (2015) Mass spectrometry-based plant metabolomics: metabolite responses to abiotic stress. Mass Spectrom Reviews PMID:25589422. doi:10.1002/mas.21449

Joyce BL, Stewart CN Jr (2012) Designing the perfect plant feedstock for biofuel production:using the whole buffalo to diversity fuels and products. Biotech Advances 30:1011–1022

Jozefczuk S, Klie S, Catchpole G, Szymanski J, Cuadros-Inostroza A, Steinhauser D, Selbig J, Willmitzer L (2010) Metabolomic and transcriptomic stress response of Escherichia coli. Mol Sys Biol 6(364):1–16

Jung JY, Kim TY, Ng CY, Oh MK (2012) Characterization of GCY1 in Saccharomyces cerevisiae by metabolic profiling. J of Appl Microbiol 113(6):1468–1478

Kaplan F, Kopka J, Sung DY, Zhao W, Popp M, Porat R, Guy CL (2007) Transcript and metabolite profiling during cold acclimation of Arabidopsis reveals an intricate relationship of cold-regulated gene expression with modifications in metabolite content. Plant J 50(6):967–981

Kebarle PA (2000) A brief overview of the present status of the mechanisms involved in electrospray mass spectrometry. J of Mass Spectrom 35:804–817

Keurentjes JJB, Fu J, de Vos CHR, Lommen A, Hall RD, Bino RJ, van der Plas LHW, Jansen RC, Vreugdenhil D, Koornneef M (2006) The genetics of plant metabolism. Nat Genet 38:842–849

Kiyota E, Mazzafera P, Sawaya ACHF (2012) Analysis of soluble lignin in sugarcane by ultrahigh performance liquid chromatography–tandem mass spectrometry with a do–it–youself oligomer database. Anal Chem 84:7015–7020

Koek MM, Jellema RH, Greef J, Tas AC, Hankemeier T (2011) Quantitative metabolomics based on gas chromatography mass spectrometry: status and perspectives. Metabolomics 7:307–328

Kopka J, Walther D, Allwood JW, Goodacre R (2011) Progress in chemometrics and biostatistics for plant applications, or: a good red wine is a bad white wine. In: Hall RD (ed) Annual plant reviews, vol 43. Wiley-Blackwell, Oxford, pp 317–342

Krastanov A (2010) Metabolomics – the state of art. Biotechnology & Biotechnological Equipment 24:1537–1543

Kusano M, Fukushima A, Kobayashi M, Hayashi N, Jonsson P, Moritz T, Ebana K, Saito K (2007) Application of a metabolomic method combining one-dimensional and two-dimensional gas chromatography-time-of-flight/mass spectrometry to metabolic phenotyping of natural variants in rice. J Chromatogr B Analyt Technol Biomed Life Sci 855:71–79

Kusano M, Redestig H, Hirai T, Oikawa A, Matsuda F, Fukushima A, Arita M, Watanabe S, Yano M, Hiwasa-Tanase K, Ezura H, Saito K (2011) Covering chemical diversity of genetically-modified tomatoes using metabolomics for objective substantial equivalence assessment. Plos One 6(2)

Lei ZT, Huhman DV, Sumner LW (2011) Mass spectrometry strategies in metabolomics. J of Biolog Chem 286:25435–25442

Leijdekkers AG, Sanders MG, Schols HA, Gruppen H (2011) Characterizing plant cell wall derivative oligosaccharides using hydrophobic interaction chromatography with mass spectrometry detection. J Chromatogr A 1218(51):9227–9235

Lisec J, Schauer N, Kopka J, Willmitzer L, Fernie AR (2006) Gas chromatography mass spectrometry-based metabolite profiling in plants. Nature Protocols 1:387–396

Lisec J, Meyer RC, Steinfath M, Redestig H, Becher M, Witucka-Wall H, Fiehn O, Torjek O, Selbig J, Altmann T, Willmitzer L (2008) Identification of metabolic and biomass QTL in Arabidopsis thaliana in a parallel analysis of RIL and IL populations. Plant J 53:960–972

Lisec J, Romisch-Margl L, Nikoloski Z, Piepho HP, Giavalisco P, Selbig J, Gierl A, Willmitzer L (2012) Corn hybrids display lower metabolite variability and complex metabolite inheritance patterns. Plant J 68:326–336

Lommen A (2009) MetAlign: interface-driven, versatile metabolomics tool for hyphenated full-scan mass spectrometry data preprocessing. Anal Chem 81:3079–3086

Luedemann A, Malotky L, Erban A, Kopka J (2012) TagFinder: preprocessing software for the fingerprinting and the profiling of gas chromatography–mass spectrometry based metabolome analyses. In: Hardy NW (ed) Plant metabolomics. Humana, Louisville, KY, pp 255–286

Lupoi JS, Singh S, Parthasarathi R, Simmons BA, Henry RJ (2015) Recent innovations in analytical methods for the qualitative and quantitative assessment of lignin. Renewable Sustainable Energy Review 49:871–906

March RE, Hughes RJ (1989) Quadrupole storage mass spectrometry. John Wiley & Sons, New York

Marshall AG, Hendrickson CL, Ernmetta MR, Rodgers RP, Blakney GT, Nilsson CL (2007) Fourier transform ion cyclotron resonance: state of the art. Eur J of Mass Spectrom 13(1):57–59

Mass Spectrometry Data Center (2014) NIST/EPA/NIH mass spectral database. Mass Spectrometry Data Center, Gaithersburg, MD, http://chemdata.nist.gov/dokuwiki/doku.php?id=chemdata:start. Accessed 12 Jun 2015

McNeely K, Xu Y, Bennette N, Bryant DA, Dismukes GC (2010) Redirecting reductant flux into hydrogen production via metabolic engineering of fermentative carbon metabolism in a cyanobacterium. Appl and Environ Microbio 76(15):5032–5038

Meyer RC, Steinfath M, Lisec J, Becher M, Witucka-Wall H, Torjek O, Fiehn O, Eckardt A, Willmitzer L, Selbig J, Altmann T (2007) The metabolic signature related to high plant growth rate in Arabidopsis thaliana. Proceedings of the Natl Acad of Sci USA 104:4759–4764

Miller PE, Denton MB (1986) The quadrupole mass filter: basic operating concepts. J of Chemical Education 63:617–622

Mol HGJ, Van Dam RCJ, Zomer P, Mulder PPJ (2011) Screening of plant toxins in food, feed and botanicals using full-scan high-resolution (Orbitrap) mass spectrometry. Food Addit Contam Part A 28:1405–1423

Moore JP, Nguema-Ona E, Fangel JU, Williats WGT, Hugo A, Vivier MA (2014) Profiling the main cell wall polysaccharides of grapevine leaves using high-throughput ans fractionation methods. Carbohydr Polymers 99:190–198

Morreel K, Kim H, Lu F, Dima O, Akiyama T, Vanholme R, Niculaes C, Goeminne G, Inzé D, Messens E, Ralph J, Boerjan W (2010) Mass spectrometry-based fragmentation as an identification tool in lignomics. Anal Chem 82:8095–8105

Nguyen Q-T, Merlo ME, Medema MH, Jankevics A, Breitling R, Takano E (2012) Metabolomics methods for the synthetic biology of secondary metabolism. FEBS Letters 586:2177–2183

Nielsen J, Pronk JT (2012) Metabolic engineering, synthetic biology and systems biology. Fems Yeast Research 12:103

Nováková L, Vlčková H (2009) A review of current trends and advances in modern bio-analytical methods: chromatography and sample preparation. Anal Chimica Acta 656(1-2):8–35

Oliver SG, Winson MK, Kell DB, Baganz F (1998) Systematic functional analysis of the yeast genome. Trends in Biotechn 16:373–378

Owen CB, Haupert LJ, Jarrell TM, Marcum CL, Parsell TH, Abu-Omar MM, Bozell JJ, Black SK, Kenttamaa HI (2012) High-performance liquid chromatography/high-resolution multiple stage tandem mass spectrometry using negative-ion mode hydroxide-doped electrospray ionization for the characterization of lignin degradation products. Anal Chem 84:6000–6007

Park C, Yun S, Lee S, Park K, Lee J (2012) Metabolic profiling of Klebsiella oxytoca: evaluation of methods for extraction of intracellular metabolites using UPLC/Q-TOF-MS. Appl Biochem and Biotechnol 167(3):425–438

Parveen I, Threadgill MD, Hauck B, Donnison I, Winters A (2011) Isolation, identification and quantitation of hydroxycinnamic acid conjugates, potential platform chemicals, in the leaves and stems of Miscanthus × giganteus using LC-ESI-MS_n. Phytochem 72(18):2376–2384

Patti GJ, Yanes O, Siuzdak G (2012) Metabolomics: the apogee of the omic triology. Nature reviews - Molecular Cell Biol 13:263–269

Peng F, Peng P, Xu F, Sun R-C (2012) Fractional purification and bioconversion of hemicelluloses. Biotech Advances 30:879–903

Perry RH, Cooks RG, Noll RJ (2008) Orbitrap mass spectrometry: instrumentation, ion motion and applications. Mass Spectrom Reviews 27:661–699

Plancot B, Vanier G, Maire F, Bardor M, Lerouge P, Farrant MJ, Driouich A, Vicré-Gibouin M, Afonso C, Loutilier-Bourhis C (2014) Structural characterization of arabinoxylans from two African species Eragrostis nindensis and Eragrostis tef using various mass spectrometric methods. Rapid Mass Spectrom 28:908–916

Quéméner B, Vigouroux J, Rathahao E, Tabet JC, Dimitrijevic A, Lahaye M (2015) Negative electrospray ionization mass spectrometry: a method for sequencing and determining linkage position in oligosaccharides from branched hemicelluloses. J Mass Spectrom 50:247–264

Ragauskas AJ, Beckham GT, Biddy MJ, Chandra R, Chen F, Davis MF, Davison BH, Dixon RA, Gilna P, Keller M, Langan P, Naskar AK, Saddler JN, Tschaplinski TJ, Tuskan GA, Wyman CE (2014) Lignin valorization: improving lignin processing in the biorefinery. Science 344:1246843-1–1246843-7

Raterink RJ, Lindenburg PW, Vreeken RJ, Ramautar R, Hankemeier T (2014) Recent developments in sample-pretreatment techniques for mass spectrometry-based metabolomics. TrAC Trends in Anal Chem 61:157–167

Reale S, Tullio A, Spreti N, De Angelis F (2004) Mass spectrometry in the biosynthetic and structural investigation of lignins. Mass Spectrom Rev 23:87–126

Rencoret J, Ralph J, Marques G, Gutiérrez A, Martínez AT, Del Río JC (2013) Structural characterization of lignin isolated from coconut (Cocos nucifera) coir fibers. J Agric Food Chem 61:2434–2445

Roberts LD, Souza AL, Gerszten RE, Clish CB (2012) Targeted metabolomics. In: Ausubel FM (ed) Current protocols in molecular biology, vol 30. John Willey, New York, NY, pp 30.2.1–30.2.24

Saito K, Watanabe Y, Shirakawa M, Matsushita Y, Imai T, Koike T, Sano FR, Fukazawa K, Fukushima K (2012) Direct mapping of morphological distribution of syringyl and guaiacyl lignin in the xylem of maple by time-of-flight secondary ion mass spectrometry. Plant J 69(3):542–552

Shulaev V (2006) Metabolomics technology and bioinformatics. Briefings in Bioinformatics 7(2):128–139

Silverstein RM, Webster FX, Kiemle DJ (2005) Spectrometric identification of organic compounds. John Wiley & Sons, Danvers

Smith CA, Want EJ, O'Maille G, Abagyan R, Siuzdak G (2006) XCMS: processing mass spectrometry data for metabolite profiling using nonlinear peak alignment, matching, and identification. Anal Chem 78:779–787

Sugimoto M, Kawakami M, Robert M, Soga T, Tomita M (2012) Bioinformatics tools for mass spectroscopy-based metabolomic data processing and analysis. Curr Bioinform 7:96–108

Sulpice R, Pyl ET, Ishihara H, Trenkamp S, Steinfath M, Witucka-Wall H, Gibon Y, Usadel B, Poree F, Piques MC, Von Korff M, Steinhauser MC, Keurentjes JJB, Guenther M, Hoehne M, Selbig J, Fernie AR, Altmann T, Stitt M (2009) Starch as a major integrator in the regulation of plant growth. Proceedings of the Natl Acad of Sci USA 106:10348–10353

Taiz L, Zeiger E (2010) Plant physiology. Sunderland, Massachusetts

Takats Z, Wiseman JM, Cooks RG (2006) Ambient mass spectrometry using desorption electrospray ionization (DESI): instrumentation, mechanisms and applications in forensics, chemistry, and biology. J of Mass Spectrom 40:1261–1275

Tian Q, Giusti MM, Stoner GD, Schwartz SJ (2005) Screening for anthocyanins using high-performance liquid chromatography coupled to electrospray ionization tandem mass spectrometry with precursor-ion analysis, product-ion analysis, common-neutral-loss analysis, and selected reaction monitoring. J Chromatogr A 1091(1-2):72–82

Tomás-Pejó E, Alvira P, Ballesteros M, Negro MJ (2011) Pretreatment technologies for lignocellulose-to-bioethanol conversion. In: Pandey A (ed) Biofuels – alternative feedstocks and conversion processes, 1st edn. Academic, San Diego, pp 149–176

Toya Y, Shimizu H (2013) Flux analysis and metabolomics for systematic metabolic engineering of microorganisms. Biotechnol Advances 31:818–826

Vaidyanathan S, Gaskell S, Goodacre R (2006) Matrix-suppressed laser desorption/ionization mass spectrometry and its suitability for metabolome analyses. Rapid Commun Mass Spectrom 20:1192–1198

Van Bramer SE (1998) An introduction to mass spectrometry. Widener University, Chester, PA, http://science.widener.edu/svb/massspec/massspec.pdf. Accessed 31 May 2015

van den Berg RA, Hoefsloot HC, Westerhuis JA, Smilde AK, van der Werf MJ (2006) Centering, scaling, and transformations: improving the biological information content of metabolomics data. BMC Genomics 7:142

Vanholme R, Morreel K, Darrah C, Oyarce P, Grabber JH, Ralph J, Boerjan W (2012a) Metabolic engineering of novel lignin in biomass crops – review. New Phytologist 196:978–1000

Vanholme R, Storme V, Vanholme B, Sundin L, Christensen JH, Goeminne G, Halpin C, Rohde A, Morreel K, Boerjan W (2012b) A systems biology view of responses to lignin biosynthesis perturbations in Arabidopsis. The Plant Cell 24:3506–3529

Vismeh R, Humpula JF, Chundawat SPS, Balan V, Dale BE, Jones AD (2013) Profiling of soluble neutral oligosaccharides from treated biomass using solid phase extraction and LC–TOF MS. Carbohydr Polym 94:791–799

Watanabe M, Kusano M, Oikawa A, Fukushima A, Noji M, Saito K (2008) Physiological roles of the beta-substituted alanine synthase gene family in arabidopsis. Plant Physiol 146:310–320

Wehren R (2011) Chemometrics with R – multivariate data analysis in the natural sciences and life sciences. Springer, Heidelberg

Williams JP, Scrivens JH (2005) Rapid accurate mass desorpition electrospray ionization tandem mass spectrometry of pharmaceutical samples. Rapid Commun Mass Spectrom 19:3643–3650

Xia J, Sinelnikov IV, Han B, Wishart DS (2015) MetaboAnalyst 3.0—making metabolomics more meaningful. Nucleic Acids Research 43:1–7

Yanes O, Tautenhahn R, Patti GJ, Siuzdak G (2011) Expanding coverage of the metabolome for global metabolite profiling. Anal Chem 83:2152–2161

Yang J, Gilmore I (2015) Application of secondary ion mass spectrometry to biomaterials, proteins and cells: a concise review. Materials Sci and Technol 31(2):131–136

Yoshida R, Tamura T, Takaoka C, Harada K, Kobayashi A, Mukai Y, Fukusaki E (2010) Metabolomics-based systematic prediction of yeast lifespan and its application for semi-rational screening of ageing-related mutants. Aging Cell 9(4):616–625

Zaia J (2010) Mass spectrometry and glycomics. OMICS 14(4):401–418

Zamboni N, Saghatelian A, Patti GJ (2015) Defining the metabolome: size, flux, and regulation. Mol Cell 58:699–706

Zhang J, Carey V, Gentleman R (2003) An extensible application for assembling annotation for genomic data. Bioinformatics 19:155–156

Ziebell AL, Barb JG, Sandhu S, Moyers BT, Sykes RW, Doeppke D, Gracom KL, Carlile M, Marek LF, Davis MF, Knapp SJ, Burke JM (2013) Sunflower as a biofuels crop: an analysis of lignocellulosic chemical properties. Biomass and Bioenergy 59:1–10

Chapter 6
Analyses of Biomass Products by Nuclear Magnetic Resonance Spectroscopy

Oigres Daniel Bernardinelli, Etelnivo Enrique Novotny, Eduardo Ribeiro de Azevêdo, and Luiz Alberto Colnago

Abstract Nuclear magnetic resonance spectroscopy has been one of the most important analytical techniques to analyze biomass materials and their transformation products. ^{1}H, ^{13}C, ^{15}N, and ^{31}P NMR techniques have been used to analyze carbohydrates, proteins, lipids, and polycondensed compounds in raw and processed biomass, from plants, animals, fungi, algae, and other living beings. NMR has been used in qualitative and quantitative analyses of biomass materials, determination of the chemical composition, and structure and dynamics of monomers, oligomers, and polymeric materials. One of the major NMR advantages is its nondestructive nature that maintains sample integrity and the analyzed samples can be analyzed by other methods. This chapter provides basic information about NMR measurements and spectroscopic parameters, analysis in solid state, liquid state and in heterogeneous samples.

Keywords Solid-state NMR • Low-field NMR • Biomass • Biochar • Sugarcane

6.1 Bases of NMR

6.1.1 Origin of the NMR Signal

The NMR phenomenon is used to observe nuclear spin transitions when a nucleus with magnetic moment (μ) and angular momentum or spin (S) is placed in a static magnetic field (B_0) and irradiated with an oscillating magnetic field (B_1), with an angular frequency ω (Eq. 6.1).

O.D. Bernardinelli • E.R. de Azevêdo
Instituto de Física de São Carlos, Universidade de São Paulo, São Carlos, SP, Brazil

E.E. Novotny
Embrapa Solos, Rio de Janeiro, RJ, Brazil

L.A. Colnago (✉)
Embrapa Instrumentação, São Carlos, SP, Brazil
e-mail: luiz.colnago@embrapa.br

S. Vaz Jr. (ed.), *Analytical Techniques and Methods for Biomass*,
DOI 10.1007/978-3-319-41414-0_6

$$\omega = \gamma B_0 \tag{6.1}$$

where γ is the magnetogyric ratio, which is a constant for each isotope.

Nuclear spin is observed only in isotopes with odd numbers of protons and/or neutrons. Therefore it is not observed in isotopes with even atomic number (Z) and even mass number (A) such as ^{12}C and ^{16}O that are the isotopes of these elements with the highest natural abundance. The major elements present in biomass: hydrogen; carbon; oxygen; and phosphorus have one or more detectable isotope. Most biomass analyses using NMR are performed with ^{1}H, ^{13}C, and ^{31}P. The oxygen analyses can be performed with ^{17}O, but it has very low γ, natural abundance, and spin 5/2.

The magnetic field (B_0) is use to breaks the degeneracy, i.e., it splits the spins (S) into $2S+1$ energy levels (Zeeman splitting) (Levitt 2008). Therefore, for $S=1/2$ (^{1}H, ^{13}C, ^{31}P), there are two energy states with an energy difference of $\Delta E = h\nu$ where h = Planck's constant and ν = excitation frequency in Hz. The nuclei of the isotopes with $S=1/2$ have uniform spherical charge distribution and are the most used in NMR analyses of biomass. Conversely, ^{17}O with $S=5/2$ has a no spherical charge distribution that generates an electrical quadruple moment that affect the spectral line width (broadens it) and is rarely used in NMR experiments.

The basic NMR phenomenon can be treated using classical and quantum mechanics. According to the classical model, in the absence of B_0 the orientation of the nuclear magnetic moment (μ) is isotropic. When exposed to B_0, the μ vector precess about the direction of B_0 (the z direction), with an angular frequency ω, known as the Larmor frequency (Eq. 6.1).

Moreover, B_0 influences the spin population at each energy level, which is related to the NMR signal intensity (sensitivity). The spin population at each energy level depends on B_0, γ, k, and temperature according to the Boltzmann Eq. (6.2):

$$N_\beta / N_\alpha = e^{-E/kT} = e^{-\left[(h\gamma B_0/2\pi)/kT\right]} \tag{6.2}$$

where N_α represents the population at the lower energy level, N_β represents the population at the higher energy level, k is the Boltzmann constant, and T is temperature (in Kelvin). The small excess of population at the lower energy state gives rise to a net magnetization M_0, where $M_0 = \Sigma\mu$.

The NMR signal is obtained when a sample inside a static magnetic field is irradiated with an oscillating magnetic field (B_1) with an angular frequency $\omega = \gamma B_0$.

In a pulsed NMR experiment, the transmitter produces very short and intense radiofrequency (RF) pulses to rotate the magnetization by an angle θ (Eq. 6.3).

$$\theta = \gamma B_1 t_p \tag{6.3}$$

where θ is the flip angle and t_p is the duration of the RF pulse.

After the pulse, the magnetization precesses around the static magnetic field inducing a NMR signal in the probe coil. This signal is known as Free Induction Decay (FID). After the pulse, the signal relaxes by two relaxation processes, the longitudinal (T_1) and transverse relaxation (T_2) times. The longitudinal relaxation is

an exponential process with a time constant T_1 involved in the return of the magnetization to the thermal equilibrium and T_2 is related to the losses of spin coherence in transverse plane.

6.1.2 Internal Nuclear Spin Interactions

The power of NMR relies mostly on the dependence of the detected signals on the so-called nuclear spin interactions. As the nuclear magnetic moments respond to internal local fields they affect the NMR signals. The local fields may have different physical origin, thus distinct information is encoded depending upon the type of interaction is producing them. The most common spin interactions for spin ½ nuclei are (Levitt 2008):

Chemical shift: The electrons around the nucleus react to the static magnetic field in which the sample is immersed by creating an extra magnetic field at the nucleus position. This extra field shields the nucleus with respect to the main applied field, producing a shift in the NMR precession frequency. Since it is created by the orbital electrons, the frequency shift depend on the symmetry, orientation and electron density of the molecular orbital, which makes it sensitive to the chemical group where the nucleus is sited in, so the name chemical shift. The chemical shifts are the primary reason why NMR is a so powerful spectroscopic technique. Chemical shift scales up with the main magnetic field, so they are better seen in high and uniform magnetic field. In general, chemical shift depend on the orientation of the molecule with respect to the main magnetic field, the so-called chemical shift anisotropy, but in solution NMR the fast tumbling of the molecules averages out this orientation dependence, and the chemical shift reduces to a single shield constant, so a single isotropic chemical shift value is observed. Thus, chemical shifts in NMR are fingerprints of the chemical groups.

Scalar or J coupling: The physical origin of the J couplings is purely quantum mechanical, i.e., there is no classical analogue. However, one can think of it as a type of dipole–dipole coupling between two nuclear magnetic moments mediated by electrons in a chemical bond. Thus, J couplings are only observed between nuclei of atoms that are part of a chemical bound. The J coupling strength depend upon how many chemical bounds the nuclei are apart to each other, so they are usually classified as J^1, J^2, J^3, and J^4 for nuclei separated by one, two, three, and four bonds, respectively. J coupling is often used as a probe of chemical connectivity and bond angles in multidimensional NMR experiments.

Dipolar coupling: The magnetic dipole–dipole interaction between nuclear spins is referred to simply as dipolar coupling in NMR. Its strength depends of the distance between the coupled nuclei, so it is an important probe of through space proximity. It is also an anisotropic interaction, but, contrary to chemical shift, it has zero average. Thus, in solution, the dipolar coupling is not directly observed in the spectra, but can contribute as relaxation and cross-relaxation mechanism, which allows it to

be use in many modern experiments devoted to structural determination. On the other hand, in solid-state NMR the anisotropy of the dipolar coupling introduces a strong broadening in the spectrum. Nevertheless, modern NMR methods, as exemplified later, are able to minimize the effect of the dipolar coupling in the NMR spectrum while retaining the orientation information, which allow to encode both structure (distances) and dynamics (molecular mobility) information.

6.1.3 Time Domain NMR

The NMR signal obtained in low field, pulsed NMR spectrometer is analyzed directly in time domain without Fourier transform, because it is a single and broad line in frequency domain (Colnago et al. 2011, 2014). Therefore, this type of NMR spectroscopy is known as low-field NMR (LF-NMR), low-resolution NMR LR-NMR) or time domain NMR (TD-NMR). The intensity of the NMR signal after a pulse has been used in quantitative analyses of oils and fats in oilseeds, fruits and algae (van Duynhoven et al. 2010). The analysis is based on the linear correlation between the NMR signal intensity at a short time after the pulse (in order of 50 μs) and lipid content (van Duynhoven et al. 2010; Colnago et al. 2011, 2014). This method has been used for more than four decades and has been recognized by several agencies as standard method (Colnago et al. 2011) and is widely used in selection and breeding program to increase the oil content in fruits, seeds and algae. Compared to conventional wet chemical methods TD-NMR is fast, nondestructive and noninvasive, simple calibration, does not use solvents (van Duynhoven et al. 2010). Compared to high-resolution NMR it is a cheap benchtop, cryogenic-free spectrometer; and does not need specialized operator (van Duynhoven et al. 2010; Colnago et al. 2014).

A high-throughput TD-NMR method for quantitative determination of oil content in seeds has been developed (Colnago et al. 2007). This *inline* method is based on continuous wave free precession pulse sequences (CWFP) and has the potential to measure several thousand samples per hour. Figure 6.1 shows a CWFP signal of 50 seeds separated by 4 cm and traveling at 13 cm s^{-1} in a 2 T magnet. In this figure, each peak is due one sample and its intensity is proportional to the oil content.

In addition to the quantitative analyses several other TD-NMR applications have been developed to measure fat/oil quality, direct in the intact seeds, fruits, and algae and in the characterization of oil/fat and their biodiesel properties (Prestes et al. 2007; Colnago et al. 2011; Berman et al. 2015). These analyses are based on the relaxation time T_1 and T_2 and diffusion measurements.

Figure 6.2 shows the NMR signal of three intact oil seeds, linseed, peanut, and castor bean obtained with Carr–Purcell–Meiboom–Gill (CPMG) pulse sequence. The time constant of the signal decay is the transverse relaxation time (T_2) which depends on chemical composition and viscosity (Prestes et al. 2007). The linseed oil shows the longest CPMG decay or T_2, attributable to its lowest viscosity, due its high content of linolenic acid, a polyunsaturated fatty acid with three double bonds.

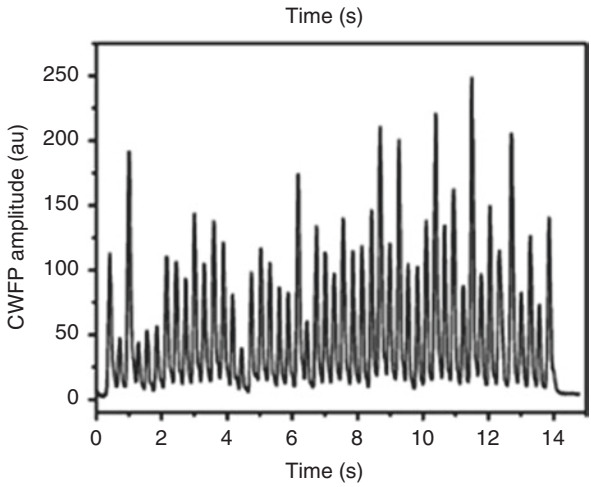

Fig. 6.1 Continuous wave free precession (CWFP) NMR signal of fifty oilseeds separated by 4 cm and traveling at 13 cm s^{-1} in a 2 T magnet. Each peak area is proportional to the oil content of the corresponding oilseed

The peanut oil shows the intermediate T_2 value, and so intermediate viscosity when compared to linseed and castor bean oils. It is rich in oleic/linoleic acid. The castor bean oil shows the shortest T_2 (highest viscosity) among the three oil seeds, because the high content of ricinoleic acid, a hydroxylated fatty acid, most likely to form intermolecular hydrogen bonds.

The use of CPMG decays and multivariate methods (e.g., Partial Least Square Regression) to predict several important biodiesel properties such as viscosity, iodine value, and cetane number (Fig. 6.3) in intact seeds has been reported in the literature (Prestes et al. 2007). Therefore, the seeds with desirable property can be used in selection and breeding program to improve biodiesel properties.

TD-NMR relaxometric and diffusometric methods have been used to study the differences in translational, segmental motion and molecular interaction of fatty acid methyl esters (FAME) that influence the physical–chemical characteristics of biodiesel and blending (Berman et al. 2015). TD-NMR has also been used to monitor transesterification reaction in situ using a unilateral magnet (Cabeça et al. 2011). The methanol is not detected in this spectrometer due to its fast diffusion and the strong magnetic field gradients employed suppress the NMR spin-echo signal of fast diffusion species.

A successful example of using TD-NMR to investigate how hydrolysis yields of lignocellulosic biomass are affected by changes in porosity and water accessibility is shown in the work reported in the following reference (Tsuchida et al. 2014). Modifications in the total surface area, hydrophilicity, porosity and water accessibility were studied using inexpensive and nondestructive time domain nuclear magnetic resonance spectrometer. This work showed that hemicellulose and lignin removal leads to changes in chemical and physical properties of biomass, such as increase in cell wall porosity and unwinding of the cellulose bundles (Tsuchida et al. 2014). Time domain NMR data revealed that water molecules occupy the cores of wide and narrow vessels, as well as the smaller pores in the cell wall internal structure. Under

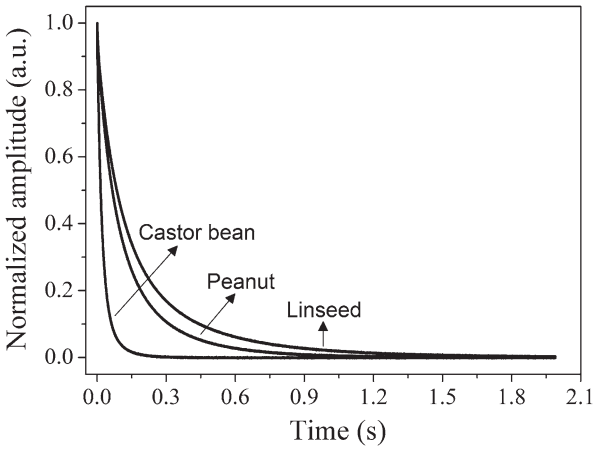

Fig. 6.2 CPMG decays of the oil in intact linseed, peanut and castor bean seeds

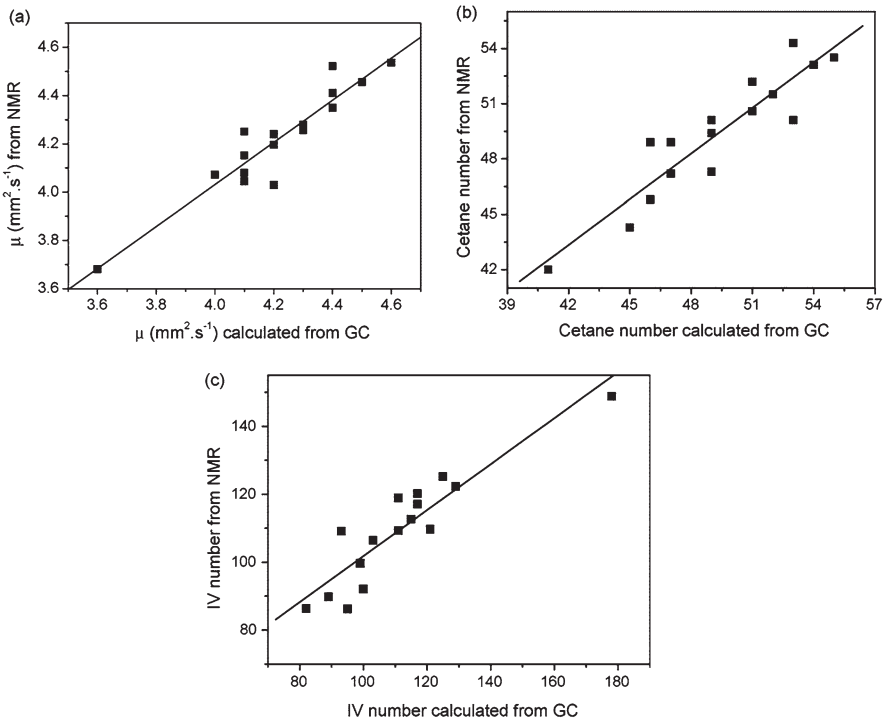

Fig. 6.3 The PLS regression curves predicted from CPMG data and biodiesel properties: (**a**) viscosity (μ); (**b**) cetane number (CN); and (**c**) iodine value (IV), calculated from gas chromatography (GC) data

drying, water is firstly removed from the cores of lumens and, in the dry sample, the only remaining water molecules are those strongly bound to the cell wall hydrophilic structures. In pretreated samples, the stronger interaction of water molecules with the cell wall, when compared to the untreated samples, is consistent with the better enzyme accessibility to cellulose in the substrates (Tsuchida et al. 2014).

6.1.3.1 High-Resolution Liquid-State NMR

Analyses of samples in liquid state or solution are the major application of NMR. These analyses are known as high-resolution NMR (HR-NMR) and usually are performed in high magnetic field (>9 T) with high homogeneity (<0.01 ppm) and have been used to study the structure and dynamics of molecules, in qualitative and quantitative analysis; monitor chemical reactions among many others applications (Levitt 2008). Because they are the most common application of NMR they are not discussed in detail here. In biomass, HR-NMR has been used in the determination of the structure and dynamics of fatty acids, fatty acid methyl esters (biodiesel) (Berman et al. 2015), triacylglycerides (oil and fat) as well as the structure and dynamics of monosaccharides and oligosaccharides (Vliegenthart and Woods 2006). These analyses have been performed using ^{1}H and ^{13}C NMR and are based on chemical shift, spin-spin coupling, signals area, relaxation times using unidimensional and multidimensional pulse sequences (Levitt 2008).

6.1.4 High-Resolution Solid-State NMR in Biomass

In organic matter, such as biomasses, solid-state NMR (SSNMR) is mostly restricted to spin ½ nuclei, mainly ^{13}C and ^{1}H. Thus, we restrict our initial discussion of SSNMR principles to methods commonly applied to organic samples containing only ^{13}C and ^{1}H nuclei.

The main difference between solution and SSNMR is the presence of the so-called anisotropic components of the spin interactions in the later. In solution, the fast and random molecular tumbling averages out these anisotropic components, so only the isotropic parts (average values) of the interactions are observed in the spectra. Since the dipolar coupling has no isotropic part, the solution spectra is dictated by the isotropic part of the chemical shift and the J-coupling, which have well defined values for a given nucleus at a chemical site, granting a high spectral resolution. These motions are restricted in solid samples, so the anisotropic components are not fully averaged and manifest directly in the spectra.

The presence of the anisotropic components of the spin interactions makes the NMR frequency of a nucleus sited in a molecular segment to be dependent on the orientation of that segment relative to the main magnetic field B_0. Thus, since the analyzed samples are usually amorphous; semicrystalline; or grounded till powder,

all molecular orientations are present, resulting in a considerable spread in the resonance frequencies resulting in broad spectra (powder pattern).

In general, the low natural abundance of ^{13}C imply not only in weak NMR signals but also in long spin–lattice relaxation times, requiring many scans and long recycle delays between experiments. Furthermore, in solid state the spectral broadening due to the anisotropic spin interaction and the conformation dependence of the NMR signal makes the situation even worst. Fortunately, very clever developments were proposed to circumvent the aforementioned problems and, nowadays, obtaining a ^{13}C SSNMR spectrum with resolution enough to distinguish different chemical groups, as in liquid state NMR, is a routing task. Since these developments are the core of the SSNMR of organic matter, they are briefly discussed in the following sections.

Given the above discussions, it may seem that anisotropic nature of the spin interactions in solid-state only imposes difficulties for NMR. However, as it becomes clear later, the orientation dependence and other specific features of the anisotropic interactions is the heart of many SSNMR techniques, making possible to explore further beyond the chemical composition. Some of these techniques are mentioned and briefly explained along this chapter.

6.2 Basic High-Resolution SSNMR Methods for Organic Matter Characterization

6.2.1 Dipolar Decoupling

As already mentioned, the dipolar coupling is a primary source of spectral broadening in SSNMR. However, the dipolar interaction between the rare ^{13}C nuclei (^{13}C-^{13}C homonuclear dipolar coupling) is negligible and the only important dipolar interaction comes from the abundant ^{1}H nuclei. The so-called dipolar decoupling method is used to suppress the magnetic dipolar interaction between nuclear spins. To suppress the ^{13}C-^{1}H dipolar interaction, the method used is called *heteronuclear decoupling* and was proposed by Sarles and Cotts in 1958 (Sarles and Cotts 1958). In its basic form, it consists in the continuous wave (CW) irradiation with RF at the ^{1}H resonance frequency while observing the ^{13}C signal. Provided that the rotation frequency imposed by the CW irradiation of the ^{1}H is higher than the line width due to the ^{13}C-^{1}H heteronuclear dipolar interaction, this averages out the dipolar magnetic field produced by the ^{1}H at the ^{13}C position. Therefore, under this condition the dipolar interaction is averaged to zero.

The CW method can be replaced by other more robust and efficient techniques, that generally involves phase modulating, being the Two-Pulse Phase Modulation (TPPM) (Bennett et al. 1995) and Small Phase INcremental ALteration (SPINAL) (Fung et al. 2000) the most popular.

In the case of homonuclear dipolar interaction, usually ^{1}H-^{1}H dipolar interaction, the method employed is denominated *homonuclear decoupling*. There are several ways to suppress this interaction and the most common are those based on multiple

pulses, such as the Waugh–Huber–Haeberlen sequence, WaHuHa (Waugh et al. 1968), the Mansfield–Rhim–Elleman–Vaughn sequence, MREV-8 (Mansfield 1971; Rhim et al. 1973), and BR-24 (Burum and Rhim 1979), or on the Lee–Goldburg method and it variants (Lee and Goldburg 1965; Vinogradov et al. 2001). Homonuclear decoupling is usually used as part of 2D-NMR techniques.

6.2.2 Magic-Angle Spinning (MAS)

In 1959, Andrew et al. (1959) and Lowe (1959) proposed, independently, a method to suppress the magnetic dipolar interaction, which became known as Magic Angle Spinning (MAS). In 1962, Andrew and Eades (1962) showed that MAS could also be applied to eliminate other anisotropic interactions.

For the sake of simplicity, let us take the case of magnetic dipolar interaction between the nuclei ^{13}C and ^{1}H. The component of the dipolar magnetic field along the static magnetic field B_0 produced by the ^{1}H nucleus on the ^{13}C site is given by $B_{dip} \approx \left(\mu_H / r^3\right)\left(3\cos^2\theta - 1\right)$, where r is the modulus of the distance vector connecting both nuclei, and θ is the angle between $\vec{r}$ and $\vec{B}_0$. The term $\left(3\cos^2\theta - 1\right)$ describes the aforementioned orientation dependence of the dipolar interaction. Thus, if this term is equal to zero, the dipolar interaction is eliminated. One way to do that is choosing $\theta = \theta_m \approx 54.74^\circ$, where θ_m is called the magic-angle. However, if one consider that all the possible ^{13}C-^{1}H spin pairs are randomly oriented in a powder (as it is in amorphous or semicrystalline samples), it is impossible to put all the spin pairs aligned along this specific orientation.

The method name as MAS propose to mimic this condition consisting in spinning the sample around the magic-angle orientation with a rotation frequency $\nu_r > \Delta\nu_{dip}$, the so-called fast MAS condition, see Fig. 6.4a. In this situation, all the internuclear vectors $\vec{r}$ will be, on the average, along the magic direction resulting in an average dipolar field $B_{dip} = \left(\mu_H / r^3\right)\left(3\cos^2\theta_m - 1\right) \approx 0$.

The same procedure also works for suppressing the anisotropic part of the chemical shift interaction (CSA) provide the rotation frequency is higher than the line broadening introduced by the CSA, $\nu_r > \Delta\nu$, where $\Delta\nu$ is by the specific anisotropic spin interaction. In the case of ^{13}C-^{1}H dipolar interaction, $\Delta\nu_{dip}$ is in the range of 1 to 100 kHz. For ^{13}C CSA, since this interaction depends on the intensity of the magnetic field, choosing for example $B_0 \approx 10$ T, $\Delta\nu_{csa}$ is in the range of 1–10 kHz. For usual MAS systems, the maximum ν_r is around 25 kHz. In this situation, it would be relatively easy to suppress the ^{13}C CSA from the ^{13}C spectra, but it would be difficult to suppress the ^{13}C-^{1}H dipolar interaction. However, as discussed below, MAS can be used together with dipolar decoupling, which can be very effective in eliminating the ^{13}C-^{1}H dipolar interaction. In Fig. 6.4b is shown a scheme that illustrates the progressive gain in resolution in ^{13}C MAS spectra as only ^{1}H decoupling and ^{1}H decoupling + fast MAS (DECMAS) is used. Thus, the ^{13}C DECMAS spectrum can be constitute by a set of relatively sharp lines at the isotropic chemical shift frequencies as in a solution NMR spectrum. However, one should stress that, even

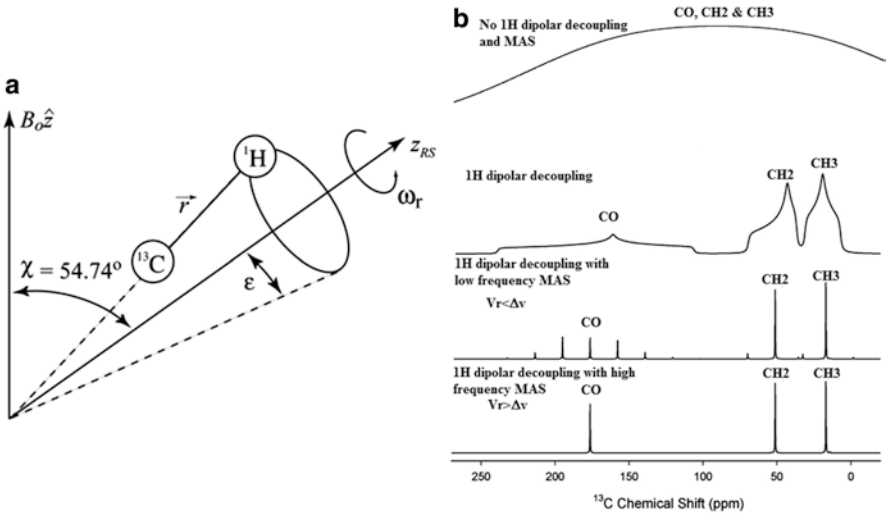

Fig. 6.4 (**a**) Sketch of sample rotation with the internuclear vector aligned along a direction different from the rotation axis (z_{RS}). (**b**) Schematic representation of the effect of the ^{1}H dipolar decoupling and MAS in the ^{13}C spectrum of a sample with three magnetic non-equivalent chemical groups (CH_3, CH_2, CO)

under DECMAS, the SSNMR lines of disordered materials are broader than in solution. This is so, mainly because the isotropic chemical shifts are also sensitive to local conformation, so the conformation distribution typical of disordered materials produces a line broadening which is not related to the anisotropy of the spin interaction, and so MAS does not eliminate it.

Despite NMR probes that reach up to 25 kHz spinning frequencies, enough to average out the ^{13}C CSA at magnetic files of ~10 T, sometimes specific features of the NMR equipments or the techniques used in the analysis requires lower spinning frequencies, so that $\nu_r < \Delta\nu$. Under this condition, considering a single ^{13}C at a given chemical site, instead of a single line at the corresponding isotropic chemical shift frequency, a set of replicas of this line appears in the ^{13}C MAS spectrum separated by the spinning frequency. These are the so-called spinning sidebands. Spinning sidebands are undesirable because they can superimpose to real lines of other chemical groups, which makes more difficult to identify the lines arising from each ^{13}C site in the sample and also to quantify each chemical group. Fortunately, there are a family of pulse trains, named as Total Suppression of Spinning Sidebands (TOSS) (Schmidt-Rohr and Spiess 1994; Dixon et al. 1982; Dixon 1982), which can be applied prior to the ^{13}C acquisition in such a way that the acquired signal is sideband free, even if $\nu_r < \Delta\nu$. The use of TOSS is very convenient, but it makes the NMR signal not quantitative, so some care should be taken when quantification of each chemical shift group. For quantitative purpose the fast MAS ($\nu_r \gg \Delta\nu$) condition is mandatory or to take in account the contribution of the spinning sidebands for

isotropic signal (add the area of the spinning sidebands to the corresponding isotropic signal).

It is important to mention, that MAS would also works for homonuclear dipolar coupling, which includes ^{1}H-^{1}H. In principle, this would make possible to obtain high resolution ^{1}H SSNMR spectra, where the major source of line broadening is the ^{1}H-^{1}H dipolar coupling. However, the strength of ^{1}H-^{1}H dipolar couplings in solids is typically in the order of 50 Hz to 100 kHz, so it would require spinning frequencies of this magnitude. NMR probes that can reach such spinning frequencies are already available, but there are not many applications in complex systems as biomasses. This is mostly because the broadening due to the conformation dependence of the chemical shift compromises the resolution of the ^{1}H ultra-fast MAS spectra.

6.2.3 Cross-Polarization (CP)

As already discussed, it is experimentally difficult to obtain spectra from solid samples for rare nuclei (low natural abundance) and with small gyromagnetic ratios, such as ^{13}C. The low sensitivity is associated to the weak NMR signal (the population difference between the α and β states is too small, see Eq. 6.2) being necessary the accumulation of thousands of spectra to improve the signal to noise ratio and the long spin–lattice relaxation times (T_1) results in very long experimental times (Tonelli 1989; Stejskal and Memory 1994). In order to circumvent these problems the Cross-Polarization method was proposed (Pines et al. 1973). This method is based on the transference of polarization between the abundant ^{1}H spins, with short T_1, and dipolar coupled to rare ^{13}C nuclei. After this polarization transfer, the rare nucleus signal intensity is increased by a factor $\gamma_{abundant}/\gamma_{rare}$, when compared with the excitation with a single ^{13}C $\pi/2$ pulse (direct polarization—DP). In the case of ^{13}C and ^{1}H this factor is about 4. Despite the fact that the NMR experiment is performed for the ^{13}C nuclei, the repetition rate for signal averaging is determined by the short ^{1}H T_1's, because the ^{13}C magnetization is now defined by the ^{1}H nuclei. This is indeed the main source of the gain in sensitivity due to CP excitation. Typically, in organic solids the ^{1}H T_1's as ~10 times shorter than the ^{13}C T_1's. This means that in the same experimental time it possible to perform ten times more scans, which together with the intensity gain of 4, makes CP excitation about 40 times more efficient than the single $\pi/2$ excitation of the ^{13}C.

In order to establish an efficient contact between ^{1}H and ^{13}C nuclei for the polarization transfer, it is necessary to satisfy the so-called Hartmann–Hahn condition $\gamma_H B_{1H} = \gamma_C B_{1C}$. This means that the RF fields have to be applied simultaneously in such a way that the precession frequencies of both nuclei around the respective resonant RF fields are the same. As a result, a resonance exchange of energy between ^{13}C and ^{1}H can readily occur through a mutual spin flip mechanism (Stejskal and Memory 1994).

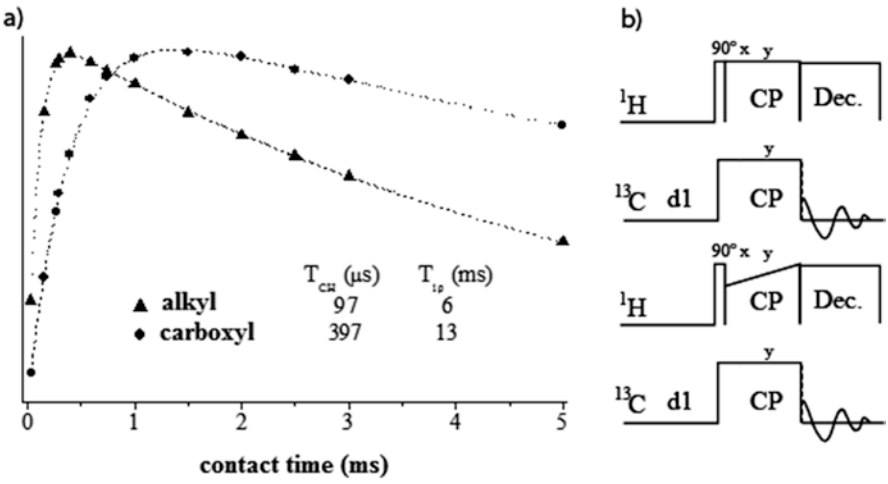

Fig. 6.5 (**a**) Typical CP build-ups for alkyl and carboxyl carbons. (**b**) Pictorial representation of a CP pulse sequence with and without radiofrequency ramp

One important issue is that the polarization transfer is mediated by the magnetic dipolar coupling between the abundant and the rare nuclei. This means that in the absence of dipolar coupling, for example in solution where the dipolar coupling is averaged to zero, the CP method cannot be used. Furthermore, the build-up of the ^{13}C polarization in CP experiment depend on the strength of the coupling to the ^{1}H network that act as a source of polarization. This is shown in Fig. 6.5 that depict the typical intensity profile of the ^{13}C as a function of the time in which the RF fields applied to the ^{13}C and ^{1}H remained on during a CP experiment (contact time). The dynamics of the cross-polarization is an initial grow with a characteristic time, known as cross polarization time (T_{CH}), followed by a decay with a characteristic time, known as T_1 relaxation time in the rotating frame ($T_{1\rho}$) of the abundant nucleus (^{1}H) (Pines et al. 1973). Both T_{CH} and $T_{1\rho}$ depend on how strong is the ^{1}H–^{13}C coupling, but, generally, T_{CH} increased with the coupling while $T_{1\rho}$ decreases. Furthermore, the presence of paramagnetic ions can reduce significantly $T_{1\rho}$ and this effect is larger for chemical groups closer to paramagnetic ion. This can lead to an underestimation of these groups but, on the other hand enables the identification of chemical groups involved in the formation of complexes of these ions (Smernik and Oades 2000).

As illustrated in Fig. 6.5a, the CP buildup can be quite different for carbons sites in different chemical groups, even in fully diamagnetic samples, since the strength of the ^{1}H-^{13}C dipolar coupling depends on the internuclear distance and intermolecular and intramolecular mobility. In regular CP experiment, a single step CP excitation is performed with constant contact time, it is impossible to make the contact time optimal for all types of carbons in the sample. Therefore, simple CP excitation is intrinsically non quantitative, in the sense that the intensity of each carbon line in the spectrum do not reflect the relative amount of that group in the sample. Moreover, if paramagnetic ions are present this is even more pronounced

since they can strongly affect $T_{1\rho}$ and consequently the CP intensity. Indeed an extreme case is that the $T_{1\rho}$ of ^{1}H nuclei near a paramagnetic ion can become so short that no CP signal is seen.

Fast MAS modulates the dipolar coupling, so the Hartmann–Hahn condition become MAS dependent and the CP transfer is affected differently for ^{13}C in distinct chemical site. This is particularly important for MAS higher than 10 kHz (considering B_0 in the order of 10 T). An alternative to minimize this effect is to vary the amplitude the RF field (B_1) applied to ^{1}H or ^{13}C during cross-polarization contact time, Fig. 6.5b. This assures that B_1 has a gradient able to cover the different Hartmann–Hahn conditions created due to the MAS modulation. This technique is called cross-polarization with variable amplitude or "Variable Amplitude Cross-Polarization." Usually the RF field is swept as a linear ramp, which is known as ramp-CP. However, as already shown in many literature reviews (Baldock and Smernik 2002; Cook 2004; Mao and Schmidt-Rohr 2004), ramp-CP does not make the cross-polarization truly quantitative.

The combination of heteronuclear decoupling, MAS, and CP techniques in only one experiment was proposed in 1976 by Schaefer and Stejskal (1976) and marked the birth of high-resolution SSNMR spectroscopy for rare nuclei.

CPMAS experiment provides the higher resolution and sensitivity available for ^{13}C SSNMR of organic solid samples. The higher resolution is associated with the use of MAS and ^{1}H dipolar decoupling while the higher sensitivity comes from the CP excitation.

6.2.4 *Quantitative ^{13}C SSNMR: SPEMAS and MultiCP Experiments*

The quantification of lignocellulosic biomass composition is extremely important. In SSNMR, the most widely accepted method for the quantification is a simple pulse sequence where the ^{13}C magnetization is excited by a single $\pi/2$ pulse followed by acquisition under ^{1}H dipolar decoupling and fast MAS (SPEMAS, from single pulse excitation under MAS[1]). To achieve the condition for quantification the recycle delay must be long enough to allow full T_1 relaxation of the ^{13}C magnetizations, i.e., it needs to be at least five times the longest T_1 value in the sample (Mao and Schmidt-Rohr 2004).

As already mentioned, the low ^{13}C natural abundance and the typically long ^{13}C T_1 in biomass samples make the quantitative ^{13}C SPEMAS method very time consuming. For instance, using a 400 MHz (9.4 T) spectrometer for acquiring a spectrum of lignocellulosic biomass with a signal–noise ratio of about 70, it will be necessary about two days for measuring a single spectrum.

[1] It is common referring to SPEMAS as DPMAS (from direct polarization under magic angle spinning).

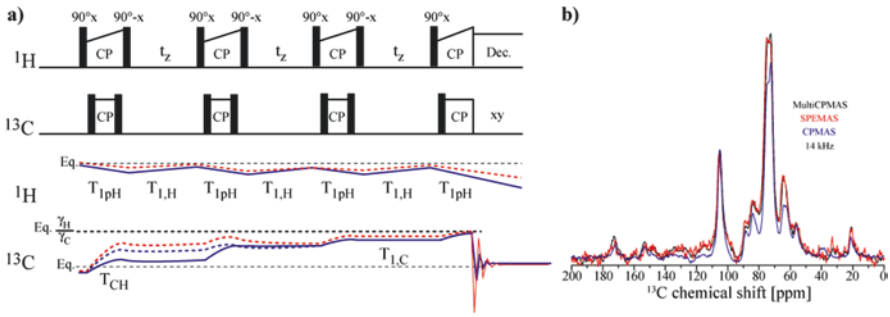

Fig. 6.6 (**a**) Schematic representation of the MultiCP pulse sequence. (**b**) Comparison between SPEMAS, rampCPMAS and MultiCP spectra of sugarcane bagasse biomass

There were many attempts to achieve quantitative ^{13}C SSNMR spectrum using CP (Baldock and Smernik 2002; Cook 2004; Mao and Schmidt-Rohr 2004). The most successful method so far is named multiCP (from multiple cross-polarization), being developed by Johnson and Schmidt-Rohr (2014). In multiCP, several periods of cross-polarization are separated by periods t_z (named as repolarization period) where the lost of ^{1}H magnetization during the CP transfer (through spin–lattice relaxation in the rotating frame) is recovered. Figure 6.6a show the general scheme of the multiCP pulse sequence.

To illustrate the general idea behind multiCP, let us consider a sample of lignocellulose biomass with different chemical groups. Quantification using rampCP would require long contact times for the complete polarization of the carbons in distinct chemical groups (Metz et al. 1996). However, in an experiment with long contact time (~10 ms), carbons with short $T_{1\rho}$ have a significant loss of polarization, which prevents quantification using a single CP period.

The main innovation of multiCP is the insertion of CP blocks separated by t_z periods (typically 0.9 s, for lignocellulosic biomass). During t_z, the ^{1}H and ^{13}C magnetizations are stored along the B_0 direction by $\pi/2$ pulses on both channels. t_z is chosen to ensure that all ^{1}H magnetizations relax, with $T_{1,H}$, to its thermal equilibrium value, while the ^{13}C magnetization is quite constant. This is possible because the ^{13}C T_1 are much longer than the ^{1}H T_1. Thus, the magnetization lost due $T_{1\rho}$ during the cross-polarization period is recovered during t_z. Furthermore, the local ^{1}H magnetization transferred to the ^{13}C nuclei during the CP will be repolarized by the phenomenon of ^{1}H spin diffusion (Johnson and Schmidt-Rohr 2014). Thus, after multiple periods of cross-polarization and ^{1}H repolarization, the several ^{13}C present the same degree of polarization no matter what is its T_{CH} and $T_{1\rho}$, i.e., the spectrum will be quantitative.

Figure 6.6b show a comparison of a quantitative SPEMAS, rampCPMAS and MultiCP spectra of sugarcane bagasse biomass. Using same number of scans the total measuring times where 24 h for the quantitative SPEMAS and 30 min for the MultiCP and 15 min for the rampCP. It is clear that, despite the huge difference in the signal to noise, the intensity profile of the SPEMAS and MultiCP spectra are

very similar, while the rampCPMAS spectrum have a significantly different spectra shape. This clearly show that MultiCP provide quantitative ^{13}C NMR spectrum with a great reduction in the measuring time.

6.3 Examples of Solid-State Applications in the Characterization of Biomass

When available, the NMR spectroscopy is one of most important analytical tool to analyze biomass and its transformation products, especially in solid state. It requires minimal sample preparation and the low solubility of the main biomass structural building blocks (cellulose and lignin) or some of its transformation products, such as acid hydrolysis residues, tar and charcoal, not preclude the analysis. In this chapter, we shall describe some specific SSNMR applications in this direction. However, one should point that many of these applications involved more advanced NMR methods, or even other techniques, the specifics of which are beyond the scope of this chapter. Therefore, we do not discuss the method in detail, but we leave the proper references for interested readers.

6.3.1 Effects of Pretreatments on the Composition of Biomass for Second-Generation Ethanol Production

SSNMR can also be used to obtain information about structure of plant cell wall of biomasses. Plant biomass is mostly made up of cellulose (35–50 %), followed by hemicellulose (20–35 %) and lignin (10–25 %). Ash, proteins and extractives make up the remaining fractions (Wall et al. 2008; Mielenz 2009; Rezende et al. 2011). Cellulose is a linear homopolymer of D-glucose units linked by 1,4-β-D-glucosidic bonds, known to be semicrystalline (Wall et al. 2008). Hemicelluloses are mostly made up of pentoses (xylose and arabinose mainly), with smaller contributions of hexoses (mannose, glucose and galactose) and sugar acid heteropolymers (Wall et al. 2008). Lignin is a phenolic polymer, which forms a tridimensional structural network surrounding the cellulose and the hemicellulose fractions (Rezende et al. 2011). Lignin has a complex structure and is very resistant to enzyme attack and degradation, thus representing, together with cellulose crystallinity, one of the most important factors determining cell wall recalcitrance to hydrolysis (Paul 2007; Wall et al. 2008; Mielenz 2009).

To obtain biofuel by renewable feedstock as biomass is essential to convert the biomass cellulose into fermentable sugars (Himmel et al. 2007; Mosier et al. 2005). Its success depends mostly on the development of effective pretreatments and on less expensive enzymatic hydrolysis processes. The former are necessary to decrease the abovementioned recalcitrance, to facilitate the enzymatic hydrolysis to ferment-

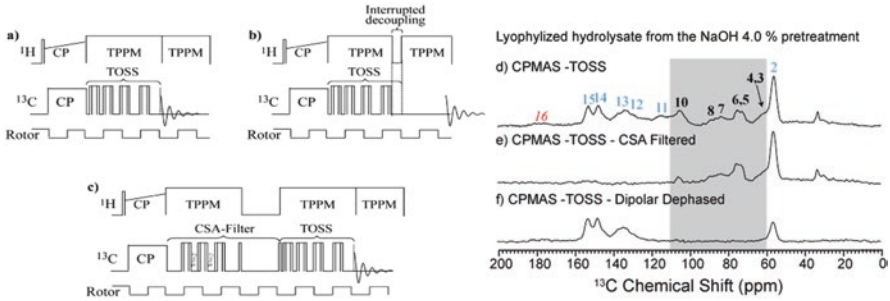

Fig. 6.7 Schematic representation of pulse sequences and resulting spectra, respectively, in hydrolysated (soluble) sugarcane bagasse. (**a**, **d**) CPMAS-TOSS. (**b**, **f**) dipolar dephased CPMAS-TOSS. (**c**, **e**) CSA filtered CPMAS-TOSS

able sugars, and to minimize the stress-tolerant microbial biocatalysts (Hallac et al. 2009; Foston et al. 2011; El Hage et al. 2010; Sannigrahi et al. 2010; Focher et al. 1981). Different pretreatments involve singular mechanisms and could improve the yields of monomeric fermentable sugars as liberated by enzymatic hydrolysis (Himmel et al. 2007). Additionally, the different pretreatment method may selectively remove hemicellulose and lignin from the biomass matrix as well increase accessible surface areas to enzymatic access (Rezende et al. 2011). An effective pretreatment strategy should minimize carbohydrate degradation and production of enzyme inhibitors (Taherzadeh and Karimi 2008; Krishnan et al. 2010). In this direction, a variety of pretreatment have been applied to different lignocellulosic biomass including physical processes (Chang and Holtzapple 2000; Gharpuray et al. 1983); physical and chemical pretreatments (Laser et al. 2002; Sasaki et al. 2003; Gollapalli et al. 2002; Zhang and Zhao 2009; Swatloski et al. 2002; Zhu et al. 2009; Shuai et al. 2010); and biological pretreatments using bacteria and fungi (Kurakake et al. 2007; Srilatha et al. 1995).

In order to understand the pretreatment and enzymatic hydrolysis efficiency, various physical techniques have been used to characterize lignocellulosic biomass before and after pretreatments. Among the main characteristics investigated are chemical composition, morphology, porosity and crystallinity. Using different techniques, NMR is able to efficiently probe all these aspects as shown, for instance, in reference (Lima et al. 2013, 2014; Rezende et al. 2011; Chandel et al. 2014; Bernardinelli et al. 2015).

Among the NMR studies in biomasses, SSNMR have been extensively used for probing the chemical composition, but there are also some efforts related to understand the evolution of the materials crystallinity, mainly cellulose, upon the pretreatments. The most standard NMR experiment used for characterization of biomass combines heteronuclear decoupling, MAS and RF ramped CP and, sometimes, total suppression of sidebands, CPMAS-TOSS (Schmidt-Rohr and Spiess 1994; Dixon 1982).

An example of probing the evolution of the biomasses composition upon the chemical pretreatments using solid-state NMR can be found in (Rezende et al. 2011).

Sugarcane bagasse was initially pretreated with sulfuric acid (1 %) followed by a second step treatment with NaOH at several concentrations (0 %—acid only, 0.25, 0.5, 2.0, 3.0, and 4.0 %) (Rezende et al. 2011). The composition of both, the solid remaining fraction and the lyophilized supernatant (hydrolysate) were analyzed.

Figure 6.7a shows the pulse sequence used for the ramped CPMAS-TOSS experiments, with the individual steps rampCP and TOSS indicated. Because relaxation and pulse imperfections effects on the carbons can affect the TOSS spectra, composite π pulses were applied in the TOSS pulse sequence in order to minimize pulse imperfections (Novotny et al. 2006).

The identification of ^{13}C signals from non-protonated carbons can be achieved using spectral editing based on dipolar dephased and ramped CPMAS-TOSS experiments. In these experiment, the dipolar decoupling is interrupted for a time period t_{deph} (~100 μs). Due to the strong ^{1}H-^{13}C dipolar coupling the magnetization from ^{13}C nuclei coupled to ^{1}H quickly dephase in this period, but the magnetization ^{13}C nuclei not coupled to ^{1}H remains. Thus, the resulting ^{13}C NMR spectrum is selective of carbons not directed bonded to ^{1}H or sited in molecular segments with high mobility, which also experience weak ^{1}H-^{13}C dipolar coupling (Schmidt-Rohr and Spiess 1994). Figure 6.7b shows this alternative pulse sequence used. As it can be noticed, the only difference to the ramped CPMAS-TOSS is the removal of the decoupling during the last delay of the TOSS sequence.

CSA filtered spectrum was also used to identify the different components in the sugarcane bagasse samples. In this experiment, only those carbons with low CSA appear in the spectrum (sp^3 hybridized ^{13}C), and so double or triple bonds ^{13}C are filtered out of the resulting spectrum, including carbon nuclei from carbonyl; carboxyl; aryl; and alkenyl (olefin ^{13}C) groups. As already mentioned, the use of fast MAS averages out the anisotropic part of the chemical shift interaction, so the NMR frequency become exclusively dependent on the isotropic chemical shifts. However, the chemical groups can also be differentiated based on their CSA, so obtaining a spectrum exclusively from segments with small CSAs may be interesting for example, to separate, and better quantify, in these chemically complex samples, overlapping signals (for example in the 120–90 ppm region) of anomeric C of carbohydrates (sp^3 hybridized ^{13}C) from aryl and alkenyl C (lower symmetry sp^2 hybridized ^{13}C).

This is achieved by the pulse sequence proposed by Mao and Schmidt-Rohr (2004), shown in Fig. 6.7c, where a π pulse train (usually known as recoupling pulses) is applied right after the CP excitation. In some cases π pulses more robust to imperfections may be also used (Novotny et al. 2006). The application of the recoupling π pulse train reintroduces the evolution under the anisotropic part of the chemical shift interaction, which makes ^{13}C nuclei in highly anisotropic sites (carbonyl, carboxyl, aryl, etc.) dephase very fast. Thus, the signal acquired after the application of the pulse sequence arises only from carbons with small CSA (i.e., sp^3 hybridized). If necessary, TOSS can be applied after the CSA filter as depicted in Fig. 6.7c.

An example of the aforementioned spectral editing methods is shown in Fig. 6.7d–f. Figure 6.7d shown the CPMAS-TOSS of the lyophilized hydrolysate (soluble fraction) obtained after acid hydrolyse (1.0 % H_2SO_4) followed alkaline

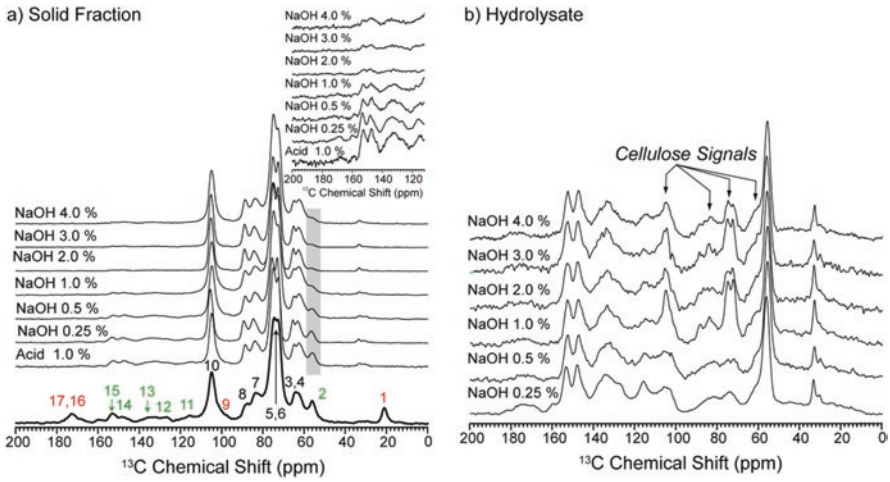

Fig. 6.8 (**a**) CPMAS-TOSS spectra of solid fractions of sugarcane bagasse samples submitted to (acid + alkaline) pretreatments. (**b**) CPMAS-TOSS spectra of lyophilized hydrolysate (supernatant) obtained after submitting sugarcane bagasse samples to (acid + alkaline) pretreatments. In the bottom spectra of (**a**) *Lines 3* and *7*: C6 and C4 carbons from amorphous cellulose; *lines 4* and *8*: C6 and C4 carbons of crystalline cellulose; *lines 2*, *11*, *12*, *13*, *14*: and *15*: lignin carbons; *lines*, *1*, *3*, *6*, *7*, *9* and *17*: hemicelluloses carbons

(4.0 % NaOH) pretreatment of sugarcane bagasse. The spectra contain a set of signals, marked in Fig. 6.7d with numbers 2: methoxyl C; 11-13: aryl C; and 14-15: O-aryl C, which could be mostly attributed to lignin (Templeton et al. 2010; Wickholm et al. 1998; Bardet et al. 2002) and the highlighted region (numbers 3–10) could be attributed to residual carbohydrates. The CPMAS-TOSS-CSA technique provides a simplification in the spectrum, Fig. 6.7e. As mentioned, after application of this technique the spectrum signals groups with large CSA are dephased, i.e., the aromatic lignin signals are removed. Interesting, the remaining signals have chemical shift with values expected for carbohydrate peaks, see the highlighted region. Besides, these signals are not present in the dipolar dephased CPMAS-TOSS spectrum, Fig. 6.7f, which would be also expected for carbohydrates where all carbons are protonated. Therefore, with the use of this spectral editing method it was possible to insure that the pretreatment with NaOH 4.0 % not only remove lignin, but also part of the cellulose (or other carbohydrates) of the sugarcane bagasse.

The CPMAS-TOSS spectra of samples submitted to pretreatments with H_2SO_4 (1.0 %) and NaOH solution with concentrations 0 % (acid only), 0.25, 0.5, 2.0, 3.0, and 4.0 %) (Rezende et al. 2011) are shown in Fig. 6.8. Both the solid fraction and the lyophilized hydrolysate are shown. The numbers in the bottom spectrum of Fig. 6.8a are signal assignments, see caption. Signals 1, 9, 16, and 17 (red) are attributed to hemicelluloses, signals 2, 11, 12, 13, 14, and 15 (green) are assigned to lignin and signals 3, 4, 5, 6, 7, 8, and 10 (blue) are due to cellulose. The removal of hemicelluloses after the acid pretreatment is clearly shown in Fig. 6.8a, as well as the progressive removal of lignin by the alkaline pretreatment with NaOH concentrations up to

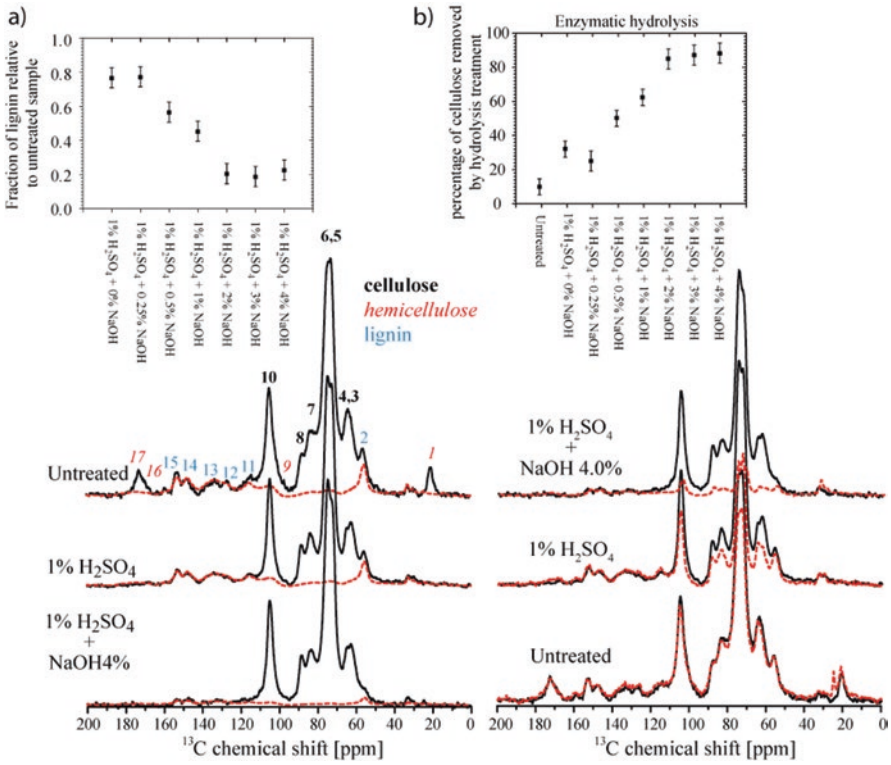

Fig. 6.9 Exemplification of the scaling procedure of the lignin reference MultiCP spectrum (lyophilized hydrolysate) in order to obtain: (**a**) the fraction of lignin in pretreated sugarcane bagasse sample (see *inset*), (**b**) percentage of cellulose removed by enzymatic hydrolysis (see *inset*). All values are relative to the untreated samples

2.0 %. For higher NaOH concentrations, the spectra become quite similar, showing a maximum in the efficiency of the alkali pretreatment (see inset). This maximum at 2.0 % was also found for other types of biomass grasses, but for biomass from wood the yield is found to be about 4.0 % (Lima et al. 2013, 2014; Rezende et al. 2011; Chandel et al. 2014; Bernardinelli et al. 2015; Himmel et al. 2007; Mosier et al. 2005; Taherzadeh and Karimi 2008; Krishnan et al. 2010). The spectra of the lyophilized hydrolysate after each step of the pretreatment are shown in Fig. 6.8b. From NaOH concentration lower than 0.5 % the spectra only contain lignin signals (Bernardinelli et al. 2015), but signals typical of carbohydrate appear in the spectra of samples pretreated with higher NaOH concentrations, suggesting the removal of cellulose.

The information obtained in Fig. 6.8 is all-qualitative due to the use of CPMAS-TOSS. More quantitative information is obtained when the MultiCP pulse sequence at MAS frequencies of 14 kHz is used. Figure 6.9 illustrates an example where MultiCP was used to obtain quantitative information from ^{13}C SSNMR. In this case, samples submitted to the same aforementioned pretreatments were analyzed using

MultiCP (Bernardinelli et al. 2015). The spectra of each pretreated sample was compared with that of a lignin reference sample (lignin extracted from samples pretreated with H_2SO_4 (1.0 %) + NaOH 0.25 %), shown in red Fig. 6.9a. This provided the relative fraction of lignin in each sample relative to the untreated sample as shown in the inset of Fig. 6.9a. The obtained profile of lignin removal is in excellent agreement with that obtained by HPLC (Rezende et al. 2011; Bernardinelli et al. 2015).

Another example of simple quantification using multiCP is shown in Fig. 6.9b. In this case the same scaling procedure was used, but the analyzed samples were the remaining solid fractions after submitting each pretreated sample to enzymatic hydrolysis. Therefore, what is the fraction of removed cellulose, Fig. 6.9a. The results are shown in the inset of Fig. 6.9b. The profile of the removed cellulose is quite similar to that of the total hydrolysis yield shown in reference (Rezende et al. 2011). This supports that the increase in the consumption of cellulose and the enzymatic hydrolysis yield are intimate related to removal of lignin and hemicelluloses from the biomass.

SSNMR techniques contributed to evaluate the efficiency of various chemical pretreatments (acid; sodium hydroxide; bisulphate; hydrothermal; and liquid ammonia) under different temperature conditions in many types of lignocellulose biomass sources derived from grasses (*Panicum maximum*, *Pennisetum purpureum*, and *Brachiaria brizantha*), wood (eucalyptus bark) (Lima et al. 2014), and pure cellulose (Park et al. 2009). The efficiency of enzymatic hydrolysis using a cocktail of specific enzymes was investigated using SSNMR along with other techniques (Chandel et al. 2014). All this studies were conducted in a multi-technique approach and SSNMR was a major player helping to elucidate the chemical transformation of the biomass.

6.3.2 Assessing Structural Information of Biomasses Components by SSNMR

SSNMR can also be used to obtain information about the biomass structure. Considering only the major components of plant biomass, lignin and hemicellulose are amorphous structures while cellulose is semicrystalline (Wall et al. 2008).

The degree of biomass crystallinity is usually quantified by the crystallinity index (CI), which is calculated as the percentage of the crystalline segments (crystalline cellulose) by the total composition of the biomass. The crystallinity index has been used to interpret changes in cellulose structure after biological and physicochemical pretreatments. While some results obtained with lignocellulosic biomass demonstrate a progressive increase in the CI of the samples as a function of pretreatments (Pu et al. 2006, 2013; Sannigrahi et al. 2010), other studies reported (Cao et al. 2012) that the crystalline index of poplar cellulose remained almost unchanged during acid pretreatments. On the other hand, it has also been shown that the CI can significantly vary depending on the choice of the measurement method

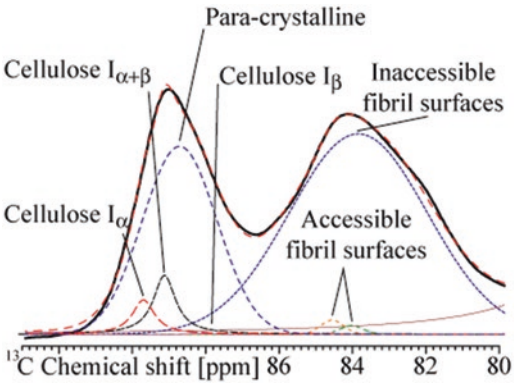

Fig. 6.10 Example of deconvolution of the cellulose MultiCP ^{13}C spectrum considering the expected structural motifs expected for cellulose

(Park et al. 2010). Besides, the influence of the CI in the recalcitrance of biomass was for long time controversial, but the most recent results tend to point that the efficiency of pretreatments in reducing the recalcitrance is not clearly correlated with the decreasing of the CI, with other parameters such as lignin/hemicelluloses contents, sample morphology and porosity being also very, or even more, important (Pu et al. 2013).

The most used method for obtaining the CI index is X-ray diffraction, XRD. The XRD diffraction peaks arising from amorphous and crystalline structures are usually well distinguishable, providing a reliable estimation about the CI. On the other hand, because the amorphous region observed in XRD refers to the total amorphous fraction of the sample and does not distinguish the source of the amorphous material (amorphous cellulose, hemicellulose or lignin), the CI obtained by XRD refers to the whole sample and not only to the cellulose fractions. This is a consequence that XRD methods usually have the disadvantage of not being able to differentiate the molecular origin of the amorphous components, which makes difficult to evaluate the crystallinity of cellulose without extracting it from the biomass, i.e., the ratio between the amount of crystalline and total (crystalline + amorphous) cellulose within the biomass.

In this sense, as a spectroscopic method SSNMR has the intrinsic advantage of making possible to obtain the CI based on signals arising from specific components of the biomass. For instance, the C4 carbon signal of cellulose in the 80–86 ppm region in Fig. 6.10 (corresponding to line 7 in Fig. 6.9) arises from disordered cellulose structures in different regions of the fibrils (inaccessible fibril surface—internal, and accessible fibril surfaces—external). On the other hand, the signal in the 86–89 ppm region are C4 carbons in ordered cellulose structures, i.e., α- and β-phase of crystalline cellulose and para-crystalline cellulose. Thus, the ratio between the integral intensity of (area) of this two signal regions, provides and estimation of the crystalline index of cellulose (Sannigrahi et al. 2010; Pu et al. 2006; Park et al. 2010).

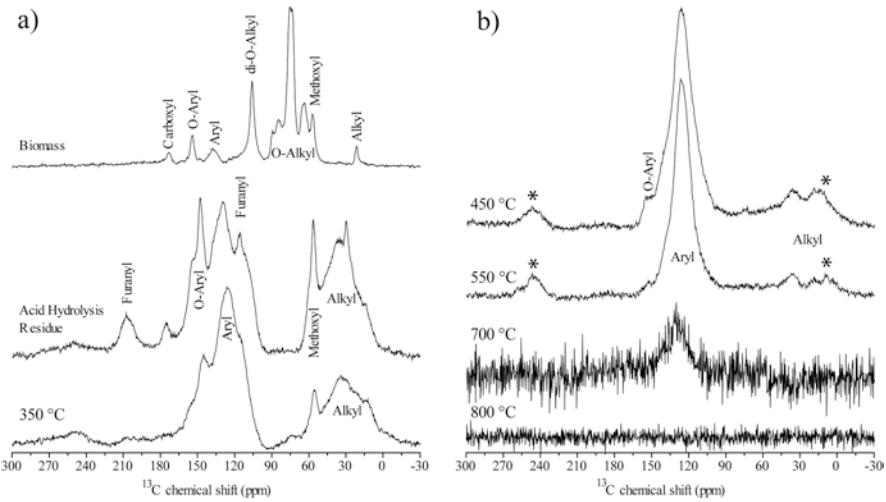

Fig. 6.11 Direct polarization ^{13}C NMR spectra of biomass and some of its solid conversion products, with emphasis in pyrolysed materials at different pyrolysis temperature. *Asterisk* indicate spinning side bands

6.3.3 Biochar Characterization by Solid-State NMR

Figure 6.11a shown the ^{13}C SSNMR spectra of biomass. The top spectrum of Fig. 6.11a was obtained from the raw biomass and shows signals corresponding to their main building blocks: cellulose and lignin. The middle spectrum correspond to sample submitted to a strong acid hydrolysis with H_2SO_4 at 170 °C seeking to solubilize the cellulose. As it can be seen, it was very effective in extracting the carbohydrates, since the main NMR signal of the solid residue are from alkyl groups (0–50 ppm) and lignin (methoxyl at 56 ppm; O-aryl at 147 ppm and aryl at 130 and 116 ppm), but the contribution of furanyl structures (207 and 115 ppm), product of thermal decomposition of cellulose, cannot be excluded (Guiotoku et al. 2012).

Pyrogenic carbon (C) is derived from the incomplete combustion of organic compounds, mainly biomass such as lignocellulosic materials. It is composed of polyaromatic units of different sizes and organizational levels (Kramer et al. 2004). Highly carbonized materials are highly resistant to thermal oxidation, chemical oxidation, and photo-oxidation (Skjemstad et al. 1996), and their incorporation in the soil is an important mechanism of carbon sequestration (Glaser et al. 2001; Masiello 2004; Rittl et al. 2015).

However, the pyrogenic C pool must be considered in a continuum model of carbonization (Goldberg 1985; Masiello 2004; Novotny et al. 2015), which is very complex and comprises different products, ranging from slightly charred, degradable biomass, to highly condensed, refractory soot, with gradual changes in properties and structures, in which the coexistence of several of the continuum products is

common. This feature turn the SSNMR analysis still more useful since it is a bulk analysis that is able to detect, under specific conditions, quantitatively, almost all the compounds of the carbonization continuum.

The mild slow pyrolysis (350 °C during 30 min) of the acid hydrolysis residue results in the loss of the furanyl structures and in the decarboxylation of the samples, besides some additional lost of other oxygenated groups, such as methoxyl from lignin (Fig. 6.11a). The further slow pyrolysis (450 °C during 30 min) results in a strong simplification of the spectrum (Fig. 6.11b), remaining just polycondensed aryl groups (symmetrical peak at 128 ppm) with a small amount of O-aryl residues (153 ppm), probably phenolic C, and also small amount of aliphatic C (0–50 ppm). The loss of alkyl and O-aryl groups continues up to 550 °C. The pyrolysis at higher temperatures resulted in the complete loss of the O-aryl signal and also increased the aromatic ring polycondensation, resulting in a graphene structure with a very high anisotropy and low electric resistance, since the ^{13}C signal result undetectable, still under ^{13}C direct polarization excitation (Fig. 6.11b).

In recent years, the interest in pyrogenic carbon (C) for agricultural use (biochar) has sharply increased (Novotny et al. 2015). The focus of this growing interest recently shifted from C sequestration and climate change mitigation to: soil fertility improvement and crop growth; water retention and movement in the soil; and soil pollution control (Cernansky 2015).

The quantification of pyrogenic C is of paramount importance to evaluate its role in soil C stocks and its fate in the environment, but is a great methodological challenge (Derenne and Largeau 2001; Masiello 2004; Simpson and Hatcher 2004; Novotny et al. 2006, 2007; Hammes et al. 2007). Except for the microscopic and molecular marker techniques, all other methods involve the removal of non-pyrogenic material by chemical oxidation, thermal oxidation, or photo-oxidation and quantification of the remaining C in the residue. However, aside from pyrogenic C, the residue can contain recalcitrant biopolymers, such as acid-insoluble components of plant waxes and lipids resistant to chemical oxidation (Knicker et al. 2008b), and therefore, this quantification of residual C alone could lead to an overestimation of pyrogenic C. To overcome this limitation, the characterization of the residues by ^{13}C SSNMR (Simpson and Hatcher 2004; Knicker et al. 2008b) can provide reliable results.

The basic chemical structure of carbonized biomass consists of the polycondensed aromatic units. The aromaticity and degree of aromatic condensation, the key parameters for its characterization, are governed mainly by the highest heat treatment temperature—HTT (Keiluweit et al. 2010; Zimmerman 2010; McBeath et al. 2011), although other pyrolysis parameters, such as: residence time (Knicker et al. 2005; Melligan et al. 2012; Rutherford et al. 2012); O_2 availability (Ascough et al. 2008); and pressure (Melligan et al. 2011), as well as the precursor biomass (Wiedemeier et al. 2015), can also significantly affect these fundamental chemical properties of biochar. These properties can be assessed by several analytical methods, described and evaluated in reference (Wiedemeier et al. 2015).

Thermal and chemical methods quantify pyrogenic C remaining after oxidation of operationally defined non-pyrogenic material by heating or chemical oxidation,

respectively; spectroscopic techniques identify signals of specific functional groups (i.e., polycondensed aromatic rings) associated with carbonized products, usually after oxidative removal (chemical oxidation, thermal oxidation, or photo-oxidation) of non-pyrogenic material, however the use of multivariate mathematical tools in spectroscopic data, e.g., Multivariate Curve Resolution, can also provide interesting results about C speciation—pyrogenic and non-pyrogenic C without requiring the removal of non-pyrogenic material (Novotny et al. 2009).

The already mentioned approach by Mao and Schmidt-Rohr (2004) was successfully applied for quantify different components of the organic matter, including the di-*O*-alkyl groups that are difficult to characterize by other NMR methods. However, the use of CSA-filter and TOSS make the pulse sequences very sensitive to imperfections in the π pulses, and this is especially problematic for pyrogenic materials because these materials present strong local magnetic susceptibility heterogeneities (Freitas et al. 1999). Novotny et al. (2006) proposed the use of composite π pulse in the protocol of Mao and Schmidt-Rohr (2004) to circumvent the problems related to the magnetic susceptibility and they demonstrated the efficiency of the procedure for the characterization of natural organic matter rich in pyrogenic C and other thermal transformed products from biomass, such as biochar.

However, in spite of what was stated in the literature (Masiello 2004), even the ^{13}C NMR spectroscopy under "quantitative" conditions (i.e., DP), when performed with high magnetic field equipment (>1.76 T), as is usual, underestimates highly condensed aromatic structures (soot and graphitic structures) in the Fig. 6.11b. This is a result of the high heterogeneity in local magnetic susceptibility and/or CSA, which are not completely averaged out at the usual rates of MAS (Freitas et al. 1999, 2001; Novotny et al. 2006). The underestimation is even worse for the cross-polarization technique, due to the inefficient H-C cross polarization (very low H content).

Besides this limitation, the only usual techniques employed for biochar characterization that provide, concomitantly, the two key parameters (aromaticity and degree of aromatic condensation) are ^{13}C SSNMR spectroscopy and benzene polycarboxilic acids (carbonization molecular markers) analysis, however the latter also has limitations (Novotny et al. 2015).

The aromaticity is provided by the quantification of aryl groups in ^{13}C CP or DP spectrum, or in more elaborated CSA filtered spectra when significant di-*O*-alkyl signals (carbohydrates) remains in the samples after low temperature pyrolysis (Novotny et al. 2006). The discussion about inefficient CP is rich in the literature (Baldock and Smernik 2002; Cook 2004; Mao and Schmidt-Rohr 2004b), but besides the general lower C observability by CP than DP, McBeath et al. 2011 showed that the aromaticity by CP or DP is quite similar, with a general slightly lower aromaticity for CP than DP, this is expected due to the poorer cross polarization of condensed aromatic structures than aliphatic ones (Mao and Schmidt-Rohr 2003; McBeath et al. 2011) since the cross polarization efficiency decrease with the carbonization and aromatic condensation. This occurs because CP efficiencies decrease with the increase of the distance between C and the nearest H (decrease of

C-H coupling strength). Empirical results have shown that the ramped CP or Variable Amplitude CP are similar to DP (Cook 2004; Simpson and Hatcher 2004; Knicker et al. 2005; Novotny et al. 2006).

However, it is important to stress that the similarity between DP and CP of carbonized materials (Simpson and Hatcher 2004; Knicker et al. 2005; Novotny et al. 2006; McBeath et al. 2011) was obtained in whole carbonized samples, but when charcoal is in mixture with non-carbonized biomass (fresh biomass), or biomass with different degree of carbonization, or with ordinary natural organic matter, probably the CP and DP results will present a significant disagreement, since the C observability under CP decrease with the carbonization degree and so low or non-carbonized material will be overestimated and high carbonized one underestimated.

The another key parameter, concerning carbonized material characterization, the degree of aromatic condensation or size of aromatic cluster, can be obtained by different ways using ^{13}C NMR, the traditional one utilize the C-H dipolar dephasing technique, where C with different C-H coupling strengths dephase with different rates. As mentioned, Carbons in close vicinity of H and in groups with low mobility have strong dipolar interactions and thus show fast dephasing. In this case, the NMR signal presents a square exponential time dependence (Gaussian component) while the C with weak dipolar interaction (Lorentzian component), such as highly mobile C and non-protonated C (e.g., polycondensed aromatic structures), show a slower dephasing (linear exponential time dependence) than the Gaussian component, and so the two component (Lorentzian and Gaussian) fitting of signal intensity (or area) of variable dipolar dephasing times, compared with experimental results from model compounds, makes possible to estimate the aromatic cluster size (number of condensed aromatic rings) (Wilson 1987; Knicker et al. 2005, 2008a).

An alternative for the classical dipolar dephasing experiment was proposed by Mao and Schmidt-Rohr (Mao and Schmidt-Rohr 2003) and applied to classify biochars (Brewer et al. 2011), in this method a train of ^{1}H π pulses is applied during the decoupling gated time every half rotation period to avoid the refocus of C-H coupling due to the rotational echoes under long dephasing times, such as 2.25 rotation periods. The authors claim that the dephasing is more efficient (three times shorter than conventional dipolar dephasing), reducing the signal lost by unrelated T_2 relaxation mechanism, such as paramagnetic dephasing; and it is independent of MAS since avoid the refocus of C-H coupling by rotational echoes.

Another approach uses the principle of increasing ring current after aromatic ring conjugation due to the biomass carbonization (Freitas et al. 1999, 2001). Labelled ^{13}C benzene is used as probe. After adsorption to the polycondensed structure, the induced ring currents in the conjugated aromatic structures upfield shift the chemical shift of the benzene, determining the degree of π electron delocalization (Smernik et al. 2006; McBeath and Smernik 2009), and according McBeath et al. (2011), by comparing the predicted upfield shift for model condensed aromatic molecules with the experimental one for charcoal samples it is possible infer the number of condensed aromatic rings and the arrangement of the cluster (i.e., peri-condensed or catacondensed).

It is important to stress that in biochar studies not only ^{13}C NMR is useful but ^{15}N NMR (Knicker 2003) and ^{31}P NMR (Novotny et al. 2012) are also employed.

References

Andrew ER, Eades RG (1962) Nuclear magnetic resonance in diamagnetic materials – possibilities for high-resolution nuclear magnetic resonance spectra of crystals. Discuss Faraday Soc 1962:38–42

Andrew ER, Bradbury A, Eades RG (1959) Removal of dipolar broadening of nuclear magnetic resonance spectra of solids by specimen rotation. Nature 183:1802–1803

Ascough PL, Bird MI, Wormald P, Snape CE, Apperley D (2008) Influence of production variables and starting material on charcoal stable isotopic and molecular characteristics. Geochim Cosmochim Acta 72:6090–6102

Baldock JA, Smernik RJ (2002) Chemical composition and bioavailability of thermally, altered *Pinus resinosa* (Red Pine) wood. Org Geochem 33:1093–1109

Bardet M, Foray MF, Tran QK (2002) High-resolution solid-state CPMAS NMR study of archaeological woods. Anal Chem 74:4386–4390

Bennett AE, Rienstra CM, Auger M, Lakshmi KV, Griffin RG (1995) Heteronuclear decoupling in rotating solids. J Chem Phys 103:6951–6958

Berman P, Meiri N, Colnago LA, Moraes TB, Linder C, Levi O, Parmet Y, Saunders M, Wiesman Z (2015) Study of liquid-phase molecular packing interactions and morphology of fatty acid methyl esters (biodiesel). Biotechnol Biofuels 8:12

Bernardinelli OD, Lima MA, Rezende CA, Polikarpov I, de Azevedo ER (2015) Quantitative ^{13}C MultiCP solid-state NMR as a tool for evaluation of cellulose crystallinity index measured directly inside sugarcane biomass. Biotechnol Biofuels 8:110

Brewer CE, Unger R, Schmidt-Rohr K, Brown RC (2011) Criteria to select biochars for field studies based on biochar chemical properties. Bioenerg Res 4:312–323

Burum DP, Rhim WK (1979) Analysis of multiple pulse NMR in solids. J Chem Phys 71:944–956

Cabeça LF, Marconcini LV, Mambrini GP, Azeredo RBV, Colnago LA (2011) Monitoring the transesterification reaction used in biodiesel production, with a low cost unilateral nuclear magnetic resonance sensor. Energy Fuels 25:2696–2701

Cao S, Pu Y, Studer M, Wyman C, Ragauskas A (2012) Chemical transformations of *Populus trichocarpa* during dilute acid pretreatment. RSC Adv 2:10925–10936

Cernansky R (2015) Agriculture: state-of-the-art soil. Nature 517:258–260

Chandel AK, Antunes FAF, Anjos V, Bell MJV, Rodrigues LN, Polikarpov I, de Azevedo ER, Bernardinelli OD, Rosa CA, Pagnocca FC, da Silva SS (2014) Multi-scale structural and chemical analysis of sugarcane bagasse in the process of sequential acid-base pretreatment and ethanol production by *Scheffersomyces shehatae* and *Saccharomyces cerevisiae*. Biotechnol Biofuels 7:63

Chang VS, Holtzapple MT (2000) Fundamental factors affecting biomass enzymatic reactivity. Appl Biochem Biotechnol 84–86:5–37

Colnago LA, Engelsberg M, Souza AA, Barbosa LL (2007) High-throughput, non-destructive determination of oil content in intact seeds by continuous wave-free precession NMR. Anal Chem 79:1271–1274

Colnago LA, Azeredo RB, Marchi Netto A, Andrade FD, Venancio T (2011) Rapid analyses of oil and fat content in agri-food products using continuous wave free precession time domain NMR. Magn Reson Chem 49:S113–S120

Colnago LA, Andrade FD, Souza AA, Azeredo RB, Lima AA, Cerioni LM, Osán DJ, Pusiol DJ (2014) Why is inline NMR rarely used as industrial sensor? Challenges and opportunities. Chem Eng Technol 37:191–203

Cook RL (2004) Coupling NMR to NOM. Anal Bioanal Chem 378:1484–1503
Derenne S, Largeau C (2001) A review of some important families of refractory macromolecules: composition, origin, and fate in soils and sediments. Soil Sci 166:833–847
Dixon WT (1982) NMR spectra in spinning samples (TOSS). J Chem Phys 77:1800
Dixon WT, Schaefer J, Sefcik MD, Stejskal EO, Mckay RA (1982) Total suppression of sidebands in CPMAS ^{13}C NMR. J Magn Reson 49:341–345
El Hage R, Brosse N, Sannigrahi P, Ragauskas A (2010) Effects of process severity on the chemical structure of Miscanthus ethanol organosolv lignin. Polym Degrad Stabil 95:997–1003
Focher B, Marzetti A, Cattaneo M, Beltrame PL, Carniti P (1981) Effects of structural features of cotton cellulose on enzymatic-hydrolysis. J Appl Polym Sci 26:1989–1999
Foston MB, Hubbell CA, Ragauskas AJ (2011) Cellulose isolation methodology for NMR analysis of cellulose ultrastructure. Materials 4:1985–2002
Freitas JCC, Bonagamba TJ, Emmerich FG (1999) C-13 High-resolution solid-state NMR study of peat carbonization. Energy Fuel 13:53–59
Freitas JCC, Emmerich FG, Cernicchiaro GRC, Sampaio LC, Bonagamba TJ (2001) Magnetic susceptibility effects on C-13 MAS NMR spectra of carbon materials and graphite. Solid State Nucl Magn Reson 20:61–73
Fung BM, Khitrin AK, Ermolaev K (2000) An improved broadband decoupling sequence for liquid crystals and solids. J Magn Reson 142:97–101
Gharpuray MM, Lee YH, Fan LT (1983) Structural modification of lignocellulosics by pretreatments to enhance enzymatic hydrolysis. Biotechnol Bioeng 25:157–172
Glaser B, Haumaier L, Guggenberger G, Zech W (2001) The 'Terra Preta' phenomenon: a model for sustainable agriculture in the humid tropics. Naturwissenschaften 88:37–41
Goldberg ED (ed) (1985) Black carbon in the environment: properties and distribution. Environmental science and technology. Wiley, New York, NY
Gollapalli LE, Dale BE, Rivers DM (2002) Predicting digestibility of ammonia fiber explosion (AFEX)-treated rice straw. Appl Biochem Biotechnol 98–100:23–35
Guiotoku M, Hansel FA, Novotny EH, Maia CMBF (2012) Molecular and morphological characterization of hydrochar produced by microwave-assisted hydrothermal carbonization of cellulose. Pesq Agropec Bras 47:687–692
Hallac BB, Sannigrahi P, Pu Y, Ray M, Murphy RJ, Ragauskas AJ (2009) Biomass characterization of *Buddleja davidii*: a potential feedstock for biofuel production. J Agric Food Chem 57:1275–1281
Hammes K, Schmidt MWI, Smernik RJ, Currie LA, Ball WP, Nguyen TH, Louchouarn P, Houel S, Gustafsson O, Elmquist M, Cornelissen G, Skjemstad JO, Masiello CA, Song J, Peng P, Mitra S, Dunn JC, Hatcher PG, Hockaday WC, Smith DM, Hartkopf-Froeder C, Boehmer A, Luer B, Huebert BJ, Amelung W, Brodowski S, Huang L, Zhang W, Gschwend PM, Flores-Cervantes DX, Largeau C, Rouzaud JN, Rumpel C, Guggenberger G, Kaiser K, Rodionov A, Gonzalez-Vila FJ, Gonzalez-Perez JA, de la Rosa JM, Manning DAC, Lopez-Capel E, Ding L (2007) Comparison of quantification methods to measure fire-derived (black/elemental) carbon in soils and sediments using reference materials from soil, water, sediment and the atmosphere. Global Biogeochem Cycles 21:1–18
Himmel ME, Ding SY, Johnson DK, Adney WS, Nimlos MR, Brady JW, Foust TD (2007) Biomass recalcitrance: engineering plants and enzymes for biofuels production. Science 315:804–807
Johnson RL, Schmidt-Rohr K (2014) Quantitative solid-state ^{13}C NMR with signal enhancement by multiple cross polarization. J Magn Reson 239:44–49
Keiluweit M, Nico PS, Johnson MG, Kleber M (2010) Dynamic molecular structure of plant biomass-derived black carbon (biochar). Environ Sci Technol 44:247–1253
Knicker H (2003) Incorporation of N-15-TNT transformation products into humifying plant organic matter as revealed by one- and two-dimensional solid state NMR spectroscopy. Sci Total Environ 308:211–220
Knicker H, Totsche KU, Almendros G, Gonzalez-Vila FJ (2005) Condensation degree of burnt peat and plant residues and the reliability of solid-state VACP MAS C-13 NMR spectra obtained from pyrogenic humic material. Org Geochem 36:1359–1377

Knicker H, Hilscher A, Gonzalez-Vila FJ, Almendros G (2008a) A new conceptual model for the structural properties of char produced during vegetation fires. Org Geochem 39:935–939
Knicker H, Wiesmeier M, Dick DR (2008b) A simplified method for the quantification of pyrogenic organic matter in grassland soils via chemical oxidation. Geoderma 147:69–74
Kramer RW, Kujawinski EB, Hatcher PG (2004) Identification of black carbon derived structures in a volcanic ash soil humic acid by Fourier transform ion cyclotron resonance mass spectrometry. Environ Sci Technol 38:3387–3395
Krishnan C, Sousa Lda C, Jin M, Chang L, Dale BE, Balan V (2010) Alkali-based AFEX pretreatment for the conversion of sugarcane bagasse and cane leaf residues to ethanol. Biotechnol Bioeng 107:441–450
Kurakake M, Ide N, Komaki T (2007) Biological pretreatment with two bacterial strains for enzymatic hydrolysis of office paper. Curr Microbiol 54:424–428
Laser M, Schulman D, Allen SG, Lichwa J, Antal MJ Jr, Lynd LR (2002) A comparison of liquid hot water and steam pretreatments of sugar cane bagasse for bioconversion to ethanol. Bioresour Technol 81:33–44
Lee M, Goldburg WI (1965) Nuclear-magnetic-resonance line narrowing by a rotating rf field. Phys Rev 140:1261–1271
Levitt MH (2008) Spin dynamics: basics of nuclear magnetic resonance, 2nd edn. John Wiley & Sons, Chichester
Lima MA, Lavorente GB, da Silva HK, Bragatto J, Rezende CA, Bernardinelli OD, de Azevedo ER, Gomez LD, McQueen-Mason SJ, Labate CA, Polikarpov I (2013) Effects of pretreatment on morphology, chemical composition and enzymatic digestibility of eucalyptus bark: a potentially valuable source of fermentable sugars for biofuel production – part 1. Biotechnol Biofuels 6:75
Lima MA, Gomez LD, Steele-King CG, Simister R, Bernardinelli OD, Carvalho MA, Rezende CA, Labate CA, Deazevedo ER, McQueen-Mason SJ, Polikarpov I (2014) Evaluating the composition and processing potential of novel sources of Brazilian biomass for sustainable biorenewables production. Biotechnol Biofuels 7:10
Lowe IJ (1959) Free induction decays of rotating solids. Phys Rev Lett 2:285–287
Mansfield P (1971) Symmetrized pulse sequences in high-resolution NMR in solids. J Phys C Solid State Phys 4:1444–1452
Mao JD, Schmidt-Rohr K (2003) Recoupled long-range C-H dipolar dephasing in solid-state NMR, and its use for spectral selection of fused aromatic rings. J Magn Reson 162:217–227
Mao JD, Schmidt-Rohr K (2004) Accurate quantification of aromaticity and nonprotonated aromatic carbon fraction in natural organic matter by ^{13}C solid-state nuclear magnetic resonance. Environ Sci Technol 38:2680–2684
Masiello CA (2004) New directions in black carbon organic geochemistry. Mar Chem 92:201–213
McBeath AV, Smernik RJ (2009) Variation in the degree of aromatic condensation of chars. Org Geochem 40:1161–1168
McBeath AV, Smernik RJ, Schneider MPW, Schmidt MWI, Plant EL (2011) Determination of the aromaticity and the degree of aromatic condensation of a thermosequence of wood charcoal using NMR. Org Geochem 42:1194–1202
Melligan F, Auccaise R, Novotny EH, Leahy JJ, Hayes MHB, Kwapinski W (2011) Pressurised pyrolysis of Miscanthus using a fixed bed reactor. Bioresour Technol 102:3466–3470
Melligan F, Dussan K, Auccaise R, Novotny EH, Leahy JJ, Hayes MHB, Kwapinski W (2012) Characterisation of the products from pyrolysis of residues after acid hydrolysis of Miscanthus. Bioresour Technol 108:258–263
Metz G, Ziliox M, Smith SO (1996) Towards quantitative CP-MAS NMR. Solid State Nucl Magn Reson 7:155–160
Mielenz JR (2009) Biofuels: methods and protocols. Springer protocols, vol 581. Humana, New York, NY
Mosier N, Wyman C, Dale B, Elander R, Lee YY, Holtzapple M, Ladisch M (2005) Features of promising technologies for pretreatment of lignocellulosic biomass. Bioresour Technol 96:673–686

Novotny EH, Hayes MH, de Azevedo ER, Bonagamba TJ (2006) Characterisation of black carbon-rich samples by (13)C solid-state nuclear magnetic resonance. Naturwissenschaften 93:447–450

Novotny EH, de Azevedo ER, Bonagamba TJ, Cunha TJF, Madari BE, Benites VD, Hayes MHB (2007) Studies of the compositions of humic acids from Amazonian Dark Earth soils. Environ Sci Technol 41:400–405

Novotny EH, Hayes MHB, Madari BE, Bonagamba TJ, de Azevedo ER, Souza AA, Song G, Nogueira CM, Mangrich AS (2009) Lessons from the Terra Preta de Índio of the Amazon region for the utilization of charcoal for soil amendment. J Braz Chem Soc 20:1003–1010

Novotny EH, Auccaise R, Velloso MHR, Correa JC, Higarashi MM, Abreu VMN, Rocha JD, Kwapinski W (2012) Characterization of phosphate structures in biochar from swine bones. Pesq Agropec Bras 47:672–676

Novotny EH, Maia CMBD, Carvalho MTD, Madari BE (2015) Biochar: pyrogenic carbon for agricultural use – a critical review. Rev Bras Ciênc Solo 39:321–344

Park S, Johnson DK, Ishizawa CI, Parilla PA, Davis MF (2009) Measuring the crystallinity index of cellulose by solid state C-13 nuclear magnetic resonance. Cellulose 16:641–647

Park S, Baker JO, Himmel ME, Parilla PA, Johnson DK (2010) Cellulose crystallinity index: measurement techniques and their impact on interpreting cellulase performance. Biotechnol Biofuels 3:10

Paul EA (2007) Soil microbiology, ecology, and biochemistry, 3rd edn. Academic, Amsterdam

Pines A, Gibby MG, Waugh JS (1973) Proton-enhanced NMR of dilute spins in solids. J Chem Phys 59:569–590

Prestes RA, Colnago LA, Forato LA, Vizzotto L, Novotny EH, Carrilho E (2007) A rapid and automated low resolution NMR method to analyze oil quality in intact oilseeds. Anal Chim Acta 596:325–329

Pu YQ, Ziemer C, Ragauskas AJ (2006) CP/MAS C-13 NMR analysis of cellulase treated bleached softwood kraft pulp. Carbohyd Res 341:591–597

Pu Y, Hu F, Huang F, Davison B, Ragauskas A (2013) Assessing the molecular structure basis for biomass recalcitrance during dilute acid and hydrothermal pretreatments. Biotechnol Biofuels 6:15

Rezende CA, de Lima MA, Maziero P, de Azevedo ER, Garcia W, Polikarpov I (2011) Chemical and morphological characterization of sugarcane bagasse submitted to a delignification process for enhanced enzymatic digestibility. Biotechnol Biofuels 4:54

Rhim WK, Elleman DD, Vaughan RW (1973) Analysis of multiple pulse NMR in solids. J Chem Phys 59:3740–3749

Rittl TF, Novotny EH, Balieiro FC, Hoffland E, Alves BJR, Kuyper TW (2015) Negative priming of native soil organic carbon mineralization by oilseed biochars of contrasting quality. Eur J Soil Sci 66:714–721

Rutherford DW, Wershaw RL, Rostad CE, Kelly CN (2012) Effect of formation conditions on biochars: compositional and structural properties of cellulose, lignin, and pine biochars. Biomass Bioenerg 46:693–701

Sannigrahi P, Miller SJ, Ragauskas AJ (2010) Effects of organosolv pretreatment and enzymatic hydrolysis on cellulose structure and crystallinity in *Loblolly pine*. Carbohyd Res 345:965–970

Sarles LR, Cotts RM (1958) Double nuclear magnetic resonance and the dipole interaction in solids. Phys Rev 111:853–859

Sasaki M, Adschiri T, Arai K (2003) Fractionation of sugarcane bagasse by hydrothermal treatment. Bioresour Technol 86:301–304

Schaefer J, Stejskal EO (1976) C-13 Nuclear magnetic-resonance of polymers spinning at magic angle. J Am Chem Soc 98:1031–1032

Schmidt-Rohr K, Spiess HW (1994) Multidimensional solid-state NMR and polymers. Academic, San Diego, CA

Shuai L, Yang Q, Zhu JY, Lu FC, Weimer PJ, Ralph J, Pan XJ (2010) Comparative study of SPORL and dilute-acid pretreatments of spruce for cellulosic ethanol production. Bioresour Technol 101:3106–3114

Simpson MJ, Hatcher PG (2004) Overestimates of black carbon in soils and sediments. Naturwissenschaften 91:436–440
Skjemstad JO, Clarke P, Taylor JA, Oades JM, McClure SG (1996) The chemistry and nature of protected carbon in soil. Aust J Soil Res 34:251–271
Smernik RJ, Oades JM (2000) The use of spin counting for determining quantitation in solid state C-13 NMR spectra of natural organic matter 1. Model systems and the effects of paramagnetic impurities. Geoderma 96:101–129
Smernik RJ, Kookana RS, Skjemstad JO (2006) NMR characterization of C-13-benzene sorbed to natural and prepared charcoals. Environ Sci Technol 40:1764–1769
Srilatha HR, Nand K, Babu KS, Madhukara K (1995) Fungal pretreatment of orange processing waste by solid-state fermentation for improved production of methane. Process Biochem 30:327–331
Stejskal EO, Memory JD (1994) High resolution NMR in the solid state: fundamentals of CP/MAS, 1st edn. Oxford University Press, New York
Swatloski RP, Spear SK, Holbrey JD, Rogers RD (2002) Dissolution of cellulose [correction of cellose] with ionic liquids. J Am Chem Soc 124:4974–4975
Taherzadeh MJ, Karimi K (2008) Pretreatment of lignocellulosic wastes to improve ethanol and biogas production: a review. Int J Mol Sci 9:1621–1651
Templeton DW, Scarlata CJ, Sluiter JB, Wolfrum EJ (2010) Compositional analysis of lignocellulosic feedstocks. 2. Method uncertainties. J Agric Food Chem 58:9054–9062
Tonelli AE (1989) NMR spectroscopy and polymer microstructure – the conformational connection, 1st edn. Methods in stereochemical analysis. VCH Publishers, Inc., New York
Tsuchida JE, Rezende CA, de Oliveira-Silva R, Lima MA, d'Eurydice MN, Polikarpov I, Bonagamba TJ (2014) Nuclear magnetic resonance investigation of water accessibility in cellulose of pretreated sugarcane bagasse. Biotechnol Biofuels 7:127
van Duynhoven J, Voda A, Witek M, Van As H (2010) Time-domain NMR applied to food products. Annu Rep NMR Spectrosc 69:145–197
Vinogradov E, Madhu PK, Vega S (2001) Phase modulated Lee-Goldburg magic angle spinning proton nuclear magnetic resonance experiments in the solid state: a bimodal Floquet theoretical treatment. J Chem Phys 115:8983–9000
Vliegenthart JFG, Woods RJ (2006) American chemical society meeting: NMR spectroscopy and computer modeling of carbohydrates: recent advances. American Chemical Society, Washington, DC
Wall JD, Harwood CS, Demain AL (2008) Bioenergy. ASM Press, Washington, DC
Waugh JS, Huber LM, Haeberlen U (1968) Approach to high-resolution NMR in solids. Phys Rev Lett 20:180–182
Wickholm K, Larsson PT, Iversen T (1998) Assignment of non-crystalline forms in cellulose I by CP/MAS C-13 NMR spectroscopy. Carbohyd Res 312:123–129
Wiedemeier DB, Abiven S, Hockaday WC, Keiluweit M, Kleber M, Masiello CA, McBeath AV, Nico PS, Pyle LA, Schneider MPW, Smernik RJ, Wiesenberg GLB, Schmidt MWI (2015) Aromaticity and degree of aromatic condensation of char. Org Geochem 78:135–143
Wilson MA (1987) NMR techniques and applications in geochemistry and soil chemistry, 1st edn. Pergamon, Oxford
Zhang Z, Zhao ZK (2009) Solid acid and microwave-assisted hydrolysis of cellulose in ionic liquid. Carbohydr Res 344:2069–2072
Zhu JY, Pan XJ, Wang GS, Gleisner R (2009) Sulfite pretreatment (SPORL) for robust enzymatic saccharification of spruce and red pine. Bioresour Technol 100:2411–2418
Zimmerman AR (2010) Abiotic and microbial oxidation of laboratory-produced black carbon (biochar). Environ Sci Technol 44:1295–1301

Chapter 7
Microscopy Applied In Biomass Characterization

Idania Valdez-Vazquez, Francisco R. Quiroz-Figueroa, Julián Carrillo-Reyes, and Artemisa Medina-López

Abstract This chapter serves as an introduction to the major types of microscopy that are applied to the characterization of lignocellulosic biomasses. The covered techniques include optical microscopies (light, Raman, and confocal microscopy), scanning probe microscopy, and electron microscopy. This chapter provides a general description of the principles, advantages and drawbacks, type of information that can be obtained using the different microscopic techniques, and includes a wide range of examples on the use of such techniques to characterize lignocellulosic biomass samples before and after pretreatments. Finally, some of the reviewed microscopic techniques were used to visualize samples of wheat straw nodes before and after acid and alkali pretreatments. This chapter is designed to help scientists select the best microscopic technique to study biomass feedstocks with recalcitrant natures.

Keywords Alkali pretreatment • Atomic force microscopy • Dilute acid pretreatment • Electron microscopy • Optical microscopy

7.1 Introduction

Lignocellulosic biomass constitutes a feedstock with unique features due to a chemical composition dominated by cellulose, hemicellulose and lignin, and their three-dimensional arrangement. Biochemical techniques may provide information about the chemical nature of the different types of cell wall components, but only advanced

I. Valdez-Vazquez (✉) • J. Carrillo-Reyes
Unidad Académica Juriquilla, Instituto de Ingeniería, Universidad Nacional Autónoma de México, Blvd. Juriquilla 3001, C.P. 76230 Querétaro, Mexico
e-mail: ivaldezv@iingen.unam.mx

F.R. Quiroz-Figueroa • A. Medina-López
Laboratorio de Fitomejoramiento Molecular, Instituto Politécnico Nacional, Centro Interdisciplinario de Investigación para el Desarrollo Integral Regional Unidad Sinaloa (CIIDIR-IPN Unidad Sinaloa), Blvd. Juan de Dios Bátiz Paredes no. 250, Col. San Joachín, C.P. 81101 Guasave, Sinaloa, Mexico

S. Vaz Jr. (ed.), *Analytical Techniques and Methods for Biomass*,
DOI 10.1007/978-3-319-41414-0_7

Table 7.1 A comparison of microscopy techniques applied to characterization of the lignocellulosic biomasses

Microscopic technique	Best spatial resolution (nm)	Typical applications
Optical microscopy	250	Determination of the particle size distribution Study of the swelling properties Visualization of morphological changes Selective identification of cellulose, xylan, and lignin
AFM	<10	Measurements of diameter and height Analysis of surface roughness Monitoring in real-time of enzymatic action Spatial localization of cellulose and lignin
TEM	<10	Visualization of cellular structures (cytoskeleton, membrane systems, organelles) Spatial localization of lignin droplets Enzyme penetration into the fibers
SEM	<10	Analysis of the sample morphology Elemental composition coupled to X-ray Analysis of the pore formation Spatial localization of lignin droplets Fungal colonization of biomass

AFM atomic force microscopy, *TEM* transmission electronic microscopy, *SEM* scanning electron microscopy

microscopic imaging can offer us a full picture of how these biomass components are organized into the plant cell wall matrix at macro-, micro-, and nanoscale levels (Table 7.1). A complete understanding of how pretreatments and enzymatic hydrolysis act on the biomass may allow us to overcome recalcitrance to degradation and to ultimately obtain simple molecules for green biorefineries. Additionally, microscopic techniques have been powerful tools for studying enzyme–substrate complexes, the progressive actions of hydrolytic enzymes, and the three-dimensional arrangement of microorganisms acting on biomass.

This chapter aims to describe the basic principles of the major microscopic techniques that have been applied to the characterization of biomasses. Our goal is to allow the reader easily identify the microscopic techniques that best suit your particular interests. Application of these microscopic techniques to the same biomass samples provides information at multiple levels of scale and resolution. When these imaging techniques are complemented with other biochemical techniques, all of them give us all of the desired information about the biomass deconstruction. This review is not intended to provide a full description of the optical design, the practical use of the techniques, or the preparations of specimens. Instead, this text is meant to serve as a quick guide about the kind of information that can be obtained from each microscopic technique and to provide an update on the latest advances in the use of microscopy for biomass characterization.

The chapter begins with optical microscopies including light, Raman, and confocal microscopy, and includes reviews of scanning probe microscopy and electron microscopy. The basic principles of each technique are presented, as well as a

selected number of examples about the use of these techniques for studying the effect of pretreatments and enzymatic hydrolysis on biomasses.

7.2 Optical Microscopy

Throughout the history of the life sciences, optical microscopes have helped biologists in many different fields to discover the microscopic world. In the literature, there is no consensus about who invented the microscope. Some texts take us back to 1609 when Galileo Galilei developed a compound microscope with a convex and a concave lens (Jean-Marie 2016). At that time, Giovanni Faber coined the term microscope from the Greek words mikron (micron) meaning "small" and skopein (skopein) meaning "to look at". In 1611, Johannes Kepler established the mathematical basis of compound microscopes with convex lenses. Only a few years later, in 1668, Anton van Leeuwenhoek popularized the use of microscopes for microbiological studies (Gunning 2013). In parallel, in 1665, Robert Hooke published his observations of cork cell walls.

The knowledge we have today was generated during three centuries of histological observations of plant cell wall architecture as revealed by optical microscopy (Blancaflor and Gilroy 2000). Thus, there are several models of how cell wall components are three-dimensionally arranged.

The current general model of the plant cell walls states that it is composed of cellulose fibrils that form a mechanical framework that is embedded in a matrix of non-cellulosic polysaccharides and lignin (Keegstra 2010). However, in different taxonomic groups, the chemical composition of the cell wall differs (Sarkar et al. 2009).

Currently, scientists are focused on using lignocellulosic plant biomass for producing transportation fuel, and they have to face the biomass recalcitrance to produce fermentable sugars. Optical microscopes will continue to be a decisive tool for studying the biomass deconstruction.

7.2.1 Light Microscopy

Optical microscopy is based on the principles of absorption, diffraction, refraction, and transmission of light waves. Optical microscopes produce images using the differential propagation of light, such as bright field, differential interference contrast or Normasky, phase contrast, dark field, polarized light, and fluorescence. The main components of conventional light microscopes are the illumination source and the system of lenses comprising an eyepiece and an objective. The image is produced when the light crosses through the specimen and enters the system of lenses (Jean-Marie 2016). With the objectives available today, the specimen's image is magnified 10×, 40× or 100× in total when the magnification of the objective is combined with

the magnification of the eyepiece (10×). In fluorescent microscopes, a steam lamp of mercury provides the illumination source that illuminates the specimen from above and excites fluorescent dyes to produce fluorescent light. Epifluorescence microscopes are equipped with filters to match the excitation and emission spectra of the labeled fluorophore (autofluorescence or dyes).

The spatial resolution of a light microscope is limited by the wavelength of visible light. All light microscopes are limited to about 1.22λ/NA, where λ is the wavelength of light and NA is the numerical aperture. Thus, diffraction limits the resolution to approximately 0.25–0.7 μm. Optical microscopes can only resolve features above the diffraction limit. In practical terms, the major cell wall layers are the smallest objects observed under a light microscope. The resolution limit is very limited, but light microscopy remains in widespread use because of their advantages. They are convenient, easy to use, and inexpensive to buy and maintain. Additionally, a wide range of techniques involving light microscopes can be used to study morphological changes in biomass.

7.2.1.1 Applications to Biomass Characterization

Studies using light microscopes include measurements of particle length and width processed with optical devices equipped with a quantitative image analysis. The particle length and width histograms give information about the different particle size distributions result of the grinding process, a critical factor in the supply chain efficiency of biofuel conversion (Crawford et al. 2016). With light images, the decrease in length of lignin-free fibers during the enzymatic hydrolysis was observed, a phenomenon called fiber cutting (Clarke et al. 2011). Fiber cutting occurs in the fiber dislocations when the enzymatic activity concentrates.

A polarized light microscope was also applied for studying the fiber cutting, since cellulose is a birefringent polymer; changes in the cellulose crystalline structure appear as bright bands across the fiber surface. Also, light microscopes easily show the swelling changes of native fibers (Lara-Vázquez et al. 2014) as well as the morphological changes of refined cellulose fibers subjected to physical, chemical, or biological treatments (Fig. 7.1).

One of the major advantages of light microscopes is the full preservation of the color information and the selective identification of substances through a wide range of stains. With this approach, studies at the tissue and cellular-scale structure are performed by light microscopy observing the disruption of the general cell morphology in the epidermis, cortex, vascular bundle, and parenchyma (Fig. 7.2).

Toluidine-staining gives general information about the lignin distribution as well as the morphological changes after pretreatments. When native lignocellulosic substrates are pretreated, they exhibit a darker color in comparison with untreated samples, which is attributed to the breakdown of lignin and polysaccharides due to the high temperatures used in pretreatments. In addition, the specific distribution of substances after pretreatments may be detected using dyes (Table 7.2). Thus, Calcofluor-staining reveals a much more abundant cellulose after pretreatment due to loss of other non-cellulosic components (Holopainen-Mantila et al. 2013). Also,

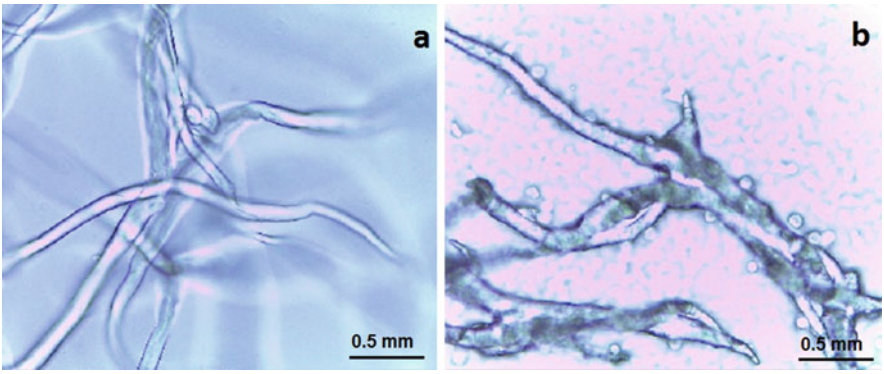

Fig. 7.1 Light microscopy images of (**a**) refined cellulose fibers and (**b**) cellulose fibers digested by a culture of *Clostridium*

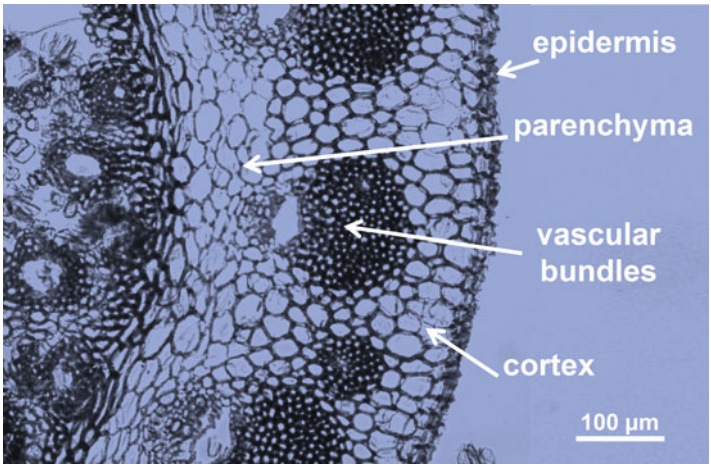

Fig. 7.2 Cross-section of wheat straw nodes under a light microscope

the lignin relocation or loss is detected using phloroglucinol-staining (Davidson et al. 1995).

Fluorescence microscopy is one of the main imaging techniques used for visualization of biomass. The lignin and phenolic acids have emission peaks at various excitation–emission wavelengths (ex. 330–385 nm, em. >420 nm; ex. 400–410 nm, em. >455 nm; ex. 420–480 nm, em. >515 nm; ex. 510–550 nm, em. >590 nm; Holopainen-Mantila et al. 2013). Thus, differences in the lignin autofluorescence are attributed to their concentration, and after pretreatments this autofluorescence decreases. An innovative use of fluorescence microscopy is immunofluorescence imaging with monoclonal antibodies to label a specific target antigen with a fluorescent dye. Thus, two rat monoclonal antibodies designated LM10 and LM11 recognize xylan with different specificities based on the substitution of the xylan backbone (McCartney et al. 2005).

Table 7.2 Representative dyes and monoclonal antibodies used in the characterization of biomasses

Name	Target molecule	Reference
Dyes		
Toluidine blue O	Phenolic compounds (blue/green) Unlignified walls (pink/purple)	O'Brien et al. (1964)
Acid fuchsin	Protein (red)	Dornez et al. (2011)
Calcofluor white	β-Glucan and chitin (blue/green)	Haigler et al. (1980)
Phloroglucinol	Lignin (red)	Davidson et al. (1995)
Monoclonal antibodies		
LM10 (rat immunoglobulin class IgG2c)	(1,4)-*β*-D-xylan (green)	McCartney et al. (2005)
LM11 (rat immunoglobulin class IgM)	Arabinoxylan and unsubstituted xylan (green)	McCartney et al. (2005)

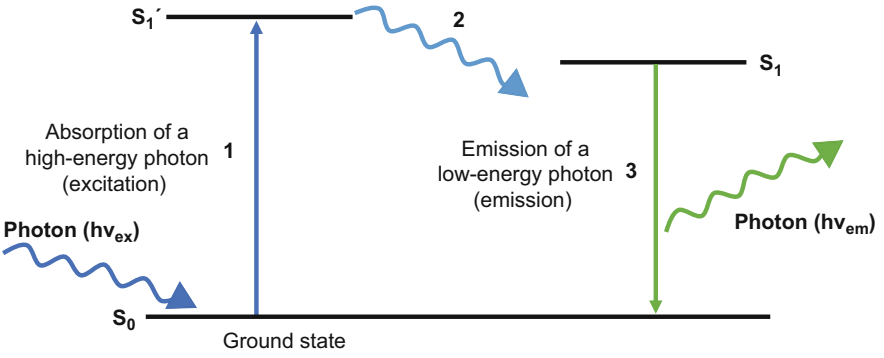

Fig. 7.3 Jablonski diagram of a fluorescence event

7.2.2 *Confocal Scanning Laser Microscopy*

Confocal microscopy represents one of the most powerful tools in optical microscopy. In the 1950s, Marvin Minsky invented the confocal scanning microscope overcoming the drawbacks of the epifluorescence microscopy (Blancaflor and Gilroy 2000). When fluorescence is generated, a substance absorbs high-energy light (at a short wavelength) and subsequently emits low-energy light (at a longer wavelength). The basic principles of fluorescence are represented in the Jablonski energy diagram (Fig. 7.3), named in honor of the physicist Alexander Jablonski. The fluorescent molecule, or fluorophore, is in its ground-energy state (S_0) before absorbing a photon of a given energy (hv) and moving to an excited electronic singlet state (S_1'), which occurs during the first phase (1) of fluorescence, typically within 1–10 ns. The fluorophore then passes to a relaxed singlet state (S_1) by partial dissipation of the absorbed energy in the second phase of fluorescence (2). Finally, in the third phase (3), a photon is emitted when the fluorophore returns to its ground-energy state (S_0).

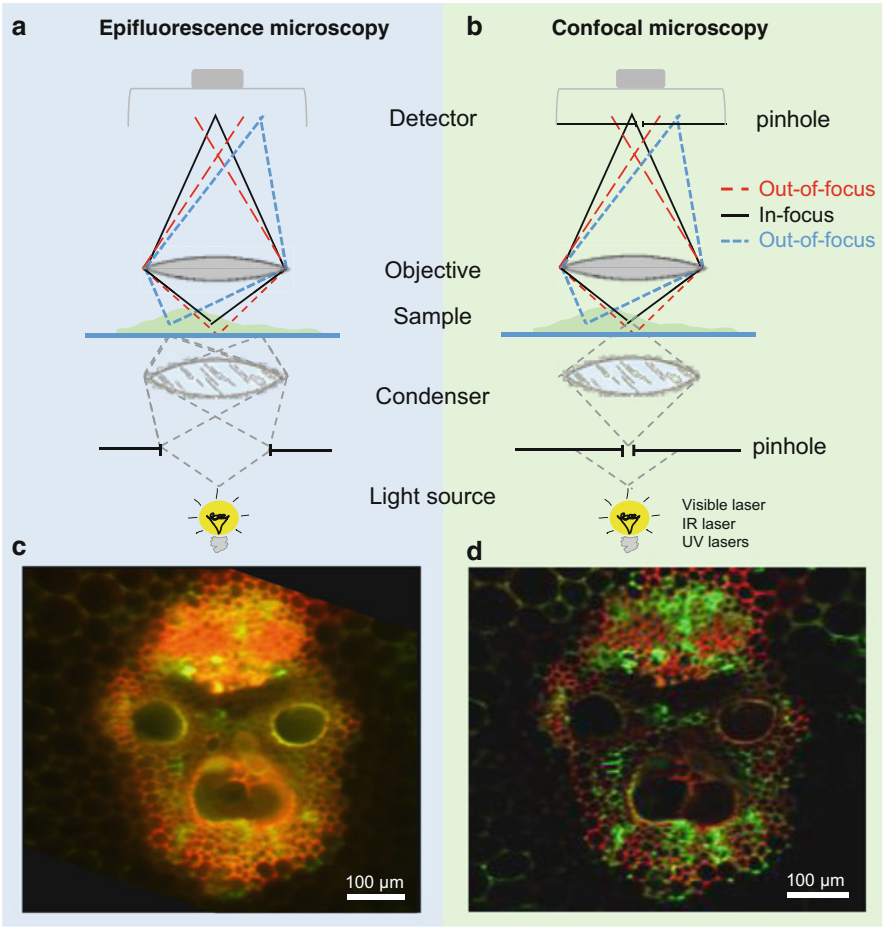

Fig. 7.4 A comparison between design and obtained images using conventional epifluorescence (**a**, **c**) and confocal (**b**, **d**) microscopes. The schemes (**a**) and (**b**) in the *upper panels* are based on Schuldt (2009). The images were taken with an epifluorescence microscope (DIM 6000CS, Leica) and a confocal microscope (TCS SP5X, Leica). The tissue was stained with propidium iodide (in *red*, Sigma-Aldrich) and Alexa Fluor® 488 conjugate of wheat germ agglutinin (in *green*, Life Technologies)

The confocal microscope derived its name from the arrangement of the light path. In a conventional epifluorescence microscope (Fig. 7.4a), the light source and condenser illuminate a large region of the sample, and the detector forms an image from a combination of the in-focus (black lines) and out-of-focus light (red and blue lines). In contrast, with a confocal microscope (Fig. 7.4b), the in-focus light is the only light to reach the detector (black lines) as the illumination and detection light paths are in a common focal plane with two pinholes (Schuldt 2009; Lou et al. 2014). A fluorescent cell might be 5–15 µm thick and have a depth of focus (i.e., the thickness of the imaging plane) of approximately 300 nm or less with a high numerical

aperture (NA) objective (≥1.3). Thus, the majority of the cell volume is out of focus (Conchello and Lichtman 2005). Removal of the out-of-focus light provides greater contrast and permits three-dimensional reconstruction of the images. The quality of the image obtained from a conventional fluorescence microscope and a confocal microscope is contrasting; for example, the image generated by epifluorescence comes from several planes (Fig. 7.4c), whereas the same image generated by confocal microscopy is formed principally in one plane (Fig. 7.4d).

The objective NA and pinhole size determine the resolution in a confocal system; the NA is the most important variable for obtaining higher quality images, in contrast to a higher magnification (Conchello and Lichtman 2005). The pinhole blocks the light from areas out of focus of the sample, whereas the in-focus light passes through the pinhole into the detector. However, as the pinhole size is reduced, more light from outside the focal plane is rejected, thus increasing depth discrimination. In practice, larger pinholes must often be used with dim samples or fluorophores that bleach rapidly.

The development of fluorophores, fluorophore-conjugated antibodies, and fluorescent proteins with improved photostability have increased quantum yields, expanded spectral palettes, are more compatible with living cells or tissues, and constitute essential microscopic imaging tools for studies of cell biology and physiology. The most significant advantages of confocal microscopy over conventional microscopy include the following (Smith 2011; Nwaneshiudu et al. 2012): (1) generation of a three-dimensional structure or reconstruction of 3-D images and video of the sample, and (2) differential identification of one or more molecules, organ or subcellular structures through the use of more than one fluorophore. However, there are also limitations in the use of fluorescence microscopy, including: (1) photobleaching, which describes the process of fluorophore fading following excitation; (2) generation of phototoxic compounds to living samples as a result of photobleaching; and (3) limits to the optical penetration and signal-to-noise ratios due to variations in the transparency of tissue samples. In spite of these disadvantages, it is currently feasible to study dynamic processes, such as transcriptional and translational gene expression (space and time), cell assembly and turnover of cytoskeletal components, and protein–protein interactions (bimolecular fluorescent complementation) by confocal microscopy (Smith 2011; Nwaneshiudu et al. 2012).

7.2.2.1 Applications to Biomass Characterization

Confocal microscopy is a robust technique applied to the characterization of the structure and dynamics of the cell wall components of untreated and treated biomasses. A routine analysis includes visualization of the differences in the cellulose content using Calcofluor White, and in the lignin content by autofluorescence (Ji et al. 2014; Sant'Anna and de Souza 2012). Immunolocalization may also elucidate the effects of the pretreatments in combination with confocal microscopy. Hell et al. (2015) obtained arabinoxylans from wheat bran using ball-milling and chemical treatments. Authors performed immunolocalization of arabinoxylan with the

monoclonal antibody LM11 and confocal microscopy. Results showed that extensive ball-milling was the best method for harvesting arabinoxylan.

In the field of enzymatic hydrolysis, confocal immunofluorescence microscopy permits the visualization of single enzymes and complexes acting on insoluble fibers. Kim et al. (2014) expressed a minicellulosome formed by two cellulolytic enzymes, endoglucanase E (CelE) and β-glucosidase A (BglA), on the surface of *Corynebacterium glutamicum*. Immunofluorescence confirmed the localization of these bi-functional cellulases complexes. An enzyme mixture, Spezyme CP blended with Novo 188 β-glucosidase, was used to depolymerize bacterial microcrystalline cellulose. The enzyme mixture was complemented with the fluorescent-labeled *Trichoderma reseii* Cel7A to measure the cellulase binding onto the fibers and enzymatic activity. The cellulose fibers were also labeled with a fluorescent dye to follow the temporal morphological changes and its depolymerization. With this experimental strategy, authors proposed three kinetic models that successfully predicted the soluble sugars released by the enzyme mixture (Luterbacher et al. 2013).

Three-dimensional images of plant cell walls were reconstructed using a series of optical sections obtained with a confocal microscopy (Travis et al. 1997). With this approach, authors measured the cell wall volume and thickness before and after fiber digestion. The effects of intensive milling of wheat straw fibers were evidenced by confocal images (Lara-Vázquez et al. 2014). The confocal images showed a shaving effect in finer fibers (0.2 mm) that had a lower swelling capacity than larger fibers (2.0 and 3.0 mm).

Confocal imaging has visualized bacterial and fungal degradation of lignocellulosic substrates. Pérez-Rangel et al. (2015) showed a very active fungal community native of wheat straw acting on insoluble fibers. Authors also published a video of the penetration hypha of the native fungi. Finally, confocal imaging in conjunction with fluorescence in situ hybridization (FISH) may allow studies on diversity, spatial arrangement, and microbial dynamic (Fig. 7.5).

7.2.3 Confocal Raman Microscopy

White light is made of a mix of different colors from red (~700 nm) to violet (~350 nm) (Fig. 7.6a). When a sample is lit with a monochromatic light (light of a single frequency or wavelength), it interacts with the sample, being reflected, absorbed, transmitted, or scattered. In this sense, spectroscopy is the study of the interaction between electromagnetic radiation and matter. During light scattering, for instance, if the violet light is isolated from the white light with a violet filter, and it passed through a sample, there are two effects: (1) most of the scattered light emerges from the sample with the same color (same wavelength) as the incident violet light, it is called the Rayleigh scattering effect, and (2) some of the scattered light may change its wavelength or frequency resulting in a different color, this light is called the Raman scattering or the Raman effect (Fig. 7.6b). The Raman effect is a very weak effect; only one in a million of the scattered light photons exhibit the

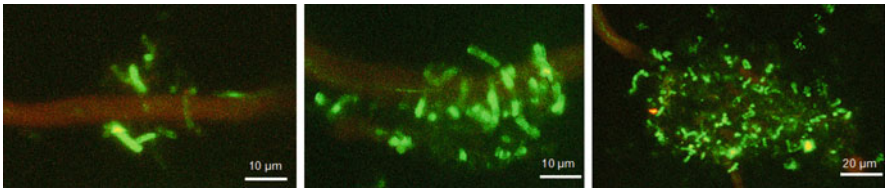

Fig. 7.5 Confocal imaging of *Clostridium* cells cultured in cellulose fibers under static conditions. The cells were stained with Alexa Fluor 488 conjugate of wheat germ agglutinin (in *green*) and fibers with Rhodamine (in *red*)

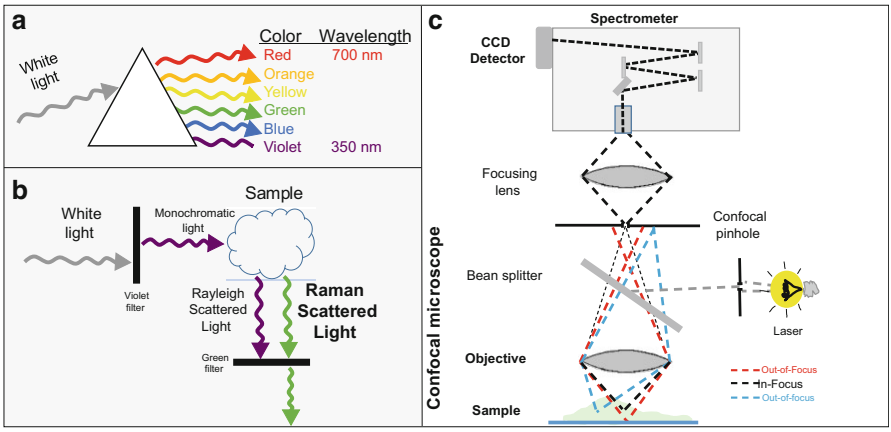

Fig. 7.6 Principle of the Raman effect. (**a**) The visible electromagnetic spectrum is a combination of lights with different wavelengths (*colors*). (**b**) Representation of the Raman scattered light. Figures are based on Bohning (1998). (**c**) Main components of a Raman microscope

change in wavelength (Bohning 1998). Each substance projects one unique spectrum of Raman scattered light; thus, it serves as a fingerprint that is used for qualitative and quantitative analyses. Additionally, the intensity of the spectral lines for such substance is related to the concentration.

When the wavelength of monochromatic light is shorter than the wavelength of scattered light, Stokes lines appear in Raman spectrum. In contrast, when the wavelength is longer than the wavelength of scattered light, anti-Stokes lines appear (for review see Bumbrah and Sharma 2015). Stokes-shifted Raman bands involve transitions from lower to upper energy vibrational levels. A change in polarizability during the molecular vibration is an essential requirement to get the Raman spectrum of samples providing information about the vibrational and rotational energies of molecular bonds. The spectral information in confocal microscopy is obtained from Raman spectroscopy; a spectrophotometer is interfaced to an optical microscope, which permits both visual and spectroscopic detection using the microscope to focus the laser beam onto the sample.

Confocal Raman microscopy fuses the Raman spectrometry and the confocal microscopy resulting in a non-destructive method for chemical analyses of organic and inorganic compounds, providing qualitative and quantitative information, and obviating the usual sample preparation and staining (Fig. 7.6c). This noninvasive method gives structural information in situ with a high spatial resolution of <0.5 μm. The most significant disadvantage of Raman microscopy is a high band overlap making difficult to interpret what components are present in the sample in small amounts (Gierlinger 2010).

7.2.3.1 Applications to Biomass Characterization

Confocal Raman spectroscopy is frequently used to evaluate the tissue-specific changes at topochemical level. Sun et al. (2013) pretreated corn stover with 1-ethyl-3-methylimidazolium acetate (an ionic liquid); different cell types such as tracheids, sclerenchyma, and parenchyma cells were analyzed. Results showed that cellulose and lignin were differentially located before the pretreatment since the lignin dissolution was faster than cellulose in the secondary cell walls. Authors provided new insights toward the mechanism of ionic liquid pretreatment where there is a synergistic mechanism of lignocellulose dissolution regarding cellulose and lignin dissolution and cell wall swelling occurring during the pretreatment. High-resolution, Raman imaging allowed to map changes in the polymer and silica contents within and between different cell wall layers (Gierlinger 2010).

Ma et al. (2014) studied the topological diversity and compositional heterogeneity of lignin and hydroxycinnamic acids in *Miscanthus sinensis*. They observed that the concentration of lignin and hydroxycinnamic acids varied among cellular types including within distinct cell wall regions. A spatial correlation between lignin and hydroxycinnamic acids was observed by microspectroscopy imaging approach.

7.3 Scanning Probe Microscopy

The family of instruments termed scanning probe microscopes (SPMs) includes the scanning tunneling microscope (STM), the atomic force microscope (AFM), and the scanning near field optical microscope (SNOM), all of which operate with a very sharp probe that interacts directly with a surface of interest to obtain a three-dimensional view (Johnson et al. 2009). In addition to topological information, SPMs record physical, chemical, and mechanical properties of such surfaces. The first STM of this family was invented in the early 1980s by Binnig and Rohrer (1982), and with these instruments, it was possible to observe atoms at surfaces for the first time. Because STMs only resolve conductive surfaces, AFM and SNOM were developed to scan any type of samples, conductive or not. Since then, AFM has been widely applied in biological fields to image three-dimensional surface structures, record physical properties of surfaces, and as a dissecting tool. Visualizations obtained by AFM

include globular proteins on the cytoplasmic surface, chromosomes and collagen fibrils and the shape and dimensions of DNA (Ushiki and Kawabata 2008). Applications of AFM on vegetal tissue started with modest visualizations of stomata (Butt et al. 1990), and individual plant cellulose microfibrils (Kirby et al. 1996). Since then, the AFM has been recognized as a powerful tool for creating three-dimensional surface structures of vegetable cell walls, before and after their pretreatment.

7.3.1 Atomic Force Microscopy

The unique features of the AFM include the study of biological samples at a micro- or nanoscale, use of nonconductive samples without any conductive treatment and under a non-vacuum environment, meaning near-physiological conditions. Additionally, the AFM measures length, height, diameter, and elasticity, simultaneously (Ushiki and Kawabata 2008).

The AFM includes four main components illustrated in Fig. 7.7a. A soft spring called cantilever is present in either a V-shape or rectangular shape with two faces: the upper surface coated with a thin layer of gold (Au) or aluminum (Al) and, at the end of the opposite surface, a very sharp probe. AFM cantilevers with integral probes are manufactured using silicon nitride (Si_3N_4) or silicon (Si). These probes are available in the form of a square-based pyramid or a cylindrical cone with sizes between 100 and 250 μm. As the probe approaches the sample surface, different interaction forces emerge causing the cantilever to deflect toward or away from the surface. A laser beam reflects off the coated surface of the cantilever recording its deflections. The detection system consists of a position-sensitive photodetector that receives and processes the normal and lateral forces from the reflected laser beam. A piezoelectric scanner, onto which the sample is placed, makes displacements in the y, x, and z directions to adjust the distance (Z) between the probe and sample. This feedback loop maintains constant laser position, and the AFM images the sample topography (Johnson et al. 2009).

The cantilevers possess the properties of a spring, with a known elastic constant k_c (N/m). As the cantilever moves in the vertical direction, it experiences attractive or repulsive forces depending on the probe–sample distance. The cantilever deflection (Δx) is a function of the vertical displacement of the piezoelectric scanner. The probe–sample forces are given by Hooke's law: $F = -k_c \Delta x$, where F is the force, k_c is the spring constant of the cantilever, and Δx is the deflection of the cantilever. As the probe approaches the sample, it experiences attractive forces such as electrostatic, van der Waals, and hydration forces.

Then, as the probe moves closer to the sample, strong repulsive forces will dominate due to the electron clouds overlapping between the atoms in the probe and those in the sample (Ushiki and Kawabata 2008).

Figure 7.7b represents a typical force–distance curve used for studying surface interactions by means of AFM with lateral (25 nm), vertical (1 Å), and force (1 pN) resolution. This curve shows the forces experienced by the probe as a function of the sample distance. At first, the probe will experience attractive forces resulting in a

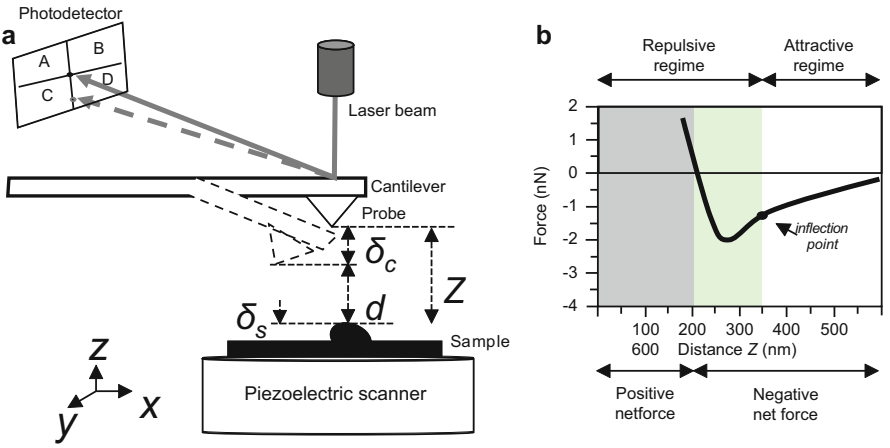

Fig. 7.7 (**a**) Main components of an atomic force microscope. (**b**) A force–distance curve

negative total force. When the probe is closer to the sample, there is an inflection point at which the repulsive forces begin their contribution to modifying the curve shape until reaching a positive total force. In this way, there are two zones where the total force contribution is repulsive (a positive net force) and where the total force contribution is attractive (a negative net force).

There are several modes of acquiring the force–distance curves. In contact mode, the probe remains in contact with the sample at all times, and repulsive forces are present. Contact mode is the most common mode chosen for imaging hard and flat samples. The drawbacks include a decrease in the resolution, damage or deformation of the probe or sample and underestimation of the height of surface features. In an intermittent contact (tapping) mode, the cantilever oscillates just above the surface at a value close to its resonant frequency. In a non-contact mode, the cantilever also oscillates above the sample but at a much-reduced amplitude than in the tapping mode. In a non-contact mode, van der Waals and electrostatic forces occur between atoms in the probe and the sample. Additionally, functionalized probes are used to study specific forces by means of their selective adherence to specific molecules (Cappella and Dietler 1999; Wang and Yadavalli 2014).

During the scanning of biological samples, capillary condensation and debris collected by the probe generate adhesive forces, resulting in a distorted image. Non-contact or tapping contact mode imaging under liquid have helped to overcome this deformation (Morris et al. 1997). However, this technique has the drawback of tip-broadening, resulting in the overestimation of crystallite dimensions.

7.3.1.1 Applications to Biomass Characterization

Early AFM studies served to determine the diameter and orientation of cellulose fibrils ranging from 3 to 5 nm. Authors led to the proposal of a model for the elementary fibril consisting of an interwoven 36-glucan chain with an inner core of 6

crystalline chains surrounded by 12 sub-crystalline chains, and finally, at the microfibril surface, another 18 amorphous chains (Ding and Himmel 2006). Additionally, high-resolution AFM served to identify and spatially locate two allomorphs of cellulose, triclinic I_α and monoclinic I_β phases in the crystalline and amorphous regions of the cell walls of wheat straw (Li et al. 2006).

Recently, AFM has been used for studying lignocellulosic biomass samples before and after pretreatment application to analyze the lignin distribution, surface roughness, progression of enzymatic hydrolysis of substrates, measurements of fibril diameter, and three-dimensional orientation of fibrils, among others. Using AFM, some authors have studied the lignin agglomeration and relocation of lignin as a result of the high temperatures applied during pretreatments (Abud et al. 2013; Haque et al. 2013). When the pretreatment temperature ranges of between 120 and 200 °C exceed the melting point of lignin, this causes its fluidization. Once the sample is cooled, lignin is deposited as droplets onto the surface of the cell wall matrix. These lignin droplets are efficiently removed using alkali pretreatments with 2.5 % of NaOH (Haque et al. 2013).

Studies on surface roughness after pretreatment reveal the total area available for enzymatic hydrolysis. For example, after application of the acid pretreatment (2 % sulfuric acid at 150 °C for 20 min), the surface roughness factor increased from 5.7 mm on the untreated sugarcane cell wall to 9.1 on the sulfuric acid-pretreated cell wall (Abud et al. 2013). Additionally, by AFM the average surface area roughness (μm^2) of rice straw was measured before and after a biological treatment with fungal enzymes. The average surface area roughness increased from 0.27 to 6.4 mv after the biological pretreatment (Dhiman et al. 2015). By AFM, it was possible to monitor the enzymatic degradation directly on cellulose fibrils.

With high-resolution AFM, Wang et al. (2013) presented direct visualizations of fungal enzymes acting on native bacterial cellulose fibers, and they demonstrated the synergistic effect between exo- and endo-acting enzymes. With an advanced version of high-speed AFM, Igarashi et al. (2011) showed real-time visualizations of cellulose degradation by single fungal enzymes. Authors demonstrated that such enzymes move unidirectionally on the surface, and at some point, "traffic jams" reduce the hydrolytic efficiency.

7.4 Electron Microscopy

Electron microscopy overcomes the limited image resolution of light microscopy led by the wavelength of visible light. This technology was developed thanks to the recognition of the optical properties of electron beams on a magnetic or electrical field. Since its early invention in 1931 by Ruska and Knoll (1987), electron microscopy has been used for the study of biological specimens. In 1934, Marton proposed a simple methodology of sample preparation involving an intense cooling and an

impregnation of objects with a less destructible material. At that time, these techniques were evaluated successfully in a 15 μm section of a *Drosera intermedia* leaf on a copper net (Marton 1934).

Two general types of electron microscopy have been developed: scanning electron microscopes (SEM) to analyze the surface of bulk specimens and transmission electron microscopes (TEM) to examine internal and external characteristics of thin specimens. Both instruments share some basic features and principles; they operate using accelerated electrons and electromagnetic lenses to generate images and require a high vacuum to allow electrons to travel down the column of microscopes without being scattered by air molecules (Bozzola 2001).

The electron microscopes generate a beam of valence electrons by heating a filament to more than 1700 K, usually of LaB_6, and applying a high voltage of negative potential in the range of 0.1–30 kV, named a thermionic gun. The electric field between the filament and the anode plate extracts and accelerates the electrons toward the anode (Fig. 7.8). Modern electron microscopes can use another source of electrons, field emission electron guns (FEG), composed of a single tungsten wire with a sharp tip. In FEG, a strong electrical field applied by an anode extracts the electrons, and a second anode accelerates them. Once electrons go through the anode plate, they travel at about half the speed of light and enter the magnetic field of the first and second lenses, focusing the electron onto the specimen (Zhou et al. 2006; Bogner et al. 2007; Williams and Carter 2009).

Electron lenses are composed of coils of wires known as electromagnets, generating a magnetic field to adjust the trajectories of electrons by the current that is applied onto these coils. Lenses are used to magnify or demagnify the electron beam diameter, varying the focal length to illuminate the specimen in the area being studied. The first lens acts as a condenser, where the electron beam is converged and collimated into a relatively parallel stream, and the second lenses act as an objective, where the electron beam is focused into a probe point at the specimen surface and supplies further demagnification (Zhou et al. 2006).

Because electrons are ionizing radiation, once they interact with the matter of the specimen being analyzed, they produce a wide range of secondary signals. Among those signals, some backscattered and secondary electrons are reflected (BSE and SE), as well as characteristic X-rays, visible light, and Auger electrons. In thin specimens, as is the case in TEM, the electron beam is transmitted by generating a weaker direct beam, elastically and inelastically scattering electrons and *bremsstrahlung* X-rays (Fig. 7.9a). It is noteworthy that those secondary signals from the specimen can be used in analytical electron microscopy, generation of chemical information from the samples, using X-ray energy-dispersive spectrometry and electron energy-loss spectrometry. For instance, spectra obtained from the X-ray exhibit characteristic peaks related to specific elements in different regions (Zhou et al. 2006; Williams and Carter 2009).

Further particular characteristics of TEM and SEM are introduced below, as well as their application in biomass characterization.

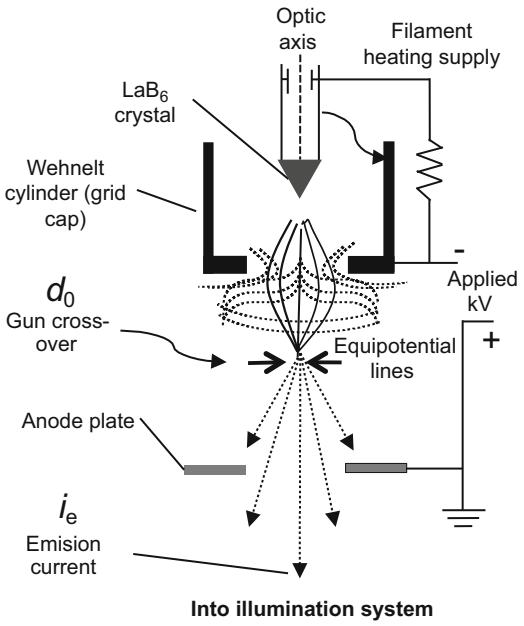

Fig. 7.8 Schematic diagram of a thermionic electron gun into electron microscopy systems. The electric field from the Wehnelt cylinder acts as a grid whereas the electric field focuses the electrons

7.4.1 Transmission Electron Microscopy (TEM)

TEM is a versatile tool for characterization of specimens over spatial ranges from the atomic scale to the nano "regime" (from <1 nm to ~100 nm) up to the micrometer level and beyond (Fig. 7.10a). Currently, the combination of intermediate voltage TEMs and the correction of spherical aberrations have led the image resolution to below the 0.1 nm (1 Å) barrier (Rose 2009; Williams and Carter 2009).

In TEM, the electrons are transmitted through the specimen revealing a two-dimensional image of the interior of cells. As shown in Fig. 7.9a, once the electrons reach the specimen, they are deflected to various degrees depending on the mass of the cellular component. In TEM, only the forward scattered electrons are considered; areas of great mass deflected electrons are removed from the optical axis and appear dark when projected onto the viewing screen. Areas of lesser mass scatter electrons to a lesser degree and appear brighter on the viewing screen. Then, images are further magnified up to a million times by additional lenses in the microscope.

The main limitation for TEM is related to sample preparation. Biological specimens require fixation (with chemicals or cryotechniques) and further sectioning, which is a lengthy procedure. Artifacts can be produced during preparation, such as distorted or disorganized organelles, and the cellular membrane continuity can be altered or material loss, making the cell appear less dense than it really is. Nonetheless, these disadvantages can be overcome by skilled scientists distinguishing between real structures and artifacts (Wilson and Bacic 2012; Winey et al. 2014).

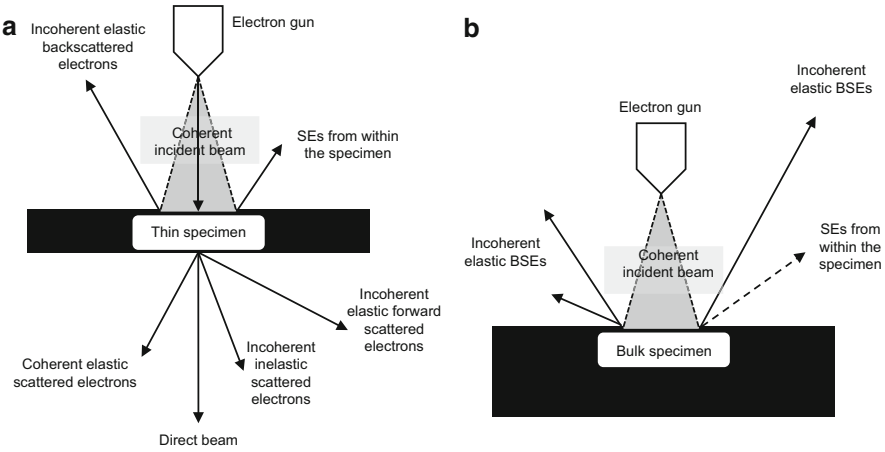

Fig. 7.9 Different types of signals from electron beam incidence in the matter: (**a**) from the thin specimen such as in TEM and (**b**) from a bulk specimen such as in SEM

7.4.1.1 Applications to Biomass Characterization

TEM has been widely used for cellular structure analysis, identifying every component, such as the cytoskeleton, membrane systems, organelles, cilia, microvilli, and the synaptonemal complex (Winey et al. 2014).

Recently, driven by the concern for producing biofuels from lignocellulosic biomass, TEM has become a useful tool for analyzing the effect of pretreatments on biomass. For instance, some effects observed were the removal of the cell wall and re-localization of lignin during chemical and hydrothermal pretreatment of switchgrass, as well as cellulase penetration in cells using immune-TEM (Donohoe et al. 2011). Indeed, TEM allowed observation of delamination and disruption of cellulose microfibrils from switchgrass following alkaline pretreatment (Karp et al. 2015). In different sources of biomass such as sugarcane bagasse, TEM allowed observation of how steam pretreatment with SO_2 and CO_2 as an impregnating agent disrupted the outer region of the cell wall resulting in the formation of pores (Corrales et al. 2012).

Considering the emerging biological pretreatments of lignocellulosic biomass, early studies proved that TEM application could evaluate biomass disruption by bacteria (Akin 1979). Also, the use of fungi was studied observing the *Cyathus stercoreus* hypha degrading the parenchyma cell wall of Bermuda grass (*Cynodon dactylon*) (Akin et al. 1995).

Of recent interest, microalgae are viewed as a source of cellulosic biomass for biofuel production. In this sense, TEM can be used to quantify microalgae populations in natural samples (Børsheim et al. 1990).

In terms of new biotechnological applications of biomass, TEM has assisted in the identification of bioplastic accumulation in the engineering crop switchgrass (*Panicum virgatum* L.) (Somleva et al. 2008).

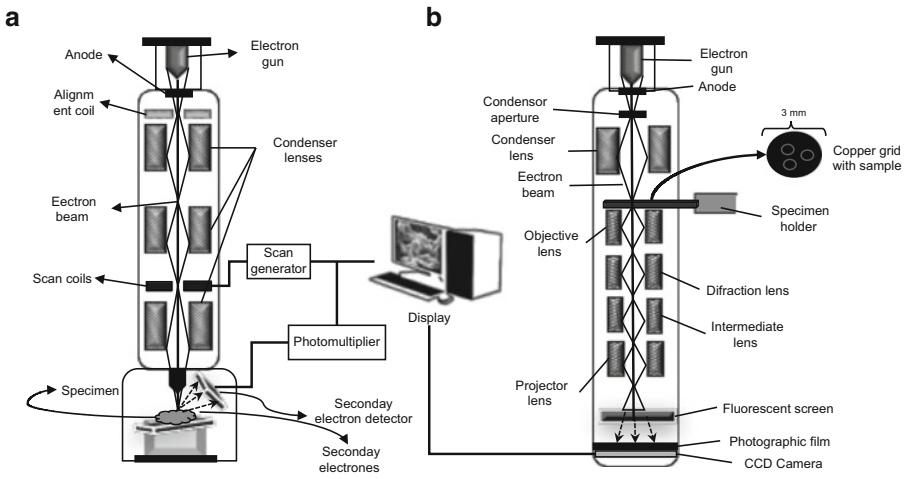

Fig. 7.10 Schematic diagram of: (**a**) a scanning electron microscope (SEM), and (**b**) a transmission electron microscope (TEM)

7.4.2 Scanning Electron Microscopy (SEM)

In SEM, the condenser lenses focused the electron beam in a tiny spot on the specimen. Once the beam of electrons strikes the specimen, several signals are emitted as is shown in Fig. 7.9b for bulk specimens. The secondary electron emission is the most widely used signal caused by loosely bound electrons through the ionization of specimen atoms, depending primarily upon topography, angle of entry of the beam into the specimen and thickness of raised portions of the specimen. Secondary electrons have low energy (3–5 eV), so they can only escape from a region of a few nanometers of the specimen surface, giving topographic information with good resolution visualization texture and roughness of surface. The topographical image depends on how many secondary electrons reach the detector, which is placed at a positive high voltage of approximately 12 kV, resolving surface structures of 10 nm or better.

Electrons that do not reach the detector will generate shadows; whereas, those that are not obstructed from the detector will generate bright areas. In this way, multiple black and white images convey three-dimensionality (Bozzola 2001; Bogner et al. 2007). A schematic diagram of a SEM is presented in Fig. 7.10b.

Modern SEM can achieve a 0.4 nm resolution with FEG at an accelerating voltage of 30 kV and three million magnifications (Nanotechnology Now 2011).

Likewise for TEM, the most relevant limitation in SEM is the sample preparation. Biological samples need to be dehydrated before being placed under the microscope. This procedure, as has been discussed, can distort cellular features or create artifacts. Moreover, specimens need to be coated with a conductive material before being viewed using SEM. Also, the thickness of the material can obscure important cellular details (Wilson and Bacic 2012).

Specimen preparation must include the high vacuum needed in electron microscopy. To overcome this restriction environmental scanning electron microscopy (ESEM) was developed since 1950, where samples are analyzed in a natural state. Two basic principles allowed the creation of ESEM: (1) maintenance of the small electron beam even through the high pressure system (a gaseous environment), and (2) the invention of a gaseous secondary electron detector, achieving resolutions approximately 5 nm.

7.4.2.1 Applications to Biomass Characterization

SEM has allowed reports of biomass morphology and composition, such as the analysis of the structure and properties of natural cellulose fibers extracted from corn stalks (Reddy and Yang 2005). In the same sense, the extraction of nanocellulose fibrils from lignocellulosic feedstocks such as banana, jute, and pineapple leaf was also evaluated with SEM (Abraham et al. 2011). The elemental composition of wheat straw nodes by energy-dispersive X-ray SEM (EDX-SEM) showed different concentrations of Si, comparing the outer to the inner surface (Ghaffar and Fan 2015).

Similar to TEM, the use of SEM has increased due to the biofuels based on lignocellulosic biomass, especially in the evaluation of biomass pretreatment methods. For instance, by analyzing the biomass solubilization due to a pretreatment with an ionic liquid, SEM showed an unpacking of macrofiber bundles, losing the hierarchical structure of switchgrass (Singh et al. 2009), pore formation over several scales (Li et al., 2010), and making the cellulose more ready for enzymatic pretreatment of palm biomass (Tan et al. 2011). Under different acid pretreatments, using SEM allowed observation of lignin deposition on corn stover surface (Wei et al. 2011), and the colonization of grass with the lignin degrader fungi *C. stercoreus* (Akin et al. 1995). Figure 7.11 provides a multi-scale imaging of wheat straw nodes before and after pretreatment. Optical and electron microscopies yield images to compare changes in the polysaccharide and lignin contents. Light images allow visualizing changes in the staining pattern due to disruption of non-cellulosic polysaccharides and lignin. Confocal images show that the dilute acid pretreatment removed more efficiently lignin than the alkali pretreatment. SEM images show the surface topography. Silica bodies and unaltered cell walls were observed in the untreated samples. Alkali pretreatment collapsed the plant cell walls and removed the silica bodies while the dilute acid pretreatment exposed the cellulosic cell walls with silica bodies still visible.

7.5 Conclusions

The last decades have resulted in the development of advanced microscopic techniques that in conjunction with biochemical and spectroscopic methods have improved our understanding of how the plant cell wall is arranged. In vivo imaging

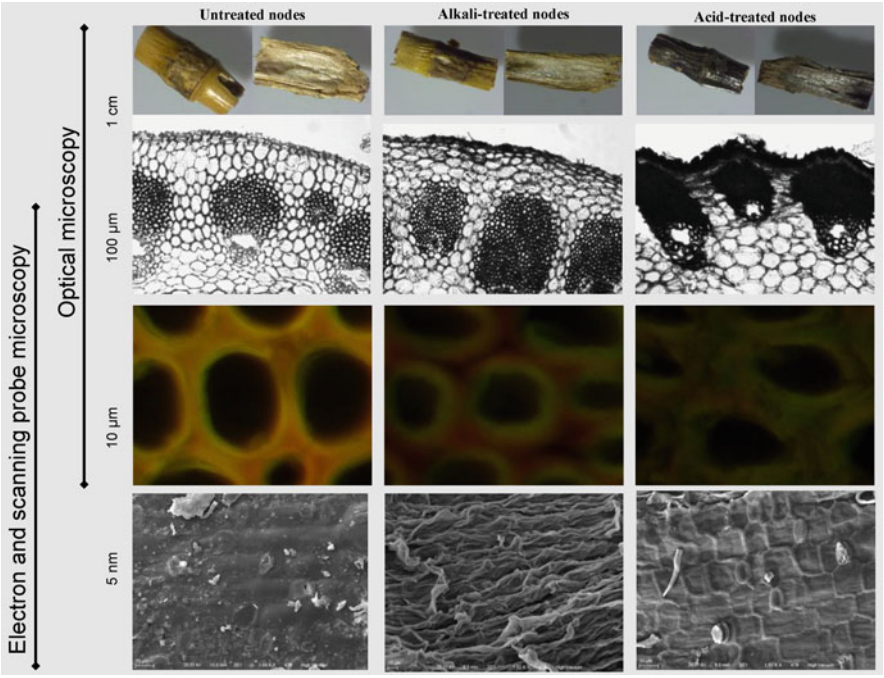

Fig. 7.11 Multi-scale imaging of wheat straw nodes before and after alkali (0.75 % NaOH) and dilute acid (0.75 % H_2SO_4) pretreatments. Both treatments were performed with 8 % w/v of total solids at 121 °C for 60 min. From top to *bottom panels*: stereomicroscopy, light microscopy, confocal microscopy, and SEM. Confocal images were captured with a TCS SP5X microscope (Leica) using a 488 nm excitation laser and an emission range of 515–565 nm for polysaccharide detection (green fluorescence) and 590–665 nm for lignin detection (red fluorescence)

has helped researchers to a better comprehension of the kinetic models as well as the physical and chemical barriers at which the hydrolytic enzymes are subjected. Nowadays, the effects of pretreatment methods are understood at a tissue and cellular scale. However, questions remain about the dynamics of the cell wall components, the relationships between the type and efficiency of pretreatments with the enzymatic hydrolysis, the type of linkages between the cellulosic- and non-cellulosic cell wall components in the different taxonomic groups, and details of the enzyme–substrate complexes. All these advances will lead to substantial improvements in the establishment of the future green biorefineries.

Acknowledgements Financial support was received from the CB CONACYT project (Grant No. CB-2011/168921), the Red Temática del Hidrógeno Subprograma de Producción de Hidrógeno (Grant No. 252003), and the CONACYT project Apoyo al Fortalecimiento y Desarrollo de la Infraestructura Científica y Tecnológica (Grant No. 250738).

References

Abraham E, Deepa B, Pothan LA, Jacob M, Thomas S, Cvelbar U, Anandjiwala R (2011) Extraction of nanocellulose fibrils from lignocellulosic fibres: a novel approach. Carbohydr Polym 86:1468–1475

Abud Y, Costa LT, de Souza W, Sant'Anna C (2013) Revealing the microfibrillar arrangement of the cell wall surface and the macromolecular effects of thermochemical pretreatment in sugarcane by atomic force microscopy. Ind Crop Prod 51:62–69

Akin DE (1979) Microscopic evaluation of forage digestion by rumen microorganisms – a review. J Anim Sci 48:701–710

Akin DE, Rigsby LL, Sethuraman A, Morrison WH, Gamble GR, Eriksson KE (1995) Alterations in structure, chemistry, and biodegradability of grass lignocellulose treated with the white rot fungi *Ceriporiopsis subvermispora* and *Cyathus stercoreus*. Appl Environ Microbiol 61:1591–1598

Binnig G, Rohrer H (1982) Scanning tunneling microscopy. Helv Phys Acta 55:726–735

Blancaflor EB, Gilroy S (2000) Plant cell biology in the new millennium: new tools and new insights. Am J Bot 87:1547–1560

Bogner A, Jouneau PH, Thollet G, Basset D, Gauthier C (2007) A history of scanning electron microscopy developments: towards "wet-STEM" imaging. Micron 38:390–401

Bohning JJ (1998) The Raman effect. American Chemical Society Indian Association for the Cultivation of Science, Kolkata

Børsheim KY, Bratbak G, Heldal M (1990) Enumeration and biomass estimation of planktonic bacteria and viruses by transmission electron microscopy. Appl Environ Microbiol 56:352–356

Bozzola JJ (2001) Electron microscopy eLS. John Wiley & Sons, New York, NY

Bumbrah GS, Sharma RM (2015) Raman spectroscopy – basic principle, instrumentation and selected applications for the characterization of drugs of abuse. J Forensic Sci (in press)

Butt HJ, Wolff EK, Gould SAC, Dixon B, Peterson CM, Hansma PK (1990) Imaging cells with the atomic force microscope. J Struct Biol 105:54–61

Cappella B, Dietler G (1999) Force-distance curves by atomic force microscopy. Surf Sci Rep 34:1–104

Clarke K, Li X, Li K (2011) The mechanism of fiber cutting during enzymatic hydrolysis of wood biomass. Biomass Bioenerg 35:3943–3950

Conchello JA, Lichtman JW (2005) Optical sectioning microscopy. Nat Methods 2:2920–2931

Corrales RCNR, Mendes FMT, Perrone CC, Sant'Anna C, Souza W, Abud Y, Bon EPS, Ferreira V (2012) Structural evaluation of sugar cane bagasse steam pretreated in the presence of CO2 and SO2. Biotechnol Biofuels 5:1–8

Crawford NC, Nagle N, Sievers DA, Stickel JJ (2016) The effects of physical and chemical preprocessing on the flowability of corn stover. Biomass Bioenerg 85:126–134

Davidson RS, Choudhury H, Origgi S, Castellan A, Trichet V, Capretti G (1995) The reaction of phloroglucinol in the presence of acid with lignin-containing materials. J Photochem Photobiol A Chem 91:87–93

Dhiman SS, Haw JR, Kalyani D, Kalia VC, Kang YC, Lee JK (2015) Simultaneous pretreatment and saccharification: green technology for enhanced sugar yields from biomass using a fungal consortium. Bioresour Technol 179:50–57

Ding SY, Himmel ME (2006) The maize primary cell wall microfibril: a new model derived from direct visualization. J Agric Food Chem 54:597–606

Donohoe BS, Vinzant TB, Elander RT, Pallapolu VR, Lee YY, Garlock RJ, Balan V, Dale BE, Kim Y, Mosier NS, Ladisch MR, Falls M, Holtzapple MT, Sierra R, Shi J, Ebrik MA, Redmond T, Yang B, Wyman CE, Hames B, Thomas S, Warner RE (2011) Surface and ultrastructural characterization of raw and pretreated switchgrass. Bioresour Technol 102:11097–11104

Dornez E, Holopainen U, Cuyvers S, Poutanen K, Delcour JA, Courtin CM, Nordlund E (2011) Study of grain cell wall structures by microscopic analysis with four different staining techniques. J Cereal Sci 54:363–373

Ghaffar SH, Fan M (2015) Revealing the morphology and chemical distribution of nodes in wheat straw. Biomass Bioenerg 77:123–134

Gierlinger N (2010) Raman imaging of plant cell walls. In: Thomas D, Olaf H, Jan T (eds) Confocal Raman microscopy. Series in optical sciences no. 158. Springer, Berlin, pp 225–235

Gunning PA (2013) Light microscopy: principles and applications to food microstructures. Woodhead Publishing Limited, Sawston

Haigler CH, Brown RM Jr, Benziman M (1980) Calcofluor white ST Alters the in vivo assembly of cellulose microfibrils. Science 210:903–906

Haque MA, Barman DN, Kang TH, Kim MK, Kim J, Kim H, Yun HD (2013) Effect of dilute alkali pretreatment on structural features and enhanced enzymatic hydrolysis of *Miscanthus sinensis* at boiling temperature with low residence time. Biosyst Eng 114:294–305

Hell J, Donaldson L, Michlmayr H, Kraler M, Kneifel W, Potthast A, Rosenau T, Böhmdorfer S (2015) Effect of pretreatment on arabinoxylan distribution in wheat bran. Carbohydr Polym 121:18–26

Holopainen-Mantila U, Marjamaa K, Merali Z, Käsper A, de Bot P, Jääskeläinen A-S, Waldron K, Kruus K, Tamminen T (2013) Impact of hydrothermal pre-treatment to chemical composition, enzymatic digestibility and spatial distribution of cell wall polymers. Bioresour Technol 138:156–162

Igarashi K, Uchihashi T, Koivula A, Wada M, Kimura S, Okamoto T, Penttilä M, Ando T, Samejima M (2011) Traffic jams reduce hydrolytic efficiency of cellulase on cellulose surface. Science 333:1279–1282

Jean-Marie E (2016) Microscopy: light microscopy and histochemical methods. Encyclopedia of food and health. Elsevier, Amsterdam

Ji Z, Ding DY, Ling Z, Zhang X, Zhou X, Xu F (2014) In situ microscopic investigation of plant cell walls deconstruction in biorefinery. In: Méndez-Vilas A (ed) Microscopy: advances in scientific research and education. Formatex, Badajoz, pp 426–433

Johnson D, Hilal N, Bowen WR (2009) Basic principles of atomic force microscopy. In: Bowen WR, Hilal N (eds) Atomic force microscopy in process engineering. Elsevier, Amsterdam, pp 1–30

Karp EM, Resch MG, Donohoe BS, Ciesielski PN, O'Brien MH, Nill JE, Mittal A, Biddy MJ, Beckham GT (2015) Alkaline pretreatment of switchgrass. ACS Sustain Chem Eng 3:1479–1491

Keegstra K (2010) Plant cell walls. Plant Physiol 154:483–486

Kim SJ, Hyeon JE, Jeon SD, Choi GW, Han SO (2014) Bi-functional cellulases complexes displayed on the cell surface of *Corynebacterium glutamicum* increase hydrolysis of lignocelluloses at elevated temperature. Enzyme Microb Technol 66:67–73

Kirby AR, Gunning AP, Waldron KW, Morris VJ, Ng A (1996) Visualization of plant cell walls by atomic force microscopy. Biophys J 70:1138–1143

Lara-Vázquez AR, Quiroz FR, Sánchez A, Valdez-Vazquez I (2014) Particle size and hydration medium effects on hydration properties and sugar release of wheat straw fibers. Biomass Bioenerg 68:67–74

Li W, Yan L, Yang J (2006) AFM study of crystalline cellulose in the cell walls of straw. Polym Int 55:87–92

Li C, Knierim B, Manisseri C, Arora R, Scheller HV, Auer M, Vogel KP, Simmons BA, Singh S (2010) Comparison of dilute acid and ionic liquid pretreatment of switchgrass: biomass recalcitrance, delignification and enzymatic saccharification. Bioresour Technol 101:4900–4906

Lou B, Peng B, Rong N, Li Y, Chen H, Sree KS, Gao Q, Varma A (2014) Root and root endophytes from the eyes of an electron microscopist. In: Asunción M, Ajit V (eds) Root Engineering, soil biology, vol 40. Springer, New York. NY, pp 469–486

Luterbacher JS, Walker LP, Moran-Mirabal JM (2013) Observing and modeling BMCC degradation by commercial cellulase cocktails with fluorescently labeled *Trichoderma reseii* Cel7A through confocal microscopy. Biotechnol Bioeng 110:108–117

Ma J, Zhou X, Ma J, Ji Z, Zhang X, Xu F (2014) Raman microspectroscopy imaging study on topochemical correlation between lignin and hydroxycinnamic acids in *Miscanthus sinensis*. Microsc Microanal 20:956–963

Marton L (1934) Electron microscopy of biological objects. Nature 133:911

McCartney L, Marcus SE, Knox JP (2005) Monoclonal antibodies to plant cell wall xylans and arabinoxylans. J Histochem Cytochem 53:543–546

Morris VJ, Gunning AP, Kirby AR, Round A, Waldron K, Ng A (1997) Atomic force microscopy of plant cell walls, plant cell wall polysaccharides and gels. Int J Biol Macromol 21:61–66

Nanotechnology Now, 2011. Press release: Hitachi launches world's highest resolution FE-SEM http://www.nanotech-now.com/news.cgi?story_id=42612. Accessed 20 Jan 2016

Nwaneshiudu A, Kuschal C, Sakamoto FH, Anderson RR, Schwarzenberger K, Young RC (2012) Introduction to confocal microscopy. J Invest Dermatol 132, e3

O'Brien TP, Feder N, McCully ME (1964) Polychromatic staining of plant cell walls by toluidine blue O. Protoplasma 59:368–373

Pérez-Rangel M, Quiroz-Figueroa FR, González-Castañeda J, Valdez-Vazquez I (2015) Microscopic analysis of wheat straw cell wall degradation by microbial consortia for hydrogen production. Int J Hydrogen Energ 1:151–160

Reddy N, Yang Y (2005) Structure and properties of high quality natural cellulose fibers from cornstalks. Polymer 46:5494–5500

Rose HH (2009) Historical aspects of aberration correction. J Electron Microsc 58:77–85

Ruska E (1987) The development of the electron microscope and of electron microscopy. Biosci Rep 7:607–629

Sant´Anna C, de Souza W (2012) Microscopy as a tool to follow deconstruction of lignocellulosic biomass. In: Méndez-Vilas A (ed) Current microscopy contributions to advances in science and technology. Formatex, Badajoz, pp 639–645

Sarkar P, Bosneaga E, Auer M (2009) Plant cell walls throughout evolution: towards a molecular understanding of their design principles. J Exp Bot 60:3615–3635

Schuldt A (2009) Seeing the wood for the trees. Nat Cell Biol 11:S12–S13

Singh S, Simmons BA, Vogel KP (2009) Visualization of biomass solubilization and cellulose regeneration during ionic liquid pretreatment of switchgrass. Biotechnol Bioeng 104:68–75

Smith CL (2011) Basic confocal microscopy. Curr Protoc Neurosci 56:2.2.1–2.2.18

Somleva MN, Snell KD, Beaulieu JJ, Peoples OP, Garrison BR, Patterson NA (2008) Production of polyhydroxybutyrate in switchgrass, a value-added co-product in an important lignocellulosic biomass crop. Plant Biotechnol J 6:663–678

Sun L, Li C, Xue Z, Simmons BA, Singh S (2013) Unveiling high-resolution, tissue specific dynamic changes in corn stover during ionic liquid pretreatment. RSC Adv 3:2017–2027

Tan HT, Lee KT, Mohamed AR (2011) Pretreatment of lignocellulosic palm biomass using a solvent-ionic liquid [BMIM] Cl for glucose recovery: an optimisation study using response surface methodology. Carbohydr Polym 83:1862–1868

Travis AJ, Murison SD, Perry P, Chesson A (1997) Measurement of cell wall volume using confocal microscopy and its application to studies of forage degradation. Ann Bot 80:1–11

Ushiki T, Kawabata K (2008) Scanning probe microscopy in biological research. In: Bharat B, Harald F, Masahiko T (eds) Applied scanning probe methods X. Springer, Berlin, pp 285–308

Wang C, Yadavalli VK (2014) Investigating biomolecular recognition at the cell surface using atomic force microscopy. Micron 60:5–17

Wang J, Quirk A, Lipkowski J, Dutcher JR, Clarke AJ (2013) Direct in situ observation of synergism between cellulolytic enzymes during the biodegradation of crystalline cellulose fibers. Langmuir 29:14997–15005

Wei H, Donohoe BS, Vinzant TB, Ciesielski PN, Wang E, Gedvilas LM, Zeng Y, Johnson DK, Ding SY, Himmel ME, Tucker MP (2011) Elucidating the role of ferrous ion cocatalyst inenhancing dilute acid pretreatment of lignocellulosic biomass. Biotechnol Biofuels 4:48

Williams DB, Carter CB (2009) The transmission electron microscope. Transmission electron microscopy. Springer, New York, NY

Wilson SM, Bacic A (2012) Preparation of plant cells for transmission electron microscopy to optimize immunogold labeling of carbohydrate and protein epitopes. Nat Protoc 7:1716–1727
Winey M, Meehl JB, O'Toole ET, Giddings TH (2014) Conventional transmission electron microscopy. Mol Biol Cell 25:319–323
Zhou W, Apkarian R, Wang ZL, Joy D (2006) Fundamentals of scanning electron microscopy (SEM). In: Zhou W, Wang ZL (eds) Scanning microscopy for nanotechnology. Springer, New York, NY

Chapter 8
Analytical Strategies Using Chromatographic Methodologies to Analyze Lignocellulosic Feedstocks and their Value-Added Compounds in Biorefinery Processes

Augusto Lopes Souto, Vanda Maria de Oliveira, Viviane Cândida da Silva, Mauro Vicentini Correia, Wesley Pereira da Silva, Magno Aparecido Gonçalves Trindade, and Clenilson Martins Rodrigues

Abstract Strategies for adding value to renewable production chains is a fairly frequent and important worldwide research theme. The mitigation of environmental impacts caused by the use of petroleum derivatives needs to be quickly established and to ensure the achievement of these renewable products the use of analytical platforms that can conduct experiments and processes to obtain these target compounds in a green manner is imperative. This chapter highlights the use of analytical tools, especially those related to chromatographic techniques—conventional and modern—that can be used in the characterization of lignocellulosic biomass and products obtained from biorefinery processes. The information presented is given in function of individual separation and detection techniques, but the most appropriate is to consider, when applicable, the use of different detectors in series. In many cases, the information generated is complementary and the correlation of analytical data is very important to conduct a more robust and accurate characterization study.

Keywords Lignocellulosic feedstock • Biomass • UHPLC • Biorefinery • High value-added compounds

A.L. Souto • V.C. da Silva • M.V. Correia • C.M. Rodrigues (✉)
EMBRAPA, Embrapa Agroenergy, Parque Estação Biológica s/n,
Av. w3 Norte (final), CEP 70770-901 Brasília, DF, Brazil
e-mail: clenilson.rodrigues@embrapa.br

V.M. de Oliveira
EMBRAPA, Embrapa Agroenergy, Parque Estação Biológica s/n,
Av. w3 Norte (final), CEP 70770-901 Brasília, DF, Brazil

UCB, Catholic University of Brasília,
Campus I, EPCT – Águas Claras, CEP 71966-700 Brasília, DF, Brazil

W.P. da Silva • M.A.G. Trindade
UFGD, Faculty of Science and Technology, Federal University of Grande Dourados,
Rodovia Dourados – Itahum, km 12, CEP 79804-970 Dourados, MS, Brazil

S. Vaz Jr. (ed.), *Analytical Techniques and Methods for Biomass*,
DOI 10.1007/978-3-319-41414-0_8

8.1 Introduction

A great fraction of worldwide fuels and chemical products come from nonrenewable sources, such as oil, the exploitation of which is predicted to decrease in the future, due to several factors such as the ongoing price increase of fossil resources, their uncertain availability, and mostly their environmental impact towards our planet. Clearly, there is strong scientific evidence that the emissions of greenhouse gases (GHG), arising from fossil fuel combustion, are affecting the Earth's environment. Therefore, in order to reduce our strong dependence on petroleum derivatives and attenuate climate change, alternative production chains of fuels and chemicals are necessary (Kamm and Kamm 2004).

The idea of a sustainable economy based on renewable sources, which will replace several petrochemicals from the energy and nonenergy sector (e.g., chemicals and materials), is becoming a reality. Governments throughout the world have begun to sponsor research and development activities for its implementation, aiming for the opportunities offered by this new and promising field (Cherubini 2010). The United States expects by 2020 to provide at least 25 % (compared with 1994 production) of organic chemicals and 10 % of liquid fuels produced from a biobased product industry (NRC 2000).

Unlike the energy economy, which may be based on several types of alternative raw materials, such as wind, water, sun, nuclear fission and fusion, the chemical economy depends mainly on only one raw material, biomass, particularly, plant biomass (NRC 2000).

Although it is clear that there are several alternatives of biomass to biofuel production via chemical or enzymatic transformation, there are many challenges regarding technological resources and research required to overcome the disadvantage that has been associated with the biofuel quality and/or the raw materials for its production. For this information, it is very hard to show the vast scientific literature to cover all features regarding the resources used to overcome these challenges. In this sense, the present chapter attempts to cover some of the more important overviews of a variety of the current state of the art on the use of lignocellulosic feedstocks and their value-added compounds in biorefinery processes. In this way, efforts have been made to cover some aspects of the diverse analytical methods based on chromatographic strategies that have been used to elucidate the composition and structural characterization of biomass feedstocks during conversion of lignocellulosic biomass to essential value-added compounds and other components.

8.1.1 Biomass as Alternative to Be Explored

The term biomass means any organic matter that is available on a renewable or recurring basis, including trees, agricultural food and feed crop residues, algae and seaweeds, wood residues, animal wastes, and other waste materials (Donate 2014). Among the variety of sustainable and economic sources that can be used as renewable

energy, the use of biomass focused on transportation biofuels has the highest domination of the recent market, in which the target biomass feedstock has the feasibility adequately to reply to the energy requirements of modern society (Lupoi et al. 2015; Santos et al. 2011; Sluiter et al. 2010). In such a scenario, bioethanol from sugarcane and corn as well as biodiesel, with a variety of sources such as rapeseed, oil palm, sunflower, peanut, soybean, and cotton and raw materials of animal origin such as beef tallow and pork fat, dominate the current transportation biofuels market.

Concurrently with the efforts to increase the production of biofuel, there is great concern about the second-generation biofuels produced from nonfood feedstocks, having alternative sources such as municipal waste, perennial grasses, wood chips, and algae. Additionally, regarding the renewable-produced biofuel from nonfood feedstocks cellulosic ethanol and biodiesel from beef tallow can be satisfactorily used as renewable transportation energy in substitution for fossil fuels.

8.1.2 Lignocellulosic Biomass

The vegetable feedstock known as lignocellulosic biomass is very complex, composed mainly of carbohydrates, such as cellulose, hemicellulose, starch, and sucrose (75 %), lignin (20 %), fats, proteins, and other substances (5 %) (Kamm and Kamm 2004). Currently, it is already globally acknowledged that this plant-based raw material serves as potential feedstock for the production of fuels and value-added compounds. This is achieved by a multistep process called biorefinery, in which firstly, the lignocellulosic feedstock (LCF) is submitted to a pretreatment in order to separate its major components, increase the surface area of each component, and make them suitable for further processing.

These pretreatments may be physical, chemical, physicochemical, or biological. Once the major components are separated, they are subjected to biological and/or chemical processes, in which they are converted into fuels and chemicals that may act as main products or as building blocks in the chemical industry (FitzPatrick et al. 2010; Fig. 8.1). Additionally, these follow-up products could furthermore enter a conventional refinery (Kamm and Kamm 2004). This concept of biorefinery is analogous to today's petroleum refinery, which produces multiple fuels and products from petroleum (Kamm et al. 2008).

In theory, all chemicals obtained from an oil refinery can be also derived from biomass (Menon and Rao 2012; van Haveren et al. 2008), however, mostly with lower yields and higher costs. The development and application of lignocellulosic biomass fractionation technologies that are technically and economically viable on a large scale are still incipient; therefore, fundamental and applied research in catalysis, polymer chemistry, biotechnology, bioengineering, and agriculture will be strongly needed in this area (Menon and Rao 2012).

Regarding the energy and fuel sector, the relatively low energy content of biomass feedstocks, along with seasonality and discrete geographic availability, has been noted as major drawbacks for large-scale production and complete

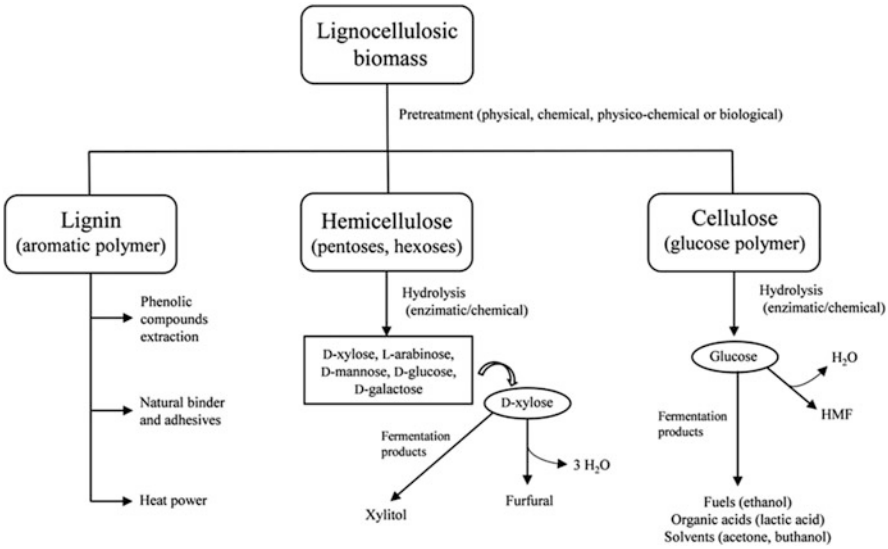

Fig. 8.1 Some renewable products obtained in biorefinery processes

replacement of fossil fuels, once fuels are low-value products and demand high volumes. In contrast, the production of chemicals requires far lower volumes of biomass to satisfy demand and its products are high value-added, which provides a greater incentive towards biobased chemical production (FitzPatrick et al. 2010; Bozell and Petersen 2009).

On the other hand, large-scale biobased chemical production from biorefineries is challenged by an overabundance of targets, which demand integrated processes of identification and isolation of not only commonly known petrochemicals, but also new structures from the biorefinery, which could basically be divided into two approaches. On the first, the value-added compounds would be identified and isolated in different processing and bioconversion steps; in the second approach, the remaining biomass would be transformed into a universal substrate and chemical products could be synthesized from it (Menon and Rao 2012; Bozell and Petersen 2009).

In fact, the carbohydrate fraction from the LCF (e.g., cellulose and hemicellulose) is expected to play a key role as a renewable carbon source for biobased products (Cherubini 2010). Once the carbohydrates are accessible by microbial or chemical processes, they may lead to a whole variety of products (Kamm and Kamm 2004).

Among these products, one may highlight the organic acids and polyols, which have a significant importance in many areas (Cherubini 2010). For instance, xylitol is used as a sweetener in place of sucrose and has odontological applications in teeth hardening and remineralization. Additionally, it is used in chewing gum and toothpaste formulations (Kumar et al. 2008). Moreover, lactic acid is utilized

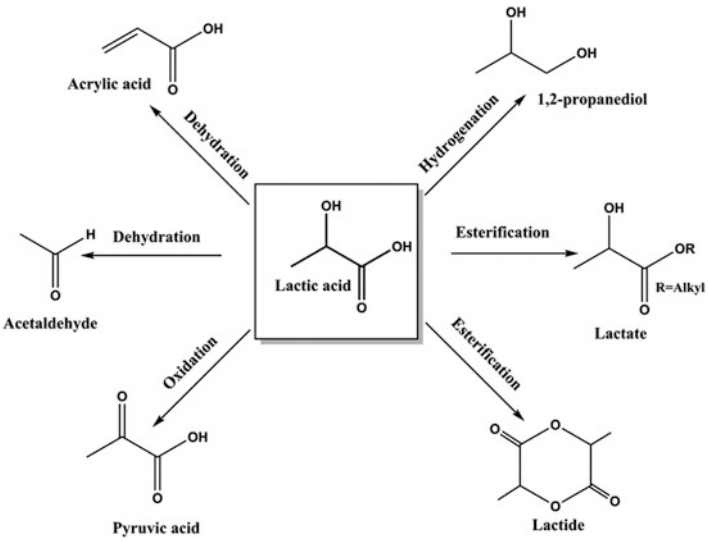

Fig. 8.2 Value-added chemicals produced from lactic acid

as a monomer to manufacture biodegradable polymers such as polylactic acids (PLA), which can be a fine replacement for conventional nonbiodegradable plastic materials such as polyethylene terephthalates (PET) (FitzPatrick et al. 2010; Corma et al. 2007). This acid may be obtained by chemical synthesis or by hexose and pentose from LCF after fermentation processes (Kumar et al. 2008; Corma et al. 2007). However, it is commercially produced today mainly by glucose fermentation due to its financial viability (Corma et al. 2007).

Many other chemical compounds are produced from lactic acid (Fig. 8.2) by several different chemical routes, such as lactide (esterification), 1,2-propanediol (hydrogenation), pyruvic acid (oxidation), and acrylic acid and acetaldehyde (dehydration) (Corma et al. 2007). The same may be applied to glucose derivatives, such as gluconic acid (oxidation), sorbitol (hydrogenation), and furans (hydrolysis) such as 5-hydroxymethylfurfural (HMF) (Wettstein et al. 2012).

Value-added chemicals, produced either by chemical or biological routes, have different structures, polarities, and physicochemical characteristics, which may lead to another challenge, on establishing an analytical method capable of identifying all these biobased products (Luo et al. 2002). Considering the potential of the substances identified by Werpy and Petersen (2004), this chapter highlights the main chromatographic techniques that can be applied to perform the monitoring of structural sugars that are available in steps of pretreatment, fermentation inhibitors produced in these processes (phenolic and furan compounds), as well as the value-added products or building blocks (polyols and organic acids) that are obtained by synthetic or biotechnological routes.

8.2 Chromatographic Techniques Used During Pretreatment of Lignocellulosic Biomass

8.2.1 Classical Chromatographic Techniques Used for Biomass Characterization

Methodologies for analysis and separation of pretreated lignocellulosic biomass have undergone rapid advances in recent years. The first chromatographic methodologies applied to analyze pretreated lignocellulosic material were paper and thin layer chromatography in a sugar analysis context (Sluiter et al. 2010; Sun and Sun 2015). These early methods were replaced by gas chromatography (GC) and by high performance liquid chromatography (HPLC) coupled to different detectors (Sun and Sun 2015).

8.2.2 Gas Chromatography (GC) Analysis

8.2.2.1 Gas Chromatography Using Mass Spectrometry Detection (GC-MS)

Among the various GC hyphenated techniques, GC coupled to mass spectrometry (MS) is the most important analytical tool that allows the separation and identification of components in a mixture, including one- or two-dimensional approaches for separation of complex samples (Marsman et al. 2008; Hope et al. 2005; Eiceman et al. 1994). The main advantage of these techniques is the peak capacity and high peak resolution when compared to other separation techniques. Another substantial benefit, when the modality of fast-GC is applied, is the reduction of time analysis, a very important parameter when the number of samples is considerable in routine studies (Snyder et al. 2010).

In GC-MS many compounds from pretreated lignocellulosic biomass can be analyzed, such as sugars, organic acid, and phenolic compounds (Luo et al. 2002; Cerdan-Calero et al. 2012; Raj et al. 2007). However, although having great resolution and capabilities of detection, GC-MS has a major drawback: any polar compound needs to pass by derivatization steps and become volatile and thermally stable before the GC analysis (e.g., sugar analysis). This derivatization step is time-consuming and to analyze different classes of compounds it could be necessary to have specific derivatization procedures, and more than one analysis of the same sample could be required. The most common derivatization method to analyze sugars by GC is silylation, which generally consists of the use of hexamethyldisilazane (HMDS) and trimethylchlorosilane (TMCS) as the agents of derivatization to formation of silyl ethers, that are stable and volatile (Ruiz-Matute et al. 2011).

8.2.3 HPLC Analysis

Another contemporaneous chromatographic technique used to analyze pretreated lignocellulosic biomass is HPLC and the literature shows that diverse columns can be used for this purpose. Additionally, simple or complex mobile phases associated with different detectors become necessary strategies for the analysis of biomass and its components. Despite HPLC resolution being considerable lower than that of CG, the absence of a derivatization step to analyze nonvolatile compounds makes HPLC a suitable technique to analyze LCF products (Snyder et al. 2010), mainly because of the presence of high polar compounds in this kind of raw material.

8.2.3.1 Chromatographic Analysis Using Refractive Index Detection (HPLC-RID)

Research involving biomass characterization usually employs the HPLC method developed by the National Renewable Energy Laboratory (NREL; NREL 2008); this procedure is capable of analyzing sugars (glucose, xylose, arabinose, galactose, and mannose), inhibitory compounds (acetic acid, furfural, and HMF), and components of interest (xylitol, glycerol, lactic acid, succinic acid, and ethanol) in liquid fractions of LCF after its hydrolysis or as an option of quality control during fermentation processes.

The NREL's method has the advantage of involving simple sample preparation (no derivatization steps) and the target components are separated by an ion exchange mechanism with the commercial columns such as Biorad Aminex HPX-87H or Agilent Hi-Plex H. The chromatographic analysis uses a simple isocratic separation with acidified water (H_2SO_4, 5 mmol L^{-1}) as the mobile phase and refractive index as detector (RID). However, each analysis takes more than 50 min per sample, and when a study involves steps of microbial bank prospecting, process optimization, and the consequent evaluation of several hundred samples, this HPLC-RID is not the best choice because it is not applicable for high-throughput analysis (Luo et al. 2002; NREL 2008; Ball et al. 2011; Castellari et al. 2001). Additionally, RID imposes some limitations including temperature sensitivity and incompatibility when used in combination with approaches that employ elution gradients, making the HPLC-RID a limited alternative for total biomass characterization (Meyer 2010).

To overcome the RID limitations, other chromatographic applications using different detectors are frequently found in the literature; among them, the most common involve the use of HPLC coupled with a photodiode array detector (PDA), evaporative light-scattering detector (ELSD), pulsed amperometric detector (PAD), and mass spectrometry detector (MS). These techniques are briefly discussed below.

8.2.3.2 Chromatographic Analysis Using Photodiode Array Detection (HPLC-PDA)

PDA detectors are frequently used to measure compounds that have chromophoric groups in their structures. This property will generate absorption spectra in the ultraviolet–visible region (UV/VIS). The advantage of the PDA detector, mainly over RID and ELSD, is during method development to determine peak identity and purity/homogeneity, because this detector provides spectra of eluting peaks that can be used to aid in peak identification, and to monitor coelutions (Swartz and Krull 2012).

Examples of PDA detector usage to analyze LCF compounds can be found in the work of Kafkas and coworkers (2006) and La Torre and coworkers (2006). The authors described the identification of organic acids and phenolic compounds (Table 4.1). However, the lack of chromophores in the structure of some LCF compounds, such as sugar, prevents the use of PDA. To overcome this limitation some researchers use derivatization to add chromophoric groups to the original compounds (Lv et al. 2009), but as mentioned with GC-MS, a derivatization step increases the analysis time and it is not a suitable strategy for biomass characterization.

8.2.3.3 Chromatographic Analysis Using Evaporative Light-Scattering Detection (HPLC-ELSD)

Another more feasible alternative applied to the analysis of nonchromophoric compounds involves the use of an ELS detector. As is RID, ELSD is a universal and nonspecific detector. The ELSD signal is independent of the intrinsic characteristics of the analyte and the detection includes three distinct stages: nebulization, evaporation, and optical detection (Webster et al. 2004; Héron et al. 2007).

All nonvolatile analytes after evaporation of the mobile phase are detected by measurement of scattered light (Webster et al. 2004). The detector is useful in the quantitative determination of nonchromophoric compounds and has the advantage of having a response independent of the solvent. Thus, it can be used with gradient elution, also, it is insensitive to flow rate and temperature fluctuation, and finally, its sensitivity is 10- to 100-fold better than RID (Snyder et al. 2010). Improvements in light-scattering detectors have led to their replacement of the RID for many applications (Valliyodan et al. 2015; Herbreteau et al. 1992).

Recently, there was an increase of methods using ELSD to analyze LCF compounds, mainly sugars. Some examples of the ELSD methods to analyze sugars and inhibitory compounds, such as HMF are presented by Valliyodan and coworkers (2015), Liu and coworkers (2012), and Ma and coworkers (2014; Table 4.1). A disadvantage of this detector is the low reproducibility and a slightly low sensitivity to low molecular weight compounds; attention should be given to the fact that nonvolatile salts cannot be used as buffer solution in the mobile phase (Snyder et al. 2010; Webster et al. 2004).

8.2.3.4 Chromatographic Analysis Using Electrochemical Detection (HPLC-ECD)

Liquid chromatographic (LC), especially HPLC techniques hyphenated with electrochemical detection (ECD), is considered very useful and can be recommended for trace quantitative analysis of reducible or oxidizable organic analytes (Kissinger 1986; Weber and Purdy 1981). If the compounds are electroactive, this detection system can probably be the first choice when low cost and low level of determination are required without using the conventional high-cost fluorescence and mass spectrometry detectors. Since Kissinger (1986), Weber and Purdy (1981), Rucki (1980), and Heineman and Kissinger (1980) reviewed the first steps of target hyphenation, there has been a significant increase in the number of electrode materials and device configurations for a variety of applications. These authors present a valuable source with notable assessments of the history and applications around ECD, discussing advantages and disadvantages of several quantitative trace analyses. Other specialized scientific texts regarding hyphenation liquid chromatographic with hydrodynamic electrochemistry were also published (Fedorowski and LaCourse 2015; Roussel et al. 2013; Gencoglu and Minerick 2014; Baldwin 1999; Pettersen 1984; Pettersen and Schwandt 1991; Davis 1998), and when appropriate, they are discussed and referenced in this section.

Lately, the combination has been advantageous due to the ECD devices—with a disposable ECD system containing multiple electrodes—which allow proper adaptation to miniaturize and use in several analytical applications with very low cost (Kissinger 1986; Fedorowski and LaCourse 2015). In addition to the reported selectivity, sensitivity, and lower detection limit (measured as low as pmol L^{-1}), the ECD has a great linear dynamic range, around six orders of magnitude. These characteristics tend to improve the applicability of separation techniques, having significant advantage over the classical spectroscopy detector (Kissinger 1986). The most common application potential modes on ECD that can be suitable for analytical application are amperometric detection (AD; Fig. 8.3a) and pulsed electrochemical detection (PAD; Fig. 8.3b), both of which are summarized in the following.

The AD (Fig. 8.3a) is the simplest form of ECD, where a constant potential is applied to the working electrode, on an electrochemical cell with a conventional three-electrode arrangement, and the current response is monitored as a function of time (Kissinger 1986; Weber and Purdy 1981; Roussel et al. 2013). Due to the fixed applied potential along the time, it can alter the working electrode surface properties by adsorption via electrogeneration products. The critical case is concerned with the noble metal electrodes that, although having an electrocatalytic surface able to directly detect organic aliphatic compounds in the absence of surface oxide (Fedorowski and LaCourse 2015), can adsorb polar organic analytes and tend to cause electrode surface fouling. As a consequence, the background signal becomes a problem, due to the difficulty of cleaning the electrode surface during simple AD, and the required electrode response cannot be accurately measured.

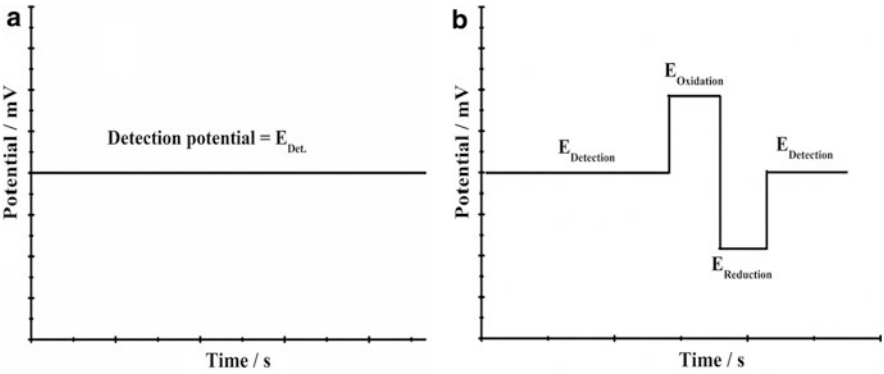

Fig. 8.3 General schematic of (**a**) amperometric detection (AD) and (**b**) pulsed electrochemical detection (PAD)

The PAD (Fig. 8.3b) differs from conventional AD because the application of potential, particularly on the noble metal electrodes, is based on repeating of pulses with three different working potentials being applied in a cyclic mode (Kissinger 1986; Weber and Purdy 1981; Rucki 1980; Heineman and Kissinger 1980; Fedorowski and LaCourse 2015). The sequence of pulses (Fig. 8.3b) enables cleaning the electrode surface with considerable intensification in the ratio of faradaic to capacitive current. Target approaches are useful when oxidizable or reducible species, containing polar groups, foul the electrode surface and require that electrogenerated products are removed from the electrode surface. According to Fedorowski and LaCourse (2015), PADs have high sensitive and selective detection modes because the several modified advanced versions allowed overcoming the electrode surface fouling, leading to an enhanced baseline drift as well as decreased background noise. The advancement in instrumentation with easily miniaturized electrochemical cells, on arrays such as microelectrodes and/or microchips, also allowed adaptability of online ECD waveforms and the application of pulsed potential has considerably amplified the number of analytical applications of HPLC-ECD (Fedorowski and LaCourse 2015; Gencoglu and Minerick 2014).

From ECD coupled with high-pressure separation systems, it is difficult, in this section, to convey all the necessary information and the challenges regarding new trends that show the advances in detection principles. Particular attention is paid to cover some examples that show the development of HPLC-ECD methods used to understand the lignocellulosic feedstock pretreatment as well as to predict chemical composition, especially quantitative analysis of their degradation products (Table 8.1).

The early application was based on anion-exchange chromatography coupled with PAD (HPAEC/PAD) and date from 1984, when Pettersen (1984) studied the chemical composition of wood. Seven years later, the researcher in collaboration with Schwandt used the HPAEC/PAD for wood sugar analysis (Pettersen and Schwandt 1991). The team focused on the overall chemical composition of lignocellulosic feedstocks—with data compiled from several countries—and methods of

Table 8.1 List of compounds of interest on LCF analysis: chromatographic methods, columns, and type of detectors recommended

Compounds	Separation	Column	Detector	Reference
(−)-Epicatechin	UHPLC	Acquity BEH C18	PDA and FL	Miranda-Hernandez et al. (2016)
(+)-Catechin	UHPLC	Acquity BEH C18	PDA and FL	Miranda-Hernandez et al. (2016)
2,3-Dihydroxypropanoic acid[a]	GC	5% Phenyl polymethylsiloxane capillary	MS (quadrupole)	Luo et al. (2002)
2,5-Dihydroxy-benzoic acid[a]	GC	5% Phenyl polymethylsiloxane capillary	MS (quadrupole)	Luo et al. (2002)
2,6-Dimethoxybenzoquinone (derivative)	UHPLC	XTerra MS C18	MS (triple quadrupole)	Stagge et al. (2015)
2-Butanedioic acid[a]	GC	5% Phenyl polymethylsiloxane capillary	MS (quadrupole)	Luo et al. (2002)
2-Deoxy-D-galactose (derivative)	UHPLC	Acquity BEH C18	MS (quadrupole)	Wang et al. (2012)
2-Deoxy-D-glucose (derivative)	UHPLC	Acquity BEH C18	MS (quadrupole)	Wang et al. (2012)
2-Furanacetic acid[a]	GC	5% Phenyl polymethylsiloxane capillary	MS (quadrupole)	Luo et al. (2002)
2-Furancarboxylic acid[a]	GC	5% Phenyl polymethylsiloxane capillary	MS (quadrupole)	Luo et al. (2002)
2-Furoic acid	HPLC	RezexTM ROA-OrganicAcid H +	MS (Q-TOF)	Ibanez and Bauer (2014)
2-Hydroxy-2-methylbutyric acid	HPLC	RezexTM ROA-OrganicAcid H +	MS (Q-TOF)	Ibanez and Bauer (2014)
2-Hydroxy-2-pentanedioic acid[a]	GC	5% Phenyl polymethylsiloxane capillary	MS (quadrupole)	Luo et al. (2002)
2-Hydroxypentanedioic acid[a]	GC	5% Phenyl polymethylsiloxane capillary	MS (quadrupole)	Luo et al. (2002)
2-methoxy-4-methylphenol	HPLC	Zorbax SB-C18/Zorbax SB-Phenyl	MS (LQIT-FT-ICR)	Owen et al. (2012)
2-Methoxy-4-propylphenol	HPLC	Zorbax SB-C18/Zorbax SB-Phenyl	MS (LQIT-FT-ICR)	Owen et al. (2012)

(continued)

Table 8.1 (continued)

Compounds	Separation	Column	Detector	Reference
2-Methoxy-α-hydroxy-benzenacetic acid[a]	GC	5% Phenyl polymethylsiloxane capillary	MS (quadrupole)	Luo et al. (2002)
2-Methyl-2-hydroxybutanoic acid[a]	GC	5% Phenyl polymethylsiloxane capillary	MS (quadrupole)	Luo et al. (2002)
3,4,5-Trimethoxy benzaldehyde (TMS)	GC	PE–5MS capillary	MS (quadrupole)	Raj et al. (2007)
3,4-Dihydroxy-benzoic acid[a]	GC	5% Phenyl polymethylsiloxane capillary	MS (quadrupole)	Luo et al. (2002)
3,5-Di-*O*-caffeoylquinic acid	UHPLC	Acquity BEH C18	PDA and FL	Miranda-Hernandez et al. (2016)
3-Acetoxy butyric acid (TMS)	GC	PE–5MS capillary	MS (quadrupole)	Raj et al. (2007)
3-Hydroxy-propanoic acid[a]	GC	5% Phenyl polymethylsiloxane capillary	MS (quadrupole)	Luo et al. (2002)
4-Hydroxybenzaldehyde	UHPLC	Acquity HSS T3	MS (QqLIT and QqTOF)	Frolov et al. (2013)
4-Hydroxybenzaldehyde	UHPLC	Hypersil Gold C18	MS (LTQ/Orbitrap)	Cavka et al. (2011)
4-Hydroxybenzoic acid	UHPLC	Acquity HSS T3	MS (QqLIT and QqTOF)	Frolov et al. (2013)
4-Hydroxybenzoic acid[a]	GC	5% Phenyl polymethylsiloxane capillary	MS (quadrupole)	Luo et al. (2002)
4-*O*-*p*-Coumaroylquinic acid	UHPLC	Acquity BEH C18	PDA and FL	Miranda-Hernandez et al. (2016)
4-Oxo-pentanoic acid[a]	GC	5% Phenyl polymethylsiloxane capillary	MS (quadrupole)	Luo et al. (2002)
5-Hydroxyferulic acid	UHPLC	Acquity HSS T3	MS (QqLIT and QqTOF)	Frolov et al. (2013)
5-Hydroxymethylfurancarboxylic acid[a]	GC	5% Phenyl polymethylsiloxane capillary	MS (quadrupole)	Luo et al. (2002)
5-Hydroxymethylfurfural	UHPLC	Hypersil Gold C18	MS (LTQ/Orbitrap)	Cavka et al. (2011)
5-Hydroxymethylfurfural	HPLC	Aminex HPX-87H	PDA	Liu et al. (2012)
5-Methoxy-2-hydroxy-benzoic acid[a]	GC	5% Phenyl polymethylsiloxane capillary	MS (quadrupole)	Luo et al. (2002)

6-Deoxy-D-glucose (derivative)	UHPLC	Acquity BEH C18	MS (quadrupole)	Wang et al. (2012)
9,12-Octadecadienoic acid[a]	GC	5% Phenyl polymethylsiloxane capillary	MS (quadrupole)	Luo et al. (2002)
Acetic acid	UHPLC	Hypersil Gold C18 (2 columns in series)	MS (triple quadrupole)	Ross et al. (2007)
Acetic acid (TMS)	GC	PE–5MS capillary	MS (quadrupole)	Raj et al. (2007)
Acetic acid[a]	GC	5% Phenyl polymethylsiloxane capillary	MS (quadrupole)	Luo et al. (2002)
Acetoguiacone (TMS)	GC	PE–5MS capillary	MS (quadrupole)	Raj et al. (2007)
Adipic acid	HPLC	RezexTM ROA-Organic Acid H +	MS (Q-TOF)	Ibanez and Bauer (2014)
Arabinose	HPAEC	Dionex HPIC-AS-6	PAD	Pettersen and Schwandt (1991) and Davis (1998)
Arabinose	HPLC	HILIC (amide-80)	PDA/MS (QTOF)	Bowman et al. (2011)
Arabinose	HPLC	Aminex HPX-87H	ELSD	Liu et al. (2012)
Arabinose (TMS)	GC	HP-5MS (5% phenyl/95% methylpolysiloxane) capillary	MS (ion trap)	Cerdan-Calero et al. (2012)
Arabitol	HPAEC[b]	CarboPac MA1	PAD[c]	Dionex (2000)
Ascorbic acid	HPLC	Reverse-phase Ultrasphere ODS	PDA	Kafkas et al. (2006)
Benzene acetic acid (TMS)	GC	PE-5MS capillary	MS (quadrupole)	Raj et al. (2007)
Benzoic acid	UHPLC	Acquity HSS T3	MS (QqLIT and QqTOF)	Frolov et al. (2013)
Butanoic acid (TMS)	GC	PE-5MS capillary	MS (quadrupole)	Raj et al. (2007)
Caffeic acid	HPLC	Supelco Discovery C18 column	PDA/MS (quadrupole)	La Torre et al. (2006)
Caffeic acid	UHPLC	Acquity HSS T3	MS (QqLIT and QqTOF)	Frolov et al. (2013)
Cellobiose	HPAEC	CarboPac PA200	PAD	Xu et al. (2013)
Cellopentaose	HPAEC	CarboPac PA200	PAD	Xu et al. (2013)
Cellotetraose	HPAEC	CarboPac PA200	PAD	Xu et al. (2013)
Cellotriose	HPAEC	CarboPac PA200	PAD	Xu et al. (2013)
Cellotriose	HPAEC	CarboPac PA200	PAD	Xu et al. (2013)

(continued)

Table 8.1 (continued)

Compounds	Separation	Column	Detector	Reference
Chlorogenic acid	UHPLC	Acquity BEH C18	PDA and FL	Miranda-Hernandez et al. (2016)
Cinnamic acid	UHPLC	Hypersil Gold C18	MS (LTQ/Orbitrap)	Cavka et al. (2011)
cis-Aconitic acid	HPLC	RezexTM ROA-OrganicAcid H +	MS (Q-TOF)	Ibanez and Bauer (2014)
Citric acid	HPLC	Reverse-phase Ultrasphere ODS	PDA	Kafkas et al. (2006)
Citric acid	HPLC	RezexTM ROA-OrganicAcid H +	MS (Q-TOF)	Ibanez and Bauer (2014)
Citric acid	UHPLC	Hypersil Gold C18 (2 columns in series)	MS (triple quadrupole)	Ross et al. (2007)
Citric acid (TMS)	GC	HP-5MS (5 % phenyl/95 % methylpolysiloxane) capillary	MS (ion trap)	Cerdan-Calero et al. (2012)
Coniferyl alcohol	HPLC	Zorbax SB-C18/Zorbax SB-Phenyl	MS (LQIT-FT-ICR)	Owen et al. (2012)
Coniferyl alcohol	UHPLC	Acquity C18-BEH	MS (triple quadrupole)	Kiyota et al. (2012)
Coniferyl alcohol	UHPLC	Acquity HSS T3	MS (QqLIT and QqTOF)	Frolov et al. (2013)
Coniferyl aldehyde	UHPLC	Acquity C18-BEH	MS (triple quadrupole)	Kiyota et al. (2012)
Coniferyl aldehyde	UHPLC	Acquity HSS T3	MS (QqLIT and QqTOF)	Frolov et al. (2013)
Coniferyl aldehyde	UHPLC	Hypersil Gold C18	MS (LTQ/Orbitrap)	Cavka et al. (2011)
Cryptochlorogenic acid	UHPLC	Acquity BEH C18	PDA and FL	Miranda-Hernandez et al. (2016)
D(−)-Arabinose	HPAEC	CarboPac PA1	PAD	Basumallick and Rohrer (2012)
D(−)-fructose	HPAEC	CarboPac PA1	PAD	Basumallick and Rohrer (2012)
D(+)-cellobiose	HPAEC	CarboPac PA1	PAD	Basumallick and Rohrer (2012)
D(+)-cellobiose	HPLC	Aminex HPX-87H	ELSD	Liu et al. (2012)
D(+)-galactose	HPAEC	CarboPac PA1	PAD	Basumallick and Rohrer (2012)
D(+)-mannose	HPAEC	CarboPac PA1	PAD	Basumallick and Rohrer (2012)

D-Allose (derivative)	UHPLC	Acquity BEH C18	MS (quadrupole)	Wang et al. (2012)
D-Arabinose (derivative)	UHPLC	Acquity BEH C18	MS (quadrupole)	Wang et al. (2012)
D-Fructose-1,6-Di P	HPAEC	CarboPac PA1	PAD	Dionex (2000)
D-Fructose-6-P	HPAEC	CarboPac PA1	PAD	Dionex (2000)
D-Fructose-1-P	HPAEC	CarboPac PA1	PAD	Dionex (2000)
D-Fucose (derivative)	UHPLC	Acquity BEH C18	MS (quadrupole)	Wang et al. (2012)
D-Galactosamine-6-P	HPAEC	CarboPac PA1	PAD	Dionex (2000)
D-Galactose (derivative)	UHPLC	Acquity BEH C18	MS (quadrupole)	Wang et al. (2012)
D-Galactose-6-P	HPAEC	CarboPac PA1	PAD	Dionex (2000)
D-Galacturonic and D-glucuronic acids	HPAEC	CarboPac PA10	PAD	Beluomini et al. (2015)
D-Glucose (derivative)	UHPLC	Acquity BEH C18	MS (quadrupole)	Wang et al. (2012)
D-Glucose, monohydrate	HPAEC	DionexCarboPac PA1	PAD	Basumallick and Rohrer (2012)
D-Glucose, monohydrate	HPAEC	DionexCarboPac PA1	PAD	Basumallick and Rohrer (2012)
D-Glucose-6-P	HPAEC	CarboPac PA1	PAD	Dionex (2000)
Dulcitol	HPAEC	CarboPac MA1	PAD	Dionex (2000)
D-Xylose	HPAEC	CarboPac PA100	PAD	Li et al. (2013)
D-Xylose	HPAEC	Dionex CarboPac PA1	PAD	Basumallick and Rohrer (2012)
D-Xylose (derivative)	UHPLC	Acquity BEH C18	MS (quadrupole)	Wang et al. (2012)
Ethanedioic acid (TMS)	GC	PE–5MS capillary	MS (quadrupole)	Raj et al. (2007)
Ethanedioic acid[a]	GC	5 % Phenyl polymethylsiloxane capillary	MS (quadrupole)	Luo et al. (2002)
Ferulic acid	HPLC	Supelco Discovery C18 column	PDA/MS (quadrupole)	La Torre et al. (2006)
Ferulic acid	UHPLC	Acquity HSS T3	MS (QqLIT and QqTOF)	Frolov et al. (2013)
Ferulic acid	UHPLC	Hypersil Gold C18	MS (LTQ/Orbitrap)	Cavka et al. (2011)
Ferulic acid (TMS)	GC	PE–5MS capillary	MS (quadrupole)	Raj et al. (2007)

(continued)

Table 8.1 (continued)

Compounds	Separation	Column	Detector	Reference
Ferulic acid[a]	GC	5 % Phenyl polymethylsiloxane capillary	MS (quadrupole)	Luo et al. (2002)
Fructose	HPAEC	CarboPac MA1	PAD	Dionex (2000)
Fructose	HPLC	Heater from Chrom Tech	MS (triple quadrupole)	Matias et al. (2011)
Fructose	HPLC	Luna 5u NH2 column	ELSD	Ma et al. (2014)
Fructose	HPLC	Prevail Carbohydrate ES	ELSD	Valliyodan et al. (2015)
Fructose (TMS)	GC	HP-5MS (5 % phenyl/95 % methylpolysiloxane) capillary	MS (ion trap)	Cerdan-Calero et al. (2012)
Fucose	HPAEC	CarboPac PA1	PAD	Dionex (2000)
Fucose	HPAEC	CarboPac PA1	PAD	Basumallick and Rohrer (2012)
Fumaric acid	HPLC	RezexTM ROA-OrganicAcid H +	MS (Q-TOF)	Ibanez and Bauer (2014)
Fumaric acid	UHPLC	Hypersil Gold C18 (2 columns in series)	MS (triple quadrupole)	Ross et al. (2007)
Fumaric acid (TMS)	GC	HP-5MS (5 % phenyl/95 % methylpolysiloxane) capillary	MS (ion trap)	Cerdan-Calero et al. (2012)
Furan carboxylic acid (TMS)	GC	PE–5MS capillary	MS (quadrupole)	Raj et al. (2007)
Furfural	UHPLC	Hypersil Gold C18	MS (LTQ/Orbitrap)	Cavka et al. (2011)
Furfural	HPLC	Aminex HPX-87H	ELSD	Liu et al. (2012)
Galactosamine	HPAEC	CarboPac PA1	PAD	Dionex (2000)
Galactose	HPAEC	CarboPac MA1	PAD	Dionex (2000)
Galactose	HPAEC	CarboPac PA1	PAD	Dionex (2000)
Galactose	HPAEC	Dionex HPIC-AS-6	PAD	Pettersen and Schwandt (1991) and Davis (1998)
Galactose	HPLC	Prevail Carbohydrate ES	ELSD	Valliyodan et al. (2015)
Galacturonic acid	HPLC	RezexTM ROA-OrganicAcid H +	MS (Q-TOF)	Ibanez and Bauer (2014)
Galacturonic acid (TMS)	GC	HP-5MS (5 % phenyl/95 % methylpolysiloxane) capillary	MS (ion trap)	Cerdan-Calero et al. (2012)

Gallic acid	HPLC	Supelco Discovery C18 column	PDA/MS (quadrupole)	La Torre et al. (2006)
Gallic acid (TMS)	GC	PE–5MS capillary	MS (quadrupole)	Raj et al. (2007)
Gluconic acid	HPLC	RezexTM ROA-OrganicAcid H +	MS (Q-TOF)	Ibanez and Bauer (2014)
Glucosamine	HPAEC	CarboPac PA1	PAD	Dionex (2000)
Glucose	HPAEC	CarboPac MA1	PAD	Dionex (2000)
Glucose	HPAEC	CarboPac PA1	PAD	Dionex (2000)
Glucose	HPAEC	Dionex HPIC-AS-6	PAD	Pettersen and Schwandt (1991) and Davis (1998)
Glucose	HPLC	Acquity UPLC BEH amide	MS (TOF)	Westereng et al. (2013)
Glucose	HPLC	Heater from Chrom Tech	MS (triple quadrupole)	Matias et al. (2011)
Glucose	HPLC	Luna 5u NH2	ELSD	Ma et al. (2014)
Glucose	HPLC	Prevail Carbohydrate ES	ELSD	Valliyodan et al. (2015)
Glucose	HPLC	Aminex HPX-87H	ELSD	Liu et al. (2012)
Glucuronic acid	HPAEC	CarboPac PA1	PAD	Dionex (2000)
Glucuronic acid	HPLC	RezexTM ROA-OrganicAcid H +	MS (Q-TOF)	Ibanez and Bauer (2014)
Glutaric acid	HPLC	RezexTM ROA-OrganicAcid H +	MS (Q-TOF)	Ibanez and Bauer (2014)
Glycerol	HPAEC	CarboPac MA1	PAD	Dionex (2000)
Glycolic acid	HPLC	RezexTM ROA-OrganicAcid H +	MS (Q-TOF)	Ibanez and Bauer (2014)
Glyoxylic acid	HPLC	RezexTM ROA-OrganicAcid H +	MS (Q-TOF)	Ibanez and Bauer (2014)
Glyoxylic acid (TMS)	GC	PE–5MS capillary	MS (quadrupole)	Raj et al. (2007)
Guaiacol	HPLC	Zorbax SB-C18/Zorbax SB-Phenyl	MS (LQIT-FT-ICR)	Owen et al. (2012)
Guaiacol (TMS)	GC	PE–5MS capillary	MS (quadrupole)	Raj et al. (2007)
Guaiacylglycerol-ß-guaiacylether	HPLC	Zorbax SB-C18/Zorbax SB-Phenyl	MS (LQIT-FT-ICR)	Owen et al. (2012)
Guaiacylglycerol-ß-syringylether	HPLC	Zorbax SB-C18/Zorbax SB-Phenyl	MS (LQIT-FT-ICR)	Owen et al. (2012)
Hexadecanoic acid (TMS)	GC	PE–5MS capillary	MS (quadrupole)	Raj et al. (2007)
Hexanedioic acid[a]	GC	5 % Phenyl polymethylsiloxane capillary	MS (quadrupole)	Luo et al. (2002)

(continued)

Table 8.1 (continued)

Compounds	Separation	Column	Detector	Reference
Hexanoic acid (TMS)	GC	PE–5MS capillary	MS (quadrupole)	Raj et al. (2007)
Hydroxybutanedioic acid[a]	GC	5 % Phenyl polymethylsiloxane capillary	MS (quadrupole)	Luo et al. (2002)
Hydroxymethylfurfural	HPAEC	DionexCarboPac PA1	PAD	Basumallick and Rohrer (2011)
Inositol	HPAEC	CarboPac MA1	PAD	Dionex (2000)
Isoeugenol	HPLC	Zorbax SB-C18/Zorbax SB-Phenyl	MS (LQIT-FT-ICR)	Owen et al. (2012)
Isoferulic acid[a]	GC	5 % Phenyl polymethylsiloxane capillary	MS (quadrupole)	Luo et al. (2002)
Kaempferol glucoside acylated by *p*-coumaric acid	UHPLC	Acquity BEH C18	PDA and FL	Miranda-Hernandez et al. (2016)
Kaempferol-3-*O*-galactoside	UHPLC	Acquity BEH C18	PDA and FL	Miranda-Hernandez et al. (2016)
Kaempferol-3-*O*-glucoside	UHPLC	Acquity BEH C18	PDA and FL	Miranda-Hernandez et al. (2016)
Kaempferol-3-*O*-rutinoside	UHPLC	Acquity BEH C18	PDA and FL	Miranda-Hernandez et al. (2016)
Kestose	HPLC	Heater from Chrom Tech	MS (triple quadrupole)	Matias et al. (2011)
Lactic acid	HPLC	RezexTM ROA-OrganicAcid H +	MS (Q-TOF)	Ibanez and Bauer (2014)
Lactic acid	UHPLC	Hypersil Gold C18 (2 columns in series)	MS (triple quadrupole)	Ross et al. (2007)
L-Allose (derivative)	UHPLC	Acquity BEH C18	MS (quadrupole)	Wang et al. (2012)
L-Arabinose (derivative)	UHPLC	Acquity BEH C18	MS (quadrupole)	Wang et al. (2012)
Levulinic acid	HPLC	RezexTM ROA-OrganicAcid H +	MS (Q-TOF)	Ibanez and Bauer (2014)
L-Fucose (derivative)	UHPLC	Acquity BEH C18	MS (quadrupole)	Wang et al. (2012)
L-Glucose (derivative)	UHPLC	Acquity BEH C18	MS (quadrupole)	Wang et al. (2012)
L-Rhamnose (derivative)	UHPLC	Acquity BEH C18	MS (quadrupole)	Wang et al. (2012)

L-Xylose (derivative)	UHPLC	Acquity BEH C18	MS (quadrupole)	Wang et al. (2012)
L-Xylose(TMS)	GC	HP-5MS (5 % phenyl/95 % methylpolysiloxane) capillary	MS (ion trap)	Cerdan-Calero et al. (2012)
Malic acid	HPLC	Reverse-phase Ultrasphere ODS	PDA	Kafkas et al. (2006)
Malic acid	UHPLC	Hypersil Gold C18 (2 columns in series)	MS (triple quadrupole)	Ross et al. (2007)
Malic acid (TMS)	GC	HP-5MS (5 % phenyl/95 % methylpolysiloxane) capillary	MS (ion trap)	Cerdan-Calero et al. (2012)
Malonic acid	HPLC	RezexTM ROA-OrganicAcid H +	MS (Q-TOF)	Ibanez and Bauer (2014)
Malonic acid	UHPLC	Hypersil Gold C18 (2 columns in series)	MS (triple quadrupole)	Ross et al. (2007)
Maltose (TMS)	GC	HP-5MS (5 % phenyl/95 % methylpolysiloxane) capillary	MS (ion trap)	Cerdan-Calero et al. (2012)
Mannitol (TMS)	GC	HP-5MS (5 % phenyl/95 % methylpolysiloxane) capillary	MS (ion trap)	Cerdan-Calero et al. (2012)
Mannitol	HPAEC	CarboPac MA1	PAD	Dionex (2000)
Mannose	HPAEC	CarboPac PA1	PAD	Dionex (2000)
Mannose	HPAEC	Dionex HPIC-AS-6	PAD	Pettersen and Schwandt (1991) and Davis (1998)
Melibiose	HPLC	Prevail Carbohydrate ES	ELSD	Valliyodan et al. (2015)
Methyl butanedioic acid[a]	GC	5 % Phenyl polymethylsiloxane capillary	MS (quadrupole)	Luo et al. (2002)
Methyl propanedioic acid[a]	GC	5 % Phenyl polymethylsiloxane capillary	MS (quadrupole)	Luo et al. (2002)
Methylmalonic acid	HPLC	RezexTM ROA-OrganicAcid H +	MS (Q-TOF)	Ibanez and Bauer (2014)
Myo-inositol	HPLC	Lichrosphere 100 DIOL	ELSD/MS (quadrupole)	Pazourek (2014)
Myo-inositol (TMS)	GC	HP-5MS (5 % phenyl/95 % methylpolysiloxane) capillary	MS (ion trap)	Cerdan-Calero et al. (2012)
N-Acetylneuraminic acid	HPAEC	CarboPac PA1	PAD	Dionex (2000)

(continued)

Table 8.1 (continued)

Compounds	Separation	Column	Detector	Reference
Neochlorogenic acid	UHPLC	Acquity BEH C18	PDA and FL	Miranda-Hernandez et al. (2016)
N-Glycolylneuraminic acid	HPAEC	CarboPac PA1	PAD	Dionex (2000)
Octadecanoic acid (TMS)	GC	PE–5MS capillary	MS (quadrupole)	Raj et al. (2007)
Oleic acid[a]	GC	5 % Phenyl polymethylsiloxane capillary	MS (quadrupole)	Luo et al. (2002)
Oligosaccharides	HPAEC	CarboPac PA100	PAD	Dionex (2000)
Oligosaccharides	UHPLC	HILIC (BEH Amide)	ELSD-MS(ion trap)	Remoroza et al. (2012)
Palmitic acid[a]	GC	5 % Phenyl polymethylsiloxane capillary	MS (quadrupole)	Luo et al. (2002)
p-Coumaryl alcohol	UHPLC	Acquity C18-BEH	MS (triple quadrupole)	Kiyota et al. (2012)
phenyl propionyl (TMS)	GC	PE–5MS capillary	MS (quadrupole)	Raj et al. (2007)
Procyanidin B1	UHPLC	Acquity BEH C18	PDA and FL	Miranda-Hernandez et al. (2016)
Procyanidin B2	UHPLC	Acquity BEH C18	PDA and FL	Miranda-Hernandez et al. (2016)
Procyanidin C1	UHPLC	Acquity BEH C18	PDA and FL	Miranda-Hernandez et al. (2016)
Propanedioic acid (TMS)	GC	PE–5MS capillary	MS (quadrupole)	Raj et al. (2007)
Propanoic acid (TMS)	GC	PE–5MS capillary	MS (quadrupole)	Raj et al. (2007)
Propionic acid	UHPLC	Hypersil Gold C18 (2 columns in series)	MS (triple quadrupole)	Ross et al. (2007)
Protocatechuic acid	HPLC	Supelco Discovery C18 column	PDA/MS (quadrupole)	La Torre et al. (2006)
Protocatechuic acid	UHPLC	Acquity HSS T3	MS (QqLIT and QqTOF)	Frolov et al. (2013)
Pyruvic acid	HPLC	RezexTM ROA-OrganicAcid H +	MS (Q-TOF)	Ibanez and Bauer (2014)

Pyruvic acid	UHPLC	Hypersil Gold C18 (2 columns in series)	MS (triple quadrupole)	Ross et al. (2007)
Quercetin	UHPLC	Acquity BEH C18	PDA-Q-TOF	Escrig et al. (2013)
Quercetin glucoside acylated by *p*-coumaric acid	UHPLC	Acquity BEH C18	PDA and FL	Miranda-Hernandez et al. (2016)
Quercetin-3-(2″-*O*-acetyl) arabinofuranoside	UHPLC	Acquity BEH C18	PDA-Q-TOF	Escrig et al. (2013)
Quercetin-3-arabinoside	UHPLC	Acquity BEH C18	PDA-Q-TOF	Escrig et al. (2013)
Quercetin-3-*O*-galactoside	UHPLC	Acquity BEH C18	PDA and FL	Miranda-Hernandez et al. (2016)
Quercetin-3-*O*-glucoside	UHPLC	Acquity BEH C18	PDA and FL	Miranda-Hernandez et al. (2016)
Quercetin-3-*O*-rutinoside	UHPLC	Acquity BEH C18	PDA and FL	Miranda-Hernandez et al. (2016)
Quercetin-3-xyloside	UHPLC	Acquity BEH C18	PDA-Q-TOF	Escrig et al. (2013)
Quercetin-3-β-glucoside	UHPLC	Acquity BEH C18	PDA-Q-TOF	Escrig et al. (2013)
Quercitrin	UHPLC	Acquity BEH C18	PDA-Q-TOF	Escrig et al. (2013)
Quinic acid (TMS)	GC	HP-5MS (5 % phenyl/95 % methylpolysiloxane) capillary	MS (ion trap)	Cerdan-Calero et al. (2012)
Raffinose	HPLC	Prevail carbohydrate ES	ELSD	Valliyodan et al. (2015)
Raffinose (TMS)	GC	HP-5MS (5 % phenyl/95 % methylpolysiloxane) capillary	MS (ion trap)	Cerdan-Calero et al. (2012)
Rhamnose	HPAEC	Dionex HPIC-AS-6	PAD	Davis (1998)
Rhamnose (TMS)	GC	HP-5MS (5 % phenyl/95 % methylpolysiloxane) capillary	MS (ion trap)	Cerdan-Calero et al. (2012)
Ribose (TMS)	GC	HP-5MS (5 % phenyl/95 % methylpolysiloxane) capillary	MS (ion trap)	Cerdan-Calero et al. (2012)
Salicylic acid	UHPLC	Acquity HSS T3	MS (QqLIT and QqTOF)	Frolov et al. (2013)

(continued)

Table 8.1 (continued)

Compounds	Separation	Column	Detector	Reference
Scyllo-inositol (TMS)	GC	HP-5MS (5 % phenyl/95 % methylpolysiloxane) capillary	MS (ion trap)	Cerdan-Calero et al. (2012)
Sinapaldehyde	UHPLC	Acquity HSS T3	MS (QqLIT and QqTOF)	Frolov et al. (2013)
Sinapic acid	UHPLC	Acquity HSS T3	MS (QqLIT and QqTOF)	Frolov et al. (2013)
Sinapyl alcohol	HPLC	Zorbax SB-C18/Zorbax SB-Phenyl	MS (LQIT-FT-ICR)	Owen et al. (2012)
Sinapyl alcohol	UHPLC	Acquity C18-BEH	MS (triple quadrupole)	Kiyota et al. (2012)
Sinapyl alcohol	UHPLC	Acquity HSS T3	MS (QqLIT and QqTOF)	Frolov et al. (2013)
Sinapyl aldehyde	UHPLC	Acquity C18-BEH	MS (triple quadrupole)	Kiyota et al. (2012)
Sorbitol	HPAEC	CarboPac MA1	PAD	Dionex (2000)
Sorbitol	HPLC	Luna 5u NH2	ELSD	Ma et al. (2014)
Sorbitol (TMS)	GC	HP-5MS (5% phenyl/95 % methylpolysiloxane) capillary	MS (ion trap)	Cerdan-Calero et al. (2012)
Stachyose	HPLC	Prevail Carbohydrate ES	ELSD	Valliyodan et al. (2015)
Stearic acid[a]	GC	5 % Phenyl polymethylsiloxane capillary	MS (quadrupole)	Luo et al. (2002)
Succinic acid	HPLC	RezexTM ROA-OrganicAcid H +	MS (Q-TOF)	Ibanez and Bauer (2014)
Succinic acid	UHPLC	Hypersil Gold C18 (2 columns in series)	MS (triple quadrupole)	Ross et al. (2007)
Succinic acid (TMS)	GC	HP-5MS (5 % phenyl/95 % methylpolysiloxane) capillary	MS (ion trap)	Cerdan-Calero et al. (2012)
Sucrose	HPAEC	CarboPac MA1	PAD	Dionex (2000)
Sucrose	HPAEC	DionexCarboPac PA1	PAD	Basumallick and Rohrer (2012)
Sucrose	HPLC	Heater from Chrom Tech	MS (triple quadrupole)	Matias et al. (2011)
Sucrose	HPLC	Luna 5u NH2	ELSD	Ma et al. (2014)
Sucrose	HPLC	Prevail Carbohydrate ES	ELSD	Valliyodan et al. (2015)

Sucrose (TMS)	GC	HP-5MS (5 % phenyl/95 % methylpolysiloxane) capillary	MS (ion trap)	Cerdan-Calero et al. (2012)
Syringaldehyde	UHPLC	Acquity HSS T3	MS (QqLIT and QqTOF)	Frolov et al. (2013)
Syringaldehyde[a]	GC	5 % Phenyl polymethylsiloxane capillary	MS (quadrupole)	Luo et al. (2002)
Syringic acid	HPLC	Supelco Discovery C18 column	PDA/MS (quadrupole)	La Torre et al. (2006)
Syringic acid	UHPLC	Acquity HSS T3	MS (QqLIT and QqTOF)	Frolov et al. (2013)
Syringic acid[a]	GC	5 % Phenyl polymethylsiloxane capillary	MS (quadrupole)	Luo et al. (2002)
Tartaric acid (TMS)	GC	HP-5MS (5 % phenyl/95 % methylpolysiloxane) capillary	MS (ion trap)	Cerdan-Calero et al. (2012)
t-Cinnamic acid (TMS)	GC	PE–5MS capillary	MS (quadrupole)	Raj et al. (2007)
Tetradecanoic acid (TMS)	GC	PE–5MS capillary	MS (quadrupole)	Raj et al. (2007)
trans-Aconitic acid	HPLC	RezexTM ROA-OrganicAcid H +	MS (Q-TOF)	Ibanez and Bauer (2014)
Tricarballylic acid	HPLC	RezexTM ROA-OrganicAcid H +	MS (Q-TOF)	Ibanez and Bauer (2014)
Tyrosol	HPLC	Supelco Discovery C18 column	PDA/MS (quadrupole)	La Torre et al. (2006)
Valeric acid (TMS)	GC	PE–5MS capillary	MS (quadrupole)	Raj et al. (2007)
Vanillic acid	HPLC	Supelco Discovery C18 column	PDA/MS (quadrupole)	La Torre et al. (2006)
Vanillic acid	UHPLC	Acquity HSS T3	MS (QqLIT and QqTOF)	Frolov et al. (2013)
Vanillic acid[a]	GC	5 % Phenyl polymethylsiloxane capillary	MS (quadrupole)	Luo et al. (2002)
Vanillin	HPLC	Zorbax SB-C18/Zorbax SB-Phenyl	MS (LQIT-FT-ICR)	Owen et al. (2012)
Vanillin	UHPLC	Acquity HSS T3	MS (QqLIT and QqTOF)	Frolov et al. (2013)
Vanillin	UHPLC	Hypersil Gold C18	MS (LTQ/Orbitrap)	Cavka et al. (2011)
Vanillin[a]	GC	5 % Phenyl polymethylsiloxane capillary	MS (quadrupole)	Luo et al. (2002)
Vanillyl alcohol	HPLC	Zorbax SB-C18/Zorbax SB-Phenyl	MS (LQIT-FT-ICR)	Owen et al. (2012)
Xylobiose	HPAEC	CarboPac PA100	PAD	Li et al. (2013)

(continued)

Table 8.1 (continued)

Compounds	Separation	Column	Detector	Reference
Xylobiose	HPAEC	CarboPac PA200	PAD	Xu et al. (2013)
Xylohexaose	HPAEC	CarboPac PA200	PAD	Xu et al. (2013)
Xylopentaose	HPAEC	CarboPac PA200	PAD	Xu et al. (2013)
Xylopentaose	HPAEC	CarboPac PA200	PAD	Xu et al. (2013)
Xylose	HPAEC	CarboPac PA100	PAD	Li et al. (2013)
Xylose	HPAEC	Dionex HPIC-AS-6	PAD	Pettersen and Schwandt (1991)
Xylose	HPLC	Aminex HPX-87H	ELSD	Liu et al. (2012)
Xylose	HPLC	HILIC (amide-80)	PDA/MS (QTOF)	Bowman et al. (2011)
Xylotetraose	HPAEC	CarboPac PA200	PAD	Xu et al. (2013)
Xylotetraose	HPAEC	CarboPac PA200	PAD	Xu et al. (2013)
Xylotriose	HPAEC	CarboPac PA100	PAD	Li et al. (2013)
Xylotriose	HPAEC	CarboPac PA200	PAD	[99]
α-(1-4)-Linked galacturonic acid oligosaccharides	UHPLC	Acquity UPLC BEH amide	ELSD/MS (ion trap)	Leijdekkers et al. (2011)
α-D-Galactosamine-1-P	HPAEC	CarboPac PA1	PAD	Dionex (2000)
α-D-Galactose-1-P	HPAEC	CarboPac PA1	PAD	Dionex (2000)
α-D-Glucosamine-1-P	HPAEC	CarboPac PA1	PAD	Dionex (2000)
α-D-Glucose-1,6-Di P	HPAEC	CarboPac PA1	PAD	Dionex (2000)
α-D-Glucose-1-P	HPAEC	CarboPac PA1	PAD	Dionex (2000)
α-D-Glucuronic acid-1-P	HPAEC	CarboPac PA1	PAD	Dionex (2000)
α-D-Ribose-1-P	HPAEC	CarboPac PA1	PAD	Dionex (2000)
β-(1-4)-Linked glucose oligosaccharides	HPLC	Acquity UPLC BEH amide	MS (TOF)	Westereng et al. (2013)
β-(1-4)-Linked xylose oligosaccharides	HPLC	HILIC (amide-80)	PDA/MS (QTOF)	Bowman et al. (2011)
β-D-Fructose-2,6-Di P	HPAEC	CarboPac PA1	PAD	Dionex (2000)
β-D-Glucose-6-P	HPAEC	CarboPac PA1	PAD	Dionex (2000)

analysis after their hydrolyzation in acid medium prior to detecting sugar monomers using the hyphenation HPAEC/PAD. Later, Davis (1998) proposed modified chromatographic conditions based on HPAEC-PAD with high pH anion exchange for rapid compositional carbohydrate analysis of lignocellulosics. The author also discussed some critical factors concentrating on improving selectivity for all studied sugars while maintaining the precision and efficiency of the application.

Following this trend, two years later, the Dionex Company started a sequence of some full technical notes containing information on application of HPAEC/PAD able to detect carbohydrates (Dionex 2000), total free monosaccharides (Basumallick and Rohrer 2009), and HMF (Basumallick and Rohrer 2011) in biological samples even as different biomass feedstocks. In target works, the feasibility of HPAEC-PAD was proved for accurate and reliable analysis of biofuel samples such as sugar levels in biomass applications with minimal sample treatment. Moreover, such methods can be adapted for online monitoring with high precision and recoveries (Dionex 2000). Li and coworkers (2013) proposed a new insight into cellulosic biomass deconstruction by characterizing the distribution of xylooligosaccharide concentrations according to chain length for high-value products. The team used gel permeation chromatography to fractionate xylooligosaccharides produced from birchwood xylan, and then each fraction was identified using HPAEC-PAD. From developed PAD responses, the hemicellulose structure was accomplished and valuable new opportunities were proposed to advance pretreatment of biomass deconstruction technologies.

Recently, Beluomini and coworkers (2015) developed a method having copper nanoparticles electrodeposited onto a glassy carbon electrode as modified detector, to determine D-galacturonic and D-glucuronic acids. The authors demonstrated the effectiveness of the method in the assessment of biomass components by quantification target acids in hydrolyzed sugarcane bagasse. The new understanding was the absence of a derivatization process as it is done in traditional spectrophotometric methods and, this way, useful for maximizing the value derived from the biomass feedstock.

Notably, pretreated processes, such as the hydrolysis step, involve drastic acid or basic medium. Also, the substrate of hydrolyzed biomass becomes ionic and can be easily separated by ionic chromatography. However, in target conditions, the ECD is subject to fouling because of the adsorption of electrogenerated products onto the electrode surface, hindering the baseline stability and/or reproducible measuring conditions. Thus, these reviewed works showed that in cases in which electrode fouling occurs rapidly, PAD is preferably used because it is more effective on a renewed electrode surface (remains in this activated condition) after each measurement.

In addition, among the carbohydrate compounds successfully detected and quantified, it was shown that the HPAEC-PAD is an analytical tool successfully used to provide information during the improvement of pretreatment processes and can be a valuable approach to predicting the chemical composition of lignocellulosic feedstocks rapidly. This section represents only a small part of some published reports and, for additional information, the references Qing et al. (2013), Jensen and Johnson (1997), and Kotnik et al. (2011) and many specific works, bring new challenges around the ECD system coupled with separation techniques that can be adapted to accomplish the chemical compositional analysis of lignocellulosic biomass feedstocks (Table 8.1).

8.2.3.5 Chromatographic Analysis Using Mass Spectrometry Detection (HPLC-MS)

The last detector coupled to classical HPLC discussed in this section is the MS, in which the analyzed compound is ionized to generate charged molecules or molecule fragments. The ions are separated, detected, and the signal is processed into the spectra of relative abundance of ions as a function of the mass-to-charge ratio. The most common ionization interfaces hyphenated with HPLC are electrospray (ESI) and atmospheric pressure chemical ionization (APCI) and the most common analyzers are single and triple quadrupole, ion trap, and time-of-flight (TOF) (Qing et al. 2013). Quadrupole analyzers are widely used in LC-MS applications owing to sensibility and selectivity, mainly to quantitative analyses (Zhou et al. 2015); on the other hand, ion trap analyzers offer great advantages over other analyzers, such as quadrupole, on MS/MS mode (March 1997), ensuring better control on fragmentations, which is very helpful in elucidation studies. The use of high-resolution mass spectrometers (HRMSs) as TOF analyzers has the advantage of mass accuracy, which allows molecular formulas to be determined, helping compound identification (Xu et al. 2010), and, with the advance of technologies, HRMS recently has been successfully used in quantitative analyses (Fung et al. 2013).

The utilities of HPLC-MS to analyze compounds of interest on pretreated lignocellulosic biomass study are confirmed by multiple methods, describing analysis of sugars, organic acids, and phenolic compounds and are presented in the literature (Ibanez and Bauer 2014; Matias et al. 2011; Owen et al. 2012; Table 8.1). Regarding the limitations, the main problems associated with HPLC-MS are the chemical diversity of the compounds to be analyzed, the simultaneous presence of more than one component in the ion source can result in ion suppression of some compounds, and a subsequent reduction in the MS signal.

The mobile phase must be of high purity to avoid interference and the use of buffers containing inorganic ions such as phosphate and sodium acetate should be avoided, because they can cause ion suppression and contaminate the ion source. Other important parameters that affect this technique are the flow rate and the type of interface used (Patel et al. 2010; Pitt 2009). All these parameters can strongly compromise the quality of the detector response, and for this reason, it is extremely hard to optimize the ionization conditions that can be suitable for all types of compounds present on LCF fractions.

8.2.4 Modern Ultra High Performance Liquid Chromatography Systems

The ultra high performance liquid chromatography (UHPLC) system has been used since 2004 due to its higher performance compared with the conventional HPLC system. The improvements done in the instrumentation make the analysis faster, including increase of sensibility, reproducibility, and lower residue produced after

the separation process (Maldaner and Jardim 2009). All these characteristics were achieved by application of small particles (sub 2 μm) of the packing material that give superior chromatographic resolution, as well as important physical modifications in this type of instrumentation. Other differences with classical HPLC are reduced column dimensions introduced by the UHPLC, height of 50–150 mm, and reduction of internal diameter and columns that can work under a pressure higher than 15,000 psi. Moreover, the highlight is the compliance with the guidelines of green chemistry, including the small volume of sample and reduced use of mobile and other reagents during the analysis (Swartz 2005).

8.2.4.1 Monitoring Value-Added Products Obtained from Biorefinery Processes by UHPLC

The UHPLC system is a technique with great potential for use, including the separation of compounds with distinct polarities, molecular weight, functional groups, and other characteristics. When it is coupled with appropriate detectors, the identification of these compounds can be quickly achieved and this type of analytical approach is interesting when desiring to investigate the chemical components present in the LCF. However, one of the great challenges for chromatographers is the use of a unique separation method of analysis that uses a single detector for the identification of all components normally found in a complex matrix.

Nowadays, the UHPLC systems are compatible with a variety of detectors that allow analysis of a broad range of compounds and the most appropriate configuration will depend much more on the laboratory infrastructure and investment capacity of research centers. As reported in the literature, UHPLC has been used for the quantification of carbohydrates, phenolic compounds, and xanthines in food samples and pharmacological preparations, but this same application can be used in the context of biomass characterization and in biorefinery processes (Dartora et al. 2011).

8.2.4.2 Chromatographic Analysis Using UHPLC-PDA

As detailed in Sect. 8.2.3.2., the photodiode array detector (PDA) allows detecting compounds with chromophoric groups, further quantifying small concentrations of analytes in the sample and detecting trace impurities. This type of instrumental configuration is not common yet for analysis of biomass and its products, but there are reports that indicate the use of UHPLC-PDA for quantitation of phenolic compounds (Nowicka and Wojdylo 2016; Carbonell-Barrachina et al. 2015; Bairwa et al. 2014), carotenoid, and other hydrophobic components that can be also observed in LCF processes (Epriliati et al. 2010).

Recently, a study was performed with *Euphorbia characias*, a potential bioenergy crop able to grow in large areas of semiarid lands (Escrig et al. 2013). In this paper, the authors investigated the metabolites of the nonpolar and polar extracts of this plant. Six flavonoids and flavonoid glycosides were quantified by UHPLC-PDA and its complete identification was performed based on the analysis of

UHPLC-PDA-Q-TOF/MS at the three phenological stages (Table 4.1). The methanol extracts of *E. characias* exhibited potential content of sugars that can be used in a biological fermentation step. The flavonoids-glycoside may be easily hydrolyzed to provide two different fractions: one containing fermentable sugars and the other with antioxidant compounds (aglycone). Additionally, the lignocellulosic content of *E. characias* can enter in a biorefinery pipeline and the second-generation fermentable sugars can be used after previous hydrolysis reactions.

The antioxidant capacity of polyphenols is extensively studied and components with this property are present in the LCF fractions and are an interesting source of value-added compounds. Recently, the monitoring of the phytochemical profile of quince liquor was analyzed and a total of 18 polyphenols were identified by LC-PDA-Q-TOF/MS and quantified with a photodiode detector (UHPLC-PDA and UHPLC-PDA and UHPLC-with florescence detection (FL)) in a single run of 15 min considering the re-equilibrate stage (Table 4.1; Carbonell-Barrachina et al. 2015).

Extracts of *Boerhaavia diffusa* have been proposed as active constituents for anticancer, spasmolytic, and anti-inflammatory activities due to the presence of phenolic compounds (boeravinones) and organic acids (Bairwa et al. 2014). As result, a study was developed using UHPLC-PDA to perform quality control of these compounds in the root extracts of *B. diffusa*. In this study, the authors used a UHPLC 1.7 μm column (BEH Shield C18, Waters: 2.1 × 100 mm) and based on a simple gradient elution with methanol and water (0.1 % acetic acid), eight boeravinone derivatives were separated and quantified within 6 min.

The advantages of UHPLC over HPLC can be easily ascertained when the same application is compared. For example, a conventional application was previously reported and the quantification of boeravinone derivatives using HPLC-PDA showed a longer analysis with greater consumption of solvents and reagents. In addition, the analysis was applied to the quantification of only two components (Bhope et al. 2013). This example shows that any HPLC-PDA migration for UPLC-PDA can be easy and effective.

8.2.4.3 Chromatographic Analysis Using UHPLC-RID

In Sect. 8.2.3.1. it was highlighted that during the analysis of compounds with absence of chromophoric groups, under isocratic conditions, the most appropriate detector is RI. In the recent literature, there are no reports on the use of UHPLC-RID applied in the biorefinery context. However, the methodologies based on HPLC-RID may be easily transferred to UHPLC-RID by using the online calculators available from the main chromatograph manufacturers (Phenomenex 2016; ThermoScientific 2016) or inside their own managing and processing software.

A successful transfer of methods can suggest a great field to be explored in the area of separation and this advantage is not only applied to UHPLC-RID, but for all other types of chromatographic techniques discussed in this chapter. All these changes lead to the adaptation or development of greener methods and this is corroborated by the increased frequency of analysis with reduced time and reduction of

solvents used. Thus, in addition to contributing to the environment, this type of approach can reduce annual costs, as can be predicted by this application provided by a chromatograph manufacturer (Waters 2016).

A different approach using the combined techniques of size-exclusion ultra-performance liquid chromatograph coupled to an ultraviolet, multiangle light scattering and refractive index (SE-UHPLC-UV-MALS-RI) was suggested by Miranda-Hernández and coauthors (2016) to determine four biotherapeutic proteins and a synthetic copolymer. The RI detector was used to evaluate possible loss mass for the injected proteins and to ensure the reliability of the proposed method.

8.2.4.4 Chromatographic Analysis Using UHPLC-ELSD

Monitoring and quality control are key steps that will validate successful technologies and processes of biomass depolymerization into its monomeric forms, inhibitory compounds, and by-products, passing by its final value-added compounds (Vaz and Dodson 2014). To meet the strong demand for analytical data generated in large quantities and in a short time, improvements of current analytical methods should be done in order to increase the throughput and efficiency, supporting more cost-effective and faster analyses.

During the analysis of nonchromophoric compounds, the UHPLC system coupled with the evaporative light-scattering detector (ELSD) appears as a promising alternative for the monitoring of sugars and organic acids in the context of high-throughput analysis. The configuration of this system supports the use of columns with short lengths (30 up to 150 mm), smaller internal diameters (1.0–2.1 mm), and stationary phase with sub 2 μm particles. For the analysis of high polar compounds (Snyder et al. 2010), UHPLC columns that deal with hydrophilic interaction chromatography (HILIC) would be ideal for the separation of biomass target compounds (carbohydrates, organic acids, by-products, and final products) (Pazourek 2014; Bowman et al. 2011). HILIC can be an alternative to reversed-phase chromatographic separation for polar compounds once it works as a normal phase column.

HILIC columns are composed mainly of classical bare silica and its few modifications with polar functionalities (including amide, diol, aminopropyl, cyano, and derivatives of polysuccinimide), developed to separate small and extremely polar compounds. Additionally, it supports an aqueous-organic mobile phase, which means that gradient elution can be performed, improving separation. Furthermore, this type of mobile phase is extremely compatible with ESI-MS, which is a very powerful analytical tool to detect and identify a wide range of polar compounds (Brokl et al. 2011; Ikegami et al. 2008; Westereng et al. 2013).

Although the number of commercially available columns designed for HILIC has been growing, this modality of separation does not have many varieties of stationary phase composition as occurs with reversed-phase columns. However, this limitation is expected to be overcome in the near future and a major structural variation in HILIC stationary phase would substantially enhance separation capacity of this type of column towards the diversity of polar compounds (Hemstrom and Irgum 2006).

There are few studies using HILIC columns with UHPLC-ELSD or combined with MS detectors to access the biomass characterization as well as its derivative products (Table 8.1); however, they do demonstrate it to be a versatile method, capable of quantifying and identifying oligosaccharides, especially the acidic ones (Remoroza et al. 2012; Leijdekkers et al. 2011). Our group has been working with a HILIC-UHPLC-ELSD approach, which was developed and validated to identify and quantify glycerol, arabitol, and mannitol during bioconversion of crude glycerol. This work highlights the necessary optimization steps which are related to chromatographic and detector parameters that will improve selectivity and sensitivity during the analysis.

8.2.4.5 Chromatographic Analysis Using UHPLC-MS/MS

Among the many advantages associated with the use of MS techniques, the most interesting are those that provide the molecular weights and unequivocal elemental compositions of unknown components in complex mixtures. This information is normally obtained by high-resolution mass spectrometry analysis. Additionally, detailed molecular-level structural information can be accessed when the tandem mass spectrometry function is used in association with the chromatographic separations (UHPLC-MS). The great advantage of mass spectrometry, when coupled with UHPLC, is because of the higher concentration of analytes at the point of detection, improving the signal-to-noise ratio, due to the reduced band spreading during a chromatographic run (Yu et al. 2006).

The rapid chromatographic analysis achieved by the UHPLC technique and its coupling with the MS detector provides important structural information during the biomass characterization step, especially when MS/MS data are obtained and this approach gives more sensitivity and specificity for the analysis (Yu et al. 2006). Therefore UHPLC-MS could be a strategic option to address the routine analysis of a great number of LCF samples (Table 8.1; Kiyota et al. 2012).

There is no report about direct applications that use UHPLC-MS for sugar analysis from LCF as products of hydrolysis, but this incipiency opens an opportunity to extend this technique to analyze this kind of matrix. An example of application uses the approach suggested by Wang and coauthors (2012). In this work, the authors developed a UHPLC-UV/MS method used for separation and characterization of chiral derivatives of 16 monosaccharides obtained after saponin hydrolysis, including six pairs of enantiomers and four other monosaccharides in a single injection.

In this case, enantiomeric aldoses were converted to diastereomeric arylthiocarbamate derivatives to be analyzed in an achiral environment. This method reports the combination of UHPLC and MS techniques to get separation of aldose enantiomers. However, there is the disadvantage of a derivatization step, which can compromise the analysis of a large number of samples.

Traditionally, organic acids have been analyzed by liquid chromatography with refractive index, conductivity, or ultraviolet as a detector option, but the methods involving these techniques have restrictions related to inadequate limits of detection

and matrix interference, and they are normally time-consuming (Ross et al. 2007). The coupling between liquid chromatography and mass spectrometry results in a more appropriate system configuration that will guarantee specificity and unequivocal detection of individual organic acids in contrast to cited detectors (Ibanez and Bauer 2014).

Ross and coworkers (2007) developed a method based on UHPLC-ESI-TripleQuad-MS/MS for the rapid identification and quantification of organic acid content after microbial fermentation, in which 10 organic acids were detected in less than 3 min (per sample). The method proposed by these authors employed a UHPLC separation system equipped with two Hypersil Gold (50 mm × 2.1 mm, 1.9 μm) columns in series and the mobile phase was water/acetonitrile (97:3, v/v) running under isocratic elution. The ionization step was obtained using an ESI probe and the multiple reaction monitoring (MRM) transition was optimized and used during the analysis of real samples by this tandem UHPLC mass spectrometry method.

Furans such as HMF and furfural display an undesired behavior during the fermentation steps and they need to be monitored during all processes of obtaining LCF samples. A successful case to monitor these inhibitory compounds was reported by Cavka and coworkers (2011), who describe UHPLC-ESI-TOF-MS and UHPLC-LTQ/Orbitrap methods to analyze furans, as well as phenolic compounds and their dithionite derivatives.

Structural elucidation of all compounds was performed using a high-resolution LTQ/Orbitrap mass spectrometer with an ESI source and the phenolic compounds were quantified using UHPLC-ESI-TOF-MS, but HMF and furfural were quantified by UV data (PDA detector) due to low ionization levels in electrospray. The combination of different detectors in a single chromatographic run is extremely useful when one of them does not fully satisfy the analysis of a complex sample.

Frolov and coworkers (2013) reported a method for the simultaneous identification and quantitation of 47 phenolic monomers and their degradation products based on a UHPLC-ESI-MS/MS method, which allowed a complete analysis in a single chromatographic run of 10 min. The MS/MS instrument configuration was a hybrid triple quadrupole linear ion trap (QqLIT) mass analyzer, which gathered a comprehensive analysis structure, rapidity, high sensitivity, and accurate quantification by multiple reaction monitoring (MRM).

Benzoquinones, also considered potent inhibitors of fermentation (Stagge et al. 2015; Larsson et al. 2000), were analyzed by UHPLC-ESI/TripleQuad-MS after derivatization with 2,4-dinitrophenylhydrazine. Chromatographic separation was achieved with an XTerra MS C18 (2.1 mm × 150 mm 5 μm) column with the flow rate constant at 0.25 mL/min and TripleQuad mass spectrometer used in negative electrospray-ionization mode.

The specific benzoquinones, *p*-benzoquinone and 2,6-dimethoxybenzoquinone, were identified as by-products of acid pretreatment of lignocellulose in six lignocellulosic hydrolysates investigated (Stagge et al. 2015), and 2,6-dimethoxybenzoquinone could tentatively be formed by degradation/oxidation of syringyl units of lignin. The monomeric constituents of lignin after acid hydrolysis are *p*-coumaryl, coniferyl, and sinapyl alcohols that through a series of oxidations become the monolignols *p*-hydroxyphenyl, guayacyl, and syringyl, respectively (Fig. 8.4; Kiyota et al. 2012).

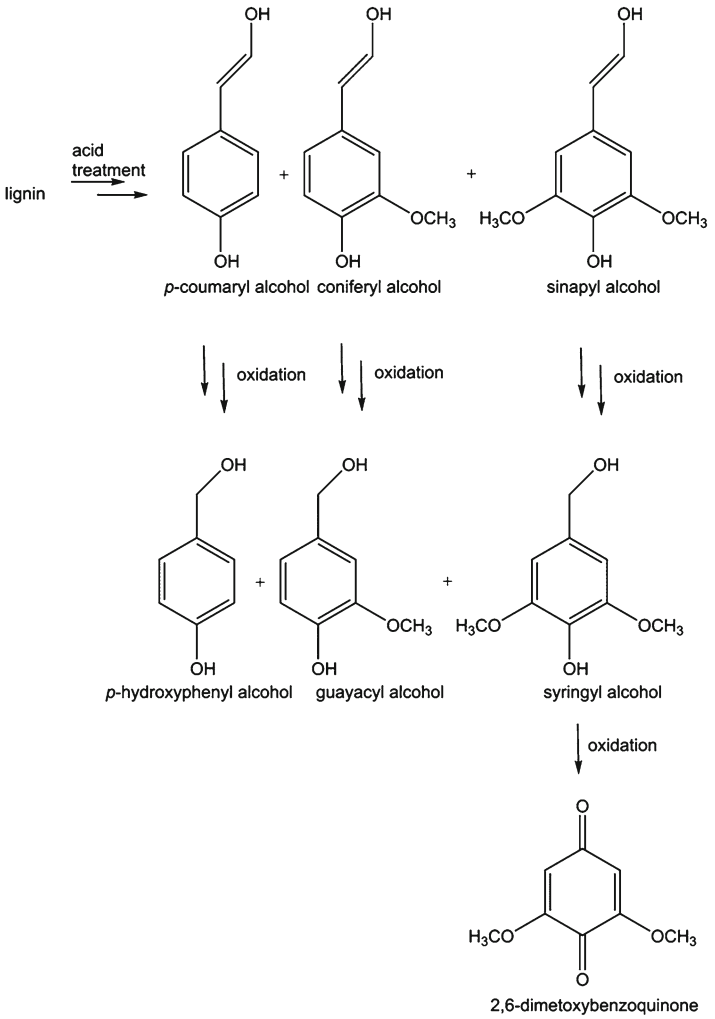

Fig. 8.4 Formation of 2,6-dimethoxybenzoquinone from lignin monomers

8.3 Conclusion

The diversification of global energy and the search for renewable substitutes for the petrochemical chain become indispensable for the balance of the planet. The environmental damages caused by petroleum derivatives must be urgently mitigated and renewable biomass, particularly lignocellulosic feedstock, is a potential candidate that can be applied as a basic input in biorefinery processes. For those products with a green label, it is necessary to perform characterization steps of the original raw material and from its products formed after the various types of processes.

An essential analytical tool is chromatography, which associated with different types of detectors can provide basic and crucial information during the production of target value-added compounds. The classical techniques, already consolidated in the literature, have a great contribution at this stage of identification and quality control of biomass conversion. However, advances in chromatographic instrumentation observed in recent decades are enabling us to obtain these results in a faster way, with more accuracy and with low environmental impact.

In this chapter the authors have chosen to present the separation and detection techniques individually, but the most appropriate is to consider, when applicable, the use of different detectors in series. In many cases, the information generated is complementary and the correlation of analytical data is very important to conduct a more robust and accurate characterization of highly complex samples.

References

Bairwa K, Srivastava A, Jachak SM (2014) Quantitative analysis of boeravinones in the roots of boerhaavia diffusa by UPLC/PDA. Phytochem Anal 25(5):415–420. doi:10.1002/pca.2509

Baldwin RP (1999) Electrochemical determination of carbohydrates: enzyme electrodes and amperometric detection in liquid chromatography and capillary electrophoresis. J Pharm Biomed Anal 19(1):69–81

Ball S, Bullock S, Lloyd L, Mapp K, Ewen A (2011) Analysis of carbohydrates, alcohols, and organic acids by ion-exchange chromatography. Agilent Technologies, Santa Clara, CA, http://www.agilent.com/cs/library/applications/5990-8801EN%20Hi-Plex%20Compendium.pdf. Accessed Jan 2016

Basumallick L, Rohrer J (2009) Rapid method for the estimation of total free monosaccharide content of corn stover hydrolysate using HPAE-PAD. http://www.dionex.com/en-us/webdocs/114769-BR-HPAE-PAD-Carbohydrate-Analysis-BR700910_E.pdf. Accessed Jan 2016

Basumallick L, Rohrer J (2012) Rapid and Sensitive Determination of Biofuel Sugars by Ion Chromatography. doi: http://www.dionex.com/enus/webdocs/113489-AN282-IC-Biofuel-Sugars-03May2012-LPN2876-R2.pdf. Accessed jan 2016

Basumallick L, Rohrer J (2011) Determination of hydroxymethylfurfural in honey and biomass. http://www.dionex.com/en-us/webdocs/109807-AN270-IC-HMF-Honey-Biomass-AN70488_E.pdf. Accessed Jan 2016

Beluomini MA, da Silva JL, Stradiotto NR (2015) Determination of uronic acids in sugarcane bagasse by anion-exchange chromatography using an electrode modified with copper nanoparticles. Anal Methods 7(6):2347–2353. doi:10.1039/c4ay03060e

Bhope SG, Gaikwad PS, Kuber VV, Patil MJ (2013) RP-HPLC method for the simultaneous quantitation of boeravinone E and boeravinone B in Boerhaavia diffusa extract and its formulation. Nat Prod Res 27(6):588–591. doi:10.1080/14786419.2012.676550

Bowman MJ, Dien BS, O'Bryan PJ, Sarath G, Cotta MA (2011) Selective chemical oxidation and depolymerization of switchgrass (Panicum virgatum L.) xylan with oligosaccharide product analysis by mass spectrometry. Rapid Commun Mass Spectrom 25(7):941–950. doi:10.1002/rcm.4949

Bozell JJ, Petersen GR (2009) Technology development for the production of biobased products from biorefinery carbohydrates-the US Department of Energy's "Top 10" revisited. Green Chem 12(4):539–554. doi:10.1039/b922014c

Brokl M, Hernández-Hernández O, Soria AC, Sanz ML (2011) Evaluation of different operation modes of high performance liquid chromatography for the analysis of complex mixtures of neutral oligosaccharides. J Chromatogr A 1218(42):7697–7703. doi:10.1016/j.chroma.2011.05.015

Carbonell-Barrachina AA, Szychowski PJ, Veronica Vasquez M, Hernandez F, Wojdylo A (2015) Technological aspects as the main impact on quality of quince liquors. Food Chem 167:387–395. doi:10.1016/j.foodchem.2014.07.012

Castellari M, Sartini E, Spinabelli U, Riponi C, Galassi S (2001) Determination of carboxylic acids, carbohydrates, glycerol, ethanol, and 5-HMF in beer by high-performance liquid chromatography and UV-refractive index double detection. J Chromatogr Sci 39(6):235–238

Cavka A, Alriksson B, Ahnlund M, Jonsson LJ (2011) Effect of sulfur oxyanions on lignocellulose-derived fermentation inhibitors. Biotechnol Bioeng 108(11):2592–2599. doi:10.1002/bit.23244

Cerdan-Calero M, Sendra JM, Sentandreu E (2012) Gas chromatography coupled to mass spectrometry analysis of volatiles, sugars, organic acids and aminoacids in Valencia Late orange juice and reliability of the Automated Mass Spectral Deconvolution and Identification System for their automatic identification and quantification. J Chromatogr A 1241:84–95. doi:10.1016/j.chroma.2012.04.014

Cherubini F (2010) The biorefinery concept: using biomass instead of oil for producing energy and chemicals. Energ Convers Manage 51(7):1412–1421. doi:10.1016/j.enconman.2010.01.015

Corma A, Iborra S, Velty A (2007) Chemical routes for the transformation of biomass into chemicals. Chem Rev 107(6):2411–2502. doi:10.1021/cr050989d

Dartora N, de Souza LM, Santana AP, Iacomini M, Valduga AT, Gorin PAJ, Sassaki GL (2011) UPLC-PDA-MS evaluation of bioactive compounds from leaves of Ilex paraguariensis with different growth conditions, treatments and ageing. Food Chem 129(4):1453–1461. doi:10.1016/j.foodchem.2011.05.112

Davis MW (1998) A rapid modified method for compositional carbohydrate analysis of lignocellulosics by high pH anion-exchange chromatography with pulsed amperometric detection (HPAEC/PAD). J Wood Chem Technol 18(2):235–252. doi:10.1080/02773819809349579

Dionex (2000) Analysis of carbohydrates by high performance anion exchange chromatography with pulsed amperometric detection (HPAE-PAD). http://www.dionex.com/en-us/webdocs/5023-TN20_LPN032857-04.pdf. Accessed Jan 2016

Donate PM (2014) Sintese ambientalmente correta a partir de biomassa. Orbital 6(2):101–117

Eiceman GA, Hill HH, Davani B (1994) Gas chromatography. Anal Chem 66(12):621R–633R. doi:10.1021/ac00084a023

Epriliati I, Kerven G, D'Arcy B, Gidley MJ (2010) Chromatographic analysis of diverse fruit components using HPLC and UPLC. Anal Methods 2(10):1606–1613. doi:10.1039/c0ay00244e

Escrig PV, Iglesias DJ, Corma A, Primo J, Primo-Millo E, Cabedo N (2013) Euphorbia characias as bioenergy crop: a study of variations in energy value components according to phenology and water status. J Agric Food Chem 61(42):10096–10109. doi:10.1021/jf403015a

Fedorowski J, LaCourse WR (2015) A review of pulsed electrochemical detection following liquid chromatography and capillary electrophoresis. Anal Chim Acta 861:1–11. doi:10.1016/j.aca.2014.08.035

FitzPatrick M, Champagne P, Cunningham MF, Whitney RA (2010) A biorefinery processing perspective: treatment of lignocellulosic materials for the production of value-added products. Bioresour Technol 101(23):8915–8922. doi:10.1016/j.biortech.2010.06.125

Frolov A, Henning A, Boettcher C, Tissier A, Strack D (2013) An UPLC-MS/MS method for the simultaneous identification and quantitation of cell wall phenolics in Brassica napus seeds. J Agric Food Chem 61(6):1219–1227. doi:10.1021/jf3042648

Fung EN, Jemal M, Aubry A-F (2013) High-resolution MS in regulated bioanalysis: where are we now and where do we go from here? Bioanalysis 5(10):1277–1284. doi:10.4155/bio.13.81

Gencoglu A, Minerick AR (2014) Electrochemical detection techniques in micro- and nanofluidic devices. Microfluid Nanofluid 17(5):781–807. doi:10.1007/s10404-014-1385-z

Heineman WR, Kissinger PT (1980) Analytical electrochemistry – methodology and applications of dynamic techniques. Anal Chem 52(5):R138–R151

Hemstrom P, Irgum K (2006) Hydrophilic interaction chromatography. J Sep Sci 29(12):1784–1821. doi:10.1002/jssc.200600199

Herbreteau B, Lafosse M, Morinallory L, Dreux M (1992) High-performance liquid-chromatography of raw sugars and polyols using bonded silica-gels. Chromatographia 33(7-8):325–330. doi:10.1007/bf02275911

Héron S, Dreux M, Alain T (2007) Factors affecting sensitivity of evaporative light scattering detection. LG GC Eur 20(7):414–419

Hope JL, Prazen BJ, Nilsson EJ, Lidstrom ME, Synovec RE (2005) Comprehensive two-dimensional gas chromatography with time-of-flight mass spectrometry detection: analysis of amino acid and organic acid trimethylsilyl derivatives, with application to the analysis of metabolites in rye grass samples. Talanta 65(2):380–388. doi:10.1016/j.talanta.2004.06.025

Ibanez AB, Bauer S (2014) Analytical method for the determination of organic acids in dilute acid pretreated biomass hydrolysate by liquid chromatography-time-of-flight mass spectrometry. Biotechnol Biofuels 7:145. doi:10.1186/s13068-014-0145-3

Ikegami T, Tomomatsu K, Takubo H, Horie K, Tanaka N (2008) Separation efficiencies in hydrophilic interaction chromatography. J Chromatogr A 1184(1-2):474–503. doi:10.1016/j.chroma.2008.01.075

Jensen MB, Johnson DC (1997) Fast wave forms for pulsed electrochemical detection of glucose by incorporation of reductive desorption of oxidation products. Anal Chem 69(9):1776–1781. doi:10.1021/ac960828x

Kafkas E, Kosar M, Turemis N, Baser KHC (2006) Analysis of sugars, organic acids and vitamin C contents of blackberry genotypes from Turkey. Food Chem 97(4):732–736. doi:10.1016/j.foodchem.2005.09.023

Kamm B, Kamm M (2004) Principles of biorefineries. Appl Microbiol Biotechnol 64(2):137–145. doi:10.1007/s00253-003-1537-7

Kamm B, Kamm M, Gruber PR, Kromus S (2008) Biorefinery systems – an overview. In: Kamm B, Gruber PR, Kamm B (eds) Biorefineries-industrial processes and products. Wiley-VCH, Berlin, pp 1–40. doi:10.1002/9783527619849.ch1

Kissinger PT (1986) Electrochemical detectors. In: Vickrey TH (ed) Liquid chromatography detectors, 1st edn. Marcel Dekker, New York, NY, pp 125–164

Kiyota E, Mazzafera P, Sawaya ACHF (2012) Analysis of soluble lignin in sugarcane by ultrahigh performance liquid chromatography-tandem mass spectrometry with a do-it-yourself oligomer database. Anal Chem 84(16):7015–7020. doi:10.1021/ac301112y

Kotnik D, Novic M, LaCourse WR, Pihlar B (2011) Cathodic re-activation of the gold electrode in pulsed electrochemical detection of carbohydrates. J Electroanal Chem 663(1):30–35. doi:10.1016/j.jelechem.2011.09.026

Kumar R, Singh S, Singh OV (2008) Bioconversion of lignocellulosic biomass: biochemical and molecular perspectives. J Ind Microbiol Biotechnol 35(5):377–391. doi:10.1007/s10295-008-0327-8

La Torre GL, Saitta M, Vilasi F, Pellicano T, Dugo G (2006) Direct determination of phenolic compounds in Sicilian wines by liquid chromatography with PDA and MS detection. Food Chem 94(4):640–650. doi:10.1016/j.foodchem.2005.02.007

Larsson S, Quintana-Sainz A, Reimann A, Nilvebrant NO, Jonsson LJ (2000) Influence of lignocellulose-derived aromatic compounds on oxygen-limited growth and ethanolic fermentation by Saccharomyces cerevisiae. Appl Biochem Biotechnol 84–6:617–632. doi:10.1385/abab:84-86:1-9:617

Leijdekkers AGM, Sanders MG, Schols HA, Gruppen H (2011) Characterizing plant cell wall derived oligosaccharides using hydrophilic interaction chromatography with mass spectrometry detection. J Chromatogr A 1218(51):9227–9235. doi:10.1016/j.chroma.2011.10.068

Li H, Qing Q, Kumar R, Wyman CE (2013) Chromatographic determination of 1, 4-beta-xylooligosaccharides of different chain lengths to follow xylan deconstruction in biomass conversion. J Ind Microbiol Biotechnol 40(6):551–559. doi:10.1007/s10295-013-1254-x

Liu XJ, Ai N, Zhang HY, Lu MZ, Ji DX, Yu FW, Ji JB (2012) Quantification of glucose, xylose, arabinose, furfural, and HMF in corncob hydrolysate by HPLC-PDA-ELSD. Carbohydr Res 353:111–114. doi:10.1016/j.carres.2012.03.029

Luo CD, Brink DL, Blanch HW (2002) Identification of potential fermentation inhibitors in conversion of hybrid poplar hydrolyzate to ethanol. Biomass Bioenerg 22(2):125–138. doi:10.1016/s0961-9534(01)00061-7

Lupoi JS, Singh S, Parthasarathi R, Simmons BA, Henry RJ (2015) Recent innovations in analytical methods for the qualitative and quantitative assessment of lignin. Renew Sust Energ Rev 49:871–906. doi:10.1016/j.rser.2015.04.091

Lv Y, Yang XB, Zhao Y, Ruan Y, Yang Y, Wang ZZ (2009) Separation and quantification of component monosaccharides of the tea polysaccharides from Gynostemma pentaphyllum by HPLC with indirect UV detection. Food Chem 112(3):742–746. doi:10.1016/j.foodchem.2008.06.042

Ma CM, Sun Z, Chen CB, Zhang LL, Zhu SH (2014) Simultaneous separation and determination of fructose, sorbitol, glucose and sucrose in fruits by HPLC-ELSD. Food Chem 145:784–788. doi:10.1016/j.foodchem.2013.08.135

Maldaner L, Jardim ICSF (2009) O estado da arte da cromatografia líquida de ultra eficiência. Quim Nova 32:214–222

March RE (1997) An introduction to quadrupole ion trap mass spectrometry. J Mass Spectrom 32(4):351–369. doi:10.1002/(sici)1096-9888(199704)32:4<351::aid-jms512>3.0.co;2-y

Marsman JH, Wildschut J, Evers P, de Koning S, Heeres HJ (2008) Identification and classification of components in flash pyrolysis oil and hydrodeoxygenated oils by two-dimensional gas chromatography and time-of-flight mass spectrometry. J Chromatogr A 1188(1):17–25. doi:10.1016/j.chroma.2008.02.034

Matias J, Gonzalez J, Royano L, Barrena RA (2011) Analysis of sugars by liquid chromatography-mass spectrometry in Jerusalem artichoke tubers for bioethanol production optimization. Biomass Bioenergy 35(5):2006–2012. doi:10.1016/j.biombioe.2011.01.056

Menon V, Rao M (2012) Trends in bioconversion of lignocellulose: biofuels, platform chemicals & biorefinery concept. Prog Energ Combust Sci 38(4):522–550. doi:10.1016/j.pecs.2012.02.002

Meyer VR (2010) Detectors. In: Practical high-performance liquid chromatography, 5th edn. John Wiley and Sons, Ltd., London, pp 91–116

Miranda-Hernandez MP, Valle-Gonzalez ER, Ferreira-Gomez D, Perez NO, Flores-Ortiz LF, Medina-Rivero E (2016) Theoretical approximations and experimental extinction coefficients of biopharmaceuticals. Anal Bioanal Chem 408(5):1523–1530. doi:10.1007/s00216-015-9261-6

Nowicka P, Wojdylo A (2016) Stability of phenolic compounds, antioxidant activity and colour through natural sweeteners addition during storage of sour cherry puree. Food Chem 196:925–934. doi:10.1016/j.foodchem.2015.10.019

NRC (2000) Overview. In: NRC (ed) Biobased industrial products, priorities for research and commercialization, 1st edn. National Academic, Washington, DC, pp 15–52

NREL (2008) Determination of sugars, byproducts, and degradation products in liquid fraction process samples. http://www.nrel.gov/docs/gen/fy08/42623.pdf. Accessed Jan 2016

Owen BC, Haupert LJ, Jarrell TM, Marcum CL, Parsell TH, Abu-Omar MM, Bozell JJ, Black SK, Kenttamaa HI (2012) High-performance liquid chromatography/high-resolution multiple stage tandem mass spectrometry using negative-ion-mode hydroxide-doped electrospray ionization for the characterization of lignin degradation products. Anal Chem 84(14):6000–6007. doi:10.1021/ac300762y

Patel KN, Patel JK, Patel MP, Rajput GC, Patel HA (2010) Introduction to hyphenated techniques and their applications in pharmacy. Pharm Methods 1(1):2–13. doi:10.1016/S2229-4708(10)11002-4

Pazourek J (2014) Fast separation and determination of free myo-inositol by hydrophilic liquid chromatography. Carbohydr Res 391:55–60. doi:10.1016/j.carres.2014.03.010

Pettersen RC (1984) The chemical-composition of wood. In: Rowell R (ed) The chemistry of solid wood, Advances in chemistry, 1st edn. American Chemical Society, Washington, DC, pp 57–126

Pettersen RC (1991) Wood sugar analysis by anion chromatography. J Wood Chem Technol 11(4):495–501. doi:10.1080/02773819108051089

Phenomenex (2016) Kinetex 2.6 µm Calculator. https://www.phenomenex.com/tools/kinetexcalculator. Accessed Jan 2016

Pitt JJ (2009) Principles and applications of liquid chromatography-mass spectrometry in clinical biochemistry. Clin Biochem Rev 30(1):19

Qing Q, Li H, Kumar R, Wyman CE (2013) Xylooligosaccharides production, quantification, and characterization in context of lignocellulosic biomass pretreatment. In: Wyman CE (ed) Aqueous pretreatment of plant biomass for biological and chemical conversion to fuels and chemicals, 1st edn. John Wiley and Sons, Oak Ridge, TN, pp 391–415

Raj A, Reddy MMK, Chandra R (2007) Identification of low molecular weight aromatic compounds by gas chromatography-mass spectrometry (GC-MS) from kraft lignin degradation by three Bacillus sp. Int Biodeterior Biodegrad 59(4):292–296. doi:10.1016/j.ibiod.2006.09.006

Remoroza C, Cord-Landwehr S, Leijdekkers AGM, Moerschbacher BM, Schols HA, Gruppen H (2012) Combined HILIC-ELSD/ESI-MSn enables the separation, identification and quantification of sugar beet pectin derived oligomers. Carbohydr Polym 90(1):41–48. doi:10.1016/j.carbpol.2012.04.058

Ross KL, Tu TT, Smith S, Dalluge JJ (2007) Profiling of organic acids during fermentation by ultraperformance liquid chromatography-tandem mass spectrometry. Anal Chem 79(13):4840–4844. doi:10.1021/ac0624243

Roussel TJ, Jackson DJ, Baldwin RP, Keynton RS (2013) Amperometric techniques. Encyclopedia Microfluidics Nanofluidics 2013:1–11. doi:10.1007/978-3-642-27758-0_26-2

Rucki RJ (1980) Electrochemical detectors for flowing liquid-systems. Talanta 27(2):147–156. doi:10.1016/0039-9140(80)80029-4

Ruiz-Matute AI, Hernandez-Hernandez O, Rodriguez-Sanchez S, Sanz ML, Martinez-Castro I (2011) Derivatization of carbohydrates for GC and GC-MS analyses. J Chromatogr B Anal Technol Biomed Life Sci 879(17-18):1226–1240. doi:10.1016/j.jchromb.2010.11.013

Santos AL, Takeuchi RM, Fenga PG, Stradiotto NR (2011) Electrochemical methods in analysis of biofuels. In: Ivanov O (ed) Applications and experiences of quality control, 1st edn. InTech, Rijeka, pp 451–494

Sluiter JB, Ruiz RO, Scarlata CJ, Sluiter AD, Templeton DW (2010) Compositional analysis of lignocellulosic feedstocks. 1. Review and description of methods. J Agric Food Chem 58(16):9043–9053. doi:10.1021/jf1008023

Snyder LR, Kirkland JJ, Dolan JW (2010) Introduction to modern liquid chromatography, 3rd edn. Wiley & Sons, Hoboken, NJ

Stagge S, Cavka A, Jonsson LJ (2015) Identification of benzoquinones in pretreated lignocellulosic feedstocks and inhibitory effects on yeast. AMB Express 5:61. doi:10.1186/s13568-015-0149-9

Sun F, Sun Q (2015) Current trends in lignocellulosic analysis with chromatography. Ann Chromatogr Sep Tech 1(2):03

Swartz ME (2005) UPLC (TM): an introduction and review. J Liq Chromatogr Relat Technol 28(7-8):1253–1263. doi:10.1081/jlc-200053046

Swartz ME, Krull IS (2012) HPLC method development and optimization with validation in mind. In: Swartz ME, Krull IS (eds) Handbook of analytical validation, 1st edn. Taylor & Francis Group, Boca Raton, FL, pp 37–60

ThermoScientific (2016) HPLC method development calculator. http://www.hplctransfer.com/. Accessed Jan 2016

Valliyodan B, Shi H, Nguyen HT (2015) A simple analytical method for high-throughput screening of major sugars from soybean by normal-phase HPLC with evaporative light scattering detection. Chromatogr Res Int 2015:8. doi:10.1155/2015/757649

van Haveren J, Scott EL, Sanders J (2008) Bulk chemicals from biomass. Biofuels Bioprod Biorefin 2(1):41–57. doi:10.1002/bbb.43

Vaz S Jr, Dodson JR (2014) Application of analytical chemistry in the production of liquid biofuels. In: Domingos Padula A, Silveira dos Santos M, Benedetti Santos OI, Borenstein D (eds) Liquid biofuels: emergence, development and prospects, vol 27. Springer, London, pp 173–187

Wang Y-H, Avula B, Fu X, Wang M, Khan IA (2012) Simultaneous determination of the absolute configuration of twelve monosaccharide enantiomers from natural products in a single injection by a UPLC-UV/MS method. Planta Med 78(8):834–837. doi:10.1055/s-0031-1298432

Waters (2016) Increase productivity and reduce solvent consumption with UPLC. http://www.waters.com/waters/promotionDetail.htm?id=10102140&locale=pt_BR. Accessed Jan 2016

Weber SG, Purdy WC (1981) Electrochemical detectors in liquid-chromatography – a short review of detector design. Ind Eng Chem Prod Res Dev 20(4):593–598. doi:10.1021/i300004a003

Webster GK, Jensen JS, Diaz AR (2004) An investigation into detector limitations using evaporative light-scattering detectors for pharmaceutical applications. J Chromatogr Sci 42(9):484–490. doi:10.1093/chromsci/42.9.484

Werpy T, Petersen G (2004) Top value added chemicals from biomass: volume I – results of screening for potential candidates from sugars and synthesis gas, 1st edn. States, United

Westereng B, Agger JW, Horn SJ, Vaaje-Kolstad G, Aachmann FL, Stenstrøm YH, Eijsink VGH (2013) Efficient separation of oxidized cello-oligosaccharides generated by cellulose degrading lytic polysaccharide monooxygenases. J Chromatogr A 1271(1):144–152. doi:10.1016/j.chroma.2012.11.048

Wettstein SG, Alonso DM, Gurbuz EI, Dumesic JA (2012) A roadmap for conversion of lignocellulosic biomass to chemicals and fuels. Curr Opin Chem Eng 1(3):218–224. doi:10.1016/j.coche.2012.04.002

Xu J, Chen D, Yan X, Chen J, Zhou C (2010) Global characterization of the photosynthetic glycerolipids from a marine diatom Stephanodiscus sp. by ultra performance liquid chromatography coupled with electrospray ionization-quadrupole-time of flight mass spectrometry. Anal Chim Acta 663(1):60–68. doi:10.1016/j.aca.2010.01.026

Xu Y, Fan L, Wang X, Yong Q, Yu SY (2013) Simultaneous Separation and Quantification of Linear Xylo- and Cello-Oligosaccharides Mixtures in Lignocellulosics Processing Products on High-Performance Anion-Exchange Chromatography Coupled with Pulsed Amperometric Detection. Bioresources 8 (3):3247–3259

Yu K, Little D, Plumb R, Smith B (2006) High-throughput quantification for a drug mixture in rat plasma – a comparison of ultra performance (TM) liquid chromatography/tandem mass spectrometry with high-performance liquid chromatography/tandem mass spectrometry. Rapid Commun Mass Spectrom 20(4):544–552. doi:10.1002/rcm.2336

Zhou X, Cao S, Li X, Tang B, Ding X, Xi C, Hu J, Chen Z (2015) Simultaneous determination of 18 preservative residues in vegetables by ultra high performance liquid chromatography coupled with triple quadrupole/linear ion trap mass spectrometry using a dispersive-SPE procedure. J Chromatogr B 989:21–26. doi:10.1016/j.jchromb.2015.02.030

Chapter 9
Chemical Analysis and Characterization of Biomass for Biorefineries

Luz Marina Flórez-Pardo and Jorge Enrique López-Galán

Abstract The aim of this chapter is to offer different chemical analyses and characterization options for researchers or whoever is looking for an appropriate methodology to analyze results obtained in laboratory tests, especially assuming the challenge to find the best process to achieve bio-products under biorefinery concept. In this way, the information provided will be very useful to evaluate the results and moreover, to improve the research process. That is the reason why analytical techniques to characterize different lignocellulosic biomass are described with detailed data about its principles and methodology, emphasizing either physical or chemical protocols that are followed normally in research laboratories. Taking into account that lignin, cellulose, and hemicelluloses are the principal compounds of these kinds of raw materials, which in general are residues, the information is emphasized with that target of analysis. Nevertheless, as it is possible to obtain a lot of bio-products from biomass, like sugars, alcohols, aromatics, biopolymers and so on, other analytical methods are included.

Keywords Gravimetric analysis • Compositional analysis • Chemical characterization

9.1 Generalities

9.1.1 Types of Biomass

Biomass is all organic matter produced by the process of photosynthesis where many molecules are synthesized by sunlight. These molecules fulfill a specific function within the plant and denote high contents of chemical energy. Every year, about

L.M. Flórez-Pardo (✉)
Department of Energy and Mechanics, Autónoma of Occidente University, Calle 25 # 115-85, Cali, Colombia
e-mail: lmflorez@uao.edu.co

J.E. López-Galán
School of Chemical Engineering, University of Valle, Calle 13 # 100-00, Cali, Colombia
e-mail: jorge.lopez@correounivalle.edu.co

S. Vaz Jr. (ed.), *Analytical Techniques and Methods for Biomass*,
DOI 10.1007/978-3-319-41414-0_9

2.2×10^{11} dry tons of biomass (Oliva Domínguez 2015) is produced and can supply the demand for global energy, overtaking it about 9 times. It can be categorized according to its origin (Ballesteros et al. 2001) in *natural, residual*, and from *energy crops* as described below.

- Natural biomass: refers to biomass that is generated naturally in each ecosystem. Because it has not undergone any transformation and in order to maintain the habitats where it grows, this type of biomass is not considered suitable to be harnessed for energy or industrial purposes.
- Residual biomass: consists of organic residues generated after natural biomass is transformed. It is classified according to its origin as follows:
  - Agricultural residues such as those generated from *woody and herbaceous* crops, as residues obtained from periodic and annual pruning of coffee and sugar cane, cereal crops (straw, leaves, seed husks, etc.), cane (leaves and tops), palm (leaves, racemes, husks, etc.), hay, rice (straw, husks), and corn (stem, leaves, husk, silk, and tassel), among many others.
  - Forest residues arising from treatments, interventions, and/or forest improvements. In this category, forest residues that can be highlighted are pruning residues, commercial trees with imperfections or trees that need to be cut down that are close to fire zones or that are ill. Also, sawdust and other residues from the production of wood tables.
  - Agroindustrial residues: are the ones originated from papermaking (pulp, process residues), juices (husks, pulp), sugar (bagasse), and from oil extraction (fibers, palm seeds), etc. Household waste is also relevant, especially the ones generated in food storage centers, market places, and administrative facilities of companies, where meaningful quantities of paper waste are generated.
- Biomass energy crops: in this category is the biomass that comes from crops whose purpose is its use for energy production. Two subdivisions can be highlighted within this category: woody crops and fast-growing annual crops of vegetables (Oliva Domínguez 2015).

The biomass type with the greatest potential of use corresponds to the residual origin. This material is a source of energy and can be employed in the field of building materials and in the pharmaceutical, cosmetology, nutraceutical, food, biofuels, and chemical industry. Unlike oil, this biomass can be found everywhere in the world where the conditions for its production are given; it is renewable and has high contents of oxygen.

9.1.2 Biomass Composition

Biomass forms different structures within a plant: roots, stems, leaves, flowers, and fruits. Each of these structures meets different functions in the plant and therefore, the composition is very heterogeneous. They also change between species and

within the same plant and are composed primarily by water, soluble substances (sugars, organic acids), pectin, fiber, lipids, and proteins. The heterogeneity is seen for example, in the study by Cardoen et al (2015), who evaluated the composition of carbon, hydrogen, oxygen, and nitrogen from residues of more than 22 species of plants grown in India. Table 9.1 shows the significant differences in composition between species and between components of the same plant. It is noted how the carbon content in these biomasses is around 30.4 % for corn stalks, mustard and onion and 52.3 % for coconut husk. The next component in greater composition is oxygen. The oily substances from coconut and peanut have a higher content of this component with 63.5 % and 59.9 %, respectively. In the lower range, water hyacinth (34 %) and rice husk (35.9 %) are found. Hydrogen is between 2 and 8.8 %. Other features that may affect this characterization in addition to the ones already stated are the growing conditions, plant growth, soil and agro-climatic characteristics, age,

Table 9.1 Moisture content and elemental analysis of several biomass samples

Crop name (s)	Residue name	Moisture content at in harvest/ production %)	Moisture content in dried air (%)	C (%)	H (%)	O (%)	N (%)
Banana	Leaves, pseudostems						
Banana	Peels	84					1.06
Cabbage	Stem and leaves	85					
Chickpea	Stalks	20	10				0.80
Chickpea Coconut	Husk Fronds	20	10	48.6[a]	5.8[a]	42.4[a]	0.80
Coconut	Husk	20	10				
Coconut	Shell	20	4.4	52.3	6.6	39.5	0.30
Coconut	Meal/oil cake	7		15.9	2.3	63.5	0.50
Coconut	Coir pith			50.3	5.1	39.6	0.45
Cotton	Stalks	20	10	41.5	6.2	47.5	1.81
Cotton	Hull/Boll shell		7	50.4	8.4	39.8	1.40
Cotton Cotton	Gin trash Meal/oil cake	5		42.7	6.1	49.5	0.18 6.45[b]
Eggplant	Stalks	85					
Groundnut	Stalks	30	10				1.60
Groundnut	Shell	30	8	33.9	2.0	59.9	1.10
Groundnut	Meal/oil cake	10					8.00
Maize/corn	Stover	60	10	46.9	5.5	45.0	0.56
Maize/corn	Cobs	50	10	41.4	6.0	51.3	0.14
Maize/corn Mango	Corn fiber/grain hull Pruning wood Pruning wood	50		47.4[a]	6.1	44.4	0.60
Mango	Peels	80		46.4[a]	5.8[a]	43.1[a]	

(continued)

Table 9.1 (continued)

Crop name (s)	Residue name	Moisture content at in harvest/ production %)	Moisture content in dried air (%)	C (%)	H (%)	O (%)	N (%)
Mango	Seed	45	13	47.8[a]	5.8[a]	43.1[a]	0.85[b]
Mango	Meal/oilcake	10					0.96[b]
Mustard	Stalks	20	10	33.7	3.9		0.67
Mustard	Seedpod	20	5.6	44.3	8.8	43.0	0.38
Mustard	Meal/oilcake e	10		50.2	6.9		5.05
Onion	Stalks	85					
Paddy/rice	Straw	30	10	36.0	5.3		0.70
Paddy/rice	Husk	30	10	36.4	4.9	35.9	0.59
Paddy/rice Paddy/rice	Bran De-oiled bran			38.9	5.1	36.8	0.55 2.88[b]
Pearl millet	Stalks	30	10				0.70
Pearl millet	Cobs	30	10				0.70
Pearl millet	Husk	30	10				0.70
Pigeon pea	Stalks	20	10	38.1	6.2	53.8	1.01
Pigeon pea	Husk	20	10				0.80
Potato	Stalks	60					1.90
Sorghum	Stalks	30	10				0.77
Sorghum	Cobs	30	10				0.77
Sorghum	Husk	30	10				0.77
Soybean	Stalks	50	10				0.80
Soybean	Husk	9	6.3	43.1	6.4	44.5	0.80
Soybean	Meal/oilcake	11					7.60[b]
Sugarcane	Tops and leaves	60	10	39.8	5.6	46.8	1.70
Sugarcane	Bagasse	50		48.6	5.9	42.8	0.16
Sugarcane	Depithed bagasse	50		46.1	6.5	46.0	0.41
Sugarcane	Press mud/filter cake			30.4[a]	3.8[a]	28.7[a]	2.00
Sugarcane Cassava Cassava	Molasses Peels Fibrous residue/ bagasse	20.6 75	11.2				0.51[b] 0.84[b] 0.25[b]
Cassava	Stalks/hay		10				1.90
Tomato	Stems	85					4.80
Water hyacinth Agua de jacinto	Whole	90		40.3	4.6	34.0	1.51
Wheat	Straw	20	10	44.9	5.5	41.8	0.44
Wheat	Chaff	20	10				
Wheat	Bran	20	10				

Source: Adapted from Cardoen et al. (2015)

but also the techniques used in this quantification of the different components (Szcrbowski et al. 2014).

It is important to understand how the biomass is chemically constituted in order to set the techniques for its chemical characterization. Biomass consists primarily of cells, which have a cell wall containing the cytoplasm with its organelles and nuclei. The cell wall has primary swellings (primary wall) or secondary (secondary wall) depending on the type of structure that is forming. The primary is rich in hemicellulose and pectin with some cellulose and lignin. Instead, the secondary are richer in cellulose and lignin. The cement that binds a cell with another in the middle lamella is pectin.

9.1.2.1 Cellulose

Cellulose is a lineal carbohydrate with crystalline structure and a molecular formula $(C_6H_{10}O_5)_n$ (in ranges from 1000 to 5000) and is composed of β-D-glucose units in pyranose shape, which can be broken into glucose units by hydrolysis (Bian et al. 2014). Its structure is organized by hydrogen bonding between hydroxyl groups of different juxtaposed glucose chains offering impermeability to water, making it insoluble in this solvent and thus, forming compact fibers that make up the wall structure in plant cells which becomes into a relevant property to this polymer. The distribution of these fibers may be different at the levels of the secondary wall favoring it with great strength. Since this polymer is the major component of the cell wall in vascular plants (Bhattacharya et al. 2008), it becomes the most abundant molecule in plants. Thanks to this abundance, this molecule is in a lot of manufactured products like paper, building, and textile materials made form fibrous plants such as cotton and linen.

9.1.2.2 Hemicellulose

It is a heterogeneous branched polymer with molecular formula $(C_6H_{10}O_5)_n$ or $(C_5H_8O_4)_n$ and is present in the cell walls with amorphous or paracrystalline distribution. The structure contains amorphous polymers, such as pentoses, hexoses, deoxyhexoses, and uronic acids, which form a branched straight chain. In addition, other polysaccharides like xylan, arabinoxylans, galactomannans, glucuroarabinoxilanes, glucomannan, and xyloglucan can be found. With regards to the structural characteristics of this polymer, the following can be mentioned (Martín-Lara 2008):

- Hemicellulose consists of a sugar chain linked by β-(1-4) bonds assuming the shape of a backbone with branches of one or two types of sugar (xylan, mannan, galactan, glucan, glucuronoxylan, galactoglucomannan, etc.).
- It cannot generate aggregates unlike cellulose due to the structure. Yet, hemicellulose can join the cellulose chains by building hydrogen bonds.
- It degrades easily by having short chain branching (Fengel and Wegener 1984).

– Additionally, hemicellulose is in charge of binding lignin with cellulose and has little resistance to hydrolysis or heat.
– Following cellulose, this polymer is found most abundantly in the cell wall of plants.

9.1.2.3 Lignin

Lignin is a tridimensional (Higuchi 1985; Boerjan et al. 2003) aromatic polymer with molecular formula $(C_9H_{10}O_2(OCH_3)_n)$. It is formed by dehydrogenation of enzymes from the phenylpropilic alcohols (coumaryl, coniferyl, and sinapyl) first, and then, by polymerization causing different types of distribution among its components and determining that lignin has no single structure due to lack of enzyme control and free radicals reaction that react together (Turrel and Fisher 1942). In cell growth, this rigid and hydrophobic substance is adhered to the cell wall by filing the empty spaces between the cellulose fibrils joining covalently to the matrix of polysaccharides. Lignin is part of the secondary cell walls of plants generating a resistant structure difficult to degrade. This polymer provides support to the structure of plant tissues and due to the chemical composition, protects against humidity and/or attack of atmospheric organisms and mechanical stress. It also acts as a type of fiber binder (Sarkanen and Ludwig 1971)

After cellulose and hemicellulose, lignin is the non-carbohydrate component found in higher quantities on cell walls and on the surface (Buranov and Mazza 2008).

9.1.2.4 Pectin

Pectic substances are linear molecules of galacturonic acid (α-D-1,4-galacturonan), with insertions at certain intervals of rhamnose units (α-L rhamnosil residue), where side chains emerge rich in neutral sugars (hairy regions). These side chains are attached by glycosidic linkages to the carbon atoms 3 and 4 of rhamnose units and to the atoms 2 and 3 of the galacturonic acid units. The predominant sugars depend on the structure of the pectin where the most important are D-galactose, L-arabinose, and xylose (Pilnik and Voragen 1993). Pectin contributes to offer mechanical strength, porosity, adhesion, and rigidity to the cell wall. They are mostly found in the middle lamella and the primary walls of upper plants.

9.1.2.5 Other Components

Other components are constituted of proteins, ash, lipids and solubles (sugars and organic acids), as well as waxes and gums.

9.2 Chemical Analysis of the Major Components of the Cell Wall

As mentioned in Sect. 9.1, the chemical characterization of biomass is complex due to the factors that affect its structure: type of tissue within plants, age of crop, type of soil, variety, agro-climatic growing conditions, etc. Szcrbowski et al. (2014) observed these factors thoroughly on sugar cane bagasse and cane straw. They found that tilage, soil, and weather factors are probably the main reasons why there is a wide range of differences in reporting the chemical composition of both residues. Additional methods used in the characterization of biomass also influence as follows: (a) the use of free-contaminant extractives for lignin analysis, (b) the degree of removal of extractives during treatment with different solvents, (c) proper quantification of minor components, such as pectin and proteins, (d) the use of HPLC columns with different resolutions for monosaccharides analysis, and (e) applying suitable hydrolysis factors to consider sugar losses due to dehydration. Therefore, there is no 100 % method approved by the scientific community to study its composition. The methods that have been most accepted are the following.

9.2.1 Methods for Extractives Extraction

9.2.1.1 Characterization of Soluble Extractives in Water

There are several methods to extract water-soluble compounds, among them are:

- Soxhlet method.
- Liquid–liquid extraction (Golander 2011).
- Cold water-solubility method (ASTM D1110-84 2013).
- Hot water-solubility method (Szcrbowski et al. 2014).
- Ultrasound-assisted extraction (Luque de Castro and García-Ayuso 1998).
- Microwave-assisted extraction (Golander 2011).

Soxhlet has been the standard technique for over a century and is referent to be compared against other modern extraction techniques (Luque de Castro and Priego-Capote 2010). Furthermore, this method has various advantages since the sample is contacted repeatedly with fresh solvent portions, which contributes to shift the equilibrium of transfer. On the other hand, the system temperature remains relatively high because the heat applied to distillation reaches the extraction unit. Also, it is not necessary to filter at the end of extraction. The equipment is basic and thus, economic. It is a very simple methodology that requires little specialized training and has the ability to extract more compounds from the sample than the majority of modern methods (microwave extraction for example) (Luque de Castro and García-Ayuso 1998).

Principles

Soxhlet extraction is based on the following steps: (1) Solvent-location in a flask. (2) Solvent boiling which is evaporated to a reflux condenser. (3) Formation of condensate falling on a vessel containing a porous cartridge with the sample therein. (4) Solvent level rise covering the cartridge until a point that reflux occurs. (5) The process is repeated as necessary until the sample is exhausted.

The technique relies on the extraction of water-soluble compounds (solvent used). Soxhlet is considered a continues–discontinuous hybrid technique since the solvent is involved in several cycles and each complete cycle is appreciated as a bath type system. At the same time, the solvent offers the system a continuous character when it recirculates. On the other hand, because water is in prolonged contact with the sample, it allows the extraction of compounds that solubilize therein like secondary metabolites and those that store energy which are critical for photosynthesis and plant growth (sucrose and pectin) (Szcrbowski et al. 2014). In addition, sugars like glucose and fructose can be found. The fact that these compounds are extracted is attributed to the polar character for both the extractant and the metabolites. An analytical technique well known as Fourier transform infrared spectroscopy (FTIR) identifies such metabolites extracted due to the pronounced vibration band corresponding to the molecular hydroxyl groups (–OH). This technique will be analyzed in more detail in Sect. 9.2.2.6. For spectroscopic analysis see Sect. 9.2.2.6.

Methodology

The procedure for performing compound extraction by Soxhlet method takes as reference the protocol "Technical Report NREL/TP-510-42619 January 2008: Determination of Extractives in Biomass" (Sluiter et al. 2008a) and is as follows.

The ground sample must consist of 8–20 g, obtained in such a way that it is representative of the entire batch of material. It is required at least 8 g of the sample to do the complete analysis. The sample must be divided into smaller fragments with certain periodicity. In the case of dry lignocellulosic biomass, the material must be ground until it passes through the mesh 40 (Tappi T 264 om-82).

Preparing Sample for Extraction

1. The moisture content of a sample of biomass can change quickly when it is exposed to air. Therefore, samples have to be weighed in order to determine the total amount of solids (Sect. 9.4), and also extractives at the same time and thus, prevent errors due to humidity changes.
2. Dry the flat bottom ball in an oven at 105 ± 5 °C for a minimum of 12 h. Then, it is removed and allowed to adapt to room temperature by placing it in a desiccator. After that, boiling stones are added and the weight of the ball is registered.
3. Add 2–10 g of the sample to an extraction cartridge (cellulose thimble) that has been weighed and tared previously. Record the weight to the nearest 0.1 mg. The amount of sample needed depends on the bulk density of the biomass.

The height of the biomass present in the cartridge must not exceed the height of the siphon of the Soxhlet extraction tube. If the height of the biomass surpasses the height of the siphon, the extraction will be incomplete.

4. Add solvent (water) to fill the flask until half of its capacity. Insert the cartridge into the Soxhlet extraction tube. Assemble the equipment and turn on. Adjust the heating mantle to provide a minimum of 4–5 siphon cycles per hour.
5. Reflux for 6–24 h. The reflux time required will depend on the rate of elimination of the compounds of interest, the temperature of the capacitors, and the flow rate in the siphon. When the sample of biomass is exhausted, turn off the equipment. Dry the cartridge with the sample. The weight difference between the initial and the final weight divided by the initial weight of biomass gives the percentage of solubles extracted in water. Note that the weight of the dry cartridge has to be subtracted to the final weight of the biomass.

9.2.1.2 Analysis of Soluble Extractives in Solvents

There are diverse methods to extract soluble compounds in solvents similar to the ones mentioned previously (Sect. 9.2.1.1), where the most relevant are the following:

– Soxhlet method.
– Liquid–Liquid extraction.
– Ultrasound-assisted extraction.
– Microwave-assisted extraction.

In this case, Soxhlet is also the most common technique applied in the extraction of compound solubles in solvents because it has great resilience of solutes and simpler instrumentation. The solvent and sample are in intimate and repeated contact, so that the extraction improves greatly due to the constant use of a clean solvent, ensuring optimal performance. The organic solvent is evaporated leaving the solutes upon completion of the process.

Principles

The principle of the method is the same as is used to extract water-soluble compounds. In this case, what changes is the use of organic solvents. Soxhlet extraction has the following steps: (1) location of the solvent in the flask. (2) Solvent boiling, which evaporates to a reflux condenser. (3) Formation of condensate falling on a vessel containing a porous cartridge with the sample therein. (4) The level of the solvent rises covering the cartridge to a point that reflux occurs by the siphon, which is done with solvent extracted by the reflux sidearm system. (5) The process is repeated as many times as necessary until the sample is exhausted.

Table 9.2 Extractant used to solubilize polar and nonpolar compounds

Raw material	Extractant	Conditions	Results (%)	References
Bagasse	Ethyl ether Dichloromethane Ethanol:toluene 1:2 Ethanol 95 % v/v Water	Soxhlet extraction. Reflux for 1 h	9.0 1.0 12.0 2.2 11.5	Szcrbowski et al. (2014))
Bagasse	Hexane	Soxhlet extraction. Reflux for 4 h	0.53	Attard et al (2015)
Bagasse	Water	Soxhlet extraction. Reflux for 3 h	1.3	Del Río et al (2015)
Straw	Ethyl ether Dichloromethane Ethanol:toluene 1:2 Ethanol 95 % v/v Water	Soxhlet extraction. Reflux for 1 h	11.5 1.5 12.2 2.5 36.0	Szcrbowski et al. (2014))
Straw	Water	Soxhlet extraction. Reflux for 3 h	2.1	Del Río et al (2015)
Leaves	Hexane	Soxhlet extraction. Reflux for 4 h	1.60	Attard et al. (2015)
Peel	Hexane	Soxhlet extraction. Reflux for 4 h	0.8	Attard et al (2015)
Chlorella vulgaris (microalgae)	Cloroform:methanol 1:2	Soxhlet extraction. Reflux for 6 h	20.22	Pérez and Quishpi (2014)
Olive Pomace	*n*-Hexane	Soxhlet extraction. Reflux for 4 h	2.14	García Sánchez et al (2005)
Olives	*n*-Hexane	Soxhlet extraction. Reflux for 4 h	24.58	García Sánchez et al. (2005)

Results in % m/m

Various organic solvents have been used as shown in Table 9.2. It can be seen as the nonpolar compounds are extracted by ethanol/toluene, hexane, and chloroform-methanol. The latter mixture is the most widely applied, because it has the ability to extract lipids, fatty acids, and sterols. This mixture combines the ability from ethanol, which consists in penetrating the tissue with the power of chloroform in order to dissolve fat.

Methodology

The reference used is the protocol "Technical Report NREL/TP-510-42619 January 2008: Determination of Extractives in Biomass" (Sluiter et al. 2008a). The most specific method for performing extractions of compounds by Soxhlet is shown below. However, in characterization of water-soluble extractives the methodology for Soxhlet is explained in detail (Fig. 9.1).

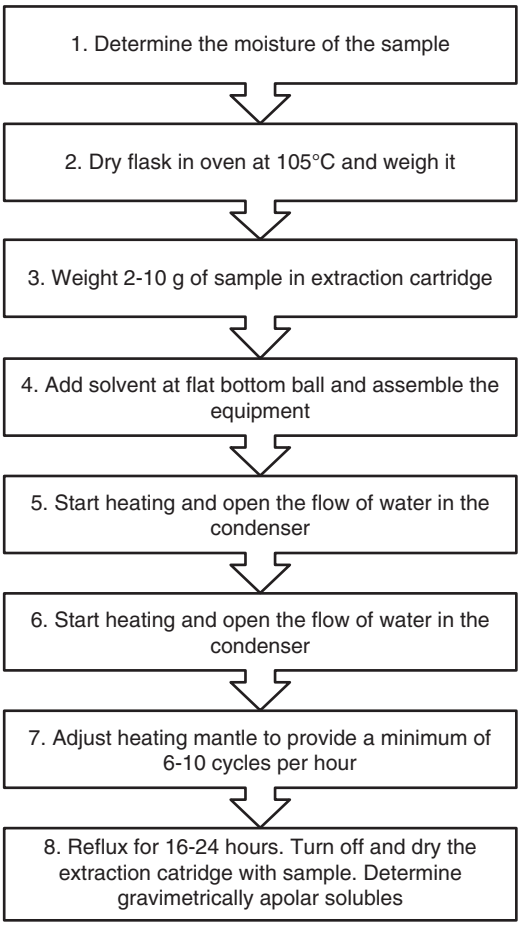

Fig. 9.1 Flow chart for water-soluble extraction by Soxhlet method

9.2.2 Analysis of Polysaccharides (Cellulose and Hemicellulose)

Hemicellulosic and cellulosic chains are joined together by internal attractive forces through the carboxyl and hydroxyl functional groups of the macromolecules of cellulose and hemicelluloses (Cataño Rueda 2009). The characterization of these polysaccharides is done through various chemical methods already established as mentioned bellow.

9.2.2.1 Van Soest Method

Principles

The Van Soest method is widely used because it measures separately cellulose, hemicellulose, and lignin. It is based on the digestion of a sample in a neutral detergent solution. The soluble fraction is cell content (CC) and the residual fraction is called neutral detergent fiber (NDF), which are cell walls. Once DC and NDF are separated, the solid residue is treated with a solution of acid detergent composed by bromide trimethyl-acetyl-ammonium in 1 mol/L sulfuric acid. The intention of this treatment is that hemicellulose can be solubilized while in the insoluble fraction, called acid detergent fiber (ADF), cellulose, lignin, and cutin remain. Once NDF is obtained, the percentage of cellulose is determined with sulfuric acid treatment. The final fractions are, on the one hand, cellulose (that is extracted), and on the other, lignin-cutin-ash residue. This residue is treated to obtain lignin employing permanganate treatment. Cutin-mineral residues that remain are incinerated in order to obtain the percentage of cutin.

Methodology

The methodology described below is based on AOAC 973.18 (1995) and AOAC 2002.04 (2002). Both the analysis NDF and ADF can be performed directly, or can be performed sequentially. The sequential method has the advantage of obtaining all the results from a single sample, although the values obtained for the second analysis may not be exactly comparable to those achieved with the same analysis done directly.

Procedure

Figure 9.2 shows the components in a Fibertest.

It is important to illustrate the way to prepare the reactives in order to perform the procedure:

ND: Neutral detergent

Sodium lauryl sulfate	30 g/L
Ethylene diamine tetra-acetic acid (EDTA) anhydrous	18.6 g/L
Borate decahydrate sodium	6.8 g/L
Disodium hydrogen phosphate anhydrous	4.6 g/L
2-Ethoxyethanol	10 mL
Distilled water	Up to 1000 mL

Mix sodium borate and EDTA in a beaker of 2 L. Add distilled water, heat to dissolve. Add the lauryl sulfate. Weigh disodium phosphate and add distilled water in another flask, heat the solution until it is completely dissolved. Mix the solutions, add 2-ethoxyethanol to limit foaming. Check the pH value is between 6.9 and 7.1.

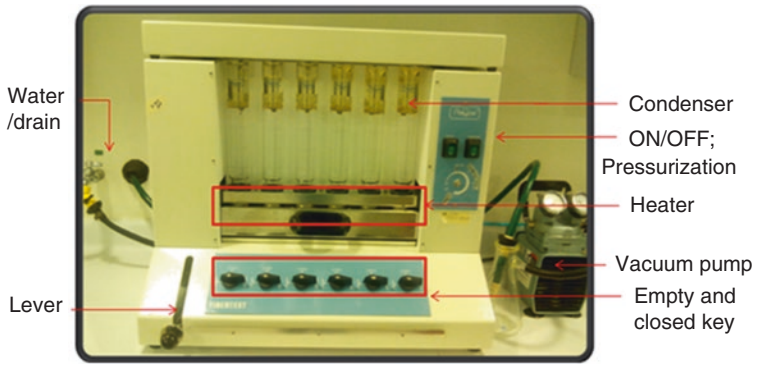

Fig. 9.2 Digestor for polysaccharides analysis

ADS: Acid detergent

Cetyl trimethyl ammonium bromide	20 g/L
Sulfuric acid 1 mol/L	1 L
Dissolve 20 g of cetyl trimethyl ammonium bromide in the sulfuric acid	1 mol/L

Amylase solution

Alpha-amylase (density: 1.13 g/mL)	2 g
Ethoxyethanol	10 mL
Distilled water	To fulfill 1 L

Dissolve 2 g of amylase in distilled water and adjust with ethoxyethanol. Keep the solution at 5 °C.

Sulfuric acid at 72 %

Dilute 750 mL of acid (96 % concentration) in water slowly to make 1 l of solution.

Note: The reaction is strongly exothermic, so it is recommended to be in a cold water bath.

(a) Sample preparation: Remove the solubles of the sample (see Sects. 9.1.1 and 9.1.2). Use the ethanol to extract apolar solubles as recommended by the NREL (Sluiter et al. 2008c). Dry at 60 ± 3 °C for 18 h and determine the moisture of the sample.
(b) Crucible preparation: wash and let the crucible submerged in a sulfochromic solution for 8 h, then rinse and dry. Weigh the dried crucible with a smaller difference of 0.1 % (weight = *P*0).
(c) Weigh 1 g of the sample in the crucible with a minor difference of 0.1 % (taking weight as *E*).
(d) Fiber digestion: to locate the crucible in fibertest: lift the lever and locate the crucible in the heating zone below the glass column. Then, pull down the lever. Verify the crucible is pressed to the system.
(e) Open the water stopcock that feeds the cooling system over the columns avoiding high water pressure.

(f) Add 50 mL of neutral detergent solution (NDS) at the top of the columns, turn the equipment on and set the temperature of the heater. Once boiling point is reached, count 30 min.

Note: The boiling should not be violent to prevent the material sticking up on the walls of the columns.

(g) After 30 min, add another 50 mL of neutral detergent solution with 2 mL of alpha-amylase to solubilize the starch content in the sample. Boil for additional 30 min.
(h) After the heating is stopped, the keys are placed in a position to filter vacuum. The equipment must be connected to a vacuum and drain systems. Several washes with hot distilled water and acetone are made until foam is unnoticeable.
(i) Lift lever up to remove the crucible with the insoluble material. Heat the sample on the stove at 105 °C for 8 h or until constant weight. Then, cool the crucible with the sample in a desiccator for 20 min and weigh with a weight difference less than 0.1 % ($P1$).
(j) Place the crucible back on the fibertest and adjust to the columns.
(k) Add 50 ml of acid detergent solution (ADS) at the top of the columns, heat to boiling point, and count 1 h when boiling point is reached.
(l) Stop heating and wash with hot distilled water repeatedly until foaming runs out.
(m) Remove the crucible. Dry in the oven at 100 °C for 8 h or until constant weight. Then, place the sample in the desiccator for 20 min and weigh for a weight difference of less than 0.1 % ($P2$).
(n) After that, place the crucible in a glass container and add sulfuric acid at 72 % v/v to the sample to cover it. Shake and leave for 3 h.

Note: Do not allow a decrease on the level of sulfuric acid.

- Then, rinse with hot distilled water to remove sulfuric acid. A vacuum system can be used to facilitate washing.
- Heat the crucible with the sample at 100 °C in an oven for 8 h or until constant weight, followed by placing it in the desiccator for 20 min and weigh to obtain weight $P3$ with a minor difference of 0.1 %.
- In order to mineralize the sample, the crucible is carried muffle at 550 °C for 4 h followed by an hour in the oven at 100 °C.
- Finally, cool the sample down in the desiccator for 20 min and weigh to obtain the weight $P4$ with a minor difference of 0.1 %.

Calculi

$$\text{NFD} = \frac{P1 - P4}{E} \times 100 \tag{9.1}$$

$$\text{ADF} = \frac{P2 - P4}{E} \times 100 \tag{9.2}$$

$$\%\,\text{Hemi} = \frac{P1 - P2}{E} \times 100 \tag{9.3}$$

$$\%\,\text{Cel} = \frac{P2 - P3}{E} \times 100 \tag{9.4}$$

$$\%\,\text{Lig} = \frac{P3 - P4}{E} \times 100 \tag{9.5}$$

$$\%\,\text{Ce} = \frac{P4 - P0}{E} \times 100 \tag{9.6}$$

Note: NDF is neutral detergent fiber; FDA is acid detergent fiber; Hem is the hemicellulose fraction; Cel is cellulose; Lig, lignin; Ce, ash; and *E*, corresponds to the initial weight of the sample.

9.2.2.2 NREL Method (According to Sluiter et al. 2008a)

Principles

This protocol uses sulfuric acid hydrolysis in order to dissociate the polymeric forms of carbohydrates present in biomass into monomeric subunits. The function of the sulfuric acid is to hydrolyze glycosidic bonds to give monosaccharides. After the Oligo or monomers are quantified by high-performance liquid chromatography (HPLC). The HPLC method will be presented in Sect. 9.2.2.5.

9.2.2.3 Methodology

Sample Preparation for Analysis and Hydrolysis

1. Place a suitable number of filtering crucibles in muffle at 575 ± 25 °C for 4 h minimum. Remove the muffle crucibles and pass them directly to a desiccator. Allow to cool for about 1 h. Weigh crucibles and record. It is important to keep the melting pots in a specific order, if they are not marked properly. Do not mark the bottom of the pot, as this can prevent filtration.
2. Weigh 300.0 ± 10.0 mg of the sample or standard of quality control (standard sugars) in a pressure tube. Record the weight to the nearest 0.1 mg. This standard of quality control (standard sugar) ensures hydrolysis conditions are suitable for carrying out this process. Label the pressure tube with a permanent marker. Each sample is tested in duplicate.
3. Add 3.00 ± 0.01 mL (or 4.92 ± 0.01 g) of 72 % sulfuric acid to each pressure tube. Use a Teflon bar to stir the mixture for 1 min.
4. Place the pressure tube in a water bath at 30 ± 3 °C and incubate the sample for 60 ± 5 min. The sample is stirred every 5–10 min using the stirring bar, and

without removing the sample from the bath. Agitation is essential to ensure contact between the acid and the sample particles and thus, ensuring uniform hydrolysis.

5. After 60 min, remove the tubes from the water bath. Dilute acid at a concentration of 4 % by the addition of 84.00 ± 0.04 mL of deionized water. Dilution may also be done by adding 84.00 ± 0.04 g of purified water using a precision scale of 0.01 g. Cap the tube and shake in a vortex to eliminate phase separation between the layers of high and low acid concentration.

   Note: 86.73 mL will be the volume of sulfuric acid solution at 4 %.

6. Prepare a set of sugar recovery standards (SRS) that be will used during remaining process to correct losses due to the destruction of sugars during dilute acid hydrolysis. The SRS should include D-(+) glucose, D-(+) xylose, D-(+) galactose, L-(+) arabinose, and D-(+) mannose. Sugar concentrations in the SRS should be chosen to resemble more closely at concentrations of sugars in the sample tested. Weigh the necessary amounts of each sugar, with accuracy of 0.1 mg, and add 10,0 mL of deionized water. Add 348 μL of sulfuric acid at 72 %. Transfer SRS to a pressure tube and cover.

A fresh solution of SRS is not required for each analysis. Large quantities of SRS can be prepared: the solution is filtered through 0.2 μm filters and dispensed in aliquots of 10.0 mL storing it in sealed and labeled containers. They can be stored in a freezer. When required, thaw and shake the frozen SRS before use.

7. Place the tubes in a safety rack and then in the autoclave. Autoclave the sealed samples and sugar recovery standards for one hour at 121 °C. Allow the hydrolyzate to slowly cool down at room temperature before removing caps from pressure tubes after completion of the autoclave cycle.

Note: To deepen in the analysis of the hydrolyzed sugars, see Sect. 9.2.2.5. If the hydrolyzate obtained determines insoluble and soluble lignin in acid, take only 1 mL for characterization by HPLC.

Sample Analysis of Acid Insoluble Lignin (According to Sluiter et al. 2008a)

1. Vacuum filter the previous hydrolysis solution through preweighed filtering crucibles. Capture filtering in a filter flask.
2. Transfer an aliquot of about 50 mL in a sample storage bottle. This sample is used to determine acid soluble lignin and carbohydrates, and acetyl if necessary. Determining acid soluble lignin must be done within 6 h following the completion of the hydrolysis. If the hydrolysis liquor should be stored, this must be done in a refrigerator for up to 2 weeks. It is important to collect the aliquot of liquor before proceeding to the next step.
3. In order to transfer all solids remaining in the pressure tube quantitatively to the filter crucible, use deionized water. Rinse the solids with a minimum of 50 mL fresh deionized water. Hot deionized water can be used instead of water at room temperature to reduce filtration time.
4. Dry the crucible with the acid insoluble residue at 105 ± 3 °C to constant weight, for at least 4 h.

5. Remove samples from oven and let cool in a desiccator. Record the weight of the dry residue nearest to 0.1 mg.
6. Place the crucibles with the residues in the muffle at 575 ± 25 °C for 24 ± 6 h. The muffle can be used with a temperature ramp:
   Programming the muffle furnace temperature:

   - Ramp from room temperature to 105 °C.
   - Temperature remains at 105 °C for 12 min.
   - Ramp to 250 °C at 10 °C/min.
   - Temperature remains at 250 °C for 30 min.
   - Ramp to 575 °C at 20 °C/min.
   - Temperature remains at 575 °C for 180 min.
   - Temperature drops to 105 °C.
   - Temperature remains 105 °C until the samples are removed.

7. Remove the crucible carefully from the oven directly into a desiccator and let cool down for a specific amount of time, which is equal to the initial cooling time of the crucibles when empty. Weigh the crucibles with ashes to the nearest 0.1 mg and record the weight.

Acid-soluble Lignin Sample Analysis

1. Place deionized water or 4 % sulfuric acid in a UV-visible spectrophotometer as a target.
2. After filtration of the hydrolyzate, use an aliquot of liquor hydrolysis obtained during the process. Measure the absorbance of the sample at a suitable wavelength (for bagasse, radiata pine and black poplar, the wavelength recommended is 240 nm; while for corn stover is 320 nm). Dilute sample as necessary for the absorbance is within range 0.7–1.0. Deionized water or 4 % sulfuric acid can be used to dilute the sample, although the same solvent has to be used as the target. Read the absorbance with three decimal places. Analyze each sample at least twice. (This step must be done within 6 h after hydrolysis.)

Calculi

- Calculation of dry weight in oven (ODW)

$$\text{ODW} = \frac{\text{Weight of dry sample} \times \%\,\text{total solids}}{100} \tag{9.7}$$

- Calculation of the percentage of acid-insoluble residue (AIR) and for acid-insoluble lignin (AIL)

$$\%\text{AIR} = \frac{\text{Weight of crucible with AIR} - \text{Weight of empty crucible}}{\text{ODW of the sample}} \times 100 \tag{9.8}$$

$$\%\text{AIL} = \frac{\begin{array}{l}\text{Weight of crusible with AIR} - \text{Weight of empty crusible} \\ -\left(\left(\text{Weight of crusible with ash}\right) - \text{Weight of empty crusible}\right) \\ -\text{Weight of protein}\end{array}}{\text{ODW of the sample}} \times 100$$

where:

the weight of the protein is the amount of protein present in the acid-insoluble residue. This quantity is necessary for biomasses that contain high amounts of protein.

- Calculation of acid-soluble lignin (ASL)

$$\%\text{ASL} = \frac{\text{UV}_{\text{abs}} \times \text{Volume}_{\text{filtrated}} \times \text{Dilution}}{\varepsilon \times \text{ODW} \times \text{cell length}} \times 100 \tag{9.9}$$

where:

UV_{abs} = UV–Vis absorbance of the sample at the appropriate wavelength (see Table 9.3).

$\text{Volume}_{\text{hydrolysis liquor}} = \text{Volume}_{\text{filtrated}} = 86.73$ mL

$$\text{Dilution} = \frac{\text{Volume}_{\text{sample}} + \text{Volume}_{\text{dilution solvent}}}{\text{Volume}_{\text{sample}}} \tag{9.10}$$

$\mathcal{E}$ = absorptivity of biomass to a specific wavelength (see Table 9.3).

ODW = weight of the sample (mg).

Cell length = cm.

Note: The maximum values of λ often contain interference peaks caused by the breakdown of carbohydrates. Recommended wavelength values are chosen to minimize interference.

- Calculi of total lignin

$$\%\text{Lignin} = \%\text{AIL} + \%\text{ASL} \tag{9.11}$$

Table 9.3 Absorptivity constants for measuring acid-soluble lignin according to the types of biomass

Type of biomass	$\lambda_{\max}$ (nm)	$\mathcal{E}$ to $\lambda_{\max}$ (L/g cm)	Recommended wavelength (nm)	Absorptivity to a recommended wavelength (L/g cm)
Pinus Radiata-NIST SRM 8493	198	25	240	12
Bagasse-NIST SRM 8491	198	40	240	25
Corn bagasse	198	55	320	30
Populus deltiodes-NIST SRM 8492	197	60	240	25

9.2.2.4 Godin Method

Godin et al. (2011) developed a new and innovative method that merges the methodology of Van Soest and NREL to analyze structural carbohydrates, cellulose, and hemicellulose in lignocellulosic biomass. In this method, they performed a modification to Van Soest extraction method using only neutral detergent (NDS) to remove all compounds that interfere with sulfuric acid hydrolysis, such as nitrogen and inorganic compounds, chlorophyll, waxes, and other minor compounds. In addition, the extraction is performed with the intention of avoiding interference in the chromatographic quantitation of hemicellulosic and cellulosic monosaccharides. Structural carbohydrates are then submitted to hydrolysis with sulfuric acid to obtain free monosaccharides which are then analyzed by liquid chromatography with Corona charged aerosol detection (LC-CAD).

Methodology

Sample Preparation

Biomass samples are dried in an oven at 60 °C for 72 h. Then, they are passed through a hammer mill to have a size sample of 4 mm, followed by a second milling by disk mill so the sample reaches 1 mm size. Samples are stored at room temperature and protected from light for later use.

1. Analysis for structural carbohydrates by the method of Van Soest modified

Weigh 2 g of dried and ground biomass in a crucible for filtration. Add 100 mL phosphate buffer at pH of 7 with a concentration of 0.1 mM containing 1000 U analytical α-amylase thermostable. The extraction is done in a reflux equipment for 15 min at 90 °C. After the first extraction, the sample in the crucible is vacuum filtered. The withheld solid is submitted to another extraction with 100 mL of neutral detergent solution (NDS) for 1 h at 100 °C. The sample is again vacuum filtered, washed with deionized water and the remaining solid is dried at 40 °C for 72 h. This solid is ground in a laboratory using a mill cooled with cold water.

1. Sulfuric acid hydrolysis.

   Weigh 200 mg of dried and ground retained solid in a 100 mL pressure tube and add 3 mL of sulfuric acid at 72 % w/w containing phenol at 0.1 % w/v. Perform washing with nitrogen in the mouth tube, cover and incubate in a water bath for 1 h at 30 °C. Subsequently, dilute H_2SO_4 at 4 % w/w by adding 84 mL of deionized water. Wash again with nitrogen in the mouth tube, cover and incubate in a forced air convection oven for 2 h at 121 °C. Phenol and nitrogen are used to prevent oxidation.

   Cool the pressure tube at room temperature before removing cap. The hydrolysis solution is filtered in a filter crucible with a pore size of 40–100 μm; then, both the pressure tube and the filter crucible are washed with deionized water. The filtrate is collected in a 100 mL flask.

Transfer 10 mL of the hydrolyzate filtrate into a 50 mL centrifuge tube and neutralize to pH 7 with solid calcium carbonate. Shake the tube and centrifuge for 5 min at 6000 × *g*. Transfer 1 mL of the supernatant to a 1.5 mL centrifuge tube containing 0.5 mL of acetonitrile to precipitate the residual calcium sulfate. The tube is stirred and centrifuged for 5 min at 6000 × *g*. The supernatant must be filtered through a 0.2 µm filter into a vial for chromatography and then quantified by LC-CAD.

To prevent overestimation of the concentration of monosaccharides due to degradation in acidic media, use a mixture of standard recovery sugars (SRS): the mixture should be prepared in a 10 mL beaker containing sulfuric acid at 72 and 0.1 % w/v phenol. The concentration of the standards should be: 60 mg/mL of D-glucose, 32.5 mg/mL of D-xylose, 2.5 mg/mL L-arabinose, and 3.1 mg/mL of D-galactose. This mixture should receive the same treatment given to biomass. Prepare a target in the same way without biomass.

2. LC-CAD analysis.

The chromatographic run-time was performed by injecting 35 µL of the solutions prepared within a separation module of liquid chromatography. It is advisable to use an analytical column Carbo Sep CHO-682 Pb with a 300 mm × 7.8 mm size ID and particle size 7 µm; and a precolumn Carbo Sep CHO-682Pb LC size of 20 mm × 4 mm ID and particle size 7 µm. Samples are circumvented with deionized water at 80 °C for 30 min with a flow 0.4 mL/min. The charged aerosol detector is set at a maximum current of 50 pA and the gas pressure is 246 kPa.

Calculi

Estimating the content of cellulose, xylan, arabinan, mannan and galactan and is calculated as the total mass of D-glucose, D-xylose, L-arabinose, D-mannose, and D-galactose respectively. The content (g/100 g DM) of a single neutral polysaccharide (NP = cellulose, xylan, arabinan, mannan and galactan) in a given anhydrous sugar is calculated as follows:

$$\mathrm{NP} = \frac{\mathrm{MF} \times \mathrm{CF} \times \mathrm{ND} \times 100}{\mathrm{RF} \times \mathrm{MS} \times \mathrm{DM}} \left(\mathrm{g} / 100\,\mathrm{g\,DM}\right) \tag{9.12}$$

where:

MF = Corresponds to the mass of a given monosaccharide in a 100 mL beaker after acid hydrolysis (in grams).

CF = Monosaccharide mass conversion factor to a polysaccharide residue (0.90 for D-glucose, D-mannose, and D-galactose; 0.88 for D-xylose and L-arabinose).

ND = Ratio of the dry mass of the retained solid after extraction with NDS on the dry mass of the sample before extraction (in g DM/g DM).

MS = Dry mass of the withheld solid used for hydrolysis with sulfuric acid (in grams of humid matter (WM)).

RF = Monosaccharide recovery factor.

DM = dry matter content obtained at 103 °C for 4 h from the sample used for the hydrolysis with sulfuric acid (in g DM/g WM).

Hemicellulose is calculated as the sum of the content of xylan, arabinan, mannan, and galactan. Cellulose + hemicellulose is calculated as the sum of the content of cellulose and hemicellulose.

9.2.2.5 Other Extraction Methods for Polysaccharides

Several methods of chemical pretreatments have been evaluated for their ability to remove lignin and hemicellulose or increasing the permeability of the hemicelluloses–cellulose–lignin matrix. Some methods include treatment with organic solvents, acids, alkali, monoethanolamine, hot water, among others (Foyle et al. 2007), besides the ultrasound and microwave-assisted extraction (Huang et al. 2010). These methods are mainly used to quantify polysaccharides obtained after each extraction based on analytical techniques.

Extraction with Organic, Acid, and Alkali Solvents

Chaa et al. (2008) set the basis for this protocol. Different methods of extraction were mentioned in Sects. 9.2.1.1 and 9.2.1.2. Nevertheless, the method described by Chaa et al. (2008) denotes the advantage of extracting several compounds through the same method, for example, hemicellulose, soluble polysaccharides in water and room temperature, hot-water solubles, solubles in EDTA, NaOH/EtOH solubles and also, solubilize lignin of the biomass.

Methodology

1. Twenty gram of ground biomass is refluxed twice with a mixture of chloroform–methanol (150 mL/150 mL) for 14 h. Then, it is treated with ethanol at room temperature for 2 h and finally with boiling ethanol for 2 h. The insoluble residue in the cell wall that is recovered by filtration with a nylon mesh must be dried at 50 °C for 48 h.
2. The cell wall is treated with stirring sequentially: (a) In water at room temperature for 2 h. (b) With boiling water for 2 h. (c) In Ethylene diamine tetra-acetic acid (EDTA) aqueous at 1 %, pH 6.8 and 80 °C for 4 h. An extraction by filtration must be done at each step that has to be precipitated with 3 volumes of 95 % v/v ethanol, centrifuged, resuspended in water and dialyzed against distilled water at room temperature in order to obtain water-soluble polysaccharides, hot-water soluble polysaccharides, and EDTA soluble polysaccharides.
3. The remaining insoluble residue is then treated with a solution of 1 % NaOH and 70 % ethanol at 80 °C for 2 h to solubilize lignin. Weight loss is defined as NaOH EtOH-lignin. NaOH-EtOH soluble polysaccharides are recovered by precipitation of the extract with 3 volumes of ethanol.
4. Finally, the insoluble residue is treated with an aqueous 14 % KOH solution at room temperature for 14 h. Then, it is filtered and acidified with glacial acetic

acid to 5–6 pH value. Acidification forms a precipitate which is recovered by centrifugation and corresponds to the fraction of hemicellulose A. The supernatant should be concentrated under reduced pressure, dialyzed against distilled water, and precipitated with 3 volumes of ethanol, resulting in the fraction called hemicellulose B. The alkali insoluble residue is dried in an oven.

Polysaccharides obtained can be quantified by gas chromatography (GC), through FTIR spectroscopy and RMN spectroscopy. If GC is used, weigh 1 mg of hemicellulose to pre-hydrolyze polysaccharides with 500 µL of trifluoroacetic acid 2 mol/L for 4 h at 80 °C; then, allow to dry at room temperature. The following step consists in incubating 100 µg of sample with 250 µL of methanol–HCl 0.5 mol/L anhydrous for 20 h at 80 °C under a nitrogen atmosphere. After drying under nitrogen flow, the methyl glycosides were acetylated and the mixture derivatized was analyzed by gas chromatography. The column suggested is Sil 5-CP (0.53 mm × 50 m fused silica). A flame ionization detector is used with nitrogen (5.5 psi) as carrier gas and the oven temperature program is as follows: start with 150 °C for 10 min and raise the temperature to 200 °C at 0.8 °C/min; hold at 200 °C for 7 min increasing it at 240 °C at 5 °C/min; finally, hold to 240 °C for 20 min.

For spectroscopic analysis see Sects. 2.2.6.1 and 2.2.6.2.

Monoethanolamine Method

Total cellulose is determined by means the monoethanolamine method as it is described by Foyle et al. (2007).

One hundred milliliters of monoethanolamine was added to a dry lignocellulosic sample and located at reflux at 170 °C for 3 h. Then, add 100 mL of water after the sample is cold. 100 mL of the supernatant liquid is decanted into a beaker and the remaining mixture should be filtered through a filtration crucible. The decanted liquid and the filtrate are re-filtered through a cellulose sphere that is formed on the glass crucible during the first filtration. The cellulose should be rinsed with 200 mL of hot water (approximately 60 °C) before washing the solid residue with water in a beaker (to a final volume of 75 mL). In order to bleach cellulose, 10 mL of H_2SO_4 at 10 % v/v and 10 mL of NaOCl (24 g/L) were added. The sample is bleached for 5 min at room temperature. The mixture is filtered through the glass crucible and any residue remaining in the beaker is also rinsed into the crucible using 15 mL of water and 15 mL of H_2SO_4 (0.25 mol/L). The sphere of bleached pulp should be rinsed with 15 mL of cold water followed by 15 mL of 3 % Na_2SO_4. The sample is transferred into a 250 mL beaker using at most 50 mL of water. 5 mL of 6 % w/v Na_2SO_4 is added. The beaker should be covered with a glass watch and incubated in a boiling water bath for 20 min. The appreciation of a pink color at this point indicates the presence of lignin. If this occurs, it is necessary to repeat bleaching. The residue is filtered through the crucible forming a cellulose sphere. Cellulose should be rinsed with 150 mL of boiling water, 50 mL of cold water, 25 mL of 10%w/v acetic acid (very quickly), 50 mL of cold water, 150 mL of boiling water, 75 mL of water

containing two drops of NH_4OH, and finally, with 200 mL of boiling water. The residue should be dried in the furnace at 105 °C and weighed. The cellulose concentration is calculated based on the initial weight of the lignocellulosic sample used.

Hot-Water Extraction

Chen et al. (2013) described the following methodology.

Accurately, weigh 5.0 g of dried and ground biomass and place them within a flask with baffles, add 200 mL of distilled water and place the flask in a bath of water with magnetic stirring (600 rpm and 90 °C). After a period of time of 4 h, the suspension is centrifuged and the pellet is extracted two more times using the same method. The supernatants obtained in each centrifugation are joined and concentrated for vaporization at 50 °C under reduced pressure. Ethanol is added to precipitate polysaccharides and left at 4 °C overnight. The precipitate is centrifuged at 5000 rpm for 10 min and rinsed several times with ethanol. The extraction should be repeated three times.

Quantification

Polysaccharides extracted with hot water can be determined by Chaa method (see Sect. 9.2.2.4.1).

In addition, the yield obtained from the extracted polysaccharides can be determined with the following equation:

$$\text{Yield}(\%) = \frac{W_1}{W_0} \times 100 \tag{9.13}$$

where:

W_1: corresponds to the weight of the extracted polysaccharides.

W_0: it is the weight of the raw material.

Ultrasound and Microwave-Assisted Extraction

This methodology was explained by Huang et al. (2010). The dry biomass is suspended in water and submitted to ultrasound and microwave-assisted extraction. The process with ultrasound takes 60 min at 50 °C while the power used corresponds to 550 W (submitted to ultrasound for a period of 5 and 5 s pause). The microwave treatment is done with 350 W for 10 min in a microwave oven. The insoluble pellet is removed by centrifugation ($5000 \times g$, 15 min) and dried under vacuum at 60 °C for 20 h to obtain residue (the humidity content is 12.26 %).

Van Soest method analyses the extraction of cellulose and hemicellulose (see Sect. 9.2.2.1).

High-Performance Liquid Chromatography (HPLC)

Principle

HPLC is a technique used to separate the different compounds within a mixture, in this case, released sugars. It consists in a nonpolar stationary phase (column) and a mobile phase. The stationary phase is usually silica, but depends on the compound to be separated while the mobile phase acts as the carrier sample. The sample in solution is injected into the mobile phase. The components of the solution migrate according to the non-covalent interactions of the compounds with the column. These chemical interactions determine the separation of the sugars contained in the sample. According to the nature of the compounds to be determined, different detectors are taken into account. HPLC is very important because it optimizes the results due to the increase in pressure to which the chromatographic run is subjected; HPLC acts in the stationary phase as an active component complementing the referential liquid mobile phase. The columns used are stainless steel and its length varies between 10 and 30 cm, with internal diameter of 4–10 mm (Orellana and Rogel 2016).

HPLC is mainly used in identifying polysaccharides as it offers various advantages: it is a simple and quick technique; it can be used from microanalytical to industrial scale; allows a continuous record of analysis; can be applied to labile substances due to the low harmfulness; denotes high precision and is not limited to volatile analytes.

Methodology (According to Sluiter et al. 2008a)

Prepare Working Solutions

Prepare a series of calibration standards containing the compounds to be quantified. See literal A and B:

A. *Preparation of standards*:

Perform dilutions in 10 mL volumetric flasks according to each of the compounds to be measured with ultra-purified water (HPLC grade). The concentration of the points of the calibration curve is: 1, 10, 15, 20, 30, and 45 g/L.

B. *Sample preparation*:

Remove 1 mL of hydrolyzate sample. Pour into eppendorf tubes. Centrifuge and then filter with nylon membrane of 0.22 μm porosity. Package in 2 mL HPLC amber vials. Finally, freeze at −10 °C.

Note: Use a micropipette or sterile glass pipette to obtain the extraction of 1 mL from the hydrolyzate obtained from the enzymatic hydrolysis.

HPLC for sugar analysis

(a) Analyze the calibration standards and samples with HPLC using a Sugar Pack or Aminex HPX-87P columns (keep the column off the compartment, which must be stored at room temperature) and a refractive index detector. Be sure to rinse the column. For this, unplug the detector off the column and dispose the waste in a container. Never wash the column with the detector plugged to avoid damages. Run the mobile phase at the same temperature of the method to be used. The flow should be maximum for about 15 min.
(b) After cleansing the column, the patterns are set to run in order to build the calibration curve. Runs should have the same conditions of the samples. Following this, run the sample according to the following conditions:

- Sample volume: 20 μL.
- Mobile phase: water 18.2 MΩ, filtrated for 0.2 μm.
- Flow: 0.5 mL/min (rising gradually to avoid column damage).
- Column temperature: 75 °C.
- Detector temperature: 75 °C.
- Duration: 20 min.
- Detector: refractive index detector (RID).

According to this methodology, the following compounds can be detected under different retention times (Table 9.4):

9.2.2.6 Non-gravimetric Techniques for Polysaccharide Analysis

Infrared Spectroscopy (IR)

Principle

Chemical analysis of lignocellulosic biomass has traditionally been conducted by conventional techniques based on gravimetric methods which result to be rather complex due to the time required to perform the analysis and the demand for large amounts of reagents.

The development of instrumental techniques has enabled analysis to lignocellulosic materials using techniques such as near infrared reflectance spectroscopy (NIRS),

Table 9.4 Retention times for sugars determined by HPLC-RID

Compound	Retention time (min)
Sacarose	7.52
Cellobiose	7.34
Galactose	9.10
Glucose	9.38
Rhamnose	9.80
Xylose	10.28
Fructose	11.69
Arabinose	11.99

analysis that allow certain advantages to gravimetric methods as: the sample requires less preparation; fewer sample-quantity; requires less time in the development of analysis; and, results are reliable (Xu et al. 2013).

IR is a technique that is based on the interaction of electromagnetic radiation with matter. Molecules have frequencies at which they rotate and vibrate (rotation and molecular vibration) and are characteristic of molecular bond types or functional groups present in the sample. This allows to collect information on the structure of a molecule, since molecular-bond information obtained from the chemical compounds of the biomass absorbs specific frequencies of infrared. The most widely used techniques are the Fourier transform infrared spectroscopy (FTIR) and NIRS. NIRS provides structural information by examining the peaks in the spectrum, while FTIR provides information about certain compounds of the plant cell wall through absorbance bands associated with each component.

The NIRS characteristic is that the frequencies of the harmonic movements of molecules are in this subregion comprising the range of wavelength from 700 to 2500 nm or wavenumber from 13,000 to 4000 cm^{-1}. It also provides information on electronic transitions, and overtone bands with symmetric stretching vibration of C–H, O–H, N–H (Cozzolino et al. 2003) are observed. The corresponding electromagnetic radiation in this range interacts with matter. Each molecular bond type has one or more wavelengths. Depending on the molecules and the corresponding bonds, specific joints between atoms vibrate at a certain frequency and each type of these joints absorbs radiation with a specific wavelength. The lengths of unabsorbed waves will be reflected and thus, allowing the construction of a spectrum which is a graphical representation of the vibrational transitions of molecules and bands that appear when the absorption of radiant energy produces changes in the energy of molecular vibration. The final result provides an insight into chemical composition and sample quantification.

For qualitative analysis, the frequencies at which a molecule absorbs radiation are one of its characteristics depending on the links and functional groups present. They also provide and give absorption spectra, while quantification is performed by the intensity of characteristic bands from each functional group associated with the molecule that can determine the concentration.

Table 9.5 describes some absorbance bands in the fundamental infrared where FTIR apply corresponding to functional groups present in the molecular structures of biomass, for example, glycan characteristic bands are used to determine glucose or xylan to determine hemicellulose.

Methodology

The following information describes the methodology employed by Pinzón and Cardona (2008).

In order to carry out FTIR spectra determination, samples of biomass are subjected to a drying process at 50–60 °C to avoid moisture and the presence of broad absorptions due to vibrations around –OH at 3500 and 1400 cm^{-1}, which overlap the existence of other possible bands in those areas. When samples are dry, pulverize

Table 9.5 Absorbance bands in the IR, which are characteristic for certain biomass compounds

Compound	Band generated by	Wave number (cm^{-1})
Cellulose	Hydroxyl groups (–OH) vibration Bond stretching –CH vibrations Asymmetric vibration of C–O–C–, characteristic of carbohydrates	3400–3200 2950–2850 1150
Hemicellulose	Hydroxyl groups (–OH) vibration Vibration of carbonyl groups (–C=O) of the carboxylic acids formed by hydrolysis of the acetyl groups Asymmetric vibration of C-O-C-, characteristic of carbohydrates	3400–3200 1730 1150
Lignin phenylpropane	Vibration bond –C=C– of the aromatic ring	1600–1400
Xyloglucan	Bond $–CH_2$	1370
Glucose	Vibration bond –C–H outside the plane characteristic of ring β-pyranose	1050–890

sample until the particle size is smaller than the wavelength of radiation (less than 2 μm) to avoid the effects of absorption band distortions. The most used technique is the formation of potassium bromide (KBr) plate but other alkali metal halides have been used. Potassium bromide is preferred for its low cost, good transmission and is also ideal for working in the mid-infrared. To prepare the pellet, mix a finely powdered milligram or less of the sample with approximately 100–300 mg of KBr powder (0.2–1 % of concentration in KBr sample). The mixture can be done with a mortar or in a small ball mill. Excessive grinding is not required because KBr will absorb more humidity from the air. Subsequently, press the mixture (between 700 and 1000 kg/cm^2) in a special hydraulic press to obtain a transparent disk. Best results are obtained if the disk is vacuumed to remove entrapped air. Then, the disk is placed on the beam path for spectroscopic examination. The frequency range used is, generally, located between 4000 and 800 cm^{-1}, since the vast majority of classical analytical infrared spectroscopy applications are based on the use of mid-infrared (MIR).

Nuclear Magnetic Resonance Spectroscopy (NMR)

Principle

NMR is the analytical tool that provides greater structural and stereochemical information in affordable time. The technique is nondestructive and has applications in all areas of Chemistry and some of Biology. NMR spectroscopy was developed to study the atomic nuclei and that is the reason why it can be used to determine the structures of organic compounds. This spectroscopic technique can be used only to study atomic nuclei with an odd number of protons or neutrons (or both). This situation occurs in ^{1}H, ^{13}C, ^{19}F, and ^{31}P atoms. Such nuclei are magnetically active, in other words, they possess spin-like electrons because the nuclei have positive charge and a rotational movement on an axis acting as tiny bar magnets.

In the case there is no magnetic field, the nuclear spins are oriented randomly. However, when a sample is placed in a magnetic field, the nuclei with positive spin are oriented in the same direction of the field in a state of minimum energy called state of spin α. Otherwise, the nuclei with negative spin are oriented oppositely to the magnetic field in a higher energy state called spin state β (McMurry 2012).

When a sample containing an organic compound is irradiated briefly by an intense radiation pulse, the nuclei in the spin state α are promoted to spin state β. For a certain field strength value, the energy required to reverse the proton coincides with the radiation, absorption occurs, and a signal is observed. This signal is originated when the nucleus return to their initial state by emitting signals whose frequency depends on the energy difference between the spin states α and β. The NMR spectrometer detects these signals and records them as a graph of frequency *vs* intensity, which is called an NMR spectrum. Thus, the term NMR comes from the fact that the nuclei are in resonance with the applied magnetic field; that is, the nucleus pass from one spin state to another in response to the radiation to which they are subjected.

The presence of many absorption peaks in the NMR spectrum reflects differences in the environment of nuclei and gives a detailed information about the molecular structure. Therefore, the following factors are crucial to interpret a spectrum:

(a) The number of signals indicating the different types of protons in a molecule.
(b) Signal-position denoting certain information about the electronic environment for each type of proton.
(c) Signal-intensity: determines the amount of types of protons present.
(d) Signal-splitting in several peaks, which reports on the environment of a proton in comparison to other nearby protons (Morrison and Boyd 1998).

Methodology

To develop this methodology, the references come from Zhang et al. (2010) and Chaa et al. (2008).

To analyze hemicelluloses fractions, NMR ^{1}H spectrum is performed at 75.5 MHz. Weight and dissolve 25 mg of sample in 1 mL of DMSO-d_6. The test is performed at 353 K and TMS is used as internal standard. For NMR ^{13}C spectrum, a probe 5 mm-BBO (^{13}C 100.67 MHz) is used.

Figure 9.3 explains an example of a NMR^{13}C for pure cellulose and hemicellulose.

9.3 Protein Analysis

There are several techniques for analyzing proteins in biomass. Among the most commonly used techniques is the determination of compounds associated with the cellular concentration of the material. Quantitation is done conveniently with colorimetric methods as the biuret method, Lowry and Bradford. Bluret and Lowry

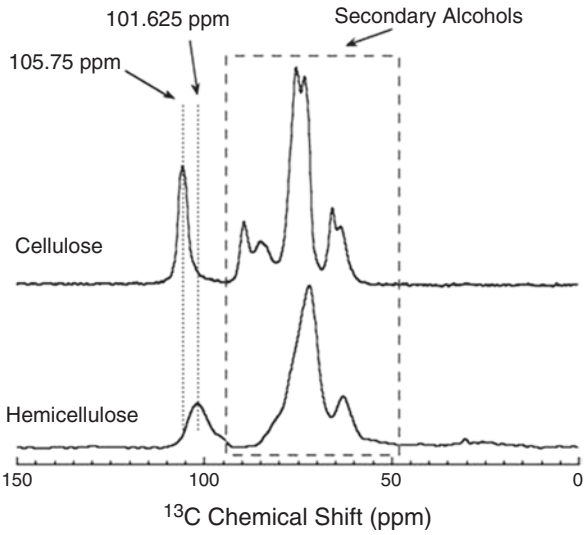

Fig. 9.3 NMR ^{13}C spectrum for pure cellulose and hemicellulose (Cody's 2016)

methods are not recommended due to the low sensitivity of the first one and the interference in the latter. Therefore, the Bradford method is determined to quantify proteins (Child Camacho 2009). In addition to these colorimetric methods, the volumetric method (Kjeldahl method) can also determine proteins.

9.3.1 Bradford Method

9.3.1.1 Principle

The method involves the binding of a dye (Coomassie blue G-250) to proteins. The dye in acidic solution may be found in two colors, one blue and one orange. Total protein binds to the blue dye to form a protein–dye complex with a higher extinction coefficient than the free one (orange dye).

9.3.1.2 Methodology

1. Perform a calibration curve from a serum albumin solution 1 mg/mL using a dilution series of different concentrations from 0.01 to 1 mg/mL.
2. Take 50 mL from each solution and mix with 2.5 mL of Bradford reagent and shake well.
3. Let stand for 3 min and measure the absorbance of the mixture at a wavelength of 595 nm.

4. Determine the standard calibration curve plotting Abs_{595nm} vs standard protein concentration in order to quantify the protein.
5. Determine the protein concentration in the samples from the standard calibration curve and Abs_{595} values. If the concentration is very high (stands outside the range of the standard), dilute the sample or to take a lower aliquot lower.

9.3.2 Kjeldahl Method

9.3.2.1 Principles

The method is based on the destruction of organic matter with concentrated sulfuric acid. In this reaction ammonium sulfate is formed immediately and in excess of sodium hydroxide, ammonia is released. This ammonia is distilled and receiving in sulfuric acid forming ammonium sulfate. The excess of acid is titrated with sodium hydroxide in the presence of methyl red or boric acid. Ammonium borate is formed which is valued with hydrochloric acid.

9.3.2.2 Methodology

The following steps explain the methodology described by Horwitz and Latimer (2005) to characterize protein in biomass:

1. Perform the analysis in duplicate.
2. Perform a control test using an organic substance without nitrogen (sucrose) that is capable of causing reduction of nitric and nitrous derivatives possibly present in the reactants.
3. Weigh to 0.1 mg, 1 g of homogenized simple in a Kjeldahl digestion flask.
4. Add three glass beads, 10 g of potassium or sodium sulfate, 0.5 g of cupric sulfate, and 20 mL of concentrated sulfuric acid.
5. Connect flask to absorption trap containing 250 mL of 15 % w/v sodium hydroxide. The porous disk creates division among fumes into fine bubbles in order to facilitate absorption. To ensure long duration, it is important to cleanse regularly before use. Sodium sulfite deposits are removed with concentrated hydrochloric acid. If sodium hydroxide solution at 15 % w/v added to phenolphthalein (contained in the absorption trap) remains colorless, it must be changed in a rate approx. to 3 analyses.
6. Heat on a blanket and once the solution is clear, let boil 15–20 min more. If the sample tends to foam, add stearic acid or antifoam-silicone-droplets and then, start warming slowly.
7. Cool and add 200 mL of water.
8. Connect the distillation equipment to the flask. Add 100 mL of NaOH at 30 % w/v slowly through the funnel and close the key.

9. Distill at least 150 ml of the solution in a flask submerged at a cooling extreme or collecting tube in:

   (a) 50 mL of sulfuric acid 0.1 mol/L; 4–5 drops of methyl red and 50 mL of distilled water. Ensure an excess of H_2SO_4 so that it can perform the titration. Titrate the excess of acid with NaOH 0.1 mol/L until yellow color appears.
   (b) Fifty milliliters of boric acid at 3 % w/v. Titrate with 0.1 mol/L hydrochloric acid to 4.6 pH using a pH meter calibrated with 4 and 7 pH buffer solutions, or in the presence of the Tashiro indicator to pH value at 4.6.

   It is necessary to check the tightness of distillation apparatus periodically by using 10 mL of a solution of ammonium sulfate 0.1 mol/L (6.6077 g/L), 100 mL of distilled water and 1–2 drops of sodium hydroxide at 30 % to release ammonia. Also, it is important to verify recovery of ammonia by destroying the organic matter from 0.25 g of L(−)-tyrosine.

9.4 Moistures Analysis

9.4.1 Principles

This analytical procedure is based on a traditional convection drying system. However, for biomass suspensions or samples prepared with 10 % (w/w) humidity the method is not recommended. Therefore, use the balance of moisture in these cases.

The gravimetric method determines the moisture content present in the sample through the drying process and by calculating the water percentage *vs* the weight loss due to the elimination of liquid after heating (under normal conditions).

9.4.2 Methodology

Wychen and Laurens (2013) describe this methodology:

Convection Oven Method

(a) Preconditioning of cleansed capsules in a muffle furnace at 575 °C for a minimum of 2 h. This is done to remove any polluting fuel.

Note: Aluminum dishes, pots or porcelain capsules may be used. If aluminum plates are used, precondition them in an oven at 105 °C for 2 h.

(b) Remove caps and cool in a desiccator employing gloves or tweezers. Weigh with an accuracy of 0.1 mg.
(c) Mix the sample and weigh 100 ± 5 mg of biomass in the pre-weighed capsule. Analyze each sample at least in duplicate and include a minimum empty crucible as the control method.

(d) Place the sample in a convection oven at 60 ± 3 °C for at least 18 h.
(e) Remove the sample from the oven and let cool at room temperature in a desiccator.
(f) According to the moisture of the sample, verify the weight of the crucible after 8 h and the weight of the dry sample every 2 h. Place the sample in a convection oven at 60 ± 3 °C again until no variations are greater than 0.01 % i.e. 0.0001 g (constant weight).

9.5 Analysis of Other Compounds

9.5.1 Lipids

9.5.1.1 Principles

It is necessary to carry out derivatization, esterification, and methylation of lipids to realize the characterization of lipids in biomass by GC. These processes are necessary to transform the analyte by chemical reaction in a derivative easier to analyze. The derivatization allows to obtain more volatile species to avoid using too high temperatures that can decompose the analytes in the equipment, or generate unwanted precipitation in the column. Another use of derivatization is to insert a functional group, which increases the resolution and detection into the column, improving the compound separation.

The reactives greatly used for esterification are NaOH, heptane (C7H16), sodium chloride (NaCl), and boron trifluoride (BF3) in methanol. They are used in the esterification of free fatty acids and acylglycerols. *Denote special attention when using BF3 in methanol as it is extremely toxic*.

The most convenient way to convert fatty acids into methyl esters is in basic medium because acid medium may provoke isomers.

The factors that affect directly the quantification of fatty acid methyl esters (FAME) are: incomplete conversion of lipids in FAME and changes in the composition of fatty acids for esterification and formation of compounds that may mistakenly be identified as fatty acids and may directly affect the quantification of FAME.

9.5.1.2 Methodology

The methodology introduced by AOAC Official Methods Ce 2-66 (2009), with the purpose of determining lipids in biomass, sets the guidelines for lipid characterization.

For Fats and Oils (Saponification):

(a) Lipid extraction can be performed through various methods, but the best known is the Soxhlet (see Sect. 9.2.1.1).
(b) Accurate weights are not required. The simple size is necessary to determine the size of balls and amounts of reagents to be applied according to the following Table 9.6.

Table 9.6 Size balls and amount of reagents required according to sample size

Sample (mg)	Balls flat bottom (mL)	NaOH 0.5 mol/L (mL)	BF_3-methanol (mL)
100–250	50	4	5
250–500	50	6	7
500–750	125	8	9
750–1000	125	10	12

(c) If the fat sample extracted from biomass is a solid which adheres to the vessel walls of the recipient, it should be dissolved with methanolic NaOH 0.5 mol/L (see Table 9.6) and heated until dissolved. Following this, pour the solution into the corresponding ball (see Table 9.6) and add three boiling stones. If the fat sample does not stick to the walls, append those to the corresponding ball (see Table 9.6) and add the required amount of NaOH according to Table 9.6.
(d) Bind to a condenser and heat the mixture in a water bath until the fat globules appear in the solution. This step may last 5–10 min.
(e) Add the specific amount of BF_3-methanol and proceed with esterification.

For fat Acids (Esterification)

(a) After adding the specific amount of BF_3-methanol, let boil for 2 min.
(b) Add 2.5 mL of heptane and boil for 1 more minute.
(c) Remove from heat, disassemble the condenser and add about 15 mL of NaCl saturated solution. Plug on the ball and shake vigorously for 15 s while the solution is still warm.
(d) Add enough NaCl saturated solution so that the heptane solution of methyl esters floats within the ball neck. Three phases are formed: organic (top), fat (intermediate), and aqueous (lower).
(e) Transfer heptane solution in the upper layer with a dropper within a test tube and add a small amount of Na_2SO_4 anhydride. Dried heptane solution (top) is transferred to chromatographic vial with a dropper and then is injected directly into the gas chromatograph. If not injected immediately, store for a maximum time of 24 h at −20 °C.

Gas Chromatography

Analyze samples derivatized by GC using two equipments: a cross-linked methyl-siloxane column (length 30 m, 0.32 mm DI) (keep the column off the compartment, it must be stored at room temperature) and a flame ionization detector (FID). Make sure to rinse the column by unpligging the cord that connects to the detector and deposing the waste in a container. Never wash the column with detector 'on' because it can damage the equipment. Run the mobile phase of work at the same temperature of the method to be used. The flow must be at maximum for about 1 h.

The sample runs after cleansing the column and under the following conditions:

- Sample volume: 2 μL
- Gas: helium

- Flow: 1.2 mL/min
- Injector temperature: 250 °C
- Detector temperature: 250 °C
- Temperature ramping: 100 °C × 4 min (3 °C/min), 240 °C × 20 min

With the intention of quantifying the fatty acid methyl esters, a standard series of increasing concentrations should be prepared. Once prepared, inject the same volume of each of the solutions into the chromatograph curve.

In both the chromatogram of each standard solution and from the sample, the peaks correspond to the methyl esters. The retention time of each peak is the same in all chromatograms. However, the area will differ depending on the concentration given to each one.

In order to create the calibration curve a graph with analyte concentration *vs* area of each peak was made according to each concentration. With the equation of the line, calculate the concentration substituting "y" for the peak area corresponding methyl ester in the sample chromatogram. Solve "x" which corresponds to the concentration of methyl ester.

9.5.2 Pectin Analysis

9.5.2.1 Principle

Degradation reactions such as depolymerization and deesterification occur when pectin is extracted of the biomass. Therefore, the conditions of the extraction must be carefully controlled to achieve the desired final properties (Muñoz (2011). Biomass can be characterized by the FTIR technique after extracting pectin from the corresponding biomass, since FTIR allows the identification of functional groups present in the pectin.

9.5.2.2 Methodology

Extraction

Muñoz (2011) described the following methodology for pectin extraction: Weigh samples of 50 g. Use concentrated hydrochloric acid as an acidifying agent of the solutions, since it requires a strong acid to hydrolyze the pectins. The extraction temperature is 93 ± 2 °C. The extraction is performed using Soxhlet equipment in order to maintain process factors without relevant changes because the extraction solvent (acidulated water) usually evaporates at environmental conditions and this could lead to change the proportions of dilution and therefore, the doses of the reagent used.

Filtration and Precipitation

After hydrolysis, pectin is isolated from the exhausted raw material by filtration with a filter cloth and precipitated from the extract with high purity ethanol.

Washing, Sterilizing, and Grinding

The precipitate obtained is rinsed with 50 % ethanol (mixed with distilled water) and pressed to remove soluble impurities. Subsequently, the pectin is dried in an oven for 24 h at an average temperature of 40 ± 3 °C. After drying, grinding is performed for homogenizing the pectin samples to a size of 80 mesh.

FTIR Characterization

This methodology is described by Kacuráková and Wilson (2001). FTIR offers the possibility to determine some functional groups of pectic derivatives in the region of 1900–1500 cm^{-1}.

To carry out the FTIR spectra, samples of extracted pectin are subjected to a drying process at 50–60 °C. Once the samples are moisture-free, they are encapsulated in disks of potassium bromide (KBr). These disks are analyzed in an infrared spectrophotometer. The frequency used for analysis of ester is 1745 cm^{-1} and for carboxylate regions is between 1605 and 1630 cm^{-1}.

9.5.3 Ash Content Determination

9.5.3.1 Principle

The inorganic content in biomass, either structural or removable, must be measured as fraction in the total composition (100 % mqm). The structural ash is inorganic material that is tied to the physical structure of biomass, while the removable ash is inorganic material that can be removed by rinsing. This ash results from soil that is attached to biomass.

Ash is generally the residue of an organic sample that has been incinerated. This is done with the purpose of analyzing the mineral and observing the presence of mineral adulterations. This is a simple method that involves the incineration of biomass at temperature of 400–600 °C. In this process occurs the destruction of all carbonaceous particles.

9.5.3.2 Methodology

The methodology used to determine ash is taken from protocol NREL/TP-510-42622 (Sluiter et al. 2008b).

Mark an appropriate number of crucibles using a porcelain marker and place them in the muffle furnace at 575 ± 25 °C for a minimum of four hours. Remove the crucibles and place them into a desiccator. Record the cooling time. Weigh the crucibles with an accuracy of 0.1 mg and record it.

Place the new crucibles into the muffle furnace at 575 ± 25 °C and dry them to constant weight, which is defined as less than ±0.3 mg of change in the weight for one hour after re-heating the crucible.

Weigh 0.5–2.0 g to the nearest 0.1 mg of the biomass into the tared crucible. Record the weight of the sample. If moisture is the target of the analysis in the sample, then store it in a desiccator until use for ash analysis. Each sample must be analyzed in duplicate at least.

The quantification of ash can be done by using a muffle furnace set at 575 °C or in a muffle furnace with a ramping program.

Determination of Ash Using a Muffle Furnace Set at 575 ± 25 °C

Place the crucible with the sample into a muffle furnace at low heating until smoke stops appearing. Let the crucible cool down before placing it into the muffle furnace. Alternatively, use a muffle furnace with a temperature ramping function to avoid pre-ignition.

Place the crucibles into the muffle furnace at 575 ± 25 °C during 24 ± 6 h. Protect the sample from airflows when handling the crucible to avoid mechanical loss of sample.

Carefully, remove the crucible from muffle furnace and place it into a desiccator. Cool the crucible for a specific amount of time, equal to the time of initial cooling of all crucibles. Weigh the crucibles and ash to the nearest 0.1 mg and record the weight.

Place the new crucibles into the muffle furnace at 575 ± 25 °C and dry them to constant weight, which is defined as less than ±0.3 mg of change in the weight upon 1 h after re-heating the crucible.

Determination of Ash into Muffle Furnace Equipped with a Ramping Program

Set the heating rate in the muffle furnace according to the following scheme:

- Ramp to room temperature at 105 °C
- Hold at 105 °C for 12 min
- Ramp to 250 °C with ratio 10 °C/min
- Hold at 250 °C for 30 min
- Ramp to 575 °C at 20 °C/min
- Hold at 575 °C for 180 min
- Allow temperature to drop to 105 °C

- Hold at 105 °C until samples are removed

Place the crucibles into muffle furnace and begin the ramping program. Protect the sample from airflows when handling the crucible to avoid mechanical loss of sample.

Carefully remove the crucible from muffle furnace and place it into a desiccator. Cool the crucible for a specific amount of time, equal to the time of initial cooling of all crucibles. Weigh the crucibles and ash to the nearest 0.1 mg and record the weight.

Place the new crucibles into the muffle furnace at 575 ± 25 °C and dry them to constant weight, which is defined as less than ±0.3 mg of change in weight for an hour after re-heating the crucible.

References

AOAC (1995) AOAC official method 973.18. Fibre (acid detergent) and Lignin in animal feed. In: AOAC (ed) AOAC official methods of analysis (vol 1, Chap. 4), 16th edn. AOAC, Rockville, MD, pp 20–21

AOAC (2002) AOAC official method 2002.04. Amylase-treated neutral detergent fiber in feeds. In: AOAC (ed) AOAC official methods of analysis, vol 85, number 6, 1st edn. AOAC, Rockville, MD, pp 20–21

AOAC (2009) AOAC official methods Ce 2–66. Preparation of methyl esters of fatty acids. Official methods 6a. AOCS, Urbana

ASTM D1110-84 (2013) Standard test methods for water solubility of wood. ASTM International, West Conshohocken, PA. www.astm.org

Attard TM, Rob Mcelroy C, Rezende CA, Polikarpovc I, Clarka JH, Hunt AJ (2015) Sugarcane waste as a valuable source of lipophilic molecules. Ind Crops Prod 76:95–103

Bhattacharya D, Germinario LT, Winter WT (2008) Isolation, preparation and characterization of cellulose microfibers obtained from bagasse. Carbohydr Polym 73:371–377

Ballesteros I, Oliva JM, Saez F, Ballesteros M (2001) Ethanol production by simultaneous saccharification and fermentation of olive oil extraction. Appl Biochem Biotechnol 91(93):237–252

Bian J, Peng F, Peng X-P, Xiao X, Peng P, Xu F (2014) Effect of [Emim]Ac pretreatment on the structure and enzymatic hydrolysis of sugarcane bagasse cellulose. Carbohydr Polym 100:211–217

Boerjan W, Ralph J, Baucher M (2003) Lignin biosynthesis. Annu Rev Plant Physiol Plant Mol Biol 54:519–546

Buranov AU, Mazza G (2008) Lignin in straw of herbaceous crops. Ind Crops Prod 28:237–259

Cardoen D, Joshi P, Diels L, Sarma PM, Pant D (2015) Agriculture biomass in India: Part 1. Estimation and characterization. Resour Conserv Recy 102:39–48

Cataño Rueda EH (2009) Obtención y caracterización de nanofibras de celulosa a partir de desechos agroindustriales. Tesis Ingeniería Química, Facultad de Minas, Escuela de Procesos y Energía, Universidad Nacional de Colombia, Medellín, Colombia, p 13. http://www.bdigital.unal.edu.co/920/1/1017137266_2009.pdf

Chaa L, Joly N, Lequart V, Faugeron C, Mollet JC, Martin P, Morvan H (2008) Isolation, characterization and valorization of hemicelluloses from Aristida pungens leaves as biomaterial. Carbohydr Polym 74:597–602

Chen J, Lai P, Shen H, Zhen H, Fang R (2013) Effect of extraction methods on polysaccharide of Clitocybe maxima stipe. Adv J Food Sci Technol 5(3):370–373

Cody's G (2016) Solid state NMR facility [Figure] recovery from. https://www.gl.ciw.edu/static/users/gcody/nmr.html

Cozzolino D, Fassio A, Fernández E (2003) Use of near infrared reflectance spectroscopy to analyze corn silage quality. Agric Téc 64(3):387–393

Del Río JC, Lino AG, Colodette JL, Lima CF, Gutierrez A, Martínez AT, Lu F, Ralph J, Rencoret J (2015) Differences in the chemical structure of the lignins from sugarcane bagasse and straw. Biomass Bioenerg 81:322–338

Fengel D, Wegener G (1984) Wood: chemistry, ultrastructure, reactions. De Gruyter, Berlin, p 613

Foyle T, Jennings L, Mulcahy P (2007) Compositional analysis of lignocellulosic materials: evaluation of methods used for sugar analysis of waste paper and straw. Bioresour Technol 98:3026–3036

García Sánchez A, Ramos Martos N, Ballesteros E (2005) Estudio comparativo de distintas técnicas analíticas (espectroscopía de NIR y RMN y extracción mediante Soxhlet) para la determinación del contenido graso y de humedad en aceitunas y orujo de Jaén. Grasas Aceites 56(3):220–227

Godin B, Agneessens R, Gerin PA, Delcarte J (2011) Composition of structural carbohydrates in biomass: precision of a liquid chromatography method using a neutral detergent extraction and a charged aerosol detector. Talanta 85:2014–2026

Golander E (2011) Characterization and methods for extraction of extractives in spent sulphite liquor. Master of science thesis, Department of Chemical and Biological Engineering, Chalmers University of Technology, p 8. http://publications.lib.chalmers.se/records/fulltext/142119.pdf

Higuchi T (1985) Lignin biosynthesis. In: Higuchi T (ed) Biosynthesis and biodegradation of wood components. Academic, Orlando, FL, pp 114–160

Horwitz W, Latimer GW (2005) Chapter 33: official methods of analysis of AOAC international, 18th edn. AOAC International, Gaithersburg, MD

Huang SQ, Li JW, Wang Z, Pan HX, Chen JX, Ning ZX (2010) Optimization of alkaline extraction of polysaccharides from Ganoderma lucidum and their effect on immune function in mice. Molecules 15:3694–3708

Kacuráková M, Wilson RH (2001) Developments in mid-infrared FT-IR spectroscopy of selected carbohydrates. Carbohydr Polym 44:291–303

Luque de Castro MD, García-Ayuso LE (1998) Soxhlet extraction of solid materials: an outdated technique with a promising innovative future. Anal Chim Acta 369:1–10

Luque de Castro MD, Priego-Capote F (2010) Soxhlet extraction: past and present panacea. J Chromatogr A 1217:2383–2389

Martín Lara, María Angela. Caracterización y aplicación de biomasa residual a a la eliminación de metales pesados [in line]. Tesis doctoral Ciencia y Tecnología del Medio Ambiente. Granada. Universidad de Granada. Facultad de Ciencias, 2008. 424 p. [consulta: 20 mayo de 2015]. In: http://hera.ugr.es/tesisugr/17514629.pdf

McMurry J (2012) Química orgánica 8a edición. Cengage Learning, México DF

Morrison RT, Boyd RN (1998) Química Orgánica. Addison Wesley Longman, México

MUÑOZ, F. J. Extracción y caracterización de la pectina obtenida a partir del fruto de dos ecotipos de cocona (Solanum sessiliflorum), en diferentes grados de madurez; a nivel de planta piloto. [In line]. Tesis Maestría en Ingeniería Agrícola. Bogotá, Colombia: Universidad Nacional de Colombia, Facultad de Ingeniería, Departamento de Ingeniería Civil y Agrícola, 2011. 18 p. [Consulta: 06 de abril de 2016] In:http://www.bdigital.unal.edu.co/4006/1/822093.2011.pdf

Niño Camacho LR (2009) Implementación de diferentes técnicas analíticas para la determinación de biomasa bacterinas de cepas *Psudomonas putida* biodegradadoras de fenol. [en línea]. Tesis Química. Facultad de Ciencias, Escuela de Quíimica, 12Universidad Industrial de Santander, Santander, Colombia, p 19. http://repositorio.uis.edu.co/jspui/bitstream/123456789/363/2/131320.pdf

Oliva Domínguez JM (2003) Efecto de los productos de degradación originados en la explosión por vapor de biomasa de chopo sobre *Kluyveromyces marxianus*. Tesis doctoral, Madrid, p 166. http://biblioteca.ucm.es/tesis/bio/ucm-t26833.pdf

Oliva Dominguez, J. Miguel. Efecto de los productos de degradación originados en la explosión por vapor de biomasa de chopo sobre Kluyveromyces marxianus. [en línea]. Tesis doctoral. Madrid, 2003. 166 p. [consulta: 5 de marzo de 2015]. Disponible en: http://biblioteca.ucm.es/tesis/bio/ucm-t26833.pdf

Orellana V, Rogel A (2016) Cromatografía de líquidos de alta resolución. Unidad Académica de Ciencias Químicas de la Salud, Universidad Técnica de Machala. https://issuu.com/toxicologia6/docs/hplc.docx_29f51bdf70a77d

Pérez MJ, Quishpi JA (2014) Evaluación cuantitativa de la producción de biodiesel de microalgas de lagunas de tratamiento de agua residual. Tesis Ingeniería Civil. Facultad de ingeniería, Escuela de Ingeniería Civil, Universidad de Cuenca, Cuenca, Ecuador, p 111. http://dspace.ucuenca.edu.ec/bitstream/123456789/20934/3/TESIS.%20PDF.pdf

Pinzón ML, Cardona AM (2008) Caracterización de la cáscara de naranja para su uso como material bioadsorbente. Bistua Rev 6(1):28–37

Sarkanen KV, Ludwig CH (1971) Lignins: occurence, formation, structure and reactions. Wiley Interscience, New York, NY, p 916

Sluiter A, Hames B, Ruiz R, Scarlata C, Sluiter J, Templeton D (2008a) Determination of extractives in biomass. NREL/TP-510-42619. National Renewable Energy Laboratory, Golden, CO

Sluiter A, Hames B, Ruiz R, Scarlata C, Sluiter J, Templeton D, Crocker D (2008b) Determination of structural carbohydrates and lignin in biomass. NREL/TP-510-42618. National Renewable Energy Laboratory, Golden, CO

Sluiter A, Hames B, Ruiz R, Scarlata C, Sluiter J, Templeton D (2008c) Determination of ash in biomass. NREL/TP-510-42622. National Renewable Energy Laboratory, Golden, CO

Szcrbowski D, Pitarelo AP, Filho AZ, Pereira L (2014) Sugarcane biomass for biorefineries: comparative composition of carbohydrate and non-carbohydrate components of bagasse and straw. Carbohydr Polym 114:95–101

Turrel FM, Fisher PL (1942) The proximate chemical constituents of citrus woods, with special reference to lignin. Plant Physiol 17(4):558–581

Pilnik W, Voragen AGJ (1993) Enzymes in food processing, 3rd edn. Copyright 1993 by Academic. 363 3 64. Capítulo 1: pectic enzymes in fruit and vegetable juice manufacture. p 363–392

Wychen SV, Laurens LM (2013) Detemination of total solids and ash in alga biomass. Tech Rep NREL/TP:5100–60956

Xu F, Yu J, Tesso T, Dowell F, Wang D (2013) Qualitative and quantitative analysis of lignocellulosic biomass using infrared techniques: a mini-review. Appl Energ 104:801–809

Zhang J, Deng H, Lin L, Sun Y, Pan C, Liu S (2010) Isolation and characterization of wheat straw lignin with a formic acid process. Bioresour Technol 101:2311–2316

Index

S. Vaz Jr. (ed.), *Analytical Techniques and Methods for Biomass*,
DOI 10.1007/978-3-319-41414-0